UNIVERSITÀ
DEGLI STUDI
DI PADOVA

Sede Amministrativa: Università degli Studi di Padova

Dipartimento di Ingegneria Industriale

CORSO DI DOTTORATO DI RICERCA IN: Ingegneria Industriale
CURRICOLO: Ingegneria Chimica ed Ambientale
CICLO: XXXV

TOWARDS A SUSTAINABLE INDUSTRY WITH LOW ENERGETIC AND ENVIRONMENTAL IMPACT, BASED ON THE INDUSTRIAL CULTIVATION OF CYANOBACTERIA

Coordinatore: Ch.mo Prof. Andrea Claudio Santomaso
Supervisore: Ch.mo Prof. Alberto Bertucco

Dottoranda: Giulia Trentin

Contents

Abstract

The aim of this PhD research project is study a feasibility investigation about the possibility of using cyanobacteria as factories for the industrial production of high value compound, namely cyanophycin. This topic was addressed from different points of view, through both laboratory experiments and mathematical modelling. Different cyanobacterial species were cultivated in batch and continuous photobioreactors at lab scale in order to study cyanophycin accumulation in the cells. The Design of Dynamic Experiments (DoDE) combined to Dynamic Response Model (DRSM) and to Response Surface Model (RSM) was applied to model the growth of *Synechocystis* sp. PCC 6803 and to investigate the effect of three dynamic operating variables on cyanophycin production in batch system.

Then, in view of an industrial prolonged campaign, the cyanophycin production was stabilized by cultivating different cyanobacterial species in continuous flat-plate photobioreactors and assessing the effect of different operating variables on the cyanophycin productivity. Also the possibility of obtaining cyanophycin in continuous system by diazotrophic cyanobacteria was addressed, exploiting N_2 as the only source of nitrogen. To further increase cyanophycin productivity an engineered strain was cultivated in continuous systems under nitrogen fixing conditions. As regards the mathematical modelling, both the nutrients uptake and the oxygen inhibition in a continuous system were accounted for. Finally, based on the results obtained at laboratory scale, a preliminary economic assessment was performed for a one-hectare cyanophycin production plant, and the total product cost was evaluated in three different scenarios.

Foreword

This research project was developed at the Department of Industrial Engineering (DII) of the University of Padova, under the supervision of Prof. Alberto Bertucco.

Part of the work reported in this Thesis has been carried out in collaboration with prof Christos Georgakis from the Department of Chemical and Biological Engineering of Tuft University. Another part is the result of a collaboration with prof. Inna Khozin-Goldberg from The French Associates Institute for Agriculture and Biotechnology of Drylands, Blaustein Institutes for Desert Research of the Ben-Gurion University of the Negev.

As a tangible result of the work completed during the Ph.D school, a number of publication and presentation to conferences has been produced, as listed below.

Publications in Refereed Journals

1. **G. Trentin**, E. Barbera, A. Bertucco, E. Sforza, Role of oxygen in tubular photobioreactors: Model-Based design and operating conditions to minimize productivity losses, Chem. Eng. Process. - Process Intensif. 157 (2020) 108151. https://doi.org/10.1016/j.cep.2020.108151.
2. **G. Trentin**, V. Lucato, E. Sforza, A. Bertucco, Stabilizing autotrophic cyanophycin production in continuous photobioreactors, Algal Res. 60 (2021) 102518. https://doi.org/10.1016/j.algal.2021.102518.
3. **G. Trentin**, E. Barbera, A. Bertucco, C. Georgakis, Experimental Test of the Design of Dynamic Experiments and Dynamic Response Surface Methodologies: Growth of a Photosynthetic Microorganism, Ind. Eng. Chem. Res. (2022). https://doi.org/10.1021/acs.iecr.2c01851.
4. **G. Trentin**, A. Bertucco, C. Georgakis, E. Sforza, E. Barbera, Using the design of dynamic experiments to optimize photosynthetic cyanophycin production by Synechocystis sp ., J. Ind. Eng. Chem. 117 (2023) 386–393. https://doi.org/10.1016/j.jiec.2022.10.026.

5. **G. Trentin**, F. Piazza, M. Carletti, B. Zorin, I. Khozin-Goldberg, A. Bertucco, E. Sforza, Fixing N_2 into cyanophycin: continuous cultivation of *Nostoc* sp. PCC 7120, Appl. Microbiol. Biotechnol. (2022). https://doi.org/10.1007/s00253-022-12292-4.
6. M. Turetta, E. Barbera, **G. Trentin**, A. Bertucco, E. Sforza, Modeling the production of cyanophycin in *Synechocystis* sp. PCC 6803 cultivated in chemostat reactors, Bioresour. Technol. Reports. 19 (2022) 101132. https://doi.org/10.1016/j.biteb.2022.101132.

Abstracts in conference proceedings

1. **Trentin G.**, Barbera E.*, Bertucco A., Kumar S., Sforza E., Trattamento di acque reflue ad elevata concentrazione di nutrienti con *Synechocystis* sp. PCC 6803, First Workshop Giovani AISAM 2019, Scuola di Agraria, Università degli Studi di Firenze, 28.10.2019, Oral presentation (*Speaker)
2. **Trentin G.**, Lucato V., Sforza E, Barbera E., Bertucco A., Production of compounds with high added value with *Synechocystis* sp. PCC 6803, Conference AISAM2020, Università degli Studi di Padova, 07.09.2020, Poster presentation
3. **Trentin G.**, Sforza E, Bertucco A., Stable production of cyanophycin by *Synechocystis* sp. PCC 6803 in continuous cultivation system, AlgaEurope 2020, Online Event, 01-04.12.2020, Poster presentation
4. **Trentin G.**, Lucato V., Sforza E., Bertucco A., Stable production of cyanophycin by *Synechocystis* sp. PCC 6803 in continuous cultivation system, International Conference on Algal Biomass, Biofuels & Bioproducts, Online Event, 14-16.06.2021, Oral presentation
5. **Trentin G.**, Sforza E., Bertucco A., Describing growth and nutrient uptake by Droop model in microalgal continuous reactors at steady state, Second Workshop Giovani AISAM, Roma, Italia, 24.09.2021, Oral Presentation
6. **Trentin G.**, Barbera E., Sforza E, Bertucco A., C. Georgakis, Photosynthetic production of cyanophycin by *Synechocystis* sp.: a data driven optimization, AlgaEurope 2021, Online Event, 07-10.12.2021, Poster presentation
7. **Trentin G.**, Carletti M., Zorin B., Khozin-Goldberg I., Sforza E., Bertucco A., Progetto INFINITRO: fissazione biologica di N_2 per la produzione di cianoficina in sistemi in continuo, Aquafarm 2022, Pordenone, Italia, 25-26.05.2022, Poster presentation

8. **Trentin G.**, Zorin B., Khozin-Goldberg I., Bertucco A., Sforza E., Progetto INFINITRO From N_2 to cyanophycin: high value compound production through biological nitrogen fixation in continuous systems, Convegno GRICU 2022, Ischia, Italia, 03-06.07.2022, Poster presentation
9. **Trentin G.**, Zorin B., Carletti M., Khozin-Goldberg I., Bertucco A., Sforza E., From N_2 to cyanophycin: high-value compound production through biological nitrogen fixation in continuous systems, AlgaEurope 2022, Roma, Italia, 13-15.12.2022, Poster presentation
10. Carletti M. *, Sforza E., **Trentin G.**, Bertucco A., Boussiba S., Khozin-Goldberg I., Zorin B., Effective conversion of atmospheric nitrogen into a storage amino acid polymer cyanophycin: mutagenesis and optimization of cultivation of *Nostoc* sp. PCC 7120, AlgaEurope 2022, Roma, Italia, 13-15.12.2022, Oral presentation (*Speaker)

Riassunto

L'aumento esponenziale della popolazione mondiale richiede alla società odierna di affrontare notevoli ed ingenti problemi che riguardano i crescenti bisogni energetici, alimentari e sanitari [1]. La disponibilità di combustibili fossili si sta progressivamente riducendo, e si rende necessario riprogettare la produzione industriale in modo da ridurre drasticamente i fabbisogni energetici. In altri termini, i processi industriali attualmente utilizzati non sono sostenibili e possono diventare la causa di significativi cambiamenti ambientali [2]. Infatti, l'anidride carbonica e altri gas serra derivanti dalla combustione di carbone, petrolio e gas naturale si accumulano nell'atmosfera, intrappolando la radiazione infrarossa emessa dalla superficie terrestre in seguito all'assorbimento della luce solare [3,4] e producendo così un effetto di riscaldamento globale. L'aumento della temperatura della superficie terrestre e degli oceani è destinato inevitabilmente a comportare un drastico cambiamento delle condizioni climatiche. Parallelamente, lo sfruttamento del suolo a fini residenziali e commerciali riduce la disponibilità di terre coltivabili [5].

Di conseguenza, negli ultimi anni sta crescendo molto l'interesse verso lo sviluppo di bioprocessi industriali sostenibili che sfruttano l'enorme potenziale dei microrganismi per ottenere cibo, medicinali ed energia [2]. Un settore industriale a base biologica ridurrebbe in modo significativo la dipendenza dai prodotti di origine fossile, porterebbe ad una crescita economica più rispettosa dell'ambiente e aiuterebbe i paesi a raggiungere gli obiettivi sui cambiamenti climatici. Questo concetto di industria bio-based si sta affermando anche nell'ottica dell'economia circolare, cioè di un'economia basata su un ciclo chiuso di vita del prodotto, attraverso il riciclo e il riutilizzo di materiali ed energia.

Alcuni microrganismi sono già sfruttati per sintetizzare molti composti commercialmente rilevanti, ed in tal senso i microorganismi fotosintetici hanno un notevole potenziale, in quanto possono utilizzare come fonte di energia sia la luce solare che le molecole di riserva immagazzinate internamente. In particolare, i cianobatteri potrebbero diventare fondamentali come fonte sostenibile di composti ad alto valore aggiunto, grazie agli elevati tassi di crescita, produttività ed efficienza di conversione dell'energia solare. Inoltre, modificandone le condizioni di coltivazione è possibile favorire la produzione di uno specifico composto di interesse e di massimizzarne la sua produttività. Fra i pigmenti

commercialmente importanti che possono essere sintetizzati dai cianobatteri, si ricordano la ficocianina, la zeaxantina e il β-carotene, ma anche i poliidrossialcanoati, una famiglia di biopoliesteri biodegradabili presenti in natura, e la cianoficina, una preziosa materia prima per ottenere polipeptidi e bioplastiche. La cianoficina potrebbe essere utilizzata come precursore per produrre sostanze chimiche contenenti azoto, come acrilonitrile, butandiammina e urea [6]. Inoltre, può essere idrolizzata nei suoi costituenti, L-arginina e acido aspartico, grazie al taglio β-idrolitico [6]. L'acido poliaspartico (PASP) è un polipeptide anionico nonché un polimero altamente versatile. Grazie alla sua struttura è un sostituto ideale dei polielettroliti anionici non degradabili e, in virtù della sua biocompatibilità e biodegradabilità, ha portato allo sviluppo di una varietà di materiali interessanti per applicazioni biomediche [7]. L'amminoacido L-arginina, invece, ha importanti ruoli fisiologici in molti disturbi cardiovascolari, gastrointestinali e immunitari [8]. Attualmente, la maggior parte della L-arginina viene prodotta per fermentazione diretta da fonti naturali di carbonio, come gli amidi [9].

In tale contesto, questa tesi di dottorato di ricerca si è proposta di studiare la coltivazione di cianobatteri per la produzione di composti ad alto valore aggiunto, focalizzando l'attenzione sulla cianoficina. La cianofician viene ottenuta sia da alcuni batteri eterotrofi come *Acinetobacter* sp., *Bordetella bronchiseptica*, *Clostridium botulinum*, *Desulfitobacterium hafniense*, sia da cianobatteri unicellulari, filamentosi, diazotrofi o meno, ad esempio appartenenti alle specie *Scytonema* sp., *Synechocystis* sp., *Synechococcus* sp. e *Anabaena* sp. [6,10,11]. A tutt'oggi, gli studi sulla cianoficina riguardano prevalentemente l'espressione eterologa dei geni della cianoficina sintetasi in microrganismi eterotrofi. Al contrario, la letteratura disponibile sulla produzione di cianoficina da microorganismi fotosintetici è ancora piuttosto scarsa. In particolare, è noto che diversi fattori possono indurre l'accumulo di cianoficina, come condizioni di crescita squilibrate, o l'aggiunta nel terreno di coltura di specifici composti come il cloramfenicolo o la rifamicina, ma questi risultati sono stati ottenuti in sistemi batch, che sono caratterizzati da un'alta variabilità nel tempo. D'altra parte, il principale vantaggio di coltivare microrganismi fotosintetici in un sistema continuo è proprio legato alla possibilità di stabilizzare nel tempo le condizioni all'interno del reattore, sia in termini di quantità che di qualità della biomassa prodotta, ottenendo così produttività più elevate e stabili, essenziali quando si deve sviluppare una produzione su larga scala. La modalità operativa in continuo appare molto più allettante, anche in considerazione della natura transitoria della cianoficina, che viene accumulata e/o consumata all'interno del microrganismo a seconda delle condizioni ambientali.

Inizialmente, seguendo un approccio statistico è stata specificatamente progettata una campagna sperimentale batch per studiare e ottimizzare l'accumulo di cianoficina all'interno della biomassa di *Synechocystis* sp. PCC 6803 e per modellare la crescita del microorganismo stesso, in funzione di tre fattori dinamici: l'intensità di luce incidente, il profilo di fosforo in ingresso e la temperatura. Si è così ottenuto un Response Surface Model (RSM) che descrive l'accumulo di cianoficina al giorno 7, e un Dynamic Response Surface Model (DRSM) per descrivere la crescita di *Synechocystis* sp. PCC 6803 in un sistema batch. Il risultante modello RSM è stato ottimizzato per ottenere il valore dei fattori, cioè delle condizioni sperimentali, che massimizzano la produzione di cianoficina. L'ottimo è stato confermato tramite esperimento di validazione, dove si è misurato un aumento della concentrazione di cianoficina di circa il 20% rispetto al valore massimo precedentemente ottenuto. Si sono stimati tre modelli DRSM: due modelli quadratici ridotti, ed un modello di interazione a due fattori. Per verificare l'accuratezza di tali modelli, sono stati progettati ed eseguiti quattro ulteriori esperimenti all'interno del dominio originale. Si è visto che quasi tutti i punti sperimentali ricadono all'interno degli intervalli di previsione, dimostrando la capacità del modello di tener conto dell'effetto di diverse variabili di processo. Pertanto, DoDE e DRSM si sono rivelati strumenti di ricerca potenti anche quando si descrivono bioprocessi estremamente complessi e altamente variabili.

Nel corso del lavoro, diverse specie di cianobatteri sono state coltivate in continuo in fotobioreattori *flat-plate*, al fine di valutare l'effetto delle variabili operative sulla produzione di biomassa e cianoficina. Per quanto riguarda gli esperimenti con *Synechocystis* sp. PCC 6803, è stata ottenuta una produzione stabile di cianoficina allo stato stazionario. Tuttavia, la cianoficina è un metabolita secondario sintetizzato in condizioni di coltivazione sbilanciate, e quindi non è stato prodotto in tutte le condizioni sperimentali studiate. L'analisi dell'effetto delle variabili operative ha evidenziato che la concentrazione e la produttività della biomassa sono più elevate a più alta concentrazione di fosforo in ingresso e mostrano un andamento classico in funzione del tempo di permanenza, con un massimo di produttività compreso tra 1 e 2 giorni. Alla maggiore concentrazione di fosforo alimentata in ingresso, la massima concentrazione di biomassa misurata è risultata pari a 0,35 g_X L^{-1} d^{-1}. La quota di cianoficina e la produttività, invece, hanno un andamento completamente diverso. Aumentando la concentrazione di fosforo in ingresso, infatti, è necessario aumentare il tempo di residenza per rilevare la presenza di cianoficina. Di conseguenza la quota massima di cianoficina è stata misurata quando la concentrazione di fosforo in ingresso è stata ridotta a circa 1 mg_P L^{-1} e il tempo di residenza è stato aumentato

fino a 11 giorni. Al contrario, il valore massimo della produttività di cianoficina è stato ottenuto non nella condizione in cui la quota era massimizzata, perché in quel caso vi era anche una contestuale riduzione della produttività di biomassa. In ogni caso, la massima produttività di cianoficina ottenuta è raddoppiata rispetto a quella misurata negli esperimenti batch preliminari effettuati sulla stessa specie. È stata proposta una correlazione quantitativa tra la quota di fosforo e la cianoficina prodotta, evidenziando una soglia di 4 mg di fosforo per g di biomassa necessaria ad innescare l'accumulo di cianoficina.

Successivamente, è stata valutata la possibilità di produrre cianoficina coltivando cianobatteri diazotrofi in sistemi continui. I cianobatteri diazotrofi hanno la capacità di fisssare l'azoto molecolare grazie all'enzima nitrogenasi. Il processo di fissazione di N_2 è inibito dall'ossigeno e i cianobatteri affrontano questo problema separando i due processi: le eterocisti sono cellule che si differenziano dalle cellule vegetative, ed al loro interno avviene la fissazione di N_2. I due tipi di cellule sono reciprocamente interdipendenti per vari processi cellulari: le eterocisti ricevono i carboidrati dalle cellule vegetative, mentre le cellule vegetative si affidano alle eterocisti per l'azoto fissato. In questo contesto, la cianoficina diventa un serbatoio dinamico per l'azoto fissato, ed infatti, per facilitarne il trasporto, si localizza principalmente nella connessione tra eterocisti e cellule vegetative. *Anabaena cylindrica* PCC 7122 e *Nostoc* sp. PCC 7120 sono stati coltivati in un sistema continuo, dove è stato valutato l'effetto della concentrazione di fosforo in ingresso. Per entrambe le specie, la concentrazione e la produttività della biomassa sono diminuite al diminuire della concentrazione di fosforo in ingresso ma, in condizione di limitazione di fosforo, la produttività della cianoficina era significativamente più alta. *Anabaena cylindrica* PCC 7122 produce cianoficina solo quando la concentrazione di fosforo in ingresso è limitante, mentre *Nostoc* sp. PCC 7120 accumulava cianoficina in tutte le condizioni sperimentali studiate. Tra le due specie, *Nostoc* sp. PCC 7120 si è mostrata la più efficiente in termini di produttività di azoto fissato, biomassa e cianoficina; quindi, le condizioni operative sono state ulteriormente ottimizzate per massimizzare la produttività di cianoficina. Nello specifico, sono stati studiati l'effetto dell'intensità della luce incidente, del tempo di permanenza e del pH. Tra queste variabili operative, il pH ha un ruolo importante nella produzione di biomassa, influenzando quindi indirettamente la produttività della cianoficina. Tuttavia, nel complesso, è stato osservato che la produzione di cianoficina è strettamente dipendente dalla concentrazione di fosforo presente nel terreno di coltura, e solo diminuendo la quota di fosforo è stato possibile misurare una maggiore

quantità di cianoficina nella biomassa. In sintesi, è stata ottenuta una produzione stabile e continua di cianoficina coltivando *Nostoc* sp. PCC 7120 in condizioni diazotrofiche, ottenendo una produttività massima di cianoficina di 15 mg_{CGP} L^{-1} d^{-1}.

Per aumentare ulteriormente la produttività della cianoficina, *Nostoc* sp. PCC 7120 è stato ingegnerizzato per ottenere ceppi che riescano a sovraprodurle. Questi ceppi, *Nostoc* 41, *Nostoc* 44, *Nostoc* 47 e *Nostoc* 53 sono stati coltivati in un sistema continuo in condizioni di fissazione dell'azoto. È stato valutato l'effetto della concentrazione di fosforo in ingresso e per tutti i ceppi mutanti la concentrazione di biomassa è diminuita al diminuire della concentrazione di fosforo in ingresso. Di conseguenza, le culture hanno cambiato il loro colore dal verde-blu al verde-giallo, come verificato tramite quantificazione dei pigmenti nella biomassa. Al contrario, la quota di cianoficina è aumentata quando il fosforo è diventato limitante. Tra i ceppi mutanti, *Nostoc* 44 è risultato il più performante, raggiungendo una produttività di cianoficina tre volte superiore rispetto al ceppo *wild type* e pari a circa 64 mg_{CGP} L^{-1} d^{-1}.

Come per *Synechocystis* sp. PCC 6803, sia per i mutanti che per i ceppi *wild type* esiste una stretta relazione tra la quota interna di fosforo e la quota di cianoficina: nello specifico queste variabili sono inversamente proporzionali. Pertanto, per aumentare la produttività della cianoficina, è necessario ridurre la quota di fosforo. Infatti, *Nostoc* 44 raggiunge una quota incredibilmente alta di cianoficina (circa il 30% w/w) proprio perché la quota interna di fosforo si riduce al minore valore misurato di $0{,}11 \pm 0{,}02$ g_P g_x^{-1}.

Per quanto riguarda la modellazione matematica della crescita delle microalghe, il modello Monod è il più utilizzato per descrivere la cinetica di crescita dei microrganismi in funzione della concentrazione dei nutrienti. Tuttavia, spesso non riesce ad adattarsi ai dati sperimentali, perché le microalghe mostrano un ritardo tra l'assorbimento dei nutrienti e la crescita della biomassa, specialmente se coltivate in substrati complessi, dove potrebbero esserci co-limitazione dei nutrienti o competizione tra diversi nutrienti che forniscono lo stesso elemento, come nel caso dell'ammonio e del nitrato per l'azoto. Un modello matematico preliminare è stato sviluppato sulla base dell'approccio di Droop, che disaccoppia la crescita dei microrganismi dall'assimilazione dei nutrienti. Il confronto con i dati sperimentali ha dimostrato che tale approccio è in grado di descrivere la crescita della biomassa per diverse variabili operative, in particolare diversi valori di tempo di residenza, spessore del reattore e concentrazioni di nutrienti, ma deve essere ulteriormente approfondito.

Ad ogni modo, gli impianti di produzione continua sono il modo più adatto per ottenere una produzione di biomassa di alto valore grazie alla maggiore e stabile produttività

ottenibile rispetto a quella discontinua. Tra le varie tipologie, i fotobioreattori tubolari garantiscono produttività microalgali più elevate grazie al loro più alto rapporto superficie/volume ma sono problematici per l'accumulo di ossigeno, che inibisce la crescita della biomassa. Pertanto, è stato sviluppato un modello matematico per comprendere l'effetto combinato della concentrazione di ossigeno, dell'intensità della luce, della geometria del reattore e della concentrazione di biomassa in reattori tubulari. Il modello matematico sviluppato è stato utilizzato dapprima per analizzare un reattore a tubo singolo, quindi per analizzare il processo completo, comprendente tutte le principali unità coinvolte in un impianto di produzione commerciale. Sono state effettuate analisi di sensitività per studiare l'effetto delle principali variabili di processo (lunghezza del tubo, intensità della luce incidente e tempo di ritenzione dei solidi), con l'obiettivo di identificare la configurazione ottimale e le condizioni operative che consentono di minimizzare la perdita di produttività a causa dell'inibizione dell'ossigeno. Nello specifico, si è visto che la concentrazione di biomassa all'ingresso del tubo è la variabile chiave per controllare l'accumulo di ossigeno e la conseguente inibizione della crescita. Dal profilo del tasso di crescita complessivo lungo il reattore, è stato possibile definire un criterio generale per determinare la lunghezza ottimale del tubo che minimizza l'effetto delle altre variabili operative (concentrazione di biomassa e di ossigeno) sull'inibizione dell'ossigeno. L'analisi ha inoltre rivelato che il monitoraggio della concentrazione di ossigeno all'uscita del reattore non è sufficiente per stimare l'andamento della produttività.

Nel corso del lavoro, è stato approfondito il metodo di quantificazione della cianoficina, il quale dipende fortemente dal composto utilizzato per creare la curva di calibrazione, dato che non è ancora disponibile uno standard commerciale di cianoficina. Questo problema impedisce un confronto corretto dei dati sperimentali con quelli della letteratura, che si riferiscono a curve di calibrazione ottenute con diversi composti amminoacidici e che influenzano la quantificazione del composto stesso. Pertanto, un campione di cianoficina è stato prodotto, estratto, essiccato, analizzato e quindi utilizzato come riferimento per la quantificazione della cianoficina. L'analisi della composizione amminoacidica mediante metodo LC-MS/MS dopo idrolisi acida ha rivelato che il campione è composto dal 36,2% di arginina e dal 48,5% di acido aspartico, a conferma dell'elevata qualità della cianoficina prodotta ed estratta.

A completamento del lavoro, è stata eseguita un'analisi economica preliminare per valutare il costo di un impianto di produzione di cianoficina, delle dimensioni di un ettaro, che comprende anche una sezione di pretrattamento della biomassa e una sezione di estrazione

della cianoficina. I calcoli sono stati effettuati in tre scenari, che corrispondono alla produttività di cianoficina ottenuta nelle migliori condizioni operative per tre specie di cianobatteri, come ottenuto nei precedenti esperimenti di laboratorio. È stato così possibile stimare il costo totale del prodotto che tiene conto sia dei costi impianto sia di quelli di energia. Se si considera solo la sezione di produzione della biomassa, il costo totale di produzione risulta pari a 82,3 € kg^{-1}, 182,0 € kg^{-1} e 121,3 € kg^{-1} rispettivamente per *Synechocystis* sp. PCC 6803, *Nostoc* sp. PCC 7120 e *Nostoc* 44. Se invece si tiene conto del costo di tutte le sezioni dell'impianto di produzione, e assumendo come prodotto non solo la cianoficina estratta ma anche la biomassa residua dopo l'estrazione, il costo totale di produzione risulta pari a 137,6 € kg^{-1}, 240,3 € kg^{-1} e 174,2 € kg^{-1} rispettivamente per *Synechocystis* sp. PCC 6803, *Nostoc* sp. PCC 7120 e *Nostoc* 44. Questi costi di produzione piuttosto elevati dipendono anche dal fatto che per produrre cianoficina i cianobatteri sono stati coltivati in condizioni sbilanciate, raggiungendo così un'efficienza fotosintetica molto bassa (di poco inferiore al 3%).

In sintesi, i risultati ottenuti durante questo progetto di dottorato possono essere considerati un buon punto di partenza per lo studio della produzione fotosintetica di cianoficina. Tuttavia, ulteriore lavoro deve essere fatto, in particolare per la produzione di uno standard commerciale universale a cui confrontare e riferire i dati sperimentali di letteratura. In vista dello sviluppo di un processo su larga scala, il protocollo per il pretrattamento della biomassa e l'estrazione della cianoficina devono essere migliorati e ottimizzati. Inoltre, sono necessarie ulteriori sperimentazioni per trovare le condizioni colturali che possano garantire un'elevata produttività di cianoficina, ma allo stesso tempo ridurre i costi operativi dovuti all'impiego dell'elettricità per l'illuminazione artificiale dei fotobioreattori, aumentando così l'efficienza fotosintetica.

Literature cited

[1] D. Tilman, R. Socolow, J.A. Foley, J. Hill, E. Larson, L. Lynd, S. Pacala, J. Reilly, T. Searchinger, C. Somerville, R. Williams, Energy. Beneficial biofuels--the food, energy, and environment trilemma., Science. 325 (2009) 270–271. https://doi.org/10.1126/science.1177970.

[2] N.K. Sharma, A.K. Rai, L.J. Stal, Cyanobacteria : an economic perspective , Wiley Blackwell, Chichester, England, 2014.

[3] S.I. Zandalinas, F.B. Fritschi, R. Mittler, Global Warming, Climate Change, and Environmental Pollution: Recipe for a Multifactorial Stress Combination Disaster, Trends Plant Sci. 26 (2021) 588–599. https://doi.org/10.1016/j.tplants.2021.02.011.

[4] Z. Chi, J. V. O'Fallon, S. Chen, Bicarbonate produced from carbon capture for algae culture, Trends Biotechnol. 29 (2011) 537–541. https://doi.org/10.1016/j.tibtech.2011.06.006.

[5] D. De Wrachien, M. Goli, Global Warming Effects on Irrigation and Drainage Development, J. Agric. Aquac. 01 (2019) 1–5. https://doi.org/10.4172/2168-9768.1000e126.

[6] J. Du, L. Li, S. Zhou, Microbial production of cyanophycin: From enzymes to biopolymers, Biotechnol. Adv. 37 (2019). https://doi.org/10.1016/j.biotechadv.2019.05.006.

[7] P.S. Yavvari, A.K. Awasthi, A. Sharma, A. Bajaj, A. Srivastava, Emerging Biomedical Applications of Polyaspartic Acid-Derived acid-derived biodegradable polyelectrolytes, (2019). https://doi.org/10.1039/C8TB02962H.

[8] A. Steinbüchel, A. Sallam, Dipeptides in nutrition and therapy: Cyanophycin-derived dipeptides as natural alternatives and their biotechnological production, Appl. Microbiol. Biotechnol. 87 (2010) 815–828. https://doi.org/10.1007/s00253-010-2641-0.

[9] T. Utagawa, Arginine Metabolism: Enzimology, Nutrition, and Clinical Significance - Production of Arginine by Fermentation, (2004) 2854–2857.

[10] J. Aravind, T. Saranya, G. Sudha, P. Kanmani, Integrated Waste Management in India, (2016) 49–58. https://doi.org/10.1007/978-3-319-27228-3.

[11] B. Watzer, K. Forchhammer, Cyanophycin: A Nitrogen-Rich Reserve Polymer, in: K.F.E.-A. Tiwari (Ed.), IntechOpen, Rijeka, 2018: p. Ch. 5. https://doi.org/10.5772/intechopen.77049.

Introduction

In recent decades, we are living an era of unprecedented technological innovation and progress [1]. Human activities are mainly based on the use of fossil fuels [2] and cause the release of large quantities of CO_2 into the environment at an alarming rate [1,3]. Industrial emissions to the atmosphere have risen by more than 70% since 2000, as a result of increasing demand of industrial goods, reaching 9.4 Gt of CO_2 in 2021, that is a quarter of global emissions [4]. Therefore, alternatives to fossil fuels need to be found within a few decades. Implementing such reductions poses significant technological, economic, social and institutional challenges [5]. The chemical sector is the third industrial sub-sector in terms of direct emissions of carbon dioxide. This is largely due to fuels that are used as a source of raw material, as well as of energy. The significant energy consumption of the sector is also driven by the demand for a wide range of primary chemicals, which has increased significantly in the recent years [4].

In this context, the industrial biotechnology sector also draws attention to "green" production alternatives [6]. For instance, the use of heterotrophic microorganisms, such as the *Escherichia coli*, is now consolidated in many industrial chemical processes. However, the economic viability of this biotechnological approach is limited by the cost of the organic substrates used in the fermentation processes [7]. A valid alternative is represented by photosynthetic microorganisms, i.e. microalgae and cyanobacteria, which have recently attracted considerable interest due to their broad renewable and potentially sustainable application potentials [8,9]. At global level, the algae products market was valued at $2,276 million in 2020, and is projected to reach $4,287 million by 2031, growing at a Compound Annual Growth Rate (CAGR) of 4.88% from 2022 to 2031 [10]. Furthermore, using mainly sunlight and CO_2 as sources of energy and carbon, the production costs related to the culture media are reduced. Photosynthetic microorganisms are more efficient in the use of sunlight, converting up to 10-20% of light energy into biomass, compared to about 2% of terrestrial plants [11], with respect to which they also require smaller areas for cultivation [7] and with an optimal growth temperature in many cases a few degrees higher [12]. Moreover, they are tolerant to different types of stress, including water stress [13] and saline stress [14]. These characteristics make the cultivation of microalgae and cyanobacteria

particularly attractive also in hostile environments, such as arid areas or oceans which are not accessible to traditional agriculture, thus minimizing the competition with food crops for human consumption [7,15]. Moreover, some species of cyanobacteria are able to perform *in vivo* nitrogen fixation, representing a valuable alternative to the Haber-Bosch process to produce ammonia, which is responsible of 0.93% of greenhouse gases emissions in the world [16]. It is clear that microalgal cultivation could contribute to the development of "carbon neutral" production processes [6,7].

Photosynthetic microorganisms are already exploited to synthetize many commercially relevant compounds, such as phycocyanin, zeaxanthin and β-carotene, with strong antioxidant properties, but also polyhydroxyalkanoates, a family of naturally-occurring biodegradable biopolyester, and cyanophycin, a valuable raw material for polypeptides and bioplastics. The industrial application of cyanophycin is not a reality right now. However, cyanophycin can be a starting point for the synthesis of many other important chemicals, as butanediamine and urea, and has recently attracted the attention of the scientific community as a biodegradable replacement for petrochemical-based industrial products. Industrial interest focuses on its chemical derivatives, as cyanophycin can be chemically converted to poly(aspartic acid) (PASP) and arginine by β-hydrolytic cleavage.

To date, studies of cyanophycin production have exploited the heterologous expression of cyanophycin synthetase genes in heterotrophic microorganisms. Instead, the available literature focused on photosynthetic cyanophycin production is still quite scarce. Different cyanobacteria strains were found to accumulate this compound, such as *Scytonema* sp., *Synechocystis* sp., *Synechococcus* sp. and *Anabaena* sp. and several factors may induce cyanophycin accumulation, such as growth under imbalanced conditions, e.g. adverse light intensities, low temperature, phosphate and sulphate starvation, or with specific substances added to culture media. So far, data available in literature regarding the cyanophycin production by photosynthetic microorganisms were carried out in batch systems, which are characterized by the variation of the experimental conditions over time, specifically with nutrients and light availability that are progressively reduced during biomass growth. On the other hand, the main advantage of cultivating microorganisms in a continuous system is the possibility of stabilizing conditions inside the reactor over time, both in terms of quantity and quality of the biomass produced, thus allowing to obtain higher and stable productivity, required for large-scale operation. The continuous operating mode appears more attractive, also considering the transient nature of cyanophycin as a storage compound, which is accumulated and/or consumed within the microorganism depending

on the evolving environmental conditions. Indeed, in the literature there is no systematic study investigating the possible combined effect of operating variables that could improve the cyanophycin productivity. In this regard, by using the Design of Experiments (DoE) approach, the information derived from experimental data can be maximized, resulting in a reduction in process development times, more efficient use of resources and, finally, greater process reliability. Mathematical models, in general, are valuable tools to aid in designing, optimizing, and controlling also industrial biochemical process, and are fundamental to perform a reliable assessment of operating variables, before investing on large scale production plants.

As regards the open issues summarized above, the aim of this PhD research project is to study the feasibility of using cyanobacteria as factories for a sustainable bio-based large-scale industrial application to obtain high value compounds, namely cyanophycin. To this purpose, several points have been addressed which have been subdivided in chapters as follows.

Chapter 1 gives an overview on the current knowledge about cyanobacterial production of cyanophycin, with a particular emphasis on the possibility to exploit diazotrophic cyanobacteria on cyanophycin applications.

Chapter 2 and Chapter 3 are dedicated to the Design of Dynamic Experiments (DoDE) statistical approach, which is used to assess the effect of three factors, the incident light intensity, the temperature, and the inlet phosphorus concentration. In **Chapter 2**, DoDE is used combined to the Response Surface Model (RSM) to describe the accumulation of cyanophycin in *Synechocystis* sp. PCC 6803. In **Chapter 3** it is developed a Dynamic Response Surface Model (DRSM) to describe the growth of *Synechocystis* sp. PCC 6803 in a batch system.

Chapter 4 to 6 are dedicated to cyanobacterial cultivation in continuous photobioreactors. Specifically, in **Chapter 4,** *Synechocystis* sp. PCC 6803 is grown in continuous system to produce cyanophycin. The effect of different inlet phosphorus concentration, and of different residence times are addressed. **Chapter 5** evaluates the possibility to produce cyanophycin by cultivating diazotrophic cyanobacteria, thus exploiting N_2 as the only source of nitrogen. Two diazotrophic cyanobacteria are cultivated in continuous system, assessing the effect of operating variables in biomass and cyanophycin production. In **Chapter 6** the continuous cultivation of engineered strains of *Nostoc* sp. PCC 7120 is considered to further increase the cyanophycin productivity.

Chapter 7 and Chapter 8 are dedicated to the mathematical modelling of microalgal growth, with analysis of general validity. In **Chapter 7**, a preliminary mathematical model was developed to decouple the microorganism growth from the nutrient assimilation, and the model results are compared to experimental measurements. **Chapter 8** is focused on the study and the development of a model to understand the combined effect of oxygen concentration, light intensity, reactor geometry, and biomass concentration on microalgal productivity in tubular photobioreactors.

Finally, in **Chapter 9**, after developing a possible process flowsheet for industrial cyanophycin production, a preliminary economic analysis in three scenarios is performed to evaluate the cost for a cyanophycin production plant, based on a one-hectare biomass production plant, a pre-treatment section and a cyanophycin extraction section.

Literature cited

[1] S.C. Peter, Reduction of CO_2 to Chemicals and Fuels: A Solution to Global Warming and Energy Crisis, ACS Energy Lett. 3 (2018) 1557–1561. https://doi.org/10.1021/acsenergylett.8b00878.

[2] T. Pulles, Engineering photosynthesis: a necessary tool to protect the world's climate?, Carbon Manag. 8 (2017) 167–173. https://doi.org/10.1080/17583004.2017.1309201.

[3] A. Gettelman, R.B. Rood, Climate Change and Global Warming, in: A. Gettelman, R.B. Rood (Eds.), Demystifying Clim. Model. A Users Guid. to Earth Syst. Model., Springer Berlin Heidelberg, Berlin, Heidelberg, 2016: pp. 23–35. https://doi.org/10.1007/978-3-662-48959-8_3.

[4] IEA (2022), Industry, Licens. CC BY 4.0 Paris. (2022). https://www.iea.org/reports/industry.

[5] IPCC 2014, Climate Change 2014: Synthesis Report. Contribution of Working Groups I, II and III to the Fifth Assessment Report of the Intergovernmental Panel on Climate Change, Core Writ. Team, R.K. Pachauri L.A. Meyer. (2014) 151.

[6] A.M. Ruffing, T. Kallas, Editorial: Cyanobacteria: The Green E. coli, Front. Bioeng. Biotechnol. 4 (2016) 7. https://doi.org/10.3389/fbioe.2016.00007.

[7] N.-S. Lau, M. Matsui, A.A.-A. Abdullah, Cyanobacteria: Photoautotrophic Microbial Factories for the Sustainable Synthesis of Industrial Products, Biomed Res. Int. 2015 (2015) 1–9. https://doi.org/10.1155/2015/754934.

[8] F. dos Santos, W. Du, K.J. Hellingwerf, Synechocystis: Not Just a Plug-Bug for CO2, but a Green E. coli, Front. Bioeng. Biotechnol. 2 (2014). https://doi.org/10.3389/fbioe.2014.00036.

[9] M.I. Khan, J.H. Shin, J.D. Kim, The promising future of microalgae: Current status, challenges, and optimization of a sustainable and renewable industry for biofuels,

feed, and other products, Microb. Cell Fact. 17 (2018) 1–21. https://doi.org/10.1186/s12934-018-0879-x.

[10] Allied Market Research, Algae Product Market, Glob. Oppor. Anal. Ind. Forecast. (2022). https://www.alliedmarketresearch.com/algae-products-market.

[11] U.B. Singh, A.S. Ahluwalia, Microalgae: A promising tool for carbon sequestration, Mitig. Adapt. Strateg. Glob. Chang. 18 (2013) 73–95. https://doi.org/10.1007/s11027-012-9393-3.

[12] B.A. Whitton, ed., Ecology of Cyanobacteria II Their Diversity in Space and Time, 1st ed., Springer Dordrecht, 2012. https://doi.org/https://doi.org/10.1007/978-94-007-3855-3.

[13] M. Potts, Desiccation tolerance of prokaryotes, Microbiol. Rev. 58 (1994) 755–805. https://doi.org/10.1128/mr.58.4.755-805.1994.

[14] J. Bauld, 8. Occurrence of benthic microbial mats in saline lakes, Hydrobiologia. 81 (1981) 87–111. https://doi.org/10.1007/BF00048708.

[15] C.J. Knoot, J. Ungerer, P.P. Wangikar, H.B. Pakrasi, Cyanobacteria: Promising biocatalysts for sustainable chemical production., J. Biol. Chem. 293 (2018) 5044–5052. https://doi.org/10.1074/jbc.R117.815886.

[16] Y. Bicer, I. Dincer, G. Vezina, F. Raso, Impact Assessment and Environmental Evaluation of Various Ammonia Production Processes, Environ. Manage. 59 (2017) 842–855. https://doi.org/10.1007/s00267-017-0831-6.

Chapter 1

Cyanobacteria as microbial cell factories: state of the art

Global challenges like climate change, land and ecosystem degradation, coupled with a growing population, force to search for new ways of producing and consuming that respect our planet. As a biological resource, microalgae could potentially provide an environmental friendly solution and contribute to meeting the increasing demands for food, feed, energy and materials. Microalgae are currently used by the food and chemical industries, with new applications emerging in the areas of food and feed, nutraceuticals, pharmaceuticals, biofuels, biomaterials and bioremediation services. Specifically, some photosynthetic microorganisms produce cyanophycin, a valuable raw material for polypeptides (feed application) and bioplastics. Moreover, the production of high value compounds by cultivating nitrogen fixing cyanobacteria represents a unique opportunity to meet the target priorities of the EU Bioeconomy Strategy.

1.1 Industrial cultivation of microalgae: a new challenge

The exponential increase in the world population places today's society in front of significant problems regarding the growing energy, food and health needs [1]. The industrial processes currently used to meet these needs are not sustainable and cause significant changes in the environment first of all the global warming effect [2]. Indeed, carbon dioxide and other greenhouse gases deriving from the combustion of coal, oil and natural gas keep accumulating in the atmosphere, trapping the infrared radiation emitted by the surface of the Earth following the absorption of sunlight [3,4]. This phenomenon causes an increase in the temperatures of land surfaces and oceans, which in turn will inevitably lead to a drastic change in climatic conditions. In parallel, the exploitation of land for residential and commercial purposes reduces the availability of arable land [5].

In recent years, the development of sustainable industrial bioprocesses that exploit the enormous potential of microorganisms to obtain food, medicines and energy is arising increasing interest [2]. An increase of 150% in the last decade was measured in the number of new algae producing companies (Figure 1.1) [6].

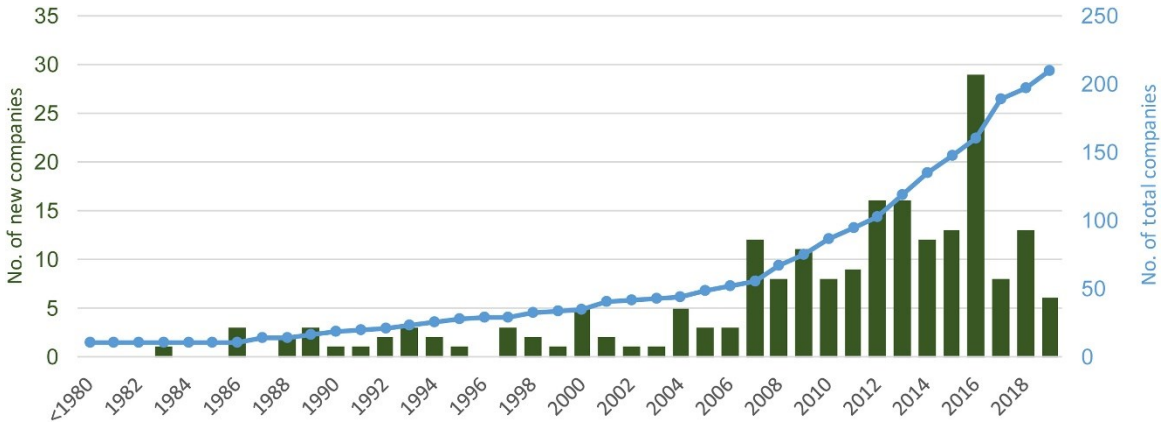

Figure 1.1. Number of algae producing companies currently operating in Europe [6]

At global level, the algae products market was valued at $2,276 million in 2020, and is projected to reach $4,287 million by 2031, growing at a Compound Annual Growth Rate (CAGR) of 4.88% from 2022 to 2031 [7]. Regarding to this, in Europe the EU Bioeconomy Strategy was adopted, aimed at implementing a sustainable and circular bioeconomy throughout the continent [8]. Some examples of the target priorities of the European Commission regard the climate neutrality by 2050, the protection of biodiversity and the

development of a sustainable food chain [9–11]. In these areas, microalgae can provide a relevant contribution. Indeed, they were already used in the past as "super food" thanks to their nutritional properties. New application, instead, regard their use as feed, or for bioremediation, to produce biofuels, biofertilizers, biostimulant and biopolymers [12–15]. The term algae actually describe a diverse group of more than 72,500 species of aquatic photosynthetic organisms. The larger, pluricellular, types of algae are called macroalgae. These can be several millimetres to 70 m in length and make up 20% of all algae species. The remaining 80% is made up of microalgae. Classes of microalgae commonly cultivated are *Chlorophyceae*, *Euglenophyceae*, *Bacillariophyceae* and *Cyanophyceae* [16]. This last class refers to cyanobacteria, a phylum of bacteria used to be called and classified in the past as "blue-green algae". Specifically, cyanobacteria are Gram-negative photosynthetic prokaryotic organisms capable of surviving in different types of habitats, both in aquatic (lakes, rivers, oceans, wastewater) and terrestrial environments. They are the oldest photosynthetic organisms on Earth and originated about 2.6-3.5 billion years ago [17]. They have had a significant impact on global ecosystems thanks to their photosynthetic activity, which supplies oxygen to aerobic life forms [18]. These microorganisms are able to survive even in extreme environmental conditions, i.e. in the presence of limiting concentrations of nutrients, in drought conditions and in polluted environments [19]. Morphologically, they can be distinguished according to the different forms: in fact, either unicellular or filamentous ones, or organisms or in the form of colonies can be found [17]. They are also often involved in symbiotic relationships with eukaryotic plants, fungi, lichens and algae [18]. Cyanobacteria are metabolically versatile, flexible and reactive: in fact, they have the ability to switch rapidly from one metabolic mode to another. All species carry out oxygenic photosynthesis, using water as an electron donor, while some can also support anoxygenic photosynthesis, in which the electron donor is dihydrogen sulphide [20]. In the dark, these microorganisms instantly switch to aerobic respiration, using reserve intracellular carbohydrates and exploiting oxygen as a terminal electron acceptor. In anaerobic conditions, instead, the fermentation of intracellular reserve compounds becomes the most used way to produce energy [21]. Cyanobacteria can also grow under mixotrophic conditions, i.e. by combining autotrophic and heterotrophic metabolism and therefore using, respectively, both inorganic carbon and organic carbon sources, such as glucose, glycerol and acetate [22]. Finally, some species have evolved the ability to fix atmospheric nitrogen, thanks to the development of different types of adaptations [17].

1.2 Biological nitrogen fixation

In view of developing a greener agriculture, biological nitrogen fixation might play a major role, since it offers the possibility to reduce the consumption of chemical fertilizers with the related energy and fossil fuel duties, and to mitigate green-house gas emissions. Industrial processes to produce nitrogen fertilizers are highly dependent on fossil energy sources. In particular, the Haber-Bosch one to obtain ammonia requires large quantities of H_2 that is mainly produced from natural gas [23]:

$$N_2 + 3H_2 \rightleftharpoons 2NH_3 \qquad \Delta H_{298} = -46.22\ kJ\ mol^{-1} \tag{1.1}$$

The main problem of this process is that it is highly energy intensive, as the total energy consumption is about 11 times greater than the theoretical minimum energy required by the ammonia production reaction. It is also responsible of 0.93% of greenhouse gases (GHGs) emissions in the world [24]. In particular, 2 to 3 tons of carbon dioxide are disperded to the environment when manufacturing 1 ton of NH_3, since 72% of the ammonia synthesis is currently realized starting from natural gas [24].

Since the ammonia reaction is an exothermic and equilibrium one, and the number of moles decreases, it is favoured by low pressure and high temperature, that implies lower reaction rate and lower catalyst activity. Hence, most of the industrial process find a compromise and work at 200-400 atm with a decreasing temperature along the catalyst bed [25]. The most employed catalyst is iron promoted by metal oxides: a typical composition is 78-82% of Fe, 1.5-3% of Al_2O_3, 0.1-0.7% of K_2O, 0.1-4% of CaO, 0.3-0.6% of MgO and 0.2-0.7% of SiO_2 [26]. Potassium oxide improves the activity of the catalyst while other oxides serve as inhibitors of the sintering. Ammonia synthesis catalysts are sensitive to poisons, in particular to oxygen-containing compounds such as CO, H_2O, O_2 and CO_2, which have a reversible effect on the catalyst at quite low temperatures. Some studies focused on improving heterogeneous catalysis by developing more efficient catalysts. Carbon-supported ruthenium catalysts were proposed in the 1990s. Their activity is higher than that of iron-based ones, thus reducing operating temperature and pressure. However, they are easily deactivated by sulphur or chlorine and significantly more expensive. More recently, ternary nitrides such as Fe_3Mo_3N and Co_3Mo_3N were proposed [27].

Other alternative routes were studied, as the electrochemical ammonia synthesis or the direct oxidation induced by plasma. In the first case, H_2 passes over the anode and is

converted to H^+. By imposing the adequate voltage, the produced protons are transported to the cathode where they react with N_2 to produce ammonia [28]. In the second case, an improvement of the Birkeland-Eyde process, according to which air is converted into valuable products using electricity only, without using solvents [27].

However, since the major demand for nitrogen compounds come from agriculture, the main alternative to the traditional Haber-Bosch process is represented by the biological processes able to perform *in vivo* fixation of atmospheric nitrogen. Biological nitrogen fixation has been studied since 1888, when the first research on the fixation of N_2 in legumes appeared [27]. The ability to fix atmospheric nitrogen was later observed for many prokaryotic organisms and symbiotic systems, in particular the interactions legumes-*Rhizobium* and Azolla-*Anabaena* are well-known [23]. On the contrary, eukaryotes do not have this ability. The core of the biological nitrogen fixation is the nitrogenase enzyme.

1.2.1 Nitrogenase enzyme complex

Nitrogenase is an enzymatic complex made up of two enzymes, dinitrogenase reductase and dinitrogenase (Figure 1.2), which cooperate, as individually they do not have any catalytic activity [29,30].

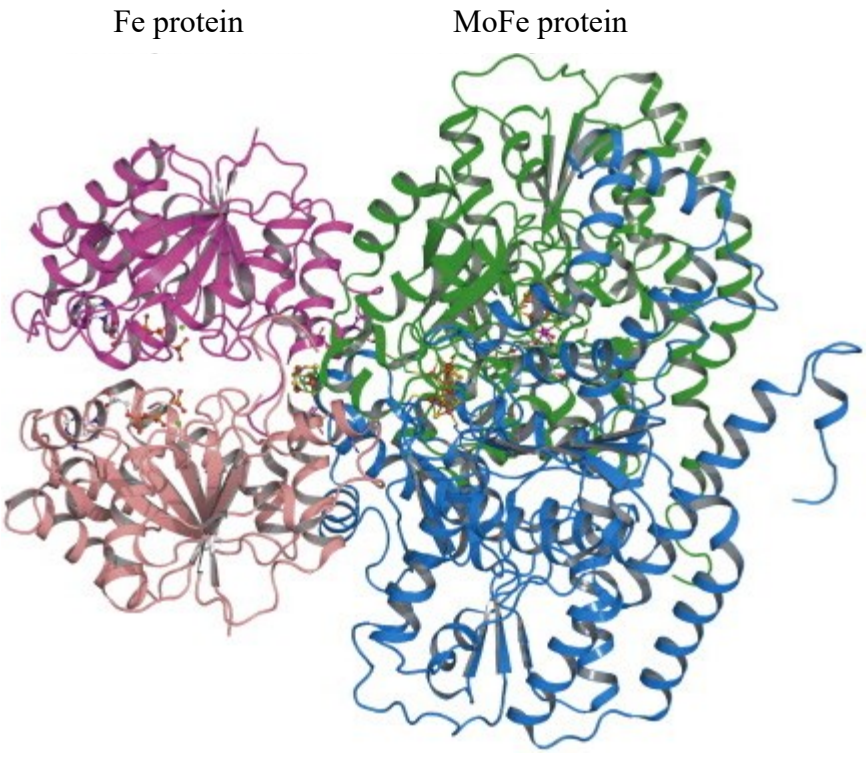

Figure 1.2. Mo-nitrogenase with cofactors, adapted from [31]

Dinitrogenase reductase is a homodimeric iron protein having an iron-sulfur cluster (4Fe-4S), which binds ATP and transfers electrons to dinitrogenase. Dinitrogenase is a molybdenum-iron heterotetrameric protein containing two types of clusters, the molybdenum-iron-sulfur (FeMo cofactor) and the iron-sulfur (8Fe-7S, also called P group) [30]. In some cyanobacteria, since molybdenum is rare, alternative nitrogenases have also been found which use vanadium or iron to allow nitrogen fixation depending on the precursor availability [32]. These last nitrogenases have a lower catalytic efficiency than MoFe-nitrogenase. For example, at 30°C the estimated specific activity of the VFe-nitrogenase is around 1.5 times lower than that of MoFe-nitrogenase [33]. Furthermore, the nitrogenase complex is non-specific and catalyses not only the reduction of N_2, but also the reduction of H+ to H_2 and the reduction of other substrates such as acetylene, hydrogen cyanide, hydrogen azide and nitrous oxide [34].
Overall, the reaction catalysed by the nitrogenase complex in diazotrophic organisms can be represented as [34]:

$$N_2 + 8e^- + 8H^+ + 16ATP \rightarrow 2NH_3 + H_2 + 16ADP + 16Pi \quad (1.2)$$

The process of nitrogen fixation is inhibited by the presence of oxygen, resulting in a repression that can be either transient or permanent [33]. Oxygen also influences the protein structure of the enzymatic complex: in particular, the dinitrogenase reductase is inactivated by O_2 in a few seconds, while the dinitrogenase within a few minutes [30]. Furthermore, reactive oxygen species (ROS) also cause problems in the nitrogen fixation pathway [33].

1.2.2 Nitrogen fixing cyanobacteria

Nitrogen fixing cyanobacteria developed different strategies to cope with the problem of the sensibility to oxygen. They can be divided in two main categories: symbiotic diazotrophs and free-living diazotrophs. As regards the symbiotic ones, a wide variety of associations was found between diazotrophs and other organisms. In most of these symbioses, the non-diazotroph organism gives carbon compounds to the diazotroph and the diazotroph gives N-containing compounds to its host. Instead, free-living diazotrophs comprise both bacteria and cyanobacteria. They are divided into two further categories as the photosynthesis can be either spatially or temporally separated from the nitrogen fixation [33]. The spatial separation is observed in heterocystous cyanobacteria, where nitrogenase

is confined to an anaerobic cell, the heterocyst, which differentiates completely 12-20 h after the nitrogen source is removed from the cultivation medium. Heterocysts differentiate irreversibly following a regular pattern. These cells are not able to replicate themselves and to fix atmospheric carbon dioxide. Thus, the sources of fixed carbon are the adjacent vegetative cells that build up organic carbon-containing molecules and transfer them to the heterocyst through microplasmodesmata. These are micro-channels which allow the product of photosynthesis to reach the heterocyst, and the product of nitrogen fixation to reach the vegetative cells. To protect the heterocysts from reactive oxygen species, the cells are equipped with a specific membrane that slows their diffusion. Example of heterocystous cyanobacteria are *Anabaena cylindrica* and *Nostoc commune*. On the other hand, non-heterocystous cyanobacteria temporally separate the photosynthesis from nitrogen fixation, so nitrogenase is found in all cells. These microorganisms usually fix dinitrogen during the night. In fact, high nitrogenase activity is registered when high respiration rate occurs, about 12 h after the peak of the photosynthetic process activity. Examples are filamentous *Symploca* and *Lyngbya majuscula*, and the unicellular *Gloeothece* sp. and *Cyanothece* sp..

1.3 Production of high value compound by microalgae

Photosynthetic microorganisms are a precious biological resource that can be exploited for sustainable development: they contain similar raw material as traditional crops, high-quality oils, proteins, pigments as well as hydrocarbons and sugars. Culturing microalgae has several advantages over conventional farming such as high yields, the ability to grow in a range of environment and the lower requirement of land compared to plants [17]. Moreover, the use of algae opens the possibility of utilizing inorganic carbon source, i.e. CO_2, thus neutralizing greenhouse gas emissions from factories or power plants [22]. Furthermore, they can be used for the bioremediation, presenting a unique opportunity to achieve simultaneously nutrient removal and production of high value algal biomass [17,35]. A biorefinery approach can be applied for the extraction of several active components from the biomass [36], which is a promising source of fatty acids, carotenoids, vitamins and others. With respect to carotenoids, β-carotene and astaxanthin play an important role in the food, feed, cosmetics and biopharma sectors. Specifically, there compounds have antioxidant activity and are therapeutic for diseases related to oxidative stress, as diabetes, cancer and obesity [22,37,38]. Phycobiliproteins are water soluble and have a wide applications in the food sector as functional food, in cosmetics as colour, in

immunology laboratories due to their characteristic absorption properties and in molecular biology as fluorescent markers [37,39]. Many polysaccharides are obtained from algae, and have been employed in pharmaceutical and nutraceutical industries, and as good metal ion chelators [39]. Other interesting products of microalgal cultivations are the polyunsaturated fatty acids (PUFAs). These molecules cannot be produced by humans, but are essential for the development of the nervous system, of visual abilities, and they reduce the occurrence of chronic diseases (e.g. diabetes, arthritis, cardiovascular disease, obesity) [40]. Microalage represent also a high protein source, which can meet the needs of malnourished people in developing countries [41]. In addition, most of the microalgal species are able to produce phytohormones, a class of molecules serving as chemical messengers to coordinate cellular processes in higher plants. Among the classical phytohormones, there are auxin, abscisic acid, cytokinin, ethylene, gibberellins, polyamines, jasmonides, salicylates, signal peptides, and brassinosteroids [42]. A diverse variety of biofuels such as biooil, biodiesel, bioethanol, bioethane, biohydrogen, syngas, and charcoal can be derived from algal biomass using multidisciplinary bioconversion technologies. However, this process is not considered applicable for the high economic costs associated to cultivation and downstream processing, that make microalgae not competitive with respect to fossil fuel and other renewable technologies [43]. In response to conditions of physiological stress and to promote long-term survival of microorganism under nutrient-starvation conditions by acting as carbon and energy reserves, various microalgal species produce polyhydroxyalkanoates (PHA), a family of naturally occurring biodegradable polyester. Depending on the composition and resulting properties, PHA have many and wide-ranging potential applications: thanks to their impermeability and gas barrier property, they are suitable for films, bottles and fibers. Their biocompatibility and biodegradability, instead, were exploited to make swabs and materials for surgery or novel drug delivery system [44,45]. Another microbial polymer produced by microalgae is cyanophycin, a non-protein, non-ribosomally generated amino acid copolymer, composed of equimolar amounts of aspartic acid and arginine. It is a zwitterion, as it possesses negatively charged α-hydroxyl groups and positively charged arginine side chains. Purified cyanophycin is a white or a mixture of white/white-brown powder, depending on whether it is soluble or insoluble [46]. As regards it properties, cyanophycin is stable up to 200°C, being pyrolyzed at a temperature greater than 700°C, whereas its Young's modulus is 560 MPa [47].

1.4 Cyanophycin Granule Polypeptide (CGP)

1.4.1 General aspect

Cyanophycin (CGP) is a polyaminoacid compound of non-ribosomal synthesis, which acts as a temporary reserve of nitrogen, because of the carbon-nitrogen ratio equal to 2:1 [48]. It consists of a backbone of poly-L-aspartic acid where an arginine residue is linked to the β-carboxylic group of each aspartic acid via isopeptide bonds (Figure 1.3). Cyanophycin was first discovered in 1887 by the Italian botanist Borzi in cyanobacteria, and initially it was described as a polymer that exclusively occurs in cyanobacteria [49]. Afterwards, it was also found in few heterotrophic bacteria, like *Acinetobacter* sp., *Bordetella bronchiseptica*, *Clostridium botulinum*, *Desulfitobacterium hafniense* [50]. The molecular masses of the polymer range from 25 to 100 kDa [51]. However, the heterotrophic bacteria *Acinetobacter* sp. ADP1 synthetizes CGP with a lower molecular weight, ranging from 21 to 28 kDa [52]. The cyanophycin produced by genetically modified microorganisms, instead, have molecular weight in the range of 25-45 kDa [53,54], thus CGP synthesis in cyanobacteria involves additional factors contributing to the polymer length [55]. Moreover, cyanobacterial CGP is exclusively composed of aspartic acid and arginine, whereas CGP of recombinant microorganisms contains also further amino acids, as lysin, citrulline and ornithine [54,56]. The different amino acidic composition affects also its typical solubility [57]: cyanophycin in water is soluble under acidic (pH<2) or alkaline (pH>9) conditions, and insoluble at physiological pH [58,59].

The first studies on cyanophycin were performed in the 70s in *Anabaena cylindrica*: its maximum production rate was measured at the end of the exponential phase, while its maximum quantity was measured during the stationary phase. Moreover, if the culture was diluted and growth resumes, the granules disappeared [60]. In further studies, it was found that the accumulation of cyanophycin is triggered by stress conditions that reduce or stop cells growth, such as entry into the stationary phase, light or temperature stress, macronutrient limitation (except for nitrogen deficiency), or the inhibition of translation by the addition of antibiotics such as chloramphenicol [55]. Indeed, in conditions of growth limitation, the protein synthesis is slowed down, causing an excess of amino acids present at the cytoplasmic level and thus prompting the biosynthesis of cyanophycin granules [55]. The intracellular synthesis of cyanophycin takes place by the enzyme cyanophycin synthetase (CphA1), which catalyses an ATP-dependent elongation reaction (Figure 1.3).

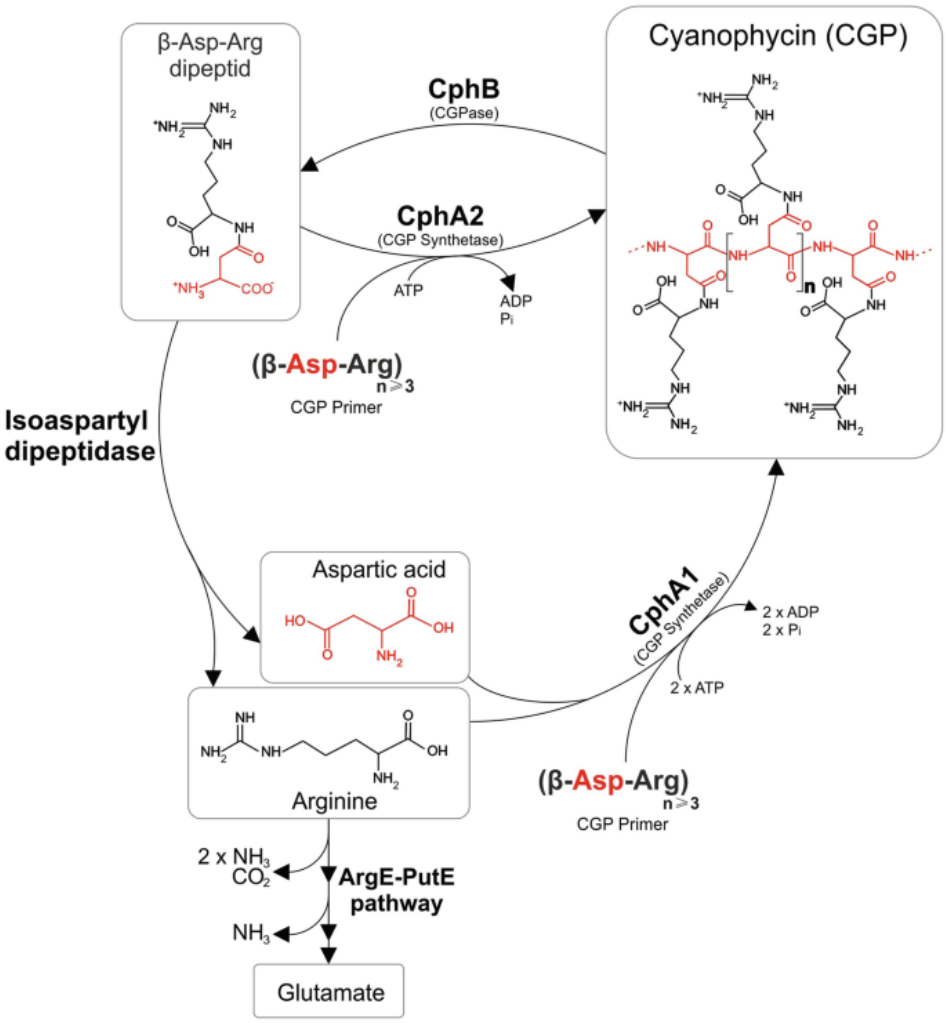

Figure 1.3. Scheme of cyanophycin metabolism [61]

Initially, the α-carboxylic group of the aspartic acid backbone is activated by phosphorylation, then the aspartic acid is bound to the C-terminal of the backbone through a peptide bond. Finally, the γ-carboxylic group of aspartic acid is activated by phosphorylation, and arginine is linked to the polymer through an isopeptide bond [62]. Cyanophycin can be degraded by the intracellular enzyme cyanophycinase (CphB1) which allows to obtain aspartate-arginine dipeptides. These dipeptides are subsequently hydrolysed by isoaspartyl dipeptidase (ISO), releasing aspartate and arginine. Further, an additional cyanophycin synthetase (CphA2) is present in many nitrogen-fixing cyanobacteria, which utilizes dipeptides for cyanophycin synthesis [55]. This enzyme contributes to the process of nitrogen transfer that takes place inside the filaments, being the aspartate-arginine dipeptide the main transport unit of N between heterocysts and vegetative cells [63,64]. However, some unicellular diazotrophic cyanobacteria also possess this enzyme, and therefore its activity must be considered not only in relation to

the transfer of nitrogen between cells, but also in the context of nitrogen fixation and mobilization [64].

1.4.2 Physiological function of cyanophycin in the context of nitrogen fixation

Cyanophycin is produced also by diazotrophic cyanobacteria of *Nostocales* sp.. Sherman et al. [65] cultured *Anabaena* sp. PCC 7120 under nitrogen fixing conditions and observed that, in the heterocysts, cyanophycin was accumulated following the peak of nitrogenase activity, forming a dense polar nodule. This nodule was located in the connection site between the heterocysts and the adjacent vegetative cells [55]. The activity of cyanophycin synthetase and cyanophycinase was higher in heterocysts than in vegetative cells by 30 and 70 times respectively, indicating that cyanophycin can be rapidly polymerized and depolymerized in heterocysts. Thus, in diazotrophic cyanobacteria, cyanophycin exists as a dynamic reservoir instead of a passive nitrogen store [66], and its location facilitates its transportation (Figure 1.4) [61,65]. Furthermore, isoaspartyl dipeptidase is preferentially expressed in vegetative cells, so the dipeptide released by cyanophycinase in heterocysts is transferred to vegetative cells to allow the activity of isoaspartyl dipeptidase and, therefore, the obtainment of the two amino acids arginine and aspartate [55].

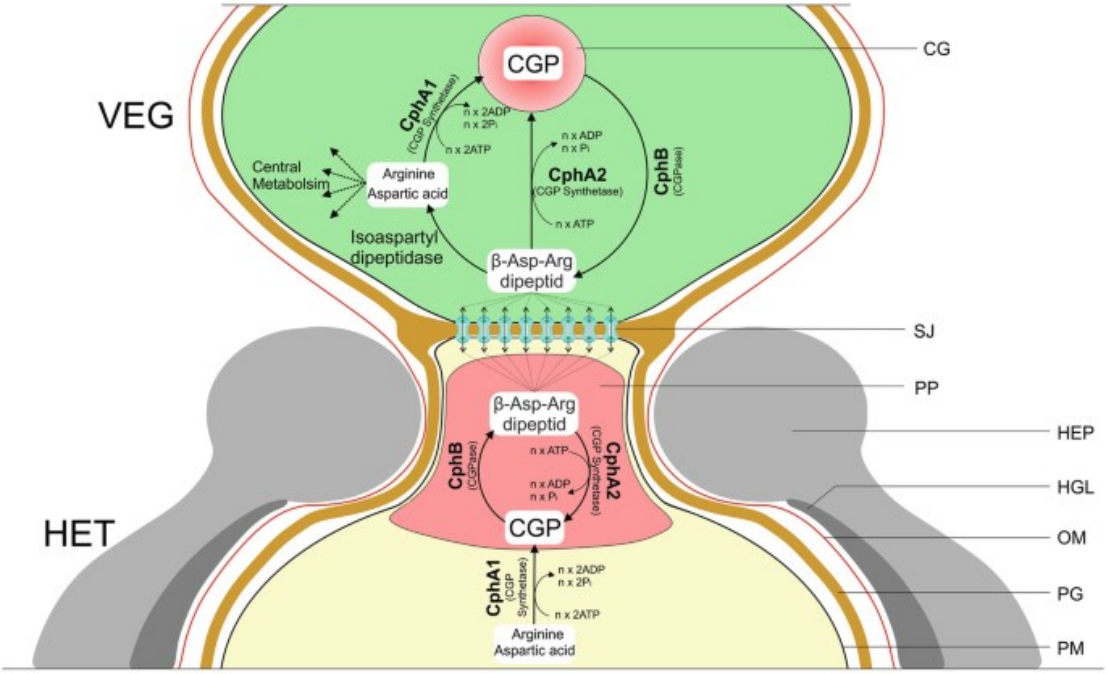

Figure 1.4. Scheme of cyanophycin-related nitrogen transport between a heterocyst (HET) and a vegetative cell (VEG) [61]

1.4.3 Cyanophycin application

Cyanophycin has recently attracted the attention of the scientific community as a biodegradable replacement for petrochemical-based industrial products, even though ther is no industrial application right now. Cyanophycin can be used as a precursor to produce nitrogen-containing chemicals, such as acrylonitrile, butanediamine, and urea [62]. Moreover, it can be hydrolysed to its constituent, amino acids, arginine and aspartic acid, thanks to β-hydrolytic cleavage [62].

Polyaspartic acid (PASP) is an anionic polypeptide that is a highly versatile, biocompatible, and biodegradable polymer fulfilling key requirements for use in a wide variety of biomedical applications. Thanks to its protein-like backbone structure it is an ideal substitute for nondegradable anionic polyelectrolytes. Moreover it allowed the development of a variety of interesting materials for biomedical applications, including tissue engineering and drug/gene delivery devices due to its biocompatibility and biodegradability [67]. Chemical structure of PASP can be customized by introducing different functional groups for diverse applications. It has also strong affinity with calcium ions, resulting in the formation of PASP-Ca complexes, which have been exploited for bone targeting and biomineralization [68–70]. To reduce its hydrophilicity, PASP was modified with long alkyl chains. In this way, the dissolution and the loading capacity of hydrophobic drugs could be improved [71]. Moreover, alkyl chains lead also to surface active properties and a new generation of degradable surfactants [72]. Mucoadhesion in drug delivery systems is a viable strategy to improve drug bioavailability [73]. By the incorporation of a high amount of thiols, PASP formulations capable of in situ gelling were developed with strong mucoadhesion in porcine conjunctiva [74]. Finally, to deliver bioactive agents and hydrogel preparation, polymers and oligomers have been grafted onto PASP [75–77].
PASP is usually synthesized by polymerization of aspartic acid or maleic anhydride (Figure 1.5). In both cases, elevated temperature, greater than 160°C and bioproduct removal are required to achieve high molecular weights and reaction yields. Indeed, if thermal exchange conditions were not properly controlled, resulted in low yields, typically in the range of 50% to 68% [78]. Whatever is the starting molecules, the intermediate product obtained is the poly(anhydroaspartic acid) (PSI), i.e. poly(succinimide), which is then hydrolysed to ring-open the succinimide to form PASP. Instead, in the presence of molecules bearing primary amines, an amidation reaction could occur, without the need of catalyst. This reaction yields poly(aspartamide) derivatives [79].

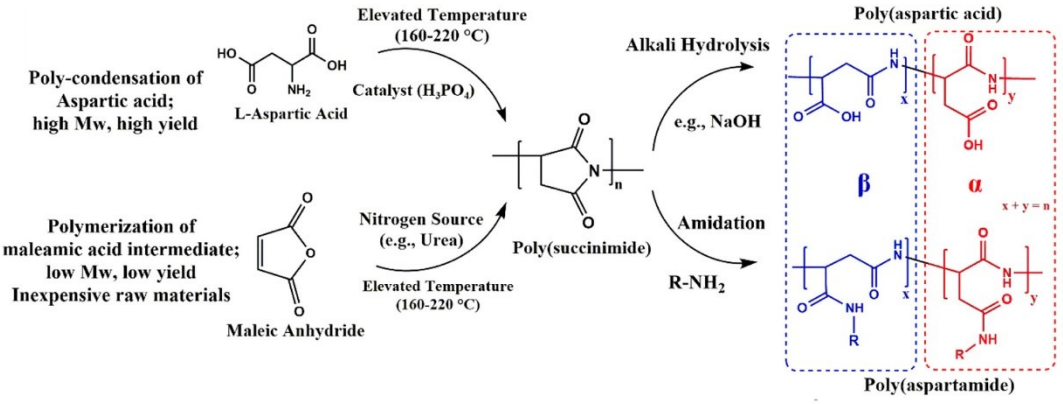

Figure 1.5. Schematic representation of the synthesis of the poly(succinimide) (PSI) intermediate to produce polyaspartic acid (PASP), adapted from [79]

The most common synthesis method of PASP is poly condensation of aspartic acid, which is carried out either in bulk or solution, in the presence or absence of a catalyst (phosphoric acid). The racemization reported during thermal condensation and the hydrolytic opening of the ring may proceed at both carbonyls. Thus, the resulting polymer has both the α and β peptide bonds in the main chain. The degree of hydrolysis can be controlled by pH; indeed, the reaction can be done catalysed by alkali or acid. The lower the pH, the higher is the proportion of the α bond in the product [80]. Depending on the reaction conditions, PASP has different yields and molecular weights. At 260°C without any catalyst, the yields was 97% with a ratio of α/β of 0.3/0.7 [78]. However, Thombre et al. reported that in the presence of phosphoric acid the polymer obtained is linear and totally biodegradable, whereas PASP obtained with thermal polymerization without a catalyst resulted to be a branched one and did not biodegrade completely [80]. The reaction can be carried out avoiding the use of solvents. Although the bulk reaction seems less complex in terms of purification and more effective in terms of yields, it was shown that as the reaction temperature increases, the optical purity of PASP decreases [81]. Furthermore, there are also problems of viscosity and mixing [82,83]. On the other hand, the solvent facilitates heat transfer, but lowers the rate of reaction because of the decreased concentration of reactive functional groups [84]. In addition, the solvent must be recovered at the end of the reaction for example through polymer precipitation and solvent evaporation [85]. Instead, to produce PASP with maleic anhydride or maleic acid, it is also necessary a source of nitrogen, such as urea or ammonia. Then, the maleamic acid obtained reacts at high temperature, in the presence of a catalyst, and produces PSI. The synthetized PASP has a relatively low degree of polymerization, but this method is still utilized owing to the inexpensiveness of the row materials [86,87].

L-arginine has numerous physiological roles in many cardiovascular, gastrointestinal and immune disorders [88]. It is essential for human infants and fish, whereas for mammals it is considered semi essential as it is synthesized endogenously [88]. For example, it is known that it stimulates secretion of growth hormones [89], prolactin [90], insulin [91] and glucagon [92], and that it promotes muscle mass [93]. It is a strongly basic amino acid with a molecular mass of 174.2 g mol^{-1}, and is found in most proteins. It was first isolated from a lupine seedling extract in 1886. Then, it was identified as a component of casein in 1895, and later it was found to be widely distributed in food and feed [94]. Amino acids as arginine are produced through protein hydrolysis, chemical synthesis, and microbiological synthesis. Specifically, most L-arginine has been obtained by the direct-fermentation method from natural carbon sources. Indeed, starches, after being hydrolysed with enzymes, form a liquid solution of glucose (>95% dextrose) [94]. Glucose from tapioca or corn, for example, is one of the best sources to produce L-arginine, but also sugar and sugar syrup are used. Because L-arginine contains 4 atoms of nitrogen, also a source of nitrogen must be supplied, like ammonia or ammonium sulphate. Moreover, the production of L-arginine is strongly inhibited by the lack of oxygen, one of the raw material needed [95,96]. After production, L-arginine must be isolated and purified, through a series of step. After a separation of the microorganism, cation and anion resins are used to minimize the impurities in the L-arginine crystal. Active carbon is then used for decolouration. Crystals are dissolved in pure water and ultrafiltered, and are concentrated and dried to minimize the moisture and achieve a purity greater than 98.5% [94].

1.4.4 Cyanophycin production: state of the art, limits and challenges

Among cyanobacteria able to synthesize cyanophycin, there are unicellular, filamentous, diazotrophic and non-diazotrophic organisms [55,62]. The intracellular content of this polymer depends on the growth phase of the microorganisms and the culture conditions [97]. Cyanophycin has been reported in different cyanobacterial strain, as *Scytonema specie*s, *Nostoc ellipsosporum* NE1, *Synechocystis* sp. PCC 6308, *Synechocystis* sp. PCC 6803, *Synechococcus* sp. MA19, *Synechococcus* sp. G2.1, *Anabaena* sp. PCC 7120, *Anabaena variabilis* ATCC 29413, *Thermosynechococcus elongatus* BP-1, *Agmenellum quadruplicatum* and *Toxifilum mysidocida* [56,59,66,98,99]. In non-diazotrophic cyanobacteria, such as *Synechocystis* sp. PCC 6803 and *Synechococcus* sp. MA19, the amount of cyanophycin obtainable is less than 1% of the dry weight of the biomass during

the exponential growth phase. During the stationary phases, instead, cyanophycin reached 18% of dry cell weight [55]. In unicellular diazotrophic cyanobacteria, like *Cyanothece* sp. ATCC 51142, nitrogen fixed under dark conditions is stored in cyanophycin granules, which are subsequently degraded during light phases to mobilize the fixed nitrogen [100]. One of the first studies concerning the cyanophycin production was performed in 1973, when Simon et al. cultivated the filamentous diazotrophic cyanobacteria *Anabaena cylindrica* in batch mode [60]. The cyanophycin quota was measured in different stages of growth: the synthesis of cyanophycin granules began at the end of the exponential phase and continued throughout the stationary phase, reaching a maximum quota of 7.8% of the dry weight. Then, by diluting the stationary phase culture, the biomass growth resumed and, contextually, the cyanophycin granules were rapidly degraded, dropping from 7.8% to 1.3% of dry weight in one day. Moreover, by adding chloramphenicol to final concentrations of 1.25 μg mL^{-1} in the exponential growth, the cyanophycin quota increased from 0.54% to 7.2% of cell dry weight in two days [101]. Other studies by Obukowicz and Kennedy and by Sherman et al. confirmed that the addition of chloramphenicol to cell cultures increases the accumulation of cyanophycin, especially at the level of the heterocyst poles [65,102]. Mackerras et al., instead, demonstrated that by adding ammonia to cultures of *Anabaena cylindrica* grown both in urea and under nitrogen fixing conditions, cyanophycin accumulated transiently and then was degraded [103,104].

As regards recombinant strains, it was shown that *E. coli* produced up to 100 mg L^{-1} of insoluble cyanophycin, mainly composed of aspartic acid and arginine, in addition to minor amount of lysin [56]. Frey et al. produced 24% (w/w) of insoluble cyanophycin by *E. coli* DH1 [53]. Moreover, if engineered *E. coli* were cultured in protamylasse medium, the main waste of industrial starch production, up to 28% (w/w) of cyanophycin was accumulated [52]. Recombinant *Corynebacterium glutamicum* resulted in the production of 14% by weight of cyanophycin [105]. Another interesting idea regards the combined production of ethanol and cyanophycin, by cultivating *Saccharomyces cerevisiae* [106]. Also transgenic plants as *Nicotiana tabacum* and *Solanum tuberosum* were used to produce cyanophycin, even if lower production yields were obtained than with bacterial strains [107].

Similarly, also cyanobacteria have been genetically modified. A deletion of the *alr2310* gene was made in *Anabaena* PCC 7120 [108]. After 8 days of culture in the presence of nitrate or ammonium, approximately 8.3-times and 4.5-times higher amounts of cyanophycin were present than in *wild type* cells. Agmatine, as it is no longer being hydrolysed into urea and putrescine, was incorporated into cyanophycin at significant

levels [63]. A strain of *Anabaena* PCC 7120 was also engineered by knocking out the gene cluster coding for AMT transporters, which allow the transport of ammonia across biological membranes and, moreover, interact with the PII protein to prevent its intracellular accumulation [109,110]. In the presence of a nitrogen source in the culture medium, the *wild type* and mutant strains accumulated approximately the same amount of cyanophycin. When nitrogen was completely depleted, the cyanophycin content decreased. However, in the *wild type* cyanophycin accumulated again two days after the nitrogen depletion, instead in the mutant strain its constant depletion occurred. This suggested that the nitrogen fixed in the *wild type* exceeded the metabolic needs and, thus, a fraction of the assimilated nitrogen was stored as cyanophycin [109]. With respect to the unicellular cyanobacteria, the cyanophycin production was increased up to 0.40 g per g of biomass by cultivating the overproducing mutant species BW86. Indeed, single point mutation in the PII signaling protein unlock the arginine pathway causing over accumulation of cyanophycin [111].

By the way, all these studies have been carried out in batch systems, thus the actual capability of large-scale production is not fully understood, as well as, at present, there is no mathematical model describing the effect of operating variable on the cyanophycin production.

Acronyms

GHGs	Greenhouse gases
CAGR	Compound Annual Growth Rate
PUFAs	Polyunsaturated fatty acids
PHA	Polyhydroxyalkanoates
CGP	Cyanophycin Granules Polypeptide
ISO	Isoaspartyl dipeptidase
PASP	Polyaspartic acid
PSI	Poly(anhydroaspartic acid), Poly(succinimide)

Literature cited

[1] D. Tilman, R. Socolow, J.A. Foley, J. Hill, E. Larson, L. Lynd, S. Pacala, J. Reilly, T. Searchinger, C. Somerville, R. Williams, Energy. Beneficial biofuels--the food, energy, and environment trilemma., Science. 325 (2009) 270–271. https://doi.org/10.1126/science.1177970.

[2] N.K. Sharma, A.K. Rai, L.J. Stal, Cyanobacteria : an economic perspective , Wiley Blackwell, Chichester, England, 2014.

[3] S.I. Zandalinas, F.B. Fritschi, R. Mittler, Global Warming, Climate Change, and Environmental Pollution: Recipe for a Multifactorial Stress Combination Disaster, Trends Plant Sci. 26 (2021) 588–599. https://doi.org/10.1016/j.tplants.2021.02.011.

[4] Z. Chi, J. V. O'Fallon, S. Chen, Bicarbonate produced from carbon capture for algae culture, Trends Biotechnol. 29 (2011) 537–541. https://doi.org/10.1016/j.tibtech.2011.06.006.

[5] D. De Wrachien, M. Goli, Global Warming Effects on Irrigation and Drainage Development, J. Agric. Aquac. 01 (2019) 1–5. https://doi.org/10.4172/2168-9768.1000e126.

[6] R. Araújo, F. Vázquez Calderón, J. Sánchez López, I.C. Azevedo, A. Bruhn, S. Fluch, M. Garcia Tasende, F. Ghaderiardakani, T. Ilmjärv, M. Laurans, M. Mac Monagail, S. Mangini, C. Peteiro, C. Rebours, T. Stefansson, J. Ullmann, Current Status of the Algae Production Industry in Europe: An Emerging Sector of the Blue Bioeconomy, Front. Mar. Sci. 7 (2021) 1–24. https://doi.org/10.3389/fmars.2020.626389.

[7] Allied Market Research, Algae Product Market, Glob. Oppor. Anal. Ind. Forecast. (2022). https://www.alliedmarketresearch.com/algae-products-market.

[8] EC, A sustainable Bioeconomy for Europe: Strengthening the connection between economy, society and the environment, Commun. FROM Comm. TO Eur. Parliam. Counc. Eur. Econ. Soc. Comm. Comm. Reg. (2018). https://eur-lex.europa.eu/legal-content/EN/TXT/?uri=CELEX%3A52018DC0673.

[9] EC, A new Circular Economy Action Plan For a cleaner and more competitive Europe, Commun. FROM Comm. TO Eur. Parliam. Counc. Eur. Econ. Soc. Comm. Comm. Reg. (2020). https://eur-lex.europa.eu/legal-content/EN/TXT/?qid=1583933814386&uri=COM:2020:98:FIN.

[10] EC, EU Biodiversity Strategy for 2030 Bringing nature back into our lives, Commun. FROM Comm. TO Eur. Parliam. Counc. Eur. Econ. Soc. Comm. Comm. Reg. (2020). https://eur-lex.europa.eu/legal-content/EN/TXT/?uri=celex%3A52020DC0380.

[11] EC, A Farm to Fork Strategy for a fair, healthy and environmentally-friendly food system, Commun. FROM Comm. TO Eur. Parliam. Counc. Eur. Econ. Soc. Comm. Comm. Reg. (2020). https://eur-lex.europa.eu/legal-content/EN/TXT/?uri=CELEX:52020DC0381.

[12] F. Jung, A. Krüger-Genge, P. Waldeck, J.-H. Küpper, Spirulina platensis, a super food?, J. Cell. Biotechnol. 5 (2019) 43–54. https://doi.org/10.3233/JCB-189012.

[13] R.D. Kinley, G. Martinez-Fernandez, M.K. Matthews, R. de Nys, M. Magnusson, N.W. Tomkins, Mitigating the carbon footprint and improving productivity of ruminant livestock agriculture using a red seaweed, J. Clean. Prod. 259 (2020) 120836. https://doi.org/https://doi.org/10.1016/j.jclepro.2020.120836.

[14] A. Chatterjee, S. Singh, C. Agrawal, S. Yadav, R. Rai, L.C. Rai, Role of Algae as a Biofertilizer, in: R.P. Rastogi, D. Madamwar, A. Pandey (Eds.), Algal Green Chem. Recent Prog. Biotechnol., Elsevier, Amsterdam, 2017: pp. 189–200. https://doi.org/https://doi.org/10.1016/B978-0-444-63784-0.00010-2.

[15] X. Zhang, M. Thomsen, Biomolecular Composition and Revenue Explained by Interactions between Extrinsic Factors and Endogenous Rhythms of Saccharina latissima, Mar. Drugs. 17 (2019). https://doi.org/10.3390/md17020107.

[16] J.M. Valigore, Microbial (microalgal-bacterial) biomass grown on municipal wastewater for sustainable biofuel production, University of Canterbury, 2011. https://doi.org/http://dx.doi.org/10.26021/3456.

[17] N.-S. Lau, M. Matsui, A.A.-A. Abdullah, Cyanobacteria: Photoautotrophic Microbial Factories for the Sustainable Synthesis of Industrial Products, Biomed Res. Int. 2015 (2015) 1–9. https://doi.org/10.1155/2015/754934.

[18] P. Dvořák, D.A. Casamatta, P. Hašler, E. Jahodářová, A.R. Norwich, A. Poulíčková, Diversity of the Cyanobacteria, in: P.C. Hallenbeck (Ed.), Mod. Top. Phototrophic Prokaryotes Environ. Appl. Asp., Springer International Publishing, Cham, 2017: pp. 3–46. https://doi.org/10.1007/978-3-319-46261-5_1.

[19] A.A. Issa, M.H. Abd-Alla, T. Ohyama, Nitrogen fixing cyanobacteria: future prospect, Adv. Biol. Ecol. Nitrogen Fixat. 2 (2014) 24–48.

[20] L.J. Stal, Nitrogen Fixation in Cyanobacteria, ELS. (2015) 1–9. https://doi.org/https://doi.org/10.1002/9780470015902.a0021159.pub2.

[21] L.J. Stal, Cyanobacteria, in: J. Seckbach (Ed.), Algae Cyanobacteria Extrem. Environ., Springer Netherlands, Dordrecht, 2007: pp. 659–680. https://doi.org/10.1007/978-1-4020-6112-7_36.

[22] M.I. Khan, J.H. Shin, J.D. Kim, The promising future of microalgae: Current status, challenges, and optimization of a sustainable and renewable industry for biofuels, feed, and other products, Microb. Cell Fact. 17 (2018) 1–21. https://doi.org/10.1186/s12934-018-0879-x.

[23] B.B. Bohlool, J.K. Ladha, D.P. Garrity, T. George, Biological nitrogen fixation for sustainable agriculture: A perspective, Plant Soil. 141 (1992) 1–11. https://doi.org/10.1007/BF00011307.

[24] Y. Bicer, I. Dincer, G. Vezina, F. Raso, Impact Assessment and Environmental Evaluation of Various Ammonia Production Processes, Environ. Manage. 59 (2017) 842–855. https://doi.org/10.1007/s00267-017-0831-6.

[25] E. Mariani, L'industria dell'azoto, in: A. Girelli, L. Matteoli, F. Parisi (Eds.), Trattato Di Chim. Ind. e Appl. Vol. 1, Zanichelli, Zanichelli, 1969: pp. 521–590.

[26] M. Appl, Ammonia, Ullmann's Encycl. Ind. Chem. (2006). https://doi.org/https://doi.org/10.1002/14356007.a02_143.pub2.

[27] N. Cherkasov, A.O. Ibhadon, P. Fitzpatrick, A review of the existing and alternative methods for greener nitrogen fixation, Chem. Eng. Process. Process Intensif. 90 (2015) 24–33. https://doi.org/10.1016/j.cep.2015.02.004.

[28] V. Kyriakou, I. Garagounis, E. Vasileiou, A. Vourros, M. Stoukides, Progress in the Electrochemical Synthesis of Ammonia, Catal. Today. 286 (2017) 2–13. https://doi.org/https://doi.org/10.1016/j.cattod.2016.06.014.

[29] R.Y. Igarashi, L.C. Seefeldt, Nitrogen Fixation: The Mechanism of the Mo-Dependent Nitrogenase, Crit. Rev. Biochem. Mol. Biol. 38 (2003) 351–384. https://doi.org/10.1080/10409230391036766.

[30] N. Rascio, N. La Rocca, Biological Nitrogen Fixation ☆, Elsevier Inc., 2013. https://doi.org/10.1016/B978-0-12-409548-9.00685-0.

[31] L.C. Seefeldt, Z.-Y. Yang, S. Duval, D.R. Dean, Nitrogenase reduction of carbon-containing compounds, Biochim. Biophys. Acta - Bioenerg. 1827 (2013) 1102–1111. https://doi.org/https://doi.org/10.1016/j.bbabio.2013.04.003.

[32] W.E. Newton, Physiology, Biochemistry, and Molecular Biology of Nitrogen Fixation, in: H. Bothe, S.J. Ferguson, W.E.B.T.-B. of the N.C. Newton (Eds.), Biol. Nitrogen Cycle, Elsevier, Amsterdam, 2007: pp. 109–129. https://doi.org/https://doi.org/10.1016/B978-044452857-5.50009-6.

[33] I. Berman-Frank, P. Lundgren, P. Falkowski, Nitrogen fixation and photosynthetic oxygen evolution in cyanobacteria, 154 (2003) 157–164. https://doi.org/10.1016/S0923-2508(03)00029-9.

[34] J.B. Howard, D.C. Rees, Structural Basis of Biological Nitrogen Fixation, Chem. Rev. 96 (1996) 2965–2982. https://doi.org/10.1021/cr9500545.

[35] I. Rawat, S. Gupta, A. Shriwastav, P. Singh, S. Kumari, F. Bux, Microalgae Applications in Wastewater Treatment, in: 2016: pp. 249–268. https://doi.org/10.1007/978-3-319-12334-9_13.

[36] A.K. Koyande, K.W. Chew, K. Rambabu, Y. Tao, D.T. Chu, P.L. Show, Microalgae: A potential alternative to health supplementation for humans, Food Sci. Hum. Wellness. 8 (2019) 16–24. https://doi.org/10.1016/j.fshw.2019.03.001.

[37] M.A. Borowitzka, High-value products from microalgae-their development and commercialisation, J. Appl. Phycol. 25 (2013) 743–756. https://doi.org/10.1007/s10811-013-9983-9.

[38] A.K. Koyande, K.W. Chew, K. Rambabu, Y. Tao, D.-T. Chu, P.-L. Show, Microalgae: A potential alternative to health supplementation for humans, Food Sci. Hum. Wellness. 8 (2019) 16–24. https://doi.org/10.1016/j.fshw.2019.03.001.

[39] M. Bilal, T. Rasheed, I. Ahmed, H.M.N. Iqbal, High-value compounds from microalgae with industrial exploitability - A review, Front. Biosci. - Sch. 9 (2017) 319–342. https://doi.org/10.2741/s490.

[40] W. Levasseur, P. Perré, V. Pozzobon, A review of high value-added molecules production by microalgae in light of the classification, Biotechnol. Adv. 41 (2020) 107545. https://doi.org/10.1016/j.biotechadv.2020.107545.

[41] E. Christaki, P. Florou-Paneri, E. Bonos, Microalgae: a novel ingredient in nutrition,

Int. J. Food Sci. Nutr. 62 (2011) 794–799. https://doi.org/10.3109/09637486.2011.582460.

[42] A. Bajguz, Brassinosteroids in Microalgae: Application for Growth Improvement and Protection Against Abiotic Stresses BT - Brassinosteroids: Plant Growth and Development, in: S. Hayat, M. Yusuf, R. Bhardwaj, A. Bajguz (Eds.), Springer Singapore, Singapore, 2019: pp. 45–58. https://doi.org/10.1007/978-981-13-6058-9_2.

[43] M. Musa, G.A. Ayoko, A. Ward, C. Rösch, R.J. Brown, T.J. Rainey, Factors Affecting Microalgae Production for Biofuels and the Potentials of Chemometric Methods in Assessing and Optimizing Productivity, Cells. 8 (2019). https://doi.org/10.3390/cells8080851.

[44] A. Shrivastav, H.-Y. Kim, Y.-R. Kim, Advances in the Applications of Polyhydroxyalkanoate Nanoparticles for Novel Drug Delivery System, Biomed Res. Int. 2013 (2013) 581684. https://doi.org/10.1155/2013/581684.

[45] S. Philip, T. Keshavarz, I. Roy, Polyhydroxyalkanoates: biodegradable polymers with a range of applications, J. Chem. Technol. Biotechnol. 82 (2007) 233–247. https://doi.org/https://doi.org/10.1002/jctb.1667.

[46] N. Kwiatos, A. Steinbüchel, Cyanophycin Modifications—Widening the Application Potential, Front. Bioeng. Biotechnol. 9 (2021). https://doi.org/10.3389/fbioe.2021.763804.

[47] N.A. Khlystov, W.Y. Chan, A.M. Kunjapur, W. Shi, K.L.J. Prather, B.D. Olsen, Material properties of the cyanobacterial reserve polymer multi-L-arginyl-poly-L-aspartate (cyanophycin), Polymer (Guildf). 109 (2017) 238–245. https://doi.org/10.1016/j.polymer.2016.11.058.

[48] R.D. Simon, P. Weathers, Preparation and Derivatization of Cyanophycin Granule Polypeptide The filamentous cyanobacterium Anabaena cylindrica Lemm . was grown as, 420 (1976) 165–176.

[49] A. Borzi, Le comunicazioni intracellulari delle Nostochinee., Malpighia I, 1887.

[50] J. Aravind, T. Saranya, G. Sudha, P. Kanmani, Integrated Waste Management in India, (2016) 49–58. https://doi.org/10.1007/978-3-319-27228-3.

[51] M.M. Allen, A.J. Smith, Nitrogen chlorosis in blue-green algae, Arch. Mikrobiol. 69 (1969) 114–120. https://doi.org/10.1007/BF00409755.

[52] Y. Elbahloul, M. Krehenbrink, R. Reichelt, A. Steinbüchel, Physiological conditions conducive to high cyanophycin content in biomass of Acinetobacter calcoaceticus Strain ADP1, Appl. Environ. Microbiol. 71 (2005) 858–866. https://doi.org/10.1128/AEM.71.2.858-866.2005.

[53] K.M. Frey, F.B. Oppermann-Sanio, H. Schmidt, A. Steinbüchel, Technical-scale production of cyanophycin with recombinant strains of Escherichia coli, Appl. Environ. Microbiol. 68 (2002) 3377–3384. https://doi.org/10.1128/AEM.68.7.3377-3384.2002.

[54] A. Steinle, K. Bergander, A. Steinbu, Metabolic Engineering of Saccharomyces cerevisiae for Production of Novel Cyanophycins with an Extended Range of Constituent Amino Acids □, 75 (2009) 3437–3446.

https://doi.org/10.1128/AEM.00383-09.

[55] B. Watzer, K. Forchhammer, Cyanophycin: A Nitrogen-Rich Reserve Polymer, in: K.F.E.-A. Tiwari (Ed.), IntechOpen, Rijeka, 2018: p. Ch. 5. https://doi.org/10.5772/intechopen.77049.

[56] K. Ziegler, A. Diener, C. Herpin, R. Richter, R. Deutzmann, W. Lockau, Molecular characterization of cyanophycin synthetase, the enzyme catalyzing the biosynthesis of the cyanobacterial reserve material multi-L- arginyl-poly-L-aspartate (cyanophycin), Eur. J. Biochem. 254 (1998) 154–159. https://doi.org/10.1046/j.1432-1327.1998.2540154.x.

[57] L. Wiefel, A. Steinbüchel, Solubility behavior of cyanophycin depending on lysine content, Appl. Environ. Microbiol. 80 (2014) 1091–1096. https://doi.org/10.1128/AEM.03159-13.

[58] N.J. Lang, R.D. Simon, C.P. Wolk, Correspondence of cyanophycin granules with structured granules in Anabaena cylindrica, Arch. Mikrobiol. 83 (1972) 313–320. https://doi.org/10.1007/BF00425243.

[59] M.M. Allen, P.J. Weathers, Structure and composition of cyanophycin granules in the cyanobacterium Aphanocapsa 6308, J. Bacteriol. 141 (1980) 959–962. https://doi.org/10.1128/jb.141.2.959-962.1980.

[60] R.D. Simon, Measurement of the cyanophycin granule polypeptide contained in the blue green alga Anabaena cylindrica, J. Bacteriol. 114 (1973) 1213–1216. https://doi.org/10.1128/jb.114.3.1213-1216.1973.

[61] B. Watzer, F. Klemke, K. Forchhammer, The Cyanophycin Granule Peptide from Cyanobacteria, in: D. Jendrossek (Ed.), Bact. Organelles Organelle-like Inclusions, Springer International Publishing, Cham, 2020: pp. 149–175. https://doi.org/10.1007/978-3-030-60173-7_7.

[62] J. Du, L. Li, S. Zhou, Microbial production of cyanophycin: From enzymes to biopolymers, Biotechnol. Adv. 37 (2019). https://doi.org/10.1016/j.biotechadv.2019.05.006.

[63] M. Burnat, A. Herrero, E. Flores, Compartmentalized cyanophycin metabolism in the diazotrophic filaments of a heterocyst- forming cyanobacterium, (2014). https://doi.org/10.1073/pnas.1318564111.

[64] F. Klemke, D.J. Nu, K. Ziegler, G. Beyer, U. Kahmann, W. Lockau, T. Volkmer, CphA2 is a novel type of cyanophycin synthetase in N 2 -fixing cyanobacteria, 2 (2016) 526–536. https://doi.org/10.1099/mic.0.000241.

[65] D.M. Sherman, D. Tucker, L.A. Sherman, Heterocyst development and localization of cyanophycin in N2-fixing cultures of Anabaena sp. PCC 7120 (Cyanobacteria), J. Phycol. 36 (2000) 932–941.

[66] M. Gupta, N.G. Carr, Enzyme Activities Related to Cyanophycin Metabolism in Heterocysts and Vegetative Cells of Anabaena spp, Microbiology. 125 (1981) 17–23. https://doi.org/https://doi.org/10.1099/00221287-125-1-17.

[67] P.S. Yavvari, A.K. Awasthi, A. Sharma, A. Bajaj, A. Srivastava, Emerging Biomedical Applications of Polyaspartic Acid-Derived acid-derived biodegradable polyelectrolytes, (2019). https://doi.org/10.1039/C8TB02962H.

[68] Y. Fu, T. Fu, H. Wang, C. Lin, G. Lee, S. Wu, C. Wang, Acta Biomaterialia Aspartic acid-based modified PLGA – PEG nanoparticles for bone targeting : In vitro and in vivo evaluation, Acta Biomater. 10 (2014) 4583–4596. https://doi.org/10.1016/j.actbio.2014.07.015.

[69] S.G. Rotman, T.F. Moriarty, B. Nottelet, D.W. Grijpma, D. Eglin, O. Guillaume, Poly (Aspartic Acid) Functionalized Poly (-Caprolactone) Microspheres with Enhanced Hydroxyapatite A ffi nity as Bone Targeting Antibiotic Carriers, (n.d.).

[70] M. Andersson, Transformation of amorphous calcium phosphate to bone-like apatite, Nat. Commun. (2018). https://doi.org/10.1038/s41467-018-06570-x.

[71] P. Das, N.R. Jana, Dopamine functionalized polymeric nanoparticle for targeted drug delivery, RSC Adv. 5 (2015) 33586–33594. https://doi.org/10.1039/C5RA03302K.

[72] H.S. Kang, S.R. Yang, J.-D. Kim, S.-H. Han, I.-S. Chang, Effects of Grafted Alkyl Groups on Aggregation Behavior of Amphiphilic Poly(aspartic acid), Langmuir. 17 (2001) 7501–7506. https://doi.org/10.1021/la0107953.

[73] S. Duggan, W. Cummins, O. O' Donovan, H. Hughes, E. Owens, Thiolated polymers as mucoadhesive drug delivery systems, Eur. J. Pharm. Sci. 100 (2017) 64–78. https://doi.org/https://doi.org/10.1016/j.ejps.2017.01.008.

[74] B. Szilágyi, B. Gyarmati, G. Horvat, Á. Laki, M. Budai-Szűcs, E. Csányi, G. Sandri, M.C. Bonferoni, A. Szilagyi, The effect of thiol content on the gelation and mucoadhesion of thiolated poly(aspartic acid), Polym. Int. 66 (2017). https://doi.org/10.1002/pi.5411.

[75] X. Dong, L. Lin, J. Chen, H. Tian, C. Xiao, Z. Guo, Y. Li, Y. Wei, X. Chen, Multi-armed poly(aspartate-g-OEI) copolymers as versatile carriers of pDNA/siRNA., Acta Biomater. 9 (2013) 6943–6952. https://doi.org/10.1016/j.actbio.2013.02.007.

[76] A. Zakeri, M.A.J. Kouhbanani, N. Beheshtkhoo, V. Beigi, S.M. Mousavi, S.A.R. Hashemi, A. Karimi Zade, A.M. Amani, A. Savardashtaki, E. Mirzaei, S. Jahandideh, A. Movahedpour, Polyethylenimine-based nanocarriers in co-delivery of drug and gene: a developing horizon, Nano Rev. Exp. 9 (2018) 1488497. https://doi.org/10.1080/20022727.2018.1488497.

[77] J.-C. Yeh, H.-H. Yang, Y.-T. Hsu, C.-M. Su, T.-H. Lee, S.-L. Lou, Synthesis and characteristics of biodegradable and temperature responsive polymeric micelles based on poly(aspartic acid)-g-poly(N-isopropylacrylamide-co-N,N-dimethylacrylamide), Colloids Surfaces A Physicochem. Eng. Asp. 421 (2013) 1–8. https://doi.org/10.1016/j.colsurfa.2012.12.014.

[78] K.C. Low, A.P. Wheeler, L.P. Koskan, Commercial Poly(aspartic acid) and Its Uses, in: Hydrophilic Polym., American Chemical Society, 1996: pp. 6–99. https://doi.org/doi:10.1021/ba-1996-0248.ch006.

[79] H. Adelnia, H.D.N. Tran, P.J. Little, I. Blakey, H.T. Ta, Poly(aspartic acid) in Biomedical Applications: From Polymerization, Modification, Properties, Degradation, and Biocompatibility to Applications, ACS Biomater. Sci. Eng. 7 (2021) 2083–2105. https://doi.org/10.1021/acsbiomaterials.1c00150.

[80] S.M. Thombre, B.D. Sarwade, Synthesis and biodegradability of polyaspartic acid:

A critical review, J. Macromol. Sci. - Pure Appl. Chem. 42 A (2005) 1299–1315. https://doi.org/10.1080/10601320500189604.

[81] E. Kokufuta, S. Suzuki, K. Harada, Temperature Effect on the Molecular Weight and the Optical Purity of Anhydropolyaspartic Acid Prepared by Thermal Polycondensation, Bull. Chem. Soc. Jpn. 51 (1978) 1555–1556. https://doi.org/10.1246/bcsj.51.1555.

[82] H. Adelnia, J. Nasrollah Gavgani, H. Riazi, H. Cheraghi Bidsorkhi, Transition behavior, surface characteristics and film formation of functionalized poly(methyl methacrylate-co-butyl acrylate) particles, Prog. Org. Coatings. 77 (2014) 1826–1833. https://doi.org/10.1016/j.porgcoat.2014.06.009.

[83] T. Nakato, A. Kusuno, T. Kakuchi, Synthesis of poly(succinimide) by bulk polycondensation of L-aspartic acid with an acid catalyst, J. Polym. Sci. Part A Polym. Chem. 38 (2000) 117–122. https://doi.org/10.1002/(SICI)1099-0518(20000101)38:1<117::AID-POLA15>3.0.CO;2-F.

[84] A. Bossion, K. V. Heifferon, L. Meabe, N. Zivic, D. Taton, J.L. Hedrick, T.E. Long, H. Sardon, Opportunities for organocatalysis in polymer synthesis via step-growth methods, Prog. Polym. Sci. 90 (2019) 164–210. https://doi.org/10.1016/j.progpolymsci.2018.11.003.

[85] H. Adelnia, J.N. Gavgani, M. Soheilmoghaddam, Fabrication of composite polymer particles by stabilizer-free seeded polymerization, Colloid Polym. Sci. 293 (2015) 2445–2450. https://doi.org/10.1007/s00396-015-3675-8.

[86] L.E. Nită, A.P. Chiriac, C.M. Popescu, I. Neamtu, L. Alecu, Possibilities for poly(aspartic acid) preparation as biodegradable compound, J. Optoelectron. Adv. Mater. 8 (2006) 663–666.

[87] S. Shi, X. Zhao, Q. Wang, H. Shan, Y. Xu, Synthesis and evaluation of polyaspartic acid/furfurylamine graft copolymer as scale and corrosion inhibitor, RSC Adv. 6 (2016) 102406–102412. https://doi.org/10.1039/c6ra22048g.

[88] A. Steinbüchel, A. Sallam, Dipeptides in nutrition and therapy: Cyanophycin-derived dipeptides as natural alternatives and their biotechnological production, Appl. Microbiol. Biotechnol. 87 (2010) 815–828. https://doi.org/10.1007/s00253-010-2641-0.

[89] J. Alba-Roth, O.A. Müller, J. Schopohl, K. von Werder, Arginine stimulates growth hormone secretion by suppressing endogenous somatostatin secretion., J. Clin. Endocrinol. Metab. 67 (1988) 1186–1189. https://doi.org/10.1210/jcem-67-6-1186.

[90] S.L. Davis, Plasma levels of prolactin, growth hormone and insulin in sheep following the infusion of arginine, leucine and phenylalanine., Endocrinology. 91

(1972) 549–555. https://doi.org/10.1210/endo-91-2-549.

[91] P. Thams, K. Capito, L-arginine stimulation of glucose-induced insulin secretion through membrane depolarization and independent of nitric oxide., Eur. J. Endocrinol. 140 (1999) 87–93. https://doi.org/10.1530/eje.0.1400087.

[92] J.P. Palmer, J.W. Benson, R.M. Walter, J.W. Ensinck, Arginine-stimulated acute phase of insulin and glucagon secretion in diabetic subjects., J. Clin. Invest. 58 (1976) 565–570. https://doi.org/10.1172/JCI108502.

[93] W. Jobgen, C.J. Meininger, S.C. Jobgen, P. Li, M.-J. Lee, S.B. Smith, T.E. Spencer, S.K. Fried, G. Wu, Dietary L-arginine supplementation reduces white fat gain and enhances skeletal muscle and brown fat masses in diet-induced obese rats., J. Nutr. 139 (2009) 230–237. https://doi.org/10.3945/jn.108.096362.

[94] T. Utagawa, Arginine Metabolism: Enzimology, Nutrition, and Clinical Significance - Production of Arginine by Fermentation, (2004) 2854–2857.

[95] K. Akashi, H. Shibai, Y. (Ajinomoto C.I. Hirose Kawasaki, Kanagawa (Japan). Central Research Labs.), Effect of oxygen supply on L-phenylalanine, L-proline, L-glutamine and L-arginine fermentations, J. Ferment. Technol. v. 57 (1979).

[96] Y. Hirose, H. Shibai, Amino-Acid Fermentation, Biotechnol. Bioeng. 22 (1980) 111–125.

[97] A. Trautmann, B. Watzer, A. Wilde, K. Forchhammer, C. Posten, Effect of phosphate availability on cyanophycin accumulation in Synechocystis sp. PCC 6803 and the production strain BW86, Algal Res. 20 (2016) 189–196. https://doi.org/10.1016/j.algal.2016.10.009.

[98] T. Hai, F.B. Oppermann-Sanio, A. Steinbüchel, Purification and characterization of cyanophycin and cyanophycin synthetase from the thermophilic Synechococcus sp. MA19, FEMS Microbiol. Lett. 181 (1999) 229–236. https://doi.org/10.1016/S0378-1097(99)00544-3.

[99] S.E. Stevens, D.A.M. Paone, D.L. Balkwill, Accumulation of Cyanophycin Granules as a Result of Phosphate Limitation in Agmenellum quadruplicatum , Plant Physiol. 67 (1981) 716–719. https://doi.org/10.1104/pp.67.4.716.

[100] L.A. Sherman, P. Meunier, M.S. Colón-López, Diurnal rhythms in metabolism: A day in the life of a unicellular, diazotrophic cyanobacterium, Photosynth. Res. 58 (1998) 25–42. https://doi.org/10.1023/A:1006137605802.

[101] R.D. Simon, The effect of chloramphenicol on the production of cyanophycin granule polypeptide in the blue-green alga Anabaena cylindrica, Arch. Mikrobiol. 92 (1973) 115–122. https://doi.org/10.1007/BF00425009.

[102] M. Obukowicz, G.S. Kennedy, The chloramphenicol altered fine structure of anabaena cylindrica, Br. Phycol. J. 15 (1980) 19–26. https://doi.org/10.1080/00071618000650021.

[103] A.H. Mackerras, N.M. de Chazal, G.D. Smith, Transient accumulations of cyanophycin in Anabaena cylindrica and Synechocystis 6308, Microbiology. 136

(1990) 2057–2065.

[104] A.H. Mackerras, B.N. Youens, R.C. Weir, G.D. Smith, Is cyanophycin involved in the integration of nitrogen and carbon metabolism in the cyanobacteria Anabaena cylindrica and Gleothece grown on light/dark cycles?, Microbiology. 136 (1990) 2049–2056.

[105] L. Wiefel, K. Wohlers, A. Steinbüchel, Re-evaluation of cyanophycin synthesis in Corynebacterium glutamicum and incorporation of glutamic acid and lysine into the polymer, Appl. Microbiol. Biotechnol. 103 (2019) 4033–4043. https://doi.org/10.1007/s00253-019-09780-5.

[106] H. Mooibroek, N. Oosterhuis, M. Giuseppin, M. Toonen, H. Franssen, E. Scott, J. Sanders, A. Steinbüchel, Assessment of technological options and economical feasibility for cyanophycin biopolymer and high-value amino acid production, Appl. Microbiol. Biotechnol. 77 (2007) 257–267. https://doi.org/10.1007/s00253-007-1178-3.

[107] H. Nausch, J. Huckauf, I. Broer, Peculiarities and impacts of expression of bacterial cyanophycin synthetases in plants, Appl. Microbiol. Biotechnol. 100 (2016) 1559–1565. https://doi.org/10.1007/s00253-015-7212-y.

[108] T. Kaneko, Y. Nakamura, C.P. Wolk, T. Kuritz, S. Sasamoto, A. Watanabe, M. Iriguchi, A. Ishikawa, K. Kawashima, T. Kimura, Y. Kishida, M. Kohara, M. Matsumoto, A. Matsuno, A. Muraki, N. Nakazaki, S. Shimpo, M. Sugimoto, M. Takazawa, M. Yamada, M. Yasuda, S. Tabata, Complete Genomic Sequence of the Filamentous Nitrogen-fixing Cyanobacterium Anabaena sp. Strain PCC 7120 , DNA Res. 8 (2001) 205–213. https://doi.org/10.1093/dnares/8.5.205.

[109] G. Perin, T. Fletcher, V. Sagi-Kiss, D.C.A. Gaboriau, M.R. Carey, J.G. Bundy, P.R. Jones, Calm on the surface, dynamic on the inside. Molecular homeostasis of Anabaena sp. PCC 7120 nitrogen metabolism, Plant. Cell Environ. 44 (2021) 1885–1907. https://doi.org/https://doi.org/10.1111/pce.14034.

[110] A. Javelle, D. Lupo, X.-D. Li, M. Merrick, M. Chami, P. Ripoche, F.K. Winkler, Structural and mechanistic aspects of Amt/Rh proteins, J. Struct. Biol. 158 (2007) 472–481. https://doi.org/https://doi.org/10.1016/j.jsb.2007.01.004.

[111] B. Watzer, A. Engelbrecht, W. Hauf, M. Stahl, I. Maldener, K. Forchhammer, Metabolic pathway engineering using the central signal processor PII, Microb. Cell Fact. 14 (2015). https://doi.org/10.1186/s12934-015-0384-4.

Chapter 2

Using the Design of Dynamic Experiments to optimize photosynthetic cyanophycin production by *Synechocystis* sp.

The production of cyanophycin by photosynthetic microorganisms, as a high-value bio-based compound, is getting increasing interest. The aim of this study is to maximize the production of this compound by the cyanobacterium *Synechocystis* sp. in semi-batch cultivation systems, by applying a data-driven modeling approach based on the Design of Dynamic Experiments (DoDE) and Response Surface Model (RSM) methodologies. A first set of experiments, carried out inside an initially defined domain, was used to find a preliminary RSM model describing cyanophycin concentration as a function of incident light intensity profile, temperature, and phosphorus supply profile. The model was then improved, according to an evolutionary optimization approach, by carrying out additional experiments in a modified domain, exploiting information derived by the initial model. The updated model was used to identify the optimal operating conditions resulting in maximum cyanophycin concentration at the end of the batch. The cyanophycin concentration found experimentally (228.2 ± 20.0 mg L^{-1}) in these conditions fell within the confidence interval of the model prediction. Remarkably, this experimentally obtained value represents a significant (about 20%) increase in the cyanophycin production with respect to the highest value found in the experiments before the optimization step (184.3 ± 0.8 mg L^{-1}).

Part of this Chapter was published as a scientific paper in *Journal of Industrial and Engineering Chemistry* (Trentin, G., Bertucco, A., Georgakis, C., Sforza, E., Barbera, E., 2023, https://doi.org/10.1016/j.jiec.2022.10.026)

2.1 Introduction

Microalgae and cyanobacteria have gained a lot of attention as a promising renewable feedstock for the production of valuable bio-based compounds. Their growth depends on several factors, such as nutrients concentration in the cultivation medium, temperature, and light availability [1]. A limitation in one of these factors greatly influences not only biomass productivity, but also its composition [2]. Indeed, cultivating microalgae under stressful conditions is a common technique to enhance the production of specific components, such as carbohydrates, lipids or pigments [3–5]. Among other compounds of interest, cyanophycin (CGP), an intracellular polypeptide that microorganisms store as a reservoir of energy, carbon and nitrogen [6], has recently attracted the attention of the scientific community.

Cyanophycin is a non-ribosomally synthesized amino acid polymer, composed by equimolar amounts of arginine and aspartic acid. It could serve as a potential biodegradable replacement for petrochemical-based industrial products. Industrial applications, not developed so far, focus on its chemical derivatives, as cyanophycin can be chemically converted into its constituents, namely poly(aspartic acid) (PASP) and arginine, by a β-hydrolytic cleavage [7]. PASP is an anionic polypeptide which is a highly versatile, biocompatible, and biodegradable polymer useful in a variety of biomedical applications [8]. Its protein-like backbone structure makes it an ideal substitute for non-degradable anionic polyelectrolytes. Moreover, thanks to its biocompatibility and biodegradability, many interesting materials for biomedical applications, including tissue engineering and drug/gene delivery were developed from modified PASP [9]. L-arginine, on the other hand, is a strongly basic amino acid (MW = 174.2 g mol^{-1}), found in most proteins. It is essential for human infants and fishes, whereas for human adults and mammals it is considered semi-essential because it is synthesized endogenously or can be taken from the diet [10].

To achieve high cyanophycin productivity, heterologous expression of cyanophycin synthetase genes (*cphA*) in heterotrophic microorganisms has been widely studied. Zhlystov et al. [11] produced 970±80 mg L^{-1} of cyanophycin with *E. coli* BL21 (DE3). Frey et al. [12] achieved a cyanophycin production of 1.5 g L^{-1}, with *E. coli* DH1. Other microorganisms have been engineered to produce cyanophycin, such as *R. eutropha* and *Pseudomonas putida*, *Corynebacterium glutamicum*, *Saccharomyces cerevisiae* [13], but interestingly also transgenic plants, as *Nicotiana tabacum* and *Solanum tuberosum*, even if the production yields obtained are lower than for bacterial strains [14].

Concerning the cyanophycin production by photosynthetic microorganism, different cyanobacteria strains were found to accumulate this compound, such as *Scytonema* sp., *Synechocystis* sp., *Synechococcus* sp. and *Anabaena* sp. [7]. It is known that several factors may induce cyanophycin accumulation: when cyanobacteria were grown under imbalanced conditions, e.g. adverse light intensities, low temperature, phosphate and sulphate starvation, or when specific substances as chloramphenicol or rifamycin were added to culture media [7,15–17], the polymer accumulation was triggered. A few studies have investigated the effect of the operating conditions that affecting cyanophycin production. As reported by Stevens et al. [18], phosphorus depletion not only increased the number of CGP granules but also their dimension. Trautmann et al. [19] and Trentin et al. [20] found a correlation in *Synechocystis* sp. between cyanophycin and phosphorus quota and identified a similar threshold value for the internal cell phosphorus quota, below which cyanophycin production was enhanced in both batch and continuous system. This behaviour was modelled by Turetta et al. [21], who considered the effect of light intensity and residence time on steady-state cyanophycin productivity in continuous photobioreactors. As regards the temperature, Elbahloul et al. [22] found that its optimum value for the growth and the CGP accumulation in *A. calcoaceticus* ADP1 was 30°C. However, the available literature focused on photosynthetic cyanophycin production is at present still quite scarce. In particular, to the best of the authors knowledge, in literature there is no systematic study investigating the possible combined effect of operating variables that could improve the productivity of cyanophycin. This task is indeed not straightforward, considering the transient nature of this storage compound, which is accumulated and/or consumed within the microorganism depending on the evolving environmental conditions [23].

In order to improve the cyanophycin production by photosynthetic microorganism, the development of mathematical models describing the effect of the main factors affecting cyanophycin concentration in the biomass is crucial. Given the complex nature of this biological process, data-driven models may be helpful, as they allow to link the system variables to the desired output, without explicit knowledge of the physical behaviour of the process. For this reason, data-driven approaches are gaining increasing attention, and they are used in a wide number of engineering fields [24], including applications based on microorganisms [25]. Specifically, the Design of Experiments (DoE) is a systematic, structured and efficient method that results in a data-driven model called Response Surface Model (RSM) [26].

In this Chapter the effect of temperature, phosphorus feed flow-rate (and consequent P concentration) and incident light intensity on the cyanophycin production by *Synechocystis* sp. PCC 6803, was studied by means of a data-driven approach in semi-batch systems. Specifically, the Design of Dynamic Experiments (DoDE) method was applied to obtain a Response Surface Model (RSM) which describes cyanophycin accumulation at the last day of the growth curve. DoDE is a recent extension of the DoE methodology, which differs from the classical approach in that some or all of the input process variables are time-varying, as described by Georgakis [27]. In this way, input factors can vary according to a defined profile, capturing the dynamic characteristic of the process. The model obtained in this work was then used to identify the optimal operating conditions that maximize the cyanophycin production. Finally, the optimum predicted by the model was experimentally validated.

2.2 DoDE: Design of Dynamic Experiments

The input variables considered in this experimental design were the incident light intensity, the phosphorus inlet flowrate and the temperature, and their effects were assessed on cyanophycin production by *Synechocystis* sp. PCC 6803 cultivated in semi-batch experiments, of 7 days duration each. A total of six factors were considered in the design: two sub-factors for the incident light intensity (dynamic factor), three sub-factors related to the phosphorus inlet profile (also a dynamic factor) and one for the temperature (fixed factor). Although a thorough knowledge of the biological process under investigation is not trivial to obtain, the partial knowledge on the qualitative effect of the main process variables involved aids the definition of the initial domain investigated by the DoDE [28].

In order to follow the increasing trend of biomass concentration along time, which increases self-shading phenomena, the light intensity was provided following a linear or quadratic increasing profile, varying from an initial value ranging between 10 and 150 μmol m^{-2} s^{-1}, and a final one is between 100 and 500 μmol m^{-2} s^{-1}. The light intensity profile is described according to Eq. (2.1), as a function of the dimensionless time $\tau_1 = t/7$.

$$I(\tau_1) = I_0(\tau_1) + \Delta I(\tau_1) w_1(\tau_1) \tag{2.1}$$

with $I_0(\tau_1) = 80 + 220\tau_1$ being the center point, and $\Delta I(\tau_1) = 70 + 130\tau_1$, being the time-varying half-width of the domain.

The term $w_1(\tau_1)$ is parametrized using the shifted Legendre polynomials. The series expansion was limited to only the first two polynomials $P_0(\tau_1) = 1,\ P_1(\tau_1) = -1 + 2\tau_1$), so that the set of dynamic subfactors, x_{i} and the corresponding number of experiments is limited. Thus, two dynamic sub-factors (i.e. factors x_1 and x_2) are used, according to:

$$w_1(\tau_1) = x_1 P_0(\tau_1) + x_2 P_1(\tau_1) = x_1 - x_2 + 2\tau_1 x_2, \ \text{with} -1 \leq x_1 \pm x_2 \leq +1 \qquad (2.2)$$

In order to ensure an increasing light intensity profile, x_1 and x_2 have to satisfy the following constraint:

$$\frac{dI(\tau_1)}{d\tau_1} \geq 0, \qquad (2.3)$$

which results in:

$$1.69 + x_1 + 4.08x_2 > 0. \qquad (2.4)$$

Temperature (i.e. factor x_3) is taken as a fixed factor, which means its value was kept constant throughout each experiment, with lower and upper boundaries of the domain equal to 26°C and 33°C [29]. So, we have:

$$T = 29.5 + 3.5x_3, \ \text{with} -1 \leq x_3 \leq +1. \qquad (2.5)$$

Finally, three factors, namely a regular factor (x_4) and two sub-factors (x_5 and x_6) were used to define a decreasing phosphorus input profile. Firstly, a dimensionless time τ_2 is defined for the P feeding interval:

$$\tau_2 = t/t_f \text{ , with } 0 \leq \tau_2 \leq 1, \qquad (2.6)$$

where the duration of the phosphorus feeding interval (t_f) was bound between 1 and 4 days, and defined as:

$$t_f = 2.5 + 1.5x_4, \ \text{with} -1 \leq x_4 \leq +1. \qquad (2.7)$$

The choice of a P feeding interval shorter than the duration of the experiment (7 days) is done to allow phosphorus starvation to occur, which is supposed to trigger cyanophycin accumulation. Note that the feeding interval is set to always start at the beginning of the experiment (day 0) to allow biomass to grow. The feed phosphorus profile is then defined by:

$$u_2(\tau_2) = u_{20}(\tau_2) + \Delta u_2(\tau_2) w_2(\tau_2) \tag{2.8}$$

where $w_2(\tau_2)$ is again expressed in terms of the first two shifted Legendre polynomials:

$$w_2(\tau_2) = x_5 P_0(\tau_2) + x_6 P_1(\tau_2) = x_5 - x_6 + 2\tau_2 x_6, \text{ with } -1 \leq x_5 \pm x_6 \leq +1 \tag{2.9}$$

Moreover, to ensure that the phosphorus feeding profile is strictly decreasing (i.e., $\frac{du_2(t)}{dt} \leq 0$) and that a positive inlet value is obtained at t=0, it must also be that $x_6 \leq 0$. The center point and the width of the phosphorus profile domain are respectively equal to:

$$u_{20}(\tau_2) = 5.5(1 - \tau_2) \qquad \Delta u_2(\tau_2) = 4.5(1 - \tau_2) \tag{2.10}$$

They are defined as the average of the upper ($u_{2u}(\tau_2)$) and the lower ($u_{2l}(\tau_2)$) boundaries of the feeding profile, which are respectively:

$$u_{2u}(\tau_2) = 10.0(1 - \tau_2) \qquad u_{2l}(\tau_2) = 1.0(1 - \tau_2) \tag{2.11}$$

The values of 10.0 and 1.0 used in Eq. (2.11) are chosen because such flow rates, if steady, would result in a total amount of P supplied within the first 0.33 days of 3.3 mg_P and 0.33 mg_P, respectively. These boundaries are selected, in the experimental set-up used for the experiments (§ 2.3), as they correspond to a P concentration ranging between 16.5 $mg_P\ L^{-1}$ and 1.65 $mg_P\ L^{-1}$, which is a reasonable inlet concentration range to investigate for cyanophycin accumulation [20]. Furthermore, to ensure that the total amount of phosphorus fed is constrained between 0.33 and 3.3 mg_P, the following inequality has to be satisfied:

$$0.33 \leq \int_0^{t_f} \Big((1 - \tau_2)\big(5.5 + 4.5 w_2(\tau_2)\big)\Big)\, dt \leq 3.3 \tag{2.12}$$

which becomes:

$$-3.5 \leq 2.2x_4 + (1 + 0.6x_4)(3x_5 - x_6) \leq -1.9. \quad (2.13)$$

All the factors' constraints are summarized in Table 2.1. The initial experimental design was aimed at estimating a Response Surface Methodology (RSM) model to optimize the value of cyanophycin concentration in the culture (c_{CGP}, mg_{CGP} L^{-1}) at the end of the batch (day 7). It was made of 25 independent experiments plus 3 additional replicates carried out at the central point of the domain to estimate the normal variability of the process and also held estimate the Lack-of-Fit (LoF) statistic. This results in a total of 28 experimental runs (R1-R28). The complete D-optimal design in terms of coded factors x_1-x_6 is reported in Table 2.2, while the corresponding actual time profiles are summarized in Table 2A.1 of Appendix. The profiles of incident light intensity and phosphorus inflow for each of the 28 experiments are shown in Figure 2.1 and Figure 2.2, respectively.

Table 2.1. Constraints for the factors

$-1 \leq x_1, x_2, x_3, x_4, x_5 \leq 1$
$-1 \leq x_6 \leq 0$
$-1 \leq x_1 \pm x_2 \leq 1$
$-1 \leq x_5 \pm x_6 \leq 1$
$x_1 + 4.08x_2 > -1.69$
$-3.5 \leq 2.2x_4 + (1 + 0.6x_4) \cdot (3x_5 - x_6) \leq -1.9$

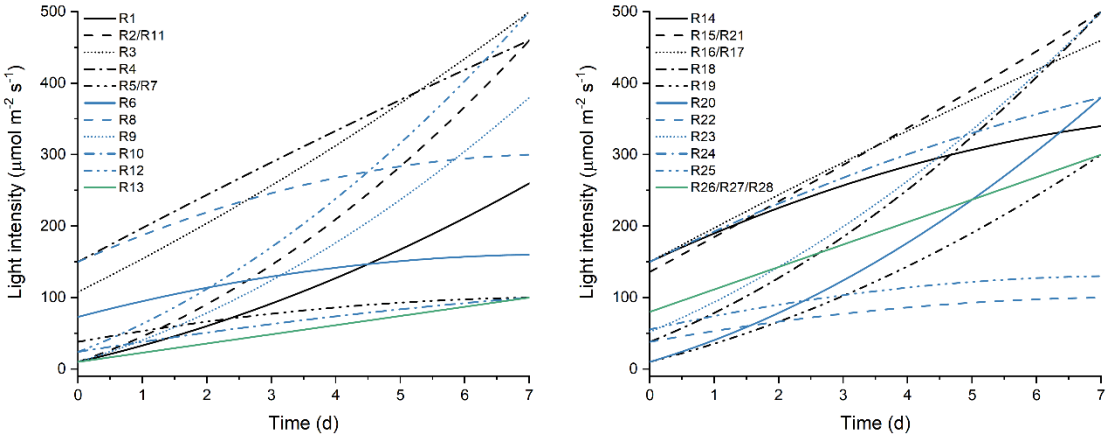

Figure 2.1. Light intensity profiles versus time for the 28 experiments. Some of the experiments have identical profiles, as indicated in the Legend

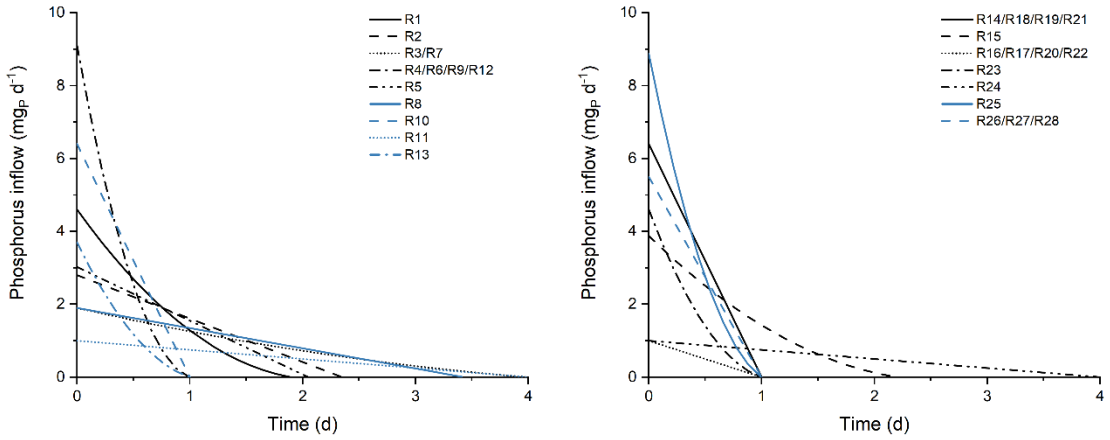

Figure 2.2. Phosphorus inflow profiles versus time for the 28 experiments. Some of the experiments have identical profiles, as indicated in the Legend

Table 2.2. The values of the coded factors defining the 28 experiments. The last three ones are replicates at the center of the domain

Run #	x_1 *Light*	x_2 *Light*	x_3 *Temperature*	x_4 *P inflow*	x_5 *P inflow*	x_6 *P inflow*
1	-0.6	0.4	-1	-0.4	-0.6	-0.4
2	-0.1	0.9	1	-0.1	-0.6	0
3	0.7	0.3	1	1	-0.9	-0.1
4	0.9	-0.1	1	-1	-0.10	-0.9
5	-0.8	-0.2	-1	-0.3	-0.55	0
6	-0.4	-0.3	-1	-1	-0.1	-0.9
7	-0.8	-0.2	1	1	-0.9	-0.1
8	0.5	-0.5	1	0.62	-0.800	0
9	-0.3	0.7	1	-1	-0.1	-0.9
10	-0.9	-0.1	-1	-1	0.2	0
11	-0.1	0.9	-1	1	-1	0
12	0.1	0.9	-1	-1	-0.085	-0.9
13	-1	0	-1	-1	-0.7	-0.3
14	0.6	-0.4	-1	-1	0.2	0
15	0.9	0.1	-1	-0.2	-0.67	-0.31
16	0.9	-0.1	-1	-1	-1	0
17	0.9	-0.1	1	-1	-1	0
18	0.2	0.8	-1	-1	0.2	0
19	-0.5	0.5	1	-1	0.2	0
20	-0.3	0.7	-1	-1	-1	0
21	0.9	0.1	1	-1	0.2	0
22	-0.8	-0.2	1	-1	-1	0
23	0.3	0.7	1	-1	-0.6	-0.4
24	0.7	-0.3	-1	1	-1	0
25	-0.6	-0.25	1	-1	0	-0.75
26	0	0	0	-1	0	0
27	0	0	0	-1	0	0
28	0	0	0	-1	0	0

2.3 Experimental setup

Synechocystis sp. PCC 6803 was purchased from Pasteur Culture of Cyanobacteria in France. It was maintained at a constant temperature of 30 ± 1°C in sterilized BG11 medium [30], buffered by 1.5 g L^{-1} of sodium bicarbonate. Maintenance and propagation of axenic culture and experiments were performed in Quickfit® Drechsel bottles with a volume of 200 mL and a diameter of 5 cm. Preinocula were renewed weekly with fresh medium, verifying axenic conditions by LB plating. Each experiment started with fresh culture medium and the initial P concentration required by the design (t = 0 d), in which a constant biomass inoculum (0.080 mg_x L^{-1}) was resuspended, following a standardized procedure to ensure that the starting culture had always the same characteristics. Then, phosphorus was added at discrete time intervals, twice per day at distance of 8 h (at 8 a.m. and 4 p.m.). Specifically, the amounts of P to be fed at time t_k for each experiment were calculated as the integrals of the continuous profiles reported in Figure 2.2, calculated between t_k and t_{k+1}. Note that the translation from a continuous feeding profile (Figure 2.2) to the amount of bolus used in the experiments does not imply any modelling ramifications, as long as it is applied consistently, and considering that we are not estimating kinetics. On the other hand, the continuous function representation results in fewer experiments required. The instantaneous amounts of phosphorus (mg_P) for each experimental run are reported in Figure 2A.1 of Appendix.

The reactor temperature was maintained constant at the value required by the design using a thermostatic bath. The culture mixing was ensured by both a stirring magnet placed at the bottom of the reactor and by the bubbling of 1 L h^{-1} of CO_2-air (5% v/v) mixture. This system ensured a bounded range for the pH within the interval 7.5-8.5, monitored daily using a Hanna portable pH-meter (code HI9124). Artificial light was provided by a LED lamp (Photon Systems Instruments), and the light intensity was measured using a photoradiometer (HD 2101.1 from Delta OHM) by means of a quantum radiometric probe which quantifies the Photosynthetically Active Radiation (PAR). A controller (LC100 Photon Systems Instruments) connected to the lamp modulated continuously the incident light intensity, according to the designed profiles.

Biomass growth was monitored twice per day at a distance of 8 h (i.e. at 8 a.m. and 4 p.m.), through optical density measurements at 750 nm (OD_{750}), using a UV-visible double beam spectrophotometer (UV1900, by Shimadzu, Japan) with 1 cm optical path length. Dry cell weight (c_x, mg_x L^{-1}) at steady state was also measured daily at 8 a.m., filtering a sample of

known volume under vacuum, through 0.22 µm previously dried nitrocellulose filters, which were then dried for 2 h at 105°C in a laboratory oven. Extraction and quantification of cyanophycin content in the biomass (q_{CGP}) was done at the first, the fourth and the last day of each experimental run, following the protocol reported in Trentin et al. (2021) [20], which uses the Bradford reaction. Then, cyanophycin concentration at time t was calculated as

$$c_{CGP} = q_{CGP} \cdot c_x \tag{2.14}$$

where the cyanophycin quota (q_{CGP}) was expressed in $mg_{CGP}\ mg_x^{-1}$.

2.4 Experimental results and first RSM model

Results of biomass and cyanophycin concentrations as a function of time in semi-batch growth curves of *Synechocystis* sp. PCC 6803 are reported in Figure 2A.2 of Appendix and in Figure 2.3, respectively.

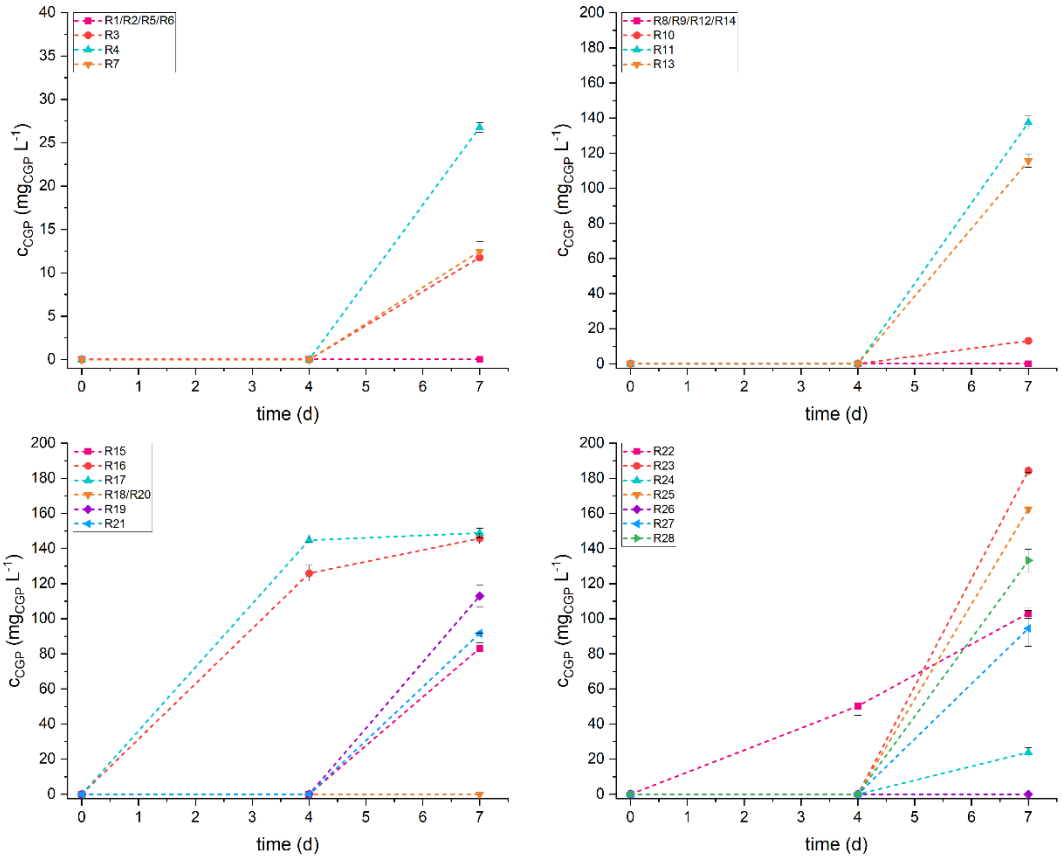

Figure 2.3. Cyanophycin concentration (c_{CGP}) as function of time (d) in semi-batch growth curves of *Synechocystis* sp. PCC 6803. Lines are just linking experimental points

The maximum biomass concentration (about 2.6 g_x L^{-1}) was measured in experimental runs number 9 and 19. All the others reached a concentration between 0.5 and 2.3 g_x L^{-1} (Figure 2A.2). Regarding the cyanophycin concentration, as shown in Figure 2.3, only experiments 16, 17 and 22 produced detectable amounts of cyanophycin at day 4. These runs corresponded to the lowest total amount of phosphorus fed (0.5 mg_P). On day 7, instead, the cyanophycin concentration varied between a minimum of 13.2 mg_{CGP} L^{-1} and a maximum of 184.3 mg_{CGP} L^{-1}, although in several experiments no cyanophycin was produced. Overall, a total of 15 experiments out of 25 resulted in cyanophycin production. Since only few experimental conditions triggered a cyanophycin accumulation at the beginning of the growth curve, a RSM for cyanophycin concentration was developed considering the results measured at day 7 only. To this purpose, the software DesignExpert from Stat-Ease® was used, imputing in the program the factors' values (i.e. x_1-x_6) and the measured responses (c_{CGP}) for each condition. Two experiments were excluded from the analysis, namely run 2 and run 26, as they were identified as unreliable data due to sudden culture crash. A preliminary analysis was carried out, starting from a full quadratic model, which has the following general formula:

$$y = \beta_0 + \sum_{i=1}^{n} \beta_i x_i + \sum_{i=1}^{n} \sum_{j=i+1}^{n} \beta_{ij} x_i x_j + \sum_{i=1}^{n} \beta_{ii} x_i^2 \quad (2.15)$$

where the response y, the cyanophycin concentration c_{CGP}, is a function of the input factors x_i through the model parameters $\beta_q | \, q = 0, i, ij,$ or ii .

The Box-Cox plot obtained by DesignExpert (Figure 2A.3) recommended a logarithmic transformation of the response data with a constant equal to 0.18, to avoid errors that are a function of the magnitude of the response. Then, through the Bayesian Information Criterion (BIC), applied in a forward direction, a reduced quadratic model retaining factors x_3x_4, x_2^2 and x_4^2 was obtained. These factors were significant, indeed their p-values were lower than 0.05 (respectively equal to 0.01, 0.003 and 0.028). Factors x_2, x_3, and x_4 were retained in the model even though they were not significant themselves, to maintain hierarchy (p-values equal to 0.9316, 0.4832, 0.1921). The Lack-of-Fit p-value was insignificant and greater than 0.05 (LoF p-value = 0.0857). In terms of actual factors, the complete model obtained was the following:

$$\ln(y + 0.18) = 1.09 + 3.66x_2 - 0.41x_3 + 0.82x_4 - 1.65x_3x_4 - 10.45x_2^2 + 3.63x_4^2 \quad (2.16)$$

Such a model was used in finding the optimal value of the factors that maximize cyanophycin production at day 7. The optimization of the function in the domain defined by the constraints of Table 2.1 was performed in Matlab®. However, the result of the optimization led to a predicted maximum cyanophycin concentration of 2750 mg_{CGP} L^{-1}, while the highest value measured experimentally was equal to 184.3 mg_{CGP} L^{-1}. The huge difference suggested that the predicted value was unrealistic, indicating that the model and its predictions had to be improved. The model inaccuracy is confirmed also by the quite large average deviation between the experimental and calculated values, which was equal to 57.52 mg_{CGP} L^{-1} in absolute terms, or to 150% in relative terms. In addition, it should be pointed out that two of the factors related to phosphorus inflow (namely x_5 and x_6) were not retained as statistically significant in the proposed model (p-values greater than 0.5), which contradicts evidence in the literature that phosphorus limitation is one of the main factors triggering cyanophycin accumulation [19,20]. Indeed, many of the experiments gave null results because they were performed in that part of the domain where cyanophycin is not accumulated. Moreover, when analyzing the optimization results (Table 2A.2 in Appendix) it can be noted that two of the factors, namely x_3 and x_4, resulted at the boundary of the investigated domain. It was suggested that the domain had to be extended to find the actual optimum.

According to these considerations, additional experiments were carried out in the part of the domain were there was a greater cyanophycin accumulation following an "evolutionary optimization approach", in order to obtain a more reliable model. Thus, the domain was enlarged in those directions were the first model indicated that cyanophycin accumulation could possibly be enhanced. Specifically, the temperature domain was enlarged to explore slightly lower as well as higher values, while the phosphorus inflow profiles was confined to lower values. More details are provided in the following section.

2.5 Evolutionary domain and final RSM model

To elaborate the new model, a set of 7 additional experiments (AR1-AR7) in an enlarged domain was performed. Factors were bounded by the constraints reported in Table 2.3. This new design (reported in terms of the coded variables x_1-x_6 in Table 2.4 and in terms of actual values in Table 2A.3 of Appendix) corresponds to the light and phosphorus profiles reported in Figure 2.4, while the instantaneous amounts of phosphorus (mg_P) for each experimental run to be fed at time t_k are reported in Figure 2A.4 of Appendix.

Table 2.3. Constraints for the factors for experiments AR1-AR7 carried out in an enlarged domain

$-1.5 \leq x_1, x_2, x_4, x_5 \leq 1.5$
$-1.5 \leq x_3 \leq 2.5$
$-1.5 \leq x_6 \leq 0$
$-1.5 \leq x_1 + x_2 \leq 1.5$
$-1 \leq x_1 - x_2 \leq 1.5$
$-1.5 \leq x_5 + x_6 \leq 1.5$

Table 2.4. The values of the coded factors defining AR1-AR7 experiments

Run #	**x1** *Light*	**x2** *Light*	**x3** *Temperature*	**x4** *P inflow*	**x5** *P inflow*	**x6** *P inflow*
1	0.7	0	-1.2	1.2	-1	0
2	0.38	0.1	-1.2	1.25	-1.1	0
3	0.3	0	-1.2	-0.10	-1.1	-0.3
4	0.05	0.10	-1.2	-1.1	-1.1	0
5	0.87	0.63	-1.2	-1.30	-1	0
6	0.44	0.56	-1.2	-1.1	-1	0
7	0.38	-0.51	2.42	-1.5	-0.65	-0.53

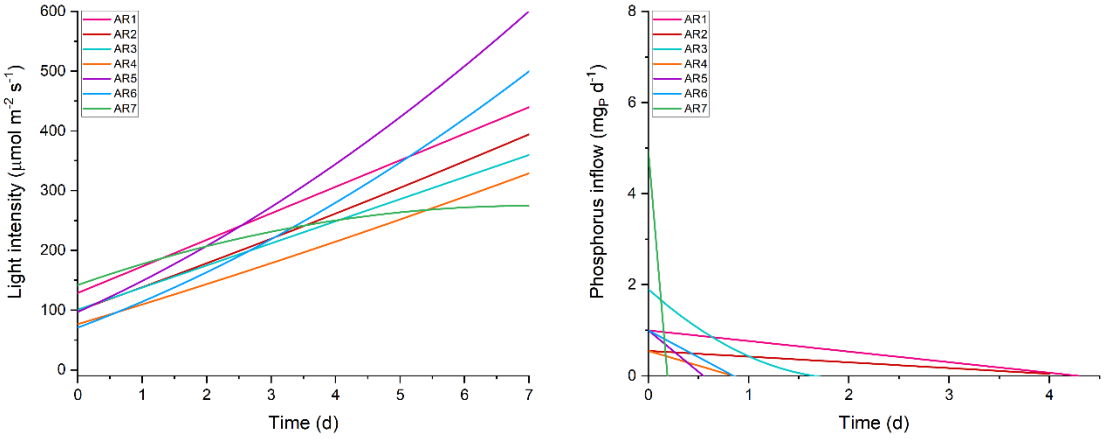

Figure 2.4. Light intensity (left) and phosphorus inflow (right) profiles versus time for AR1-AR7 experiments

In particular, the temperature domain was extended up to 38°C, as the previous model suggested that the actual optimum could be in this direction. The constraint on the total amount of P to be fed was instead shifted towards lower values, and specifically it varied between 2.150 mg_P and 0.226 mg_P. The results of cyanophycin concentration (c_{CGP}) measured at day 7 are reported in Figure 2.5.

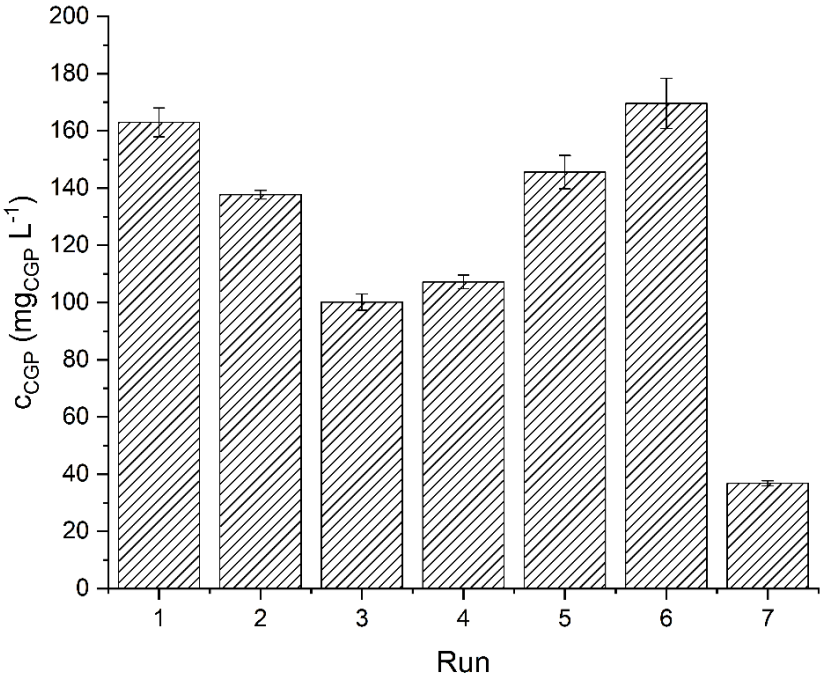

Figure 2.5. Cyanophycin concentration (c_{CGP}) measured at day 7 in semi-batch growth curves of *Synechocystis* sp. PCC 6803 for the additional experiments AR1-AR7

All the experimental conditions tested resulted in a significant cyanophycin production, indicating that the new domain was indeed more appropriate than the previous one for the desired goal. Moreover, experimental run AR7 resulted in the lowest CGP concentration, qualitatively suggesting that a too high temperature might have a negative effect.

Based on the additional experimental runs, a new model was developed, accounting for both the old and new experimental data. Also in this case data were transformed. Specifically, a square root transformation is now suggested and used with the constant k equal to 0.18. The full quadratic model (Eq. (2.15)) was reduced considering the p-value and the Variance Inflation Factors (VIF) values. Specifically, the p-value of each term must be lower than 0.05 for a significant model, and the VIF must be lower than 10 (ideally 1.0, indicating that the factors are orthogonal), to avoid multicollinearity in the estimation of the model's coefficients. The RSM model obtained in terms of coded factors is:

$$\sqrt{y + 0.18} = 9.25 - 6.89x_1 - 1.30x_2 - 5.85x_3 - 5.28x_4 - 4.71x_5 - 0.16x_6 - 3.67x_1 \cdot x_3 + 7.39x_1 \cdot x_6 - 5.77x_2 \cdot x_3 - 7.22x_3 \cdot x_4 - 13.01x_2^2 - 6.61x_3^2 \quad (2.17)$$

which is converted in terms of actual factors to:

$$\sqrt{y+0.18} = 7.90 + 0.95x_1 + 10.16x_2 - 0.09x_3 - 2.32x_4 - 3.14x_5 - 0.21x_6 - 1.22x_1 \cdot x_3 + 6.57x_1 \cdot x_6 - 2.71x_2 \cdot x_3 - 2.41x_3 \cdot x_4 - 11.49x_2^2 - 1.65x_3^2 \quad (2.18)$$

The confidence intervals for each parameter of the RSM model are reported in Table 2A.4 of the Appendix. All factors retained in the model are significant except x_2, x_6, x_1x_3. These are retained to achieve the desired hierarchy in the model. This requires that lower-order insignificant terms, like x_2, are retained because a higher-order term, like $, x_2x_3$, is significant. This is necessary to be able to accurately transform the RSM model from the coded factor values to the physical values [31]. Furthermore, the p-value of the x_1x_3 factor (0.0621) is just slightly greater than 0.05, but lower than 0.1. As regards the two-factor interaction terms, the interaction between the amount of light and phosphorus (x_1x_6), light profile slope and temperature (x_2x_3), and temperature and phosphorus feeding time (x_3x_4) were the most significant. The remaining factors, instead, were retained only to maintain the hierarchy. The p-values and VIFs for all the terms are reported in Table 2A.4 of Appendix. As regards the VIFs, the values are lower than 10 for all the factors, with only three factors with a value greater than 5 (namely x_1, x_3, and x_1x_6). The adjusted R^2_{adj} value was equal to 0.81, and it was greatly increased with respect to the one obtained with the former model (Eq. (2.16), $R^2_{adj} = 0.4724$), indicating that the new RSM model is significantly better. Similarly, the LoF p-value was increased from 0.0857 of the first RSM up to 0.4713 for the new model. The average absolute deviation between experimental and calculated values was reduced from 57.52 to 18.4 mg_{CGP} L^{-1}, and the average relative deviation was equal to 22%.

The optimization was performed in Matlab®, using the "fmincon.m" function. The optimum was searched by slightly extrapolating the results in an enlarged domain, whose boundaries are reported in Table 2.5. It has to be pointed out that some of the lower bounds, specifically the ones set for x_4, $x_1 - x_2$ and $x_5 - x_6$, were kept equal with respect to the previous domain (Table 2.3), in order to have non-negative values of the profiles in the first day, and a phosphorus feeding time (t_k) greater than 0. The initial guess used in the optimization was equal to [0, 0, 0, 0, 0, -0.5].

The maximum value of cyanophycin concentration predicted by the Matlab® optimization is equal to 304.4 mg_{CGP} L^{-1}, with a 95% confidence interval equal to (206.4, 422.0). The predicted nominal value for the operation (304.4) is 39% greater with respect to the maximum cyanophycin concentration measured experimentally (184.3 ± 0.8 mg_{CGP} L^{-1}).

Table 2.5. Constraints for the factors for Matlab® optimization

$-1.7 \leq x_1, x_2, x_5 \leq 1.7$
$-1.7 \leq x_3 \leq 2.5$
$-1.5 \leq x_4 \leq 1.7$
$-1.7 \leq x_6 \leq 0$
$-1.7 \leq x_1 + x_2 \leq 1.7$
$-1 \leq x_1 - x_2 \leq 1.7$
$-1.7 \leq x_5 + x_6 \leq 1.7$
$-1 \leq x_5 - x_6 \leq 1.7$
$x_1 + 4.08x_2 > -1.69$
$-3.5 \leq 2.2x_4 + (1 + 0.6x_4) \cdot (3x_5 - x_6) \leq -1.9$

Table 2.6 reports the optimal value for each factor corresponding to the optimal production point. It can be seen that each factor lies within the investigated domain, and so do the other constraints, with the only exception of the sum of the first two factors ($x_1 + x_2$). In this case, indeed, the optimal value of factors x_1 and x_2 is on the domain boundary, suggesting that probably this could be slightly enlarged. In any case, the result obtained was decidedly positive.

Table 2.6. Optimal value in terms of coded factors

Factors	Value
x_1	1.31
x_2	0.39
x_3	0.1
x_4	-1.3
x_5	-0.94
x_6	0

To validate the model prediction, an additional experiment was performed at the optimal condition reported in Table 2.6. This corresponds to the incident light and phosphorus inflow profiles reported in Figure 2A.5 of Appendix. The instantaneous amount of P to be added at the time instant t_k is equal to 0.293 mg of phosphorus to be fed at time 0, and it also corresponds to the total amount of P added. In this last run the cyanophycin concentration measured at day 7 was equal to 228.2 ± 20.0 mg_{CGP} L^{-1}. This value is inside the confidence interval predicted by the model, confirming its reliability. Moreover, the cyanophycin production obtained at these conditions was about 20% greater than the highest value previously measured experimentally (184.3 ± 0.8 mg_{CGP} L^{-1}) (Figure 2A.6 of

Appendix). This corresponds to a cyanophycin productivity of 32.6 mg_{CGP} L^{-1} d^{-1}, which is comparable or even slightly higher than the maximum value reported in the literature [19,20].

Our result confirms the validity and the reliability of the data-driven methodology used. In fact, although the final model obtained has a relatively large confidence interval, which is related to the intrinsic variability of biological processes (specifically those involving photosynthetic microorganisms) and the relatively large errors of the corresponding experimental measurements, it allowed identifying optimal operating conditions which resulted in a significant increase in the production of the desired compound, with a relatively small number of experimental runs. Moreover, it was shown that using the DoDE methodology, therefore allowing input variables to change over time, brings significant advancement to the conventional DoE, in which all factors are kept constant throughout the experiments. It should be mentioned that the results of this Chapter could be potentially further improved by developing a Dynamic Response Surface Model (DRSM) [32], to predict the cyanophycin concentration profile along with time, provided that enough experimental data are collected at different time intervals.

2.6 Final remarks

In this Chapter, the data-driven Design of Dynamic Experiment (DoDE) approach followed by Response Surface Methodology (RSM) was applied to model the effect of incident light intensity, phosphorus feeding profile, and temperature on cyanophycin production by *Synechocystis* sp. PCC 6803, with the aim of maximizing the production of this compound in a semi-batch system. We showed that, by applying an evolutionary optimization approach, it was possible to identify optimal operating conditions that led to a significant increase in cyanophycin production. Although the model obtained from the first set of experiment was not reliable in its predictions, it provided useful indications on how to modify the experimental domain towards more significant conditions. Following a few additional experiments performed in the enlarged domain, it was in fact possible to obtain another reduced quadratic RSM model that better fits the experimental data. The optimal condition predicted by the model, although characterized by a relatively large confidence interval, was experimentally validated, proving the effectiveness of the methodology employed.

Nomenclature

τ_1	Dimensionless time (-)
t_f	Duration of the phosphorus feeding interval (d)
τ_2	Dimensionless time (-)
c_{CGP}	Cyanophycin concentration ($mg_{CGP}\ L^{-1}$)
q_{CGP}	Cyanophycin quota ($mg_{CGP}\ mg_x^{-1}$)
c_x	Biomass concentration ($mg_x\ L^{-1}$)
β_q	Model parameters (-)

Acronyms

BIC	Bayesian Information Criterion
CGP	Cyanophycin
DoDE	Design of Dynamic Experiments
DoE	Design of Experiments
DRSM	Dynamic Response Surface Model
LoF	Lack of Fit
PAR	Photosynthetically Active Radiation
PASP	Poly(aspartic acid)
RSM	Response Surface Model
VIF	Variance Inflation Factors

Literature cited

[1] M.I. Khan, J.H. Shin, J.D. Kim, The promising future of microalgae: Current status, challenges, and optimization of a sustainable and renewable industry for biofuels, feed, and other products, Microb. Cell Fact. 17 (2018) 1–21. https://doi.org/10.1186/s12934-018-0879-x.

[2] G. Markou, I. Angelidaki, D. Georgakakis, Microalgal carbohydrates: An overview of the factors influencing carbohydrates production, and of main bioconversion technologies for production of biofuels, Appl. Microbiol. Biotechnol. 96 (2012) 631–645. https://doi.org/10.1007/s00253-012-4398-0.

[3] C.E. de Farias Silva, E. Sforza, A. Bertucco, Stability of carbohydrate production in continuous microalgal cultivation under nitrogen limitation: effect of irradiation regime and intensity on Tetradesmus obliquus, J. Appl. Phycol. 30 (2018) 261–270. https://doi.org/10.1007/s10811-017-1252-x.

[4] E. Cointet, G. Wielgosz-Collin, G. Bougaran, V. Rabesaotra, O. Gonçalves, V. Méléder, Effects of light and nitrogen availability on photosynthetic efficiency and fatty acid content of three original benthic diatom strains, PLoS One. 14 (2019) 1–28. https://doi.org/10.1371/JOURNAL.PONE.0224701.

[5] J.R. Benavente-Valdés, C. Aguilar, J.C. Contreras-Esquivel, A. Méndez-Zavala, J. Montañez, Strategies to enhance the production of photosynthetic pigments and lipids in chlorophycae species, Biotechnol. Reports. 10 (2016) 117–125. https://doi.org/10.1016/j.btre.2016.04.001.

[6] R.D. Simon, P. Weathers, Preparation and Derivatization of Cyanophycin Granule Polypeptide The filamentous cyanobacterium Anabaena cylindrica Lemm . was grown as, 420 (1976) 165–176.

[7] J. Du, L. Li, S. Zhou, Microbial production of cyanophycin: From enzymes to biopolymers, Biotechnol. Adv. 37 (2019). https://doi.org/10.1016/j.biotechadv.2019.05.006.

[8] H. Adelnia, H.D.N. Tran, P.J. Little, I. Blakey, H.T. Ta, Poly(aspartic acid) in Biomedical Applications: From Polymerization, Modification, Properties, Degradation, and Biocompatibility to Applications, ACS Biomater. Sci. Eng. 7 (2021) 2083–2105. https://doi.org/10.1021/acsbiomaterials.1c00150.

[9] P.S. Yavvari, A.K. Awasthi, A. Sharma, A. Bajaj, A. Srivastava, Emerging Biomedical Applications of Polyaspartic Acid-Derived acid-derived biodegradable

polyelectrolytes, (2019). https://doi.org/10.1039/C8TB02962H.

[10] A. Steinbüchel, A. Sallam, Dipeptides in nutrition and therapy: Cyanophycin-derived dipeptides as natural alternatives and their biotechnological production, Appl. Microbiol. Biotechnol. 87 (2010) 815–828. https://doi.org/10.1007/s00253-010-2641-0.

[11] N.A. Khlystov, W.Y. Chan, A.M. Kunjapur, W. Shi, K.L.J. Prather, B.D. Olsen, Material properties of the cyanobacterial reserve polymer multi-L-arginyl-poly-L-aspartate (cyanophycin), Polymer (Guildf). 109 (2017) 238–245. https://doi.org/10.1016/j.polymer.2016.11.058.

[12] K.M. Frey, F.B. Oppermann-Sanio, H. Schmidt, A. Steinbüchel, Technical-scale production of cyanophycin with recombinant strains of Escherichia coli, Appl. Environ. Microbiol. 68 (2002) 3377–3384. https://doi.org/10.1128/AEM.68.7.3377-3384.2002.

[13] J. Aravind, T. Saranya, G. Sudha, P. Kanmani, Integrated Waste Management in India, (2016) 49–58. https://doi.org/10.1007/978-3-319-27228-3.

[14] H. Nausch, J. Huckauf, I. Broer, Peculiarities and impacts of expression of bacterial cyanophycin synthetases in plants, Appl. Microbiol. Biotechnol. 100 (2016) 1559–1565. https://doi.org/10.1007/s00253-015-7212-y.

[15] S. Canizales, M. Sliwszcinka, A. Russo, S. Bentvelzen, H. Temmink, A.M. Verschoor, R.H. Wijffels, M. Janssen, Cyanobacterial growth and cyanophycin production with urea and ammonium as nitrogen source, J. Appl. Phycol. 33 (2021) 3565–3577. https://doi.org/10.1007/s10811-021-02575-0.

[16] M. Obst, A. Steinbüchel, Microbial degradation of poly (amino acid)s, Biomacromolecules. 5 (2004) 1166–1176. https://doi.org/10.1021/bm049949u.

[17] N.H. Lawry, R.D. Simon, The Normal And Induced Occurrence Of Cyanophycin Inclusion Bodies In Several Blue-Green Algae, J. Phycol. 18 (1982) 391–399. https://doi.org/https://doi.org/10.1111/j.1529-8817.1982.tb03201.x.

[18] S.E. Stevens, D.A.M. Paone, D.L. Balkwill, Accumulation of Cyanophycin Granules as a Result of Phosphate Limitation in Agmenellum quadruplicatum , Plant Physiol. 67 (1981) 716–719. https://doi.org/10.1104/pp.67.4.716.

[19] A. Trautmann, B. Watzer, A. Wilde, K. Forchhammer, C. Posten, Effect of phosphate availability on cyanophycin accumulation in Synechocystis sp. PCC 6803 and the production strain BW86, Algal Res. 20 (2016) 189–196. https://doi.org/10.1016/j.algal.2016.10.009.

[20] G. Trentin, V. Lucato, E. Sforza, A. Bertucco, Stabilizing autotrophic cyanophycin production in continuous photobioreactors, Algal Res. 60 (2021) 102518. https://doi.org/10.1016/j.algal.2021.102518.

[21] M. Turetta, E. Barbera, G. Trentin, A. Bertucco, E. Sforza, Modeling the production of cyanophycin in Synechocystis sp. PCC 6803 cultivated in chemostat reactors, Bioresour. Technol. Reports. 19 (2022) 101132. https://doi.org/10.1016/j.biteb.2022.101132.

[22] Y. Elbahloul, M. Krehenbrink, R. Reichelt, A. Steinbüchel, Physiological conditions conducive to high cyanophycin content in biomass of Acinetobacter calcoaceticus Strain ADP1, Appl. Environ. Microbiol. 71 (2005) 858–866. https://doi.org/10.1128/AEM.71.2.858-866.2005.

[23] A.H. Mackerras, N.M. de Chazal, G.D. Smith, Transient accumulations of cyanophycin in Anabaena cylindrica and Synechocystis 6308, Microbiology. 136 (1990) 2057–2065.

[24] F.J. Montáns, F. Chinesta, R. Gómez-Bombarelli, J.N. Kutz, Data-driven modeling and learning in science and engineering, Comptes Rendus - Mec. 347 (2019) 845–855. https://doi.org/10.1016/j.crme.2019.11.009.

[25] P.P. Peralta-Yahya, F. Zhang, S.B. Del Cardayre, J.D. Keasling, Microbial engineering for the production of advanced biofuels, Nature. 488 (2012) 320–328. https://doi.org/10.1038/nature11478.

[26] J. Santos-Marques, C.T. Georgakis, J. Mustakis, J.M. Hawkins, From dynamic response surface models to the identification of the reaction stoichiometry in a complex pharmaceutical case study, AIChE J. (2019).

[27] C. Georgakis, Design of dynamic experiments: A data-driven methodology for the optimization of time-varying processes, Ind. Eng. Chem. Res. 52 (2013) 12369–12382. https://doi.org/10.1021/ie3035114.

[28] Z. Wang, C. Georgakis, An in silico evaluation of data-driven optimization of biopharmaceutical processes, AIChE J. 63 (2017) 2796–2805. https://doi.org/https://doi.org/10.1002/aic.15659.

[29] K. Kłodawska, L. Kovács, Z. Várkonyi, M. Kis, Ö. Sozer, H. Laczkó-Dobos, O. Kóbori, I. Domonkos, K. Strzałka, Z. Gombos, P. Malec, Elevated growth temperature can enhance photosystem I trimer formation and affects xanthophyll biosynthesis in cyanobacterium synechocystis sp. PCC6803 Cells, Plant Cell Physiol. 56 (2015) 558–571. https://doi.org/10.1093/pcp/pcu199.

[30] R. Rippka, J.J.B.W. Deruelles, J.B. Waterbury, M. A. Herdman, R.Y. Stanier, Generic Assignments, Strain Histories and Properties of Pure Cultures of Cyanobacteria, Microbiology-Sgm. 111 (1979) 1–61. https://doi.org/10.1099/00221287-111-1-1.

[31] J.L. Peixoto, Hierarchical Variable Selection in Polynomial Regression Models, Am. Stat. 41 (1987) 311–313. https://doi.org/10.1080/00031305.1987.10475506.

[32] N. Klebanov, C. Georgakis, Dynamic Response Surface Models: A Data-Driven Approach for the Analysis of Time-Varying Process Outputs, Ind. Eng. Chem. Res. 55 (2016) 4022–4034. https://doi.org/10.1021/acs.iecr.5b03572.

Appendix

Table 2A.1. The values of the actual factors defining the 28 experiments. The last three ones are replicates at the center of the domain

Run #	**Light profiles** ($\mu mol\ m^{-2}\ s^{-1}$)	**Temperature** (°C)	**Phosphorus inflow** ($mg_P\ d^{-1}$)
1	$10+20.9*t+2.12*t^2$	26	$4.6-4.32*t+t^2$
2	$10+30.9t+0.4.78*t^2$	33	2.8-1.19*t
3	$108+44.9*t+1.59*t^2$	33	$1.9-0.7*t+0.06*t^2$
4	$150+48*t-0.53*t^2$	33	$9.1-17.2*t+8.1*t^2$
5	$38+16.3*t+-1.06*t^2$	26	3.03-1.48*t
6	$73+23.6*t-1.59*t^2$	26	$9.1-17.2*t+8.1*t^2$
7	$38+16.3*t-1.06*t^2$	33	$1.9-0.7*t+0.06*t^2$
8	$150+40*t-2.65*t^2$	33	1.9-0.55*t
9	$10+26.9*t+3.71*t^2$	33	$9.1-17.2*t+8.1*t^2$
10	$24+14.6*t-0.53*t^2$	26	6.4*(1-t)
11	$10+30.9*t+4.78*t^2$	26	1-0.25*t
12	$24+34.6*t+4.78*t^2$	26	$9.17-17.27*t+8.1*t^2$
13	10+12.9*t	26	$3.7-6.4*t+2.7*t^2$
14	$150+42*t-2.12*t^2$	26	6.4*(1-t)
15	$136+48.3*t+0.53*t^2$	26	$3.88-3.03*t+0.58*t^2$
16	$150+48*t-0.53*t^2$	26	1-t
17	$150+48*t-0.53*t^2$	33	1-t
18	$38+36.3*t+4.24*t^2$	26	6.4*(1-t)
19	$10+22.9*t+2.65*t^2$	33	6.4*(1-t)
20	$10+26.9*t+3.71*t^2$	26	1-t
21	$136+48.3*t+0.53*t^2$	33	6.4*(1-t)
22	$38+16.3*t-1.06*t^2$	33	1-t
23	$52+38*t+3.71*t^2$	33	$4.6-8.2*t+3.6*t^2$
24	$150+44*t-1.59*t^2$	26	1-0.25*t
25	$55.5+19.9*t-1.33*t^2$	33	$8.88-15.633*t+6.75*t^2$
26	80+31.4*t	29.5	5.5*(1-t)
27	80+31.4*t	29.5	5.5*(1-t)
28	80+31.4*t	29.5	5.5*(1-t)

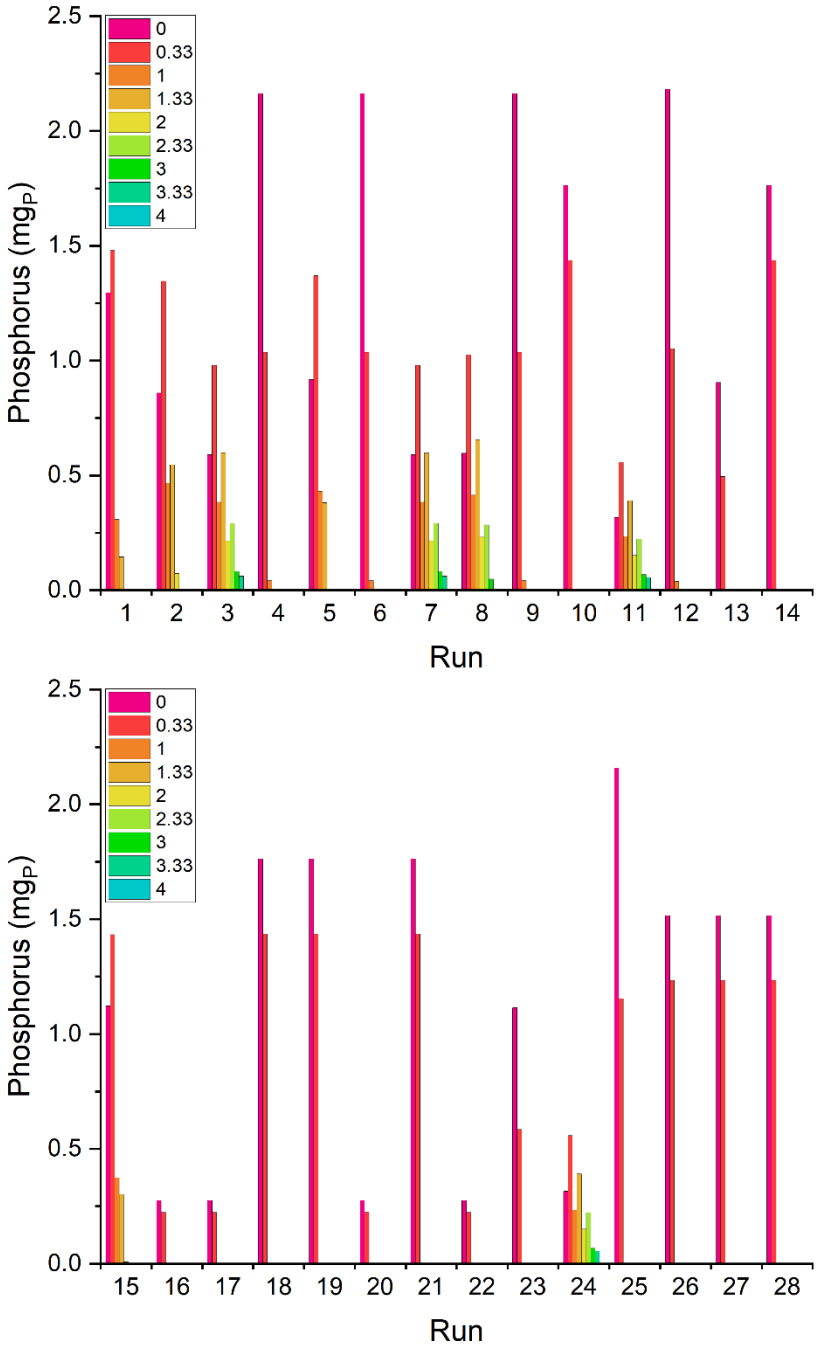

Figure 2A.1. Instantaneous amount of phosphorus (mg_P) for each experimental run at each time instant

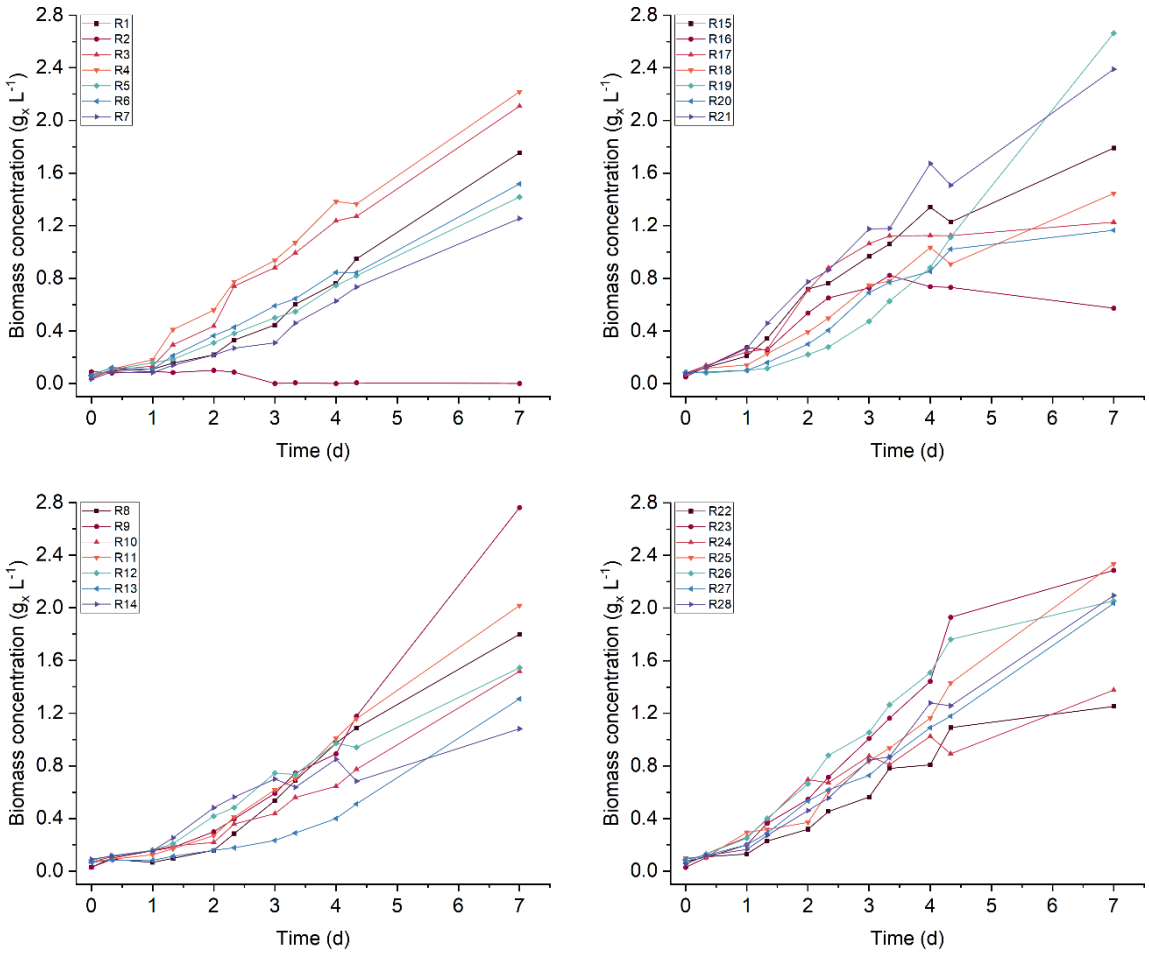

Figure 2A.2. Biomass concentration (g_x L^{-1}) as function of time (d) in semi-batch growth curves of *Synechocystis* sp. PCC 6803. Lines are just eye guides

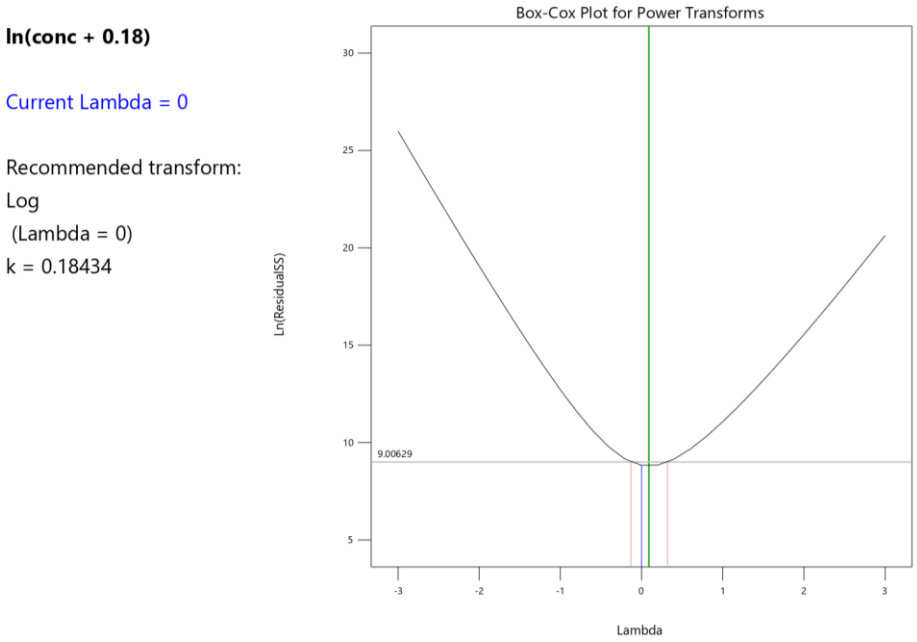

Figure 2A.3. Box-Cox plot of first RSM model

Table 2A.2. Optimal value in terms of coded factors for the first RSM model

Factors	Value
x_1	0.053
x_2	0.175
x_3	-1
x_4	1
x_5	-0.908
x_6	-0.048

Table 2A.3. The values of the actual factors defining the AR1-AR7 experiments

Run #	Light profiles ($\mu mol\ m^{-2}\ s^{-1}$)	Temperature (°C)	Phosphorus inflow ($mg_P\ d^{-1}$)
1	129+44.4*t	25.3	1.00-0.23*t
2	99.6+38.6*t+0.5*t^2	25.3	0.55-0.13*t
3	101.0+37.0*t	25.3	1.90-1.96*t+0.49*t^2
4	76.5+32.5*t+0.5*t^2	25.3	0.55-0.65*t
5	97.2+48.6*t+3.3*t^2	25.3	1.00-1.82*t
6	71.0+40.3*t+3.0*t^2	25.3	1.00-1.18*t
7	142.3+37.8*t-2.69*t^2	38.0	4.94-52.01*t+136.9*t^2

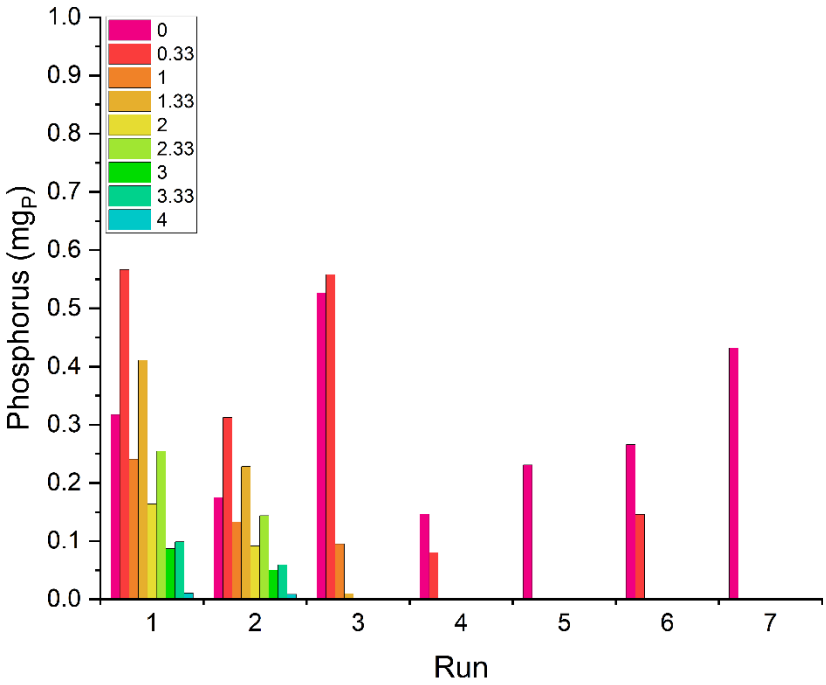

Figure 2A.4. Instantaneous amount of phosphorus (mg_P) for each experimental run AR1-AR7 in an enlarged domain.

Table 2A.4. RSM model in terms of coded variables, and 95% Confidence Interval (CI) for each parameter of the RSM model; p-values and VIF factors for the RSM model.

Terms	β_i	95% CI Low	95% CI High	p-value	VIF
intercept	9.25	6.29	12.21	-	-
x_1	-6.89	-11.44	-2.33	0.0057	6.04
x_2	-1.30	-6.22	3.62	0.5819	4.25
x_3	-5.85	-10.39	-1.31	0.0150	9.84
x_4	-5.28	-7.35	-3.22	<0.0001	2.45
x_5	-4.71	-8.27	-1.15	0.0130	2.09
x_6	-0.16	-2.55	2.24	0.8920	1.28
x_1x_3	-3.67	-7.54	0.21	0.0621	1.72
x_1x_6	7.39	2.10	12.68	0.0094	6.11
x_2x_3	-5.77	-11.27	-0.27	0.0410	4.79
x_3x_4	-7.22	-10.01	-4.43	<0.0001	2.40
x_2^2	-13.01	-20.42	-5.60	0.0020	3.91
x_3^2	-6.61	-11.95	-1.26	0.0188	4.13

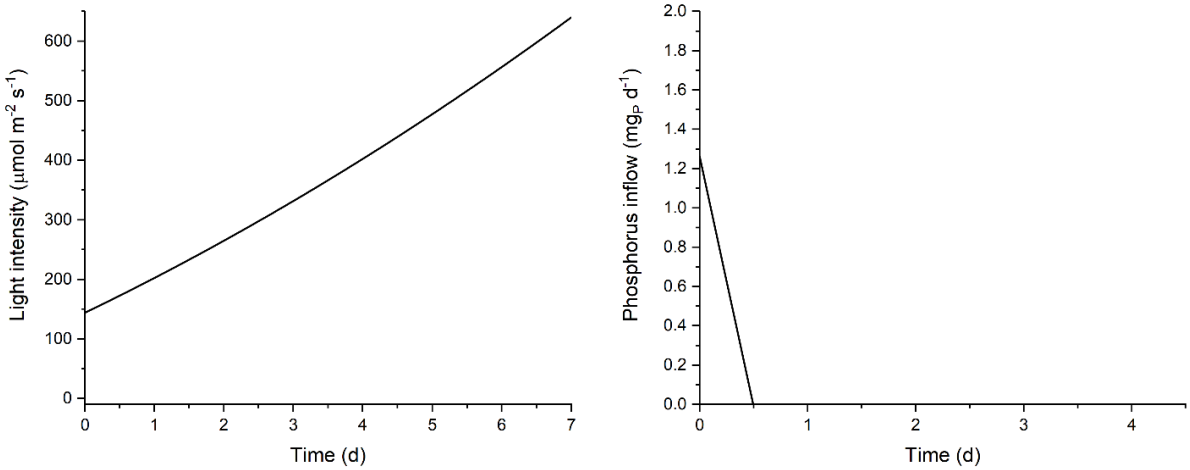

Figure 2A.5. Light intensity profile and phosphorus inflow profile of the optimum.

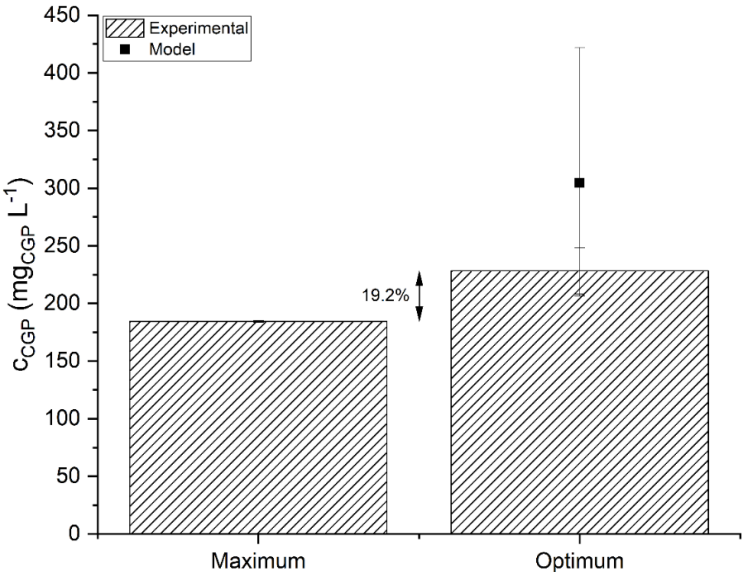

Figure 2A.6. Cyanophycin concentration (c_{CGP}) measured experimentally (*bars*) and predicted by the model (*square*)

Chapter 3

An Experimental Test of the DoDE and DRSM Methodologies: The Growth of a Photosynthetic Microorganism

The design of dynamic experiments (DoDE) and dynamic response surface methodology (DRSM) have been recently applied to accurately model and optimize several types of industrial and pharmaceutical processes. In this study, we apply the methodologies above to the growth of a photosynthetic microorganism, a bioprocess characterized by a high degree of complexity. Compared to conventional bioprocesses involving heterotrophic bacteria, the high adaptability of photosynthetic microorganisms to environmental conditions and the complexity of understanding the effect of light intensity on biomass growth make the development of a thorough knowledge-driven model a difficult task. Based on a pre-defined experimental design taking into account the effect of light, temperature, and nutrient feeding profiles, we performed a set of dynamic biomass growth experiments, from which we estimate different DRSM models. The best one was then used to predict the behaviour of a new set of experiments. We show that through such a model, valuable insights into the process can be gained and that the model is fairly reliable in predicting the growth behaviour under different experimental conditions.

Part of this Chapter was published as a scientific paper in *Industrial and Engineering Chemistry Research* (Trentin, G., Barbera, E., Bertucco, A., Georgakis, C., 2022, https://doi.org/10.1021/acs.iecr.2c01851)

3.1 Introduction

Mathematical models are a valuable tool to aid in designing, optimizing, and controlling industrial chemical and biochemical processes. When possible, knowledge-driven or "first-principles" models are developed, which allow a detailed description of the inner workings of a process. They can be used in several tasks, including process optimization. However, their development requires a significant investment of time and resources, which may not be justifiable for processes characterized by small production scales or niche applications. Data-driven models quantify only the relationship between the input and output process variables. This is achieved by performing a well-designed set of experiments on the process of interest and using the collected data to estimate the model parameters. Even though we are not increasing our understanding of the process's inner workings, this is a valuable and cost-effective alternative route to achieve the optimization of a process, especially a batch process.

A classical data-driven approach to guide the experimental campaign is the Design of Experiments (DoE) methodology [1], which defines the minimum number of experiments necessary to estimate a particular type of model. Such a model is obtained through the Response Surface Methodology (RSM), which, utilizing linear regression tools, allows to statistically estimate the relationship between input variables, called factors, and one or more output variables, called responses. The classical DoE and RSM methodologies consider only time-invariant, "static" or "fixed" input factors and relate them to a single or multiple outputs measured at a given time. This fails to capture the dynamic nature of the batch or semi-batch process. The DoE methodology has been recently generalized to incorporate time-varying input and output variables. The first generalization is called Design of Dynamic Experiments (DoDE) and allows the use of time-varying input factors, such as feeding time profiles [2]. The second generalization, called Dynamic Response Surface Methodology (DRSM), allows the description of time-evolving output measurements, thus greatly extending the applicability of data-driven models [3–5].

In previous publications, the effectiveness of the DRSM modelling methodology for process optimization was proven in silico for different industrial processes of interest, including pharmaceutical applications as well as polymerization reactions [4–6]. In this paper, we aim to experimentally test the accuracy and effectiveness of the DRSM approach to model the growth of photosynthetic microorganisms (such as microalgae or cyanobacteria) in batch or semi-batch systems. For such biological processes, developing

a knowledge-driven model is a difficult task, requiring the quantification of complex phenomena involving the effect of light intensity and other environmental factors on the physiology of the cells and consequently on their growth. The complexity is even increased in batch/semi-batch cultivation systems, where the biomass concentration and other compositions change over time. Consequently, so does the light availability per cell, which is the driving force for photosynthesis. Here, we demonstrate the usefulness and accuracy of the DRSM approach by applying it to the growth of *Synechocystis* sp. PCC 6803, which is a model cyanobacterium of industrial interest due to its potential as a cell factory for the production of valuable compounds [7,8]. We take advantage of an actual experimental campaign carried out according to a DoDE set of experiments specifically designed to optimize the accumulation of a particular compound of interest within the biomass. Here, our main process interest is the biomass concentration, measured at different instants throughout the batch. We then derive two initial variations of the DRSM model to describe the dynamic growth of the cyanobacterium as a function of the input factors. The two models differ in the number of two-factor interaction terms as well as the retention of quadratic terms in the model structure. We check the validity of these models by comparing their prediction of the time evolution of four additional experiments carried out for cross-validation purposes.

A third model where all two factor interaction (2FI) terms are given an equal chance to contribute significantly to the model is also estimated. Because the parameter estimation algorithm of the 3.0 version of the DRSM modelling methodology uses LASSO regression [9,10], the model retains only a set of the original terms. Through a follow up significance test a further reduction in the number of model terms takes place. A comparison among the final terms of these three models demonstrates that they have only minor differences.

3.2 The DRSM and DoDE Methodologies

A DRSM model has the same form as a traditional RSM model, but the model parameters are instead parametric functions of time. For example, a quadratic DRSM model is written as follows:

$$y(\theta) = \beta_0(\theta) + \sum_{i=1}^{n} \beta_i(\theta) x_i + \sum_{i=1}^{n} \sum_{j=i+1}^{n} \beta_{ij}(\theta) x_i x_j + \sum_{i=1}^{n} \beta_{ii}(\theta) x_i^2 \quad (3.1)$$

The dynamic response of interest, $y(\theta)$, is a function of an exponentially transformed dimensionless time $\theta = 1 - \exp(-t/t_c)$, where t_c is an appropriately selected constant

[4]. The variables x_i represent the input factors, which can be either fixed factors as in the classical DoE [1], or dynamic subfactors as in the DoDE approach. The parametric functions of the model are $\beta_q(\theta) \mid q = 0, i, ij, \text{or } ii$ and are parametrized with shifted Legendre polynomials, as follows:

$$\beta_q(\theta) = \gamma_{q,1}P_0(\tau\theta) + \gamma_{q,2}P_1(\theta) + \cdots + \gamma_{q,R+1}P_R(\theta) \tag{3.2}$$

Here $P_i(\theta)$ represents the i^{th} shifted Legendre polynomial order $i \in (0, \ldots, R)$ in the dimensionless time θ. The $\gamma_{q,i}$ constants are the model parameters to be estimated by linear regression. Besides the quadratic model reported above as an example, other types of DRSM models can be used, such as the two-factor interaction (2FI) model. This model lacks the pure quadratic terms, $\beta_{ii}(\theta)x_i^2$ of Eq. (3.1). It has been observed [4] that a polynomial dependence on a transformed time (θ) instead of the original time (t) results in a more accurate DRSM model.

As mentioned above, in a DoDE design several of the factors x_i represent dynamic subfactors that parametrize a time-varying input profile, called the dynamic factor, $u(\tau)$, expressed as follows:

$$u(\tau) = u_0(\tau) + \Delta u_0(\tau)w(\tau), \text{ with } -1 \leq w(\tau) \leq +1 \tag{3.3}$$

Here, $\tau = t/t_f$, is a dimensionless time where t_f is the duration of the batch experiment. The function $u_0(\tau)$ represents a reference input profile, while $\Delta u_0(\tau)$ denotes the maximum positive or negative deviation from this reference profile, defining the time-varying domain within which examples of the dynamic factor $u(\tau)$ should lie in. Finally, $w(\tau)$ represents the coded version of the dynamic factor. It is parametrized through a linear combination of n shifted Legendre polynomials, besides the first constant one, P_0:

$$w(\tau) = \sum_{i=0}^{n} x_{i+1}P_i(\tau) \tag{3.4}$$

The values of n can be as high as one wishes. However, this increases the number of dynamic subfactors x_i and, *in tandem*, the number of experiments that are needed to estimate the increased number of model parameters. Typically, up to four of five and in some special cases six polynomials have been used. To ensure that $-1 \leq w(\tau) \leq +1$ the values of the x_i could be constrained by [2]:

$$-1 \leq x_1 \pm x_2 \pm \cdots \pm x_n \leq +1 \tag{3.5}$$

This is a sufficient condition but not a necessary one for $n \geq 3$. Then a very close approximation to the necessary condition can be achieved by a set of n_k conditions, such as in Eq. (3.6), can be imposed instead of Eq. (3.5).

$$-1 \leq x_1 P_0(\tau_k) + x_2 P_1(\tau_k) + \cdots + x_n P_{n-1}(\tau_k) \leq +1 \tag{3.6}$$

One can select, for example, $n_k = 21, n_k = 41,$ or $n_k = 101$ equidistant values of τ_k in the $(0, 1)$ interval. Often 21 or 41 values are sufficient.

3.3 The DoDE design

We define here the experimental factors that we will consider. The first dynamic factor is $I(\tau_1)$ the time-varying strength of the incident light. It is defined with respect to the dimensionless time $\tau_1 = t/t_I$, where $t_I = 7\ d$ is the duration of light exposure equal to the common duration of $7\ d$ for all experiments. This dynamic factor varies with time as follows:

$$I(\tau_1) = I_0(\tau_1) + \Delta I(\tau_1) w_1(\tau_1), \text{ with } -1 \leq w_1(\tau_1) \leq +1 \tag{3.7}$$

With $I_0(\tau_1) = 80 + 220\tau_1$, and $\Delta I(\tau_1) = 70 + 130\tau_1$, denoting that the incident light will vary between 10 and 150 µmol photons m^{-2} s^{-1} at day 0, and between 100 and 500 µmol photons m^{-2} s^{-1} at day 7. The coded dynamic factor $w_1(\tau_1)$ is parametrized with two dynamic factors:

$$w_1(\tau_1) = x_1 + x_2(-1 + 2\tau_1), \text{ with } -1 \leq x_1 \pm x_2 \leq +1 \tag{3.8}$$

To ensure that the light profile is strictly increasing with time, an inequality constraint must be imposed such that $\frac{dI(\tau_1)}{d\tau_1} = \frac{d}{d\tau_1}\{I_0(\tau_1) + \Delta I(\tau_1) w_1(\tau_1)\} > 0$, that is satisfied if the following inequality is satisfied:

$$1.69 + x_1 + 4.08x_2 > 0 \tag{3.9}$$

The temperature is a time-invariant (traditional) factor, x_3, kept constant at a specific value between 26 and 33°C throughout each experiment.

$$T = 29.5 + 3.5x_3, \text{ with } -1 \leq x_3 \leq +1 \tag{3.10}$$

The second dynamic factor is related to the time-varying profile defining the addition of phosphorus to the reactor. For simplicity, it will be assumed to also be linear with time. However, the feeding duration will not be the same in all experiments, defined by the following equation through the fourth codded factor x_4:

$$t_f = 2.5 + 1.5x_4, \text{ with } -1 \leq x_4 \leq +1 \tag{3.11}$$

Using the feeding time t_f as a reference we define a new dimensional time $\tau_2 = t/t_f$. Then the phosphorous feeding profile is:

$$u_2(\tau_2) = u_{20}(\tau_2) + \Delta u_2(\tau_2) w_2(\tau_2) \tag{3.12}$$

with $u_{20}(\tau_2) = 5.5(1 - \tau_2)$ and $\Delta u_2(\tau_2) = 4.5(1 - \tau_2)$. Here $w_2(\tau_2)$ is also expressed in terms of the first two shifted Legendre polynomials:

$$w_2(\tau_2) = x_5 + x_6(-1 + 2\tau_2), \text{ with } -1 \leq x_5 \pm x_6 \leq +1 \tag{3.13}$$

Furthermore, the total amount of phosphorous to be fed is constrained between 0.33 and 3.3 mg_P, which results in the following non-linear inequality constraints:

$$-3.5 \leq 2.2x_4 + (1 + 0.6x_4)(3x_5 - x_6) \leq -1.9 \tag{3.14}$$

The inequality constraints of Eq. (3.9) and Eq. (3.14) are forcing the domain to have an irregular shape. This makes the use of classical factorial and fractional factorial designs unattractive. Here we design a D-Optimal design with the six factors defined above and the related inequalities they must observe. We aim for a two-factor interaction (2FI) model, which requires 25 distinct experiments. We arrive at the above number of experiments by first observing that the 2FI model with six factors has 22 (=1+6+15) parameters to be estimated. To these, we add three more distinct experiments to be able to estimate the Lack-of-Fit (LoF) statistic, for a total of 25. We further add three replicated experiments at the center of the domain to help us estimate the normal variability of the process. The values of the coded factors $x_1, x_2, \ldots x_6$ for each of the 28 experiments are reported in Table 3A.1 of Appendix. Light intensity profiles (μmol photons m^{-2} s^{-1}) versus time for the 28 experiments are plotted in Figure 3.1. The corresponding ones for the phosphorus inflow profiles (mg_P d^{-1}) are shown in Figure 3.2.

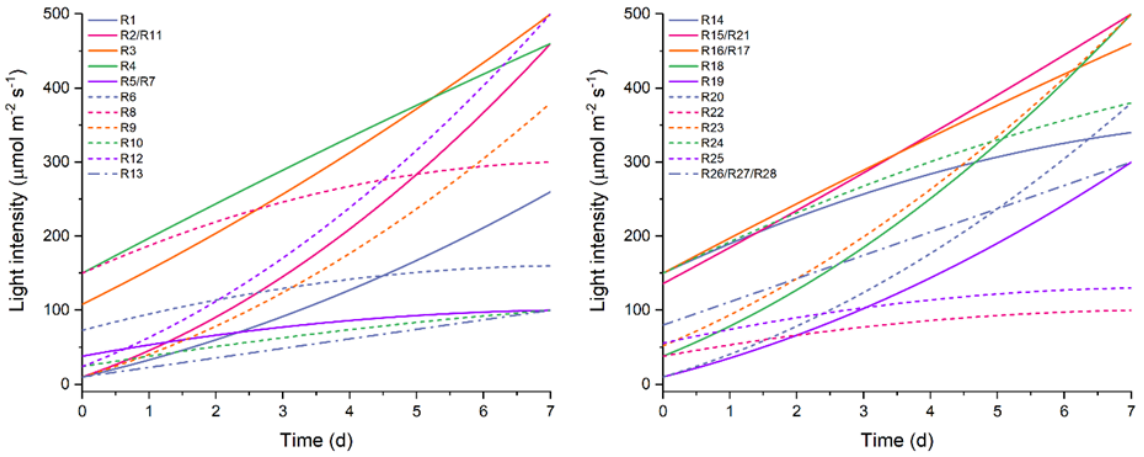

Figure 3.1. Light intensity profiles versus time for the 28 experiments. Several of the experiments have identical profiles, as indicated in the Legend

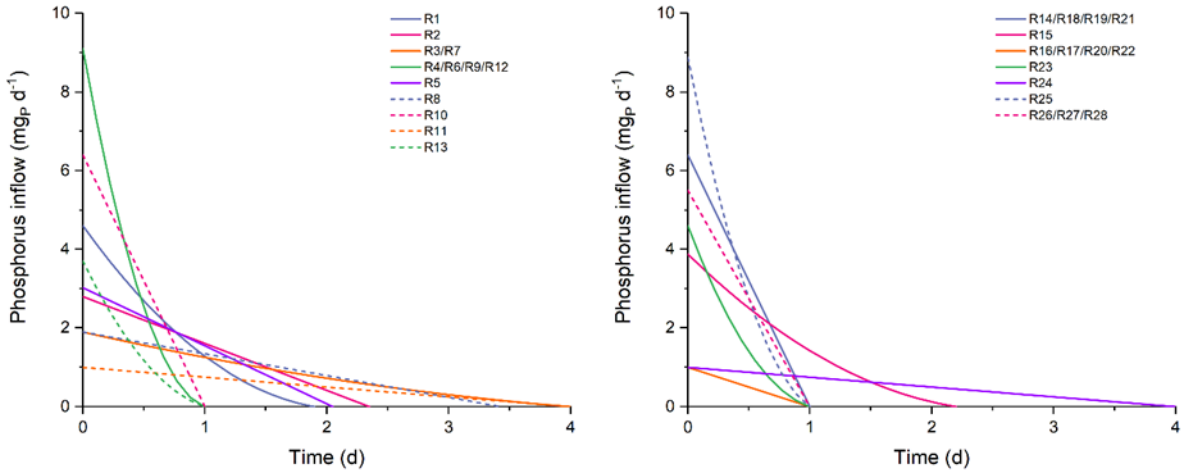

Figure 3.2. Phosphorus inflow profiles versus time for the 28 experiments. Several of the experiments have identical profiles, as indicated in the Legend

The amount of phosphorus will be added as a bolus at the following instants 0.00, 0.33, 1.00, 1.33, 2.00, 2.33, 3.00, 3.33, and 4.00 days. This is because of experimental constraints. The amount of each bolus is calculated to be the integral of the designed profile between the present time and the next time when phosphorus is introduced. So, the phosphorus bolus at t=0, is equal to $PB(0) = \int_0^{0.33} u_2(t/t_f)dt$ and at t=0.33 is equal to $PB(0.33) = \int_{0.33}^{1} u_2(t/t_f)dt$, and so on. There are no modeling ramifications, as long as the translation from continuous feeding profiles to the amount of bolus implied above is applied consistently. It is true that this relationship does not have a unique inverse relationship, but this does not present a limitation. It would have been a limitation if we were trying to represent historical data of bolus feeding with our specific linear representation.

The continuous function representation results in fewer experiments. It needs only three factors, $x_4, x_5,$ and $x_6,$ as defined earlier. The alternative through a classical DoE design would have been to define eight traditional factors representing the amount of phosphorus at each time instant bolus, some of which would have been forced to be zero. These eight factors would have required more experiments than the three used here.

3.4 Experimental setup

Synechocystis sp. PCC 6803, from Pasteur Culture collection of Cyanobacteria (France) was cultivated in sterilized freshwater medium (BG11) [11] without phosphorus (which was added separately to each experiment according to the designed profiles), and modified by substituting the organic buffer HEPES with 1.5 g L^{-1} of sodium bicarbonate, to maintain the pH within the range of 7.5-8, optimal for the cyanobacterial growth. The pH was monitored daily using a Hanna portable pH meter (code HI9124).

Maintenance and propagation of axenic culture and experiments were carried out in Quickfit® Drechsel bottles with a volume of 200 mL and a diameter of 5 cm. A CO_2-air (5:95 v/v) mixture was fed to the reactor by continuously bubbling it at the bottom of the bottle, for the overall duration of the growth curve. The total gas flow rate was 1 L h^{-1}. Additionally, to ensure good mixing within the reactor, a magnetic stirrer was used to prevent any deposition of biomass. To ensure culture axenicity, all the equipment used and the fresh medium were sterilized in an autoclave at 121°C for 20 min.

Each experiment was carried out following a standardized procedure. A constant biomass inoculum (0.080 mg_x L^{-1}) taken from a preinoculum renewed weekly was resuspended in 200 mL of fresh medium, with the P concentration required by the design at t=0 d. Then, phosphorus was added twice per day at 8 AM and 4 PM. The discrete amounts of P added at each time corresponded to the integrals of the continuous profiles reported in Figure 3.2, calculated between time t_k and time t_{k+1} (Figure 3A.1, Appendix). Sterility of the inoculum was verified regularly by plating samples on Luria Bertani Petri dishes. The reactor temperature was maintained constant at the required value using a thermostatic bath. Artificial light was provided by a LED lamp (Photon Systems Instruments), connected to a controller to modulate the incident light intensity according to the designed profiles. Light was measured using a photoradiometer (HD 2101.1 from Delta OHM), which quantifies the Photosynthetically Active Radiation (PAR, 400-700 nm). The experimental set-up is shown in Figure 3.3.

Figure 3.3. Experimental set-up: batch photobioreactor, LED lamp, LED controller

To measure the growth of the microorganisms, the value of the optical density at 750 nm (OD_{750}) was checked twice per day at 8 AM and 4 PM. The measurement was done by a double beam spectrophotometer (UV1900, by Shimadzu, Japan) with 1 cm optical path length at a wavelength of 750 nm, which is outside the absorption range of chlorophyll and other photosynthetic pigments, therefore accounting for scattering effects only. In addition, the dry cell weight concentration of biomass (c_x, $g_x\ L^{-1}$) was measured daily, at the same time (8 AM) each day. A known volume of culture sample was filtered through a 0.22 μm previously dried and weighed nitrocellulose filter, which was then dried for 2 h at 105°C in a laboratory oven. From a linear correlation between OD_{750} and c_x (Figure 3A.2, Appendix), the value of biomass concentration was obtained also at 4 PM. During weekends no measurements were taken so eventually 11 measurements (time 0 d + 10 measurement instants) are available for each 7-days experimental run.

3.5 The DRSM model

In this section, we will describe the estimation of the DRSM model. We have enough data to estimate a DRSM model with all the two-factor interaction (2FI) terms, and we will do so later. However, the possibility exists that some of the 2FI terms might be insignificant.

This might allow us to estimate some of the quadratic model terms as significant. Because the DRSM algorithm uses a LASSO regression algorithm for the estimation of the values of the gamma (γ) parameters and a test of significance for the non-zero gammas, the completely insignificant 2FI terms could be eliminated. Because the above stepwise regression in estimating the DRSM parameters is a backwards one, quadratic terms cannot be considered as there are not enough experiments for the initial estimation of all the parameters in a quadratic DRSM form. For this reason, an alternative route is explored to obtain the most accurate DRSM model for the experiment data at hand.

Because data have been collected at a set of well-determined instants, we are able to estimate one RSM model for each of the ten measurement instants: 0.33, 1.00, 1.33, 2.00, 2.33, 3.00, 3.33, 4.00, 4.33, 7.00. This is done in the DesignExpert® software, using a BIC forward stepwise regression in which quadratic terms are added as candidates for inclusion in the model. Since this is a forward approach one can have as initial model candidates the 28 possible terms of the quadratic model using the 25 district experimental conditions. One should note here that even though there are 26 distinct experiments defined in Table 3A.1, run R2 provided reliable data up until $t = 2.33\ d$ and therefore it is not included in the estimation of the ten RSMs. The structure of the estimated RSM models is summarized in Table 3.1. Terms included in the model are marked with an "X". If they are in a light-red shaded cell they were not initially in the model but were added during the Analysis of Variance (ANOVA) step for hierarchical reasons. Terms marked with an "o" in a light-blue shaded cell were removed from the model because they had a VIF value higher than 10. We note that the x_1x_3, x_4x_5, x_4x_6, x_5x_6 terms do not appear in any of the models. On the other hand, the x_3^2 term, representing temperature, appears in 8 of the 10 models, while the x_2^2 and x_4^2 terms appear in two RSMs and x_1^2 in only one. The existence of several quadratic terms in each of the 10 RSMs strongly indicates the existence of curvature. The most important statistical characteristics of these 10 models are given in Table 3.2.

We note that in the first nine of the ten models, the Lack-of-Fit p-value is larger than 0.05, indicating no lack of fit. This implies that the corresponding models have represented all the information on the data besides the normal variability of the process, which is estimated from the replicated runs. The R_{adj}^2 values range from 0.72 to 0.85, indicating that the normal variability of the process is not small as it often is the case in cell processes. Removing some model terms, marked with a light blue cell in Table 3.1, has kept the Variability Inflation Factor (VIF) below 5.00.

Table 3.1. The structure of the 10 RSM models estimated at the ten measurement instants, using the BIC Forward Stepwise regression. Terms included in the model are marked with an "X". Terms with light red shaded cell were added for hierarchy reasons. Terms marked with a "o" in a light blue shaded cell were removed from the model because they had a VIF value higher than 10

#	Time (d)	x_1	x_2	x_3	x_4	x_5	x_6	x_1x_2	x_1x_3	x_1x_4	x_1x_5	x_1x_6	x_2x_3	x_2x_4	x_2x_5
1	**0.33**	X	X	X	X	X	X	X				X			X
2	**1.00**	X	X	X	X	X	X	X		X	X	X	X		
3	**1.33**	X	X	X	X	X		X							
4	**2.00**	X	X	X	X			X							
5	**2.33**	X	X	X	X	X									
6	**3.00**	X	X	X		X		X							X
7	**3.33**	X	X	X	X	X		X							X
8	**4.00**	X	X	X	X	X	X	X							
9	**4.33**	X	X	X	X	X		X						X	X
10	**7.00**	X	X	X	X	X	X			X	X				X

#	TIME	x_2x_6	x_3x_4	x_3x_5	x_3x_6	x_4x_5	x_4x_6	x_4x_6	x_1^2	x_2^2	x_3^2	x_4^2	x_5^2	x_6^2
1	**0.33**		X	X							X			
2	**1.00**	X	X	X	X	o	o							
3	**1.33**		X	X						X	X			
4	**2.00**		X							X	X			
5	**2.33**		X			o					X			
6	**3.00**		X								X			
7	**3.33**		X								X			
8	**4.00**	X	X						X		X	X		
9	**4.33**		X								X	X		
10	**7.00**		X				o						o	o

Table 3.2. Statistical characteristics of the estimated 10 RSM models

#	Time (d)	LoF *p*-value	R^2_{adj}	BIC	AICc	max (VIF)
1	0.33	0.44	0.76	-160.0	-149.0	4.2
2	1.00	0.82	0.75	-80.0	-46.4	5.3
3	1.33	0.83	0.72	-60.6	-57.2	4.8
4	2.00	0.89	0.85	-46.1	-45.4	3.8
5	2.33	0.98	0.79	-32.9	-34.0	1.6
6	3.00	0.94	0.82	-26.3	-25.5	2.0
7	3.33	1.00	0.78	-21.3	-20.5	2.0
8	4.00	0.96	0.84	-11.4	-0.3	2.5
9	4.33	1.00	0.79	-2.1	4.6	4.8
10	7.00	0.02	0.84	15.8	22.5	4.1

Utilizing the information obtained from the ten RSM models, we define two DRSM models, A and B. Model A has as candidate terms all entries in Table 3.1 that appear in more than two RSMs. They include the six individual factors $x_1, x_2, x_3, x_4, x_5, x_6$, the following 2FI terms x_1x_2, x_1x_4, x_1x_5, x_1x_6, x_2x_5, x_2x_6, x_3x_4, x_3x_4, x_3x_5 and the x_2^2, x_3^2, x_4^2 quadratic terms. Figure 3.4 depicts model A's predictions and its prediction interval against the experimental points. It is noted that only the first six data points on the second experiment were used, as all others were considered as faulty data and were removed. Nevertheless, the DRSM model leverages degrees of freedom from the time-series data across the design space and stepwise regression to identify the significant terms. This allows the model to estimate the data that may have been collected in experiment R2. This is a significant advantage of the DRSM model. Out of the initial 21 $\beta_q(\theta)$ parametric functions of the related model terms, only 12 were retained as significant in the final model. They are: $\beta_0(\theta), \beta_1(\theta), \beta_2(\theta), \beta_3(\theta), \beta_4(\theta), \beta_5(\theta), \beta_{12}(\theta), \beta_{14}(\theta), \beta_{25}(\theta), \beta_{34}(\theta), \beta_{33}(\theta)$ and $\beta_{44}(\theta)$.

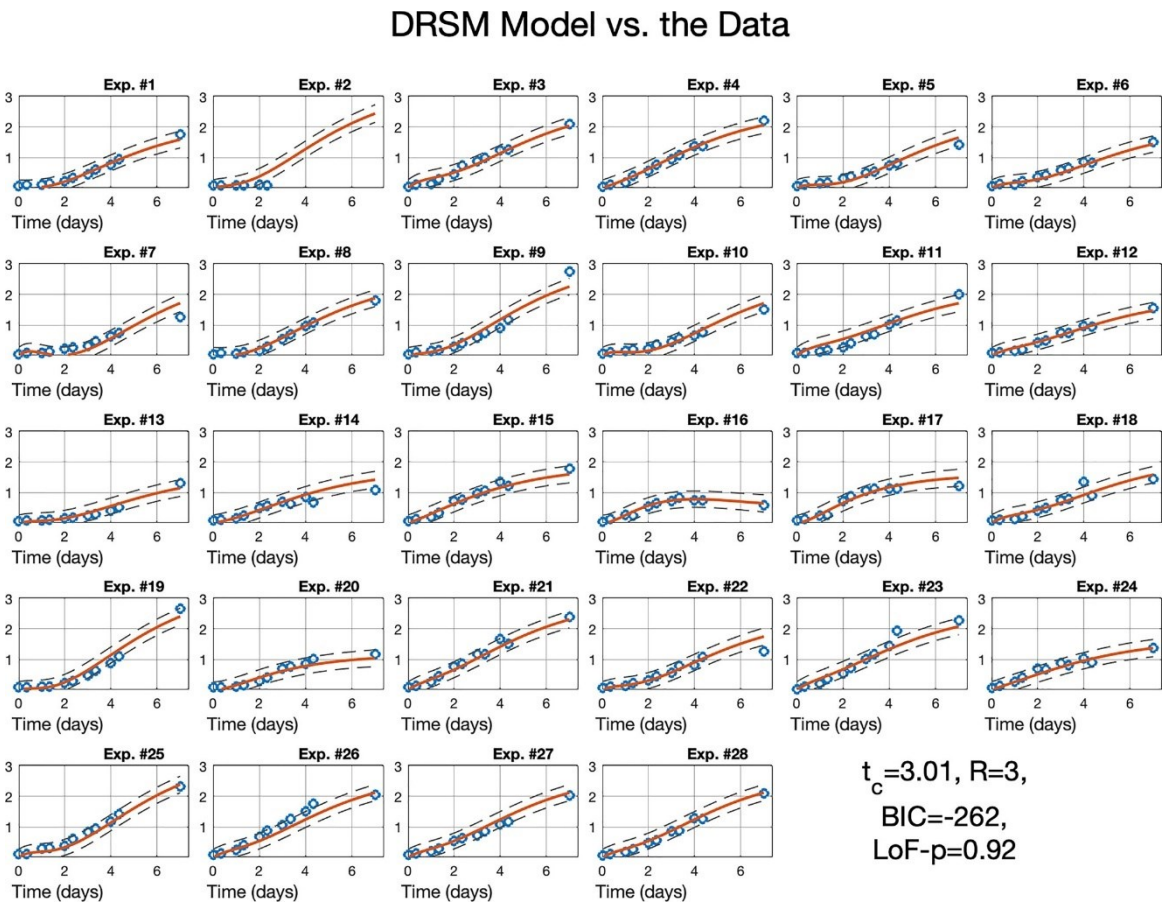

Figure 3.4. Nominal predictions and corresponding prediction intervals of Model A against the experimental data in 28 experiments

Model B has the same initial terms as Model A and three additional terms appearing in only one of the ten RSM, Table 3.2. These are the x_2x_3, x_3x_4, x_3x_6 and x_1^2 terms. A visual comparison between Figure 3.4 and the corresponding one for Model B, offered in the Appendix (Figure 3A.3), reveals very little difference between the two models. Even though Model B started with 22 candidates, only 11 $\beta_q(\theta)$ parametric functions remain in the model as significant. They are the 12 above minus the $\beta_{33}(\theta)$ one.

Table 3.3. Statistical Characteristics of three DRSM models

Name	t_c	Number of significant out of Initial $\boldsymbol{\beta(\theta)}$	Number of significant out of Initial gammas (γ_{ij})	BIC	$p(LoF)$
Model A	3.01 d	12/18	26/54	-261.89	0.92
Model B	3.20 d	11/22	24/66	-246.06	0.86
2FI Model	3.00 d	12/22	24/66	-221.15	0.76

Table 3.3 lists some statistical characteristics of these two models. Model A has a slightly smaller BIC value, with 26 significant gamma parameters out of the initial 54. By comparison, Model B has 24 significant gammas out of 66 initially. In the same table, we present the corresponding statistical characteristics of a third model, Model C, that started with all 22 terms, linear and 2FI ones. It retained as significant 12 terms and 24 significant gammas out of 66 initially. This model has no chance of retaining quadratic terms like β_{33} and β_{44} in Model A and β_{44} in Model B. The figure depicting the model predications of this third DRSM model (Model C) against the collected data, corresponding to Figure 3.4 for Model A above, is given in the Appendix (Figure 3A.4).

In the same table, one can see that the Lack-of-Fit p-value for model A is the largest. We conclude that model A has the best statistical scores though its superiority over the other two is not that large. The close similarity of these three models reveals the robust characteristics of the DRSM modeling algorithm in retaining only the significant model parameters, with minor differences in the final model.

The time dependence of the DRSM model is a linear combination of shifted Legendre polynomial on the dimensional time θ, $0 \leq \theta \leq 1$, where θ is an exponential transformation of time t: $\theta = 1 - \exp(-t/t_c)$, for an appropriately selected value of t_c [4]. There is important information in the estimated parametric functions $\beta_q(\theta)$ or $\beta_q(t)$ and their dependency on the original (t) or the transformed time (θ). Their expressions in θ are given in Eq. (3.15) and their dependence on t is plotted in Figure 3.5. For Model A, one notes that we have $\theta = 1 - \exp(-t/3.01)$.

$$\begin{aligned}
\beta_0 &= 1.36\theta - 3.90\theta^2 + 6.22\theta^3 & \beta_{12} &= 12.96\theta - 7.39\theta^2 + 4.93\theta^3 \\
\beta_0 &= 1.36\theta - 3.90\theta^2 + 6.22\theta^3 & \beta_{14} &= -0.08\theta + 0.24\theta^2 \\
\beta_2 &= 0.063\theta & \beta_{25} &= -0.30\theta \\
\beta_3 &= -0.35\theta - 0.58\theta^2 + 1.07\theta^3 & \beta_{34} &= -0.15\theta \\
\beta_4 &= 0.53\theta - 2.46\theta^2 + 2.32\theta^3 & \beta_{34} &= -0.15\theta \\
\beta_5 &= 0.62\theta - 3.36\theta^2 + 3.70\theta^3 & \beta_{44} &= 0.54\theta - 0.98\theta^2
\end{aligned} \tag{3.15}$$

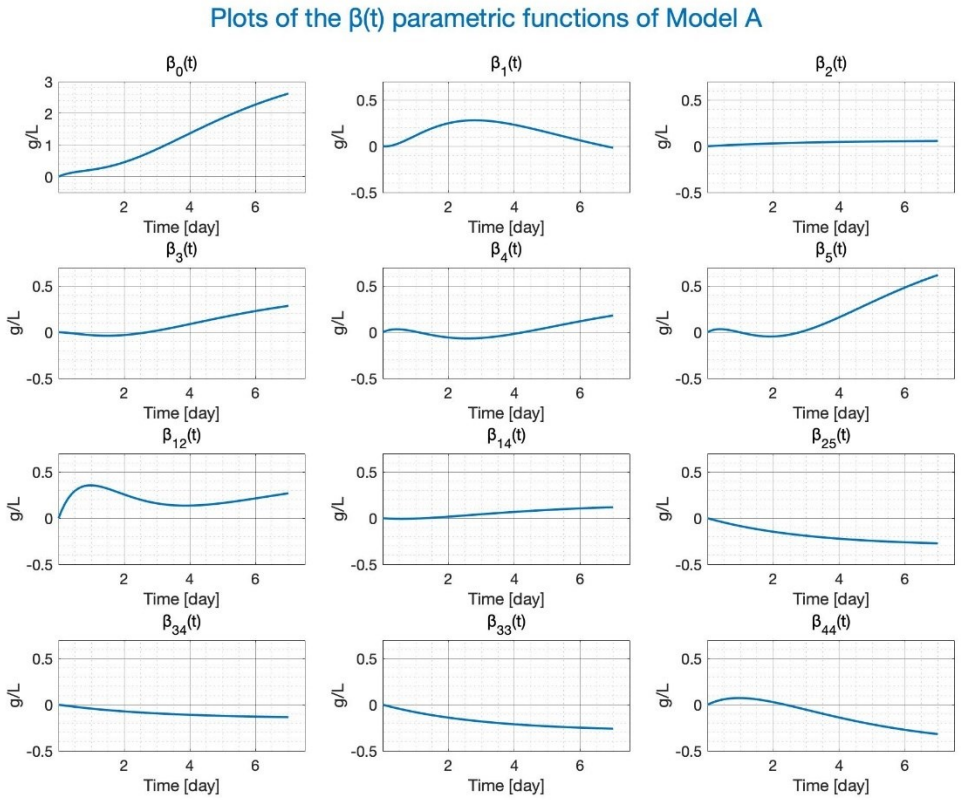

Figure 3.5. The dependence of the parametric functions $\beta_i(t)$ on time. To assess the relative magnitude, all of them, besides $\beta_0(t)$, have the same y-axis scale.

We observe that the most significant effect on the model output is exercised by the x_1 and x_5 factors, representing the amount of light and the amount of phosphorous fed to the process. One also notes a significant effect of the cross term x_1x_2, corresponding to the $\beta_{12}(t)$ parametric function. Because of the time-dependent nature of the DRSM model through the $\beta_q(t)$ functions, we observe that the light effect, represented by $\beta_1(t)$ function, is largest between days 2 and 4, and the most significant impact of the phosphorous fed ($\beta_5(t)$) is between days 4 and 7. Both effects are positive, indicating that more light at earlier times and more phosphorus at later days are desired. The latter indication is

consistent also with the trend of $\beta_4(t)$, i.e., the factor related to the duration of the phosphorus feeding profile, which has a very slight sinusoidal shape. It shows a slightly positive effect in the first two days (although values are nearly zero), and a more relevant positive effect starting from the fourth day. Both the trend of $\beta_4(t)$ and $\beta_5(t)$ are consistent with the mechanism of phosphorus uptake carried out by photosynthetic microorganisms. Indeed, microalgae and cyanobacteria have the capability to sequester more phosphorus from the environment than that immediately necessary for growth at a fast rate, storing it inside the cells. These intracellular phosphorus reserves are accumulated as polyphosphate granules, and can be used as a phosphorus source when phosphate becomes depleted in the surrounding medium [12]. Thus, the trend of $\beta_4(t)$ and $\beta_5(t)$ would explain why feeding phosphorus becomes more important after the fourth day: according to this specific design, phosphorus was supplied up to day 4 only, so that it was stored and/or used by the microorganisms in the initial days, becoming limiting in the latest growth stage. In fact, the almost zero values of $\beta_4(t)$ and the predominately negative values of $\beta_{44}(t)$ imply there exists an optimal duration of phosphorous feeding. With the following rough estimates of $\beta_4(7) = 0.2, \quad \beta_{44}(7) = -0.3$, the optimal value of x_4 alone is equal to $x_4^* = 0.2/2 \times 0.3 = 0.33$, within the range considered $-1 \leq x_4 \leq +1$.

However, we point out that this specific experimental design was not originally made to maximize the biomass production, so the optimal feeding time could be affected by domain considered in the design itself. For this reason, optimizing the process to maximize the amount of biomass produced was not the primary aim of the present paper. To achieve this goal, as the parametric functions indicate, more experiments should be performed in an enlarged domain, extending the phosphorus feeding time through the end of the batch duration. Moreover, increasing feeding profiles should be considered as well, rather than strictly decreasing ones, as was the case in this study. Note that also the nitrogen feeding profile (i.e., the second most important macronutrient in algal cultivation) should be taken into account and optimized, thereby requiring substantial additional work. Nonetheless, based on the results of this study, we are confident that the DRSM approach would be extremely helpful in this regard.

As regards the quadratic terms, because $\beta_{11}(t)$ and $\beta_{22}(t)$ for factors x_1 and x_2 have been estimated as non-significant, the conclusion is that the maximal possible light is desirable, at least, within the ranges considered in this set of experiments. The positive values of $\beta_{12}(t)$ at earlier times also implies that the incident light amount should have a steeper

increasing rate earlier than later. This is also consistent with the typical trend of cell growth, which is initially exponential, followed by a slower growth rate, until reaching a stationary phase when one of the substrates becomes limiting. As the biomass concentration increases at a steeper rate in the earlier days, light intensity should follow the same trend to avoid self-shading phenomena.

In the Appendix we present two additional figures related the Figure 3.5 above. Figure 3A.5 plots the time dependences of the $\beta_q(t)$ parametric functions of model B. One can notice that they are very similar to the one for model A given in Figure 3.5. Furthermore, Figure 3A.6 presents the difference $\beta_B(t) - \beta_A(t)$ between the corresponding $\beta_q(t)$ perimetric functions of model A and B. Here the same y-axis range is used as it was in Figures 3.5 and 3A.5. It is thus obvious that these differences are minimal, most of them very close to zero implying minimal differences between models A and B. The same can be argued about the differences with Model C.

3.6 Cross-Validation

To check the model's accuracy, four additional experiments were designed and performed inside the original domain. The data collected were not used to estimate the model parameters but only to check whether they agree with the estimated model predictions. Here we use Model A. The values of the coded factors defining these four cross-validation experiments are given in Table 3.4. The corresponding light intensity profiles (μmol m^{-2} s^{-1}) and phosphorus inflow profiles (mg_P d^{-1}) versus time for the 4 experiments are reported in the Appendix (Figure 3A.7).

Table 3.4. Statistical Characteristics of three DRSM models

Run #	x_1 *Light: 1st subfactor*	x_2 *Light: 2nd subfactor*	x_3 *Temperature*	x_4 *P inflow duration*	x_5 *P inflow: 1st subfactor*	x_6 *P inflow 2nd subfactor*
V1	0.8	0.2	1	-0.5	-0.5	-0.2
V2	0.4	0.1	1	-1	-0.6	-0.4
V3	0.6	0.15	-1	-1	-0.9	-0.05
V4	0.2	0.05	-1	-0.9	-0.3	-0.6

The plots of the Model A predictions against the data of these four runs are given in Figure 3.6.

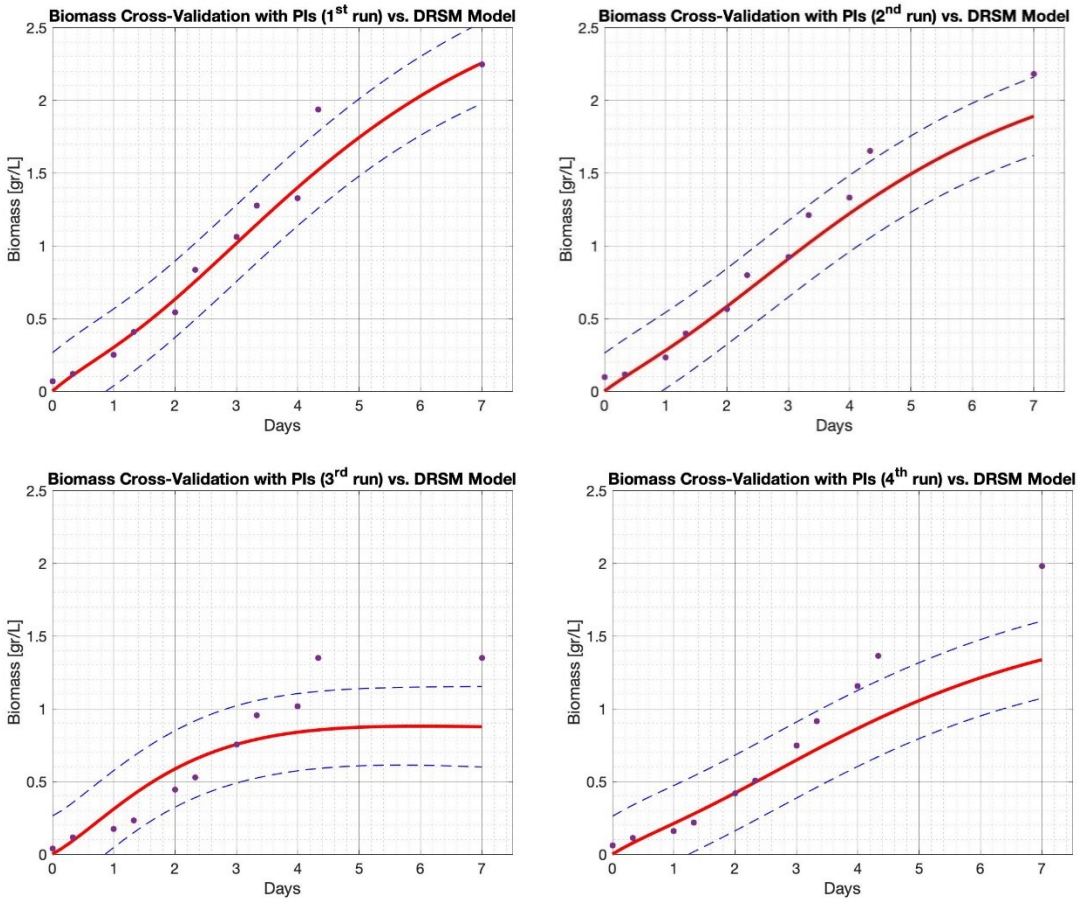

Figure 3.6. Comparison of the experimental data against Model A and its *prediction* intervals for the four cross-validation runs

One can note that all the data points, except five, are inside the prediction intervals. This reveals that model A is quite accurate. In the Appendix, the corresponding cross-validation sets of four plots for modes B and C (the 2FI one) are given in Figures 3A.8 and 3A.9. There are some minor differences between them, and the ones given here but none is very striking. The striking difference is between the width of the prediction intervals in Figure 3.6 and the uncertainty intervals in Figure 3.4, which are much narrower than the prediction intervals. This is because the latter, in Figure 3.4, are confidence intervals that are always narrower. Figure 3.7 replicates Figure 3.6, but with "confidence" instead of prediction intervals. They are much narrower. These "confidence" intervals could be interpreted as prediction intervals if the normal variability of the process were zero.

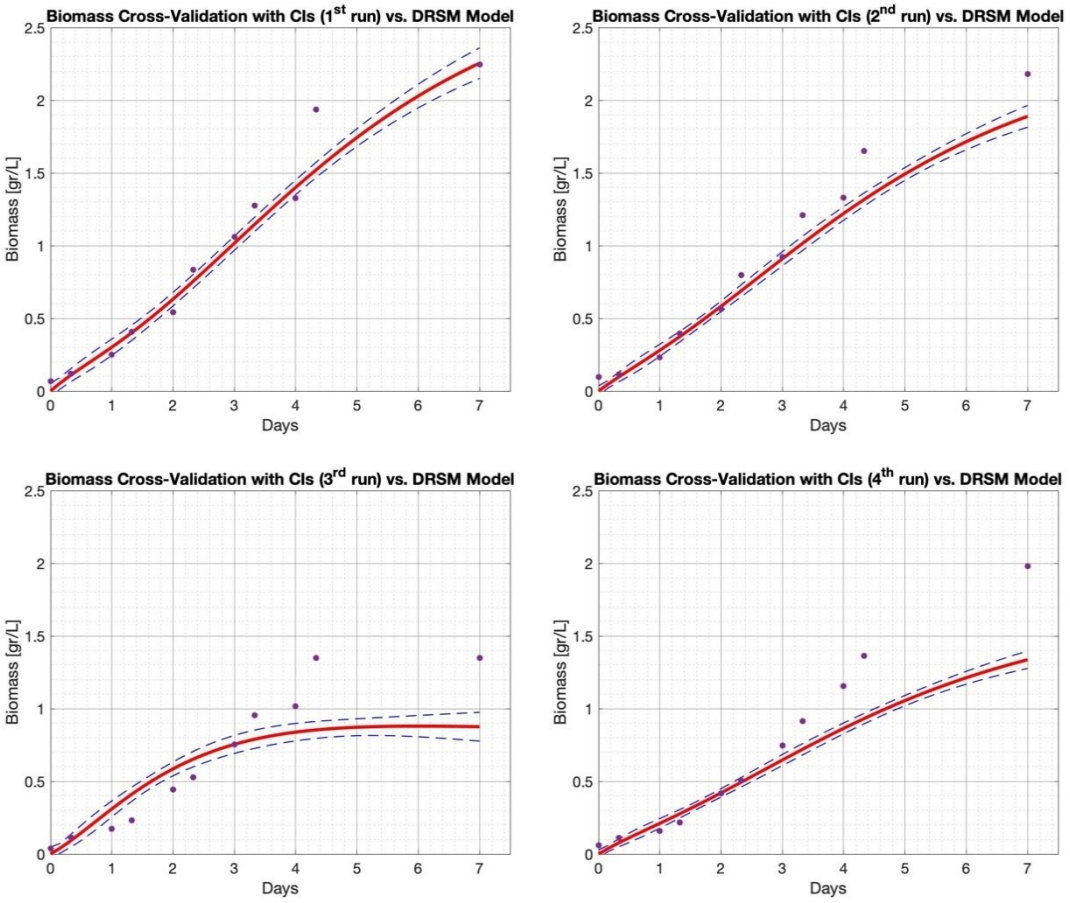

Figure 3.7. Comparison of the experimental data against Model A and its *confidence* intervals for the four cross-validation runs

This significant difference is due to the substantial normal variability of the process. Note that the average R^2_{adj} value in Table 3.2 is 0.80, indicating that approximately 20% of the total variability is normal variability due to the uncertainty of any biological process.
A more quantitative comparison between the three models is given by the cross-validation sum of squares ($cvSS$) values reported in Table 3.5.

Table 3.5. Cross-validation sum of squares ($cvSS_i$) for each of the four runs and their sum ($cvSS_t$)

	$cvSS_1$	$cvSS_2$	$cvSS_3$	$cvSS_4$	$cvSS_t$
2FI Model	0.41	0.21	0.44	0.69	1.74
Model A	0.22	0.27	0.62	0.74	1.86
Model B	0.21	0.23	0.53	0.61	1.58

There, the $cvSS$ values for each of the three models and for each of the four cross-validation experiments and their sums for each model are summarized. We see that none of the three models is definitely more accurate than the other two, either in each of the experiments or

in all four of them. This is also confirmed by the small differences in the statistical performance of the three models during their estimation step, given in Table 3.3. There we declared that model A has a slight advantage because of the smaller BIC value. However, Model B has the smallest total cross-validation sum of squares in Table 3.5.

3.7 Discussion

Batch systems are the most common method for photosynthetic microorganism cultivation, because of their ease of operation [13]. A batch system simply consists of an agitated vessel containing the culture medium with the necessary nutrients, where the biomass is inoculated and let grow. It is supplied with CO_2-enriched air and exposed to a source of light. The growth of microorganism occurs in four main phases. An initial lag phase is often observed, where the concentration of cells does not increase because the microorganism needs to adjust and adapt to the experimental conditions in which it is set to grow. After the cells have adapted to the new environment, there is an active cell proliferation, with a rapid increase of cells concentration (exponential growth phase). Cells continue to increase exponentially with the time until they reach a high concentration and the light and/or nutrients become a limiting factor for their growth. Finally, the viability of the cells is compromised, and their number contributes to inhibit further growth. As an alternative but still simple cultivation method, nutrients could be supplied according to a determined feed profile, in a fed-batch configuration.

The growth of photosynthetic microorganisms in batch or fed-batch systems depends on several factors such as light, temperature and nutrients concentrations. Light is the main source of energy, essential to support metabolism in autotrophic conditions. If too low, it can be limiting for the biomass growth because absorption and scattering phenomena do not let the light penetrate deeply into dense biomass suspension [14]; if present in excess, it can damage vegetative cells and lead to oxidative stress and photoinhibition [15]. Another important factor for the growth of algae is temperature: high values strongly reduce the growth rate and could be fatal for the cells [16], while low temperature could significantly decrease biomass productivity [17]. As for nutrients, the most relevant are nitrogen, phosphorus and carbon, but also micronutrients (e.g. iron, cobalt, manganese) are required, although in smaller amounts[18].

In the design used in this Chapter, three are the factors that diversify the various experiments: the light intensity profile, the temperature and the feeding profile of

phosphorus. The specific experimental conditions used influenced not only the final biomass concentration obtained at the end of the batch, but also the shape and duration of the different growth phases. In this regard, the dynamic data-driven methodology employed proved to be extremely valuable. The trends of the $\beta_q(t)$ provided valuable insights not simply on the effect of each input variable considered, and on their interaction, but also on the extent of this effect along with time. Indeed, using an incident light intensity profile increasing according to what suggested by the model, could be an interesting strategy to provide the necessary amount of light per cell along the growth. The DRSM model estimated proved fairly successful in predicting *Synechocystis* sp. biomass growth under the different experimental conditions of the four cross-validation experiments (V1-V4), accounting for the effect of all process variables. Specifically, experiments V1 and V2 resulted in greater biomass growth, reaching values of about 2.2 $g_x\ L^{-1}$ on the seventh day. In fact, both experiments were carried out at a temperature of 33°C, close to the optimal growth temperature for *Synechocystis* sp. [19], while V3 and V4 were carried out at a temperature of 26°C, suboptimal for *Synechocystis* sp.

The incident light profiles of the cross validation experiments have almost the same trend, but reach different light intensities towards the end of the profile, ranging from 350 to 500 $\mu mol\ m^{-2}\ s^{-1}$. V1 is the experiment carried out at the greatest light intensity, and in fact a greater quantity of biomass is obtained on the final day experimentally and in agreement with model predictions. As for the amount of phosphorus, experiments V1 and V4 had a similar integral amount of phosphorus, equal to 3.07 and 2.89 mg_P respectively. Experiment V3 was characterized by a very small amount of phosphorus fed (0.76 mg_P). This reflected the trend of the growth curve, which reached the stationary phase as early as day 4, achieving a lower final biomass concentration. Such a behaviour is correctly predicted by the model. However, one could notice that the final points of biomass concentration measured experimentally (time 4.33 d and 7 d) are higher than the predicted values and are located outside of the prediction interval. The same occurs in the case of experiment V4 as well. This result can be explained considering that the temperature control system might have failed to keep a stable set-point temperature of 26 °C, which could have been raised to 27°C in the timeframe going from day 4 to day 7, influencing in turn the biomass concentration. In fact, a different and slightly less precise temperature control system was employed for these two experiments, due to a failure of the one used in all the other experimental runs. This hypothesis is in accordance with the trend of $\beta_3(t)$ reported in

Figure 3.5, which suggests a positive effect on biomass concentration if temperature is increased, especially during the last days of the growth curves. To further check this hypothesis, the biomass growth of experiments V3 and V4 was simulated at 27°C (x_3= -0.7). Because temperature is a fixed factor throughout the batch duration in the DRSM model, it is not possible to simulate the time evolution of biomass in response to a temperature profile changing with time. Nonetheless, a constant temperature profile at 27°C can give an idea of the final biomass concentration that could be reached if the actual temperature were higher than planned. In Figure 3.8 we compare the model predictions at this higher temperature against the collected data in runs V3 and V4. It can be clearly seen that considering a temperature of 27°C, all the experimental measurements fall within the prediction interval of the model, here model A.

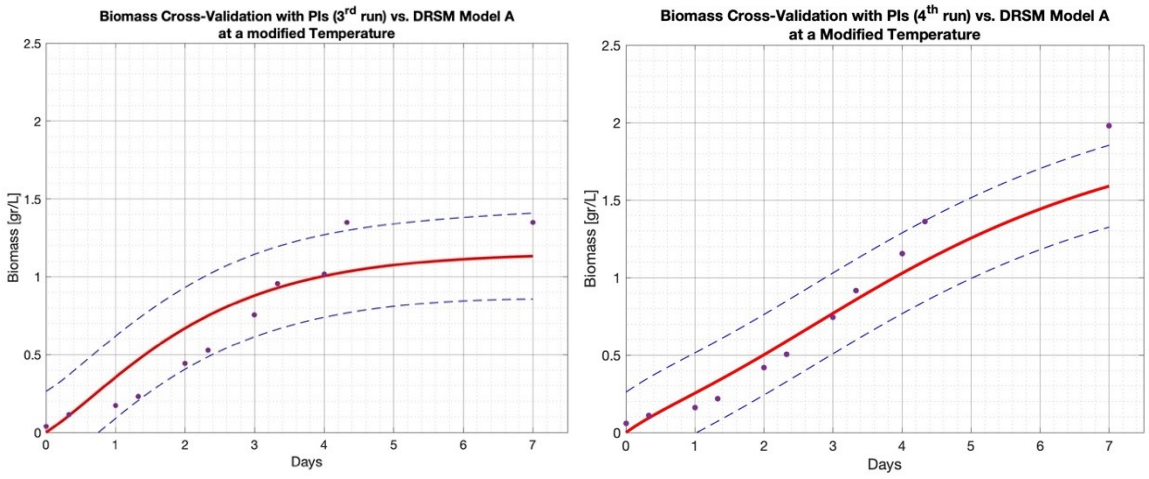

Figure 3.8. Comparison of the experimental data against Model A and its *prediction* intervals for the two cross-validation runs V3 and V4 at 27°C

3.8 Final remarks

We have here applied the Design of Dynamic Experiments (DoDE) and Dynamic Response Surface Methodology (DRSM) to model the growth of a photosynthetic microorganism. We performed a set of dynamic, fed-batch experiments, changing the values of light intensity, temperature, and nutrient inflow profiles, and measuring biomass growth at discrete time intervals. Based on the experimental results, we derived different DRSM models. The estimation of several data-driven models which appear slightly different from each other but represent the data with almost identical accuracy is not a weakness of the methodology but rather a strength. If one used these models to predict the process outputs

at new operating conditions, their prediction differences would be smaller than the normal variability of the process. One should not forget that the modeling purpose is not to find the unique model but a model that represents the data accurately enough and thus can be used to understand process behaviors and possibly predict the results of new experiments inside the domain within which the model was estimated.

We retained the model that gave the best statistical scores (smallest BIC and largest LoF) although the other two models were not significantly different, confirming the robust characteristics of the DRSM modeling algorithm in retaining only the significant model parameters. The model was able to satisfactorily predict the behavior of biomass growth of a new set of experiments performed in different conditions, demonstrating the capability of taking into account the effect of the different process variables considered. Moreover, by analyzing the trend of the parametric functions $\beta_q(t)$ of the DRSM model, we were able to gain some interesting insights on the effect of the different factors along with time. Therefore, DoDE and DRSM methodologies are two powerful data-driven tools even when dealing with extremely complex and highly variable bioprocesses, such as those involving photosynthetic organisms.

Nomenclature

τ_1	Dimensionless time (-)
t_f	Duration of the phosphorus feeding interval (d)
τ_2	Dimensionless time (-)
c_{CGP}	Cyanophycin concentration ($mg_{CGP}\ L^{-1}$)
q_{CGP}	Cyanophycin quota ($mg_{CGP}\ mg_x^{-1}$)
c_x	Biomass concentration ($mg_x\ L^{-1}$)
β_q	Model parameters (-)

Acronyms

R^2_{adj}	Adjusted R-squared
2FI	Two-factor interation
AICc	Small-sample corrected Akaike Information Criterion
ANOVA	Analysis of Variance
BIC	Bayesian Information Criterion
cvSS	Cross-validation Sum of Squares
DoDE	Design of Dynamic Experiments
DoE	Design of Experiments
DRSM	Dynamic Response Surface Model
LASSO	Least Absolute Shrinkage and Selection Operator
LoF	Lack of Fit
PAR	Photosynthetically Active Radiation
RSM	Response Surface Model
VIF	Variance Inflation Factors

Literature cited

[1] D.C. Montgomery, Design and analysis of experiments, 8th ed., John wiley & sons, New York, 2017.

[2] C. Georgakis, Design of dynamic experiments: A data-driven methodology for the optimization of time-varying processes, Ind. Eng. Chem. Res. 52 (2013) 12369–12382. https://doi.org/10.1021/ie3035114.

[3] N. Klebanov, C. Georgakis, Dynamic Response Surface Models: A Data-Driven Approach for the Analysis of Time-Varying Process Outputs, Ind. Eng. Chem. Res. 55 (2016) 4022–4034. https://doi.org/10.1021/acs.iecr.5b03572.

[4] Z. Wang, C. Georgakis, New Dynamic Response Surface Methodology for Modeling Nonlinear Processes over Semi-infinite Time Horizons, Ind. Eng. Chem. Res. 56 (2017) 10770–10782. https://doi.org/10.1021/acs.iecr.7b02381.

[5] Z. Wang, C. Georgakis, A Dynamic Response Surface Model for Polymer Grade Transitions in Industrial Plants, Ind. Eng. Chem. Res. 58 (2019) 11187–11198. https://doi.org/10.1021/acs.iecr.8b04491.

[6] Y. Dong, C. Georgakis, J. Mustakis, L. Han, J.P. McMullen, Optimization of pharmaceutical reactions using the dynamic response surface methodology, Comput. Chem. Eng. 135 (2020) 106778. https://doi.org/10.1016/j.compchemeng.2020.106778.

[7] N.-S. Lau, M. Matsui, A.A.-A. Abdullah, Cyanobacteria: Photoautotrophic Microbial Factories for the Sustainable Synthesis of Industrial Products, Biomed Res. Int. 2015 (2015) 1–9. https://doi.org/10.1155/2015/754934.

[8] M.A. Borowitzka, High-value products from microalgae-their development and commercialisation, J. Appl. Phycol. 25 (2013) 743–756. https://doi.org/10.1007/s10811-013-9983-9.

[9] R. Tibshirani, Regression Shrinkage and Selection Via the Lasso, J. R. Stat. Soc. Ser. B. 58 (1996) 267–288. https://doi.org/10.1111/j.2517-6161.1996.tb02080.x.

[10] T. Hastie, R. Tibshirani, J. Friedman, The Elements of Statistical Learning: Data Mining, Inference, and Prediction, Second Edition, Springer New York, 2009. https://books.google.it/books?id=tVIjmNS3Ob8C.

[11] R. Rippka, J.J.B.W. Deruelles, J.B. Waterbury, M. A. Herdman, R.Y. Stanier, Generic Assignments, Strain Histories and Properties of Pure Cultures of Cyanobacteria, Microbiology-Sgm. 111 (1979) 1–61.

https://doi.org/10.1099/00221287-111-1-1.

[12] N. Powell, A. Shilton, Y. Chisti, S. Pratt, Towards a luxury uptake process via microalgae--defining the polyphosphate dynamics, Water Res. 43 (2009) 4207–4213. https://doi.org/10.1016/J.WATRES.2009.06.011.

[13] Y.K. Lee, W. Chen, H. Shen, D. Han, Y. Li, H.D.T. Jones, J.A. Timlin, Q. Hu, Basic Culturing and Analytical Measurement Techniques, Handb. Microalgal Cult. Appl. Phycol. Biotechnol. Second Ed. (2013) 37–68. https://doi.org/10.1002/9781118567166.ch3.

[14] Y.S. Yun, J.M. Park, Kinetic modeling of the light-dependent photosynthetic activity of the green microalga Chlorella vulgaris, Biotechnol. Bioeng. 83 (2003) 303–311. https://doi.org/10.1002/bit.10669.

[15] E. Sforza, B. Gris, C.E. De Farias Silva, T. Morosinotto, A. Bertucco, Effects of light on cultivation of scenedesmus obliquus in batch and continuous flat plate photobioreactor, Chem. Eng. Trans. 38 (2014) 211–216. https://doi.org/10.3303/CET1438036.

[16] R. Serra-Maia, O. Bernard, A. Gonçalves, S. Bensalem, F. Lopes, Influence of temperature on Chlorella vulgaris growth and mortality rates in a photobioreactor, Algal Res. 18 (2016) 352–359. https://doi.org/10.1016/J.ALGAL.2016.06.016.

[17] M. Pawlita-Posmyk, M. Wzorek, M. Płaczek, The influence of temperature on algal biomass growth for biogas production, MATEC Web Conf. 240 (2018) 4008. https://doi.org/10.1051/matecconf/201824004008.

[18] G. Markou, D. Vandamme, K. Muylaert, Microalgal and cyanobacterial cultivation: The supply of nutrients, Water Res. 65 (2014) 186–202. https://doi.org/10.1016/j.watres.2014.07.025.

[19] T. Hasunuma, M. Matsuda, Y. Kato, C.J. Vavricka, A. Kondo, Temperature enhanced succinate production concurrent with increased central metabolism turnover in the cyanobacterium Synechocystis sp. PCC 6803, Metab. Eng. 48 (2018) 109–120. https://doi.org/10.1016/j.ymben.2018.05.013.

Appendix

Table 3A.1. The values of the coded factors defining the 28 experiments. The last three ones are replicates at the center of the domain

Run #	x_1 *Light*	x_2 *Light*	x_3 *Temperature*	x_4 *P feed duration*	x_5 *P inflow*	x_6 *P inflow*
1	-0.6	0.4	-1	-0.4	-0.6	-0.4
2	-0.1	0.9	1	-0.1	-0.6	0
3	0.7	0.3	1	1	-0.9	-0.1
4	0.9	-0.1	1	-1	-0.10	-0.9
5	-0.8	-0.2	-1	-0.3	-0.55	0
6	-0.4	-0.3	-1	-1	-0.1	-0.9
7	-0.8	-0.2	1	1	-0.9	-0.1
8	0.5	-0.5	1	0.62	-0.800	0
9	-0.3	0.7	1	-1	-0.1	-0.9
10	-0.9	-0.1	-1	-1	0.2	0
11	-0.1	0.9	-1	1	-1	0
12	0.1	0.9	-1	-1	-0.085	-0.9
13	-1	0	-1	-1	-0.7	-0.3
14	0.6	-0.4	-1	-1	0.2	0
15	0.9	0.1	-1	-0.2	-0.67	-0.31
16	0.9	-0.1	-1	-1	-1	0
17	0.9	-0.1	1	-1	-1	0
18	0.2	0.8	-1	-1	0.2	0
19	-0.5	0.5	1	-1	0.2	0
20	-0.3	0.7	-1	-1	-1	0
21	0.9	0.1	1	-1	0.2	0
22	-0.8	-0.2	1	-1	-1	0
23	0.3	0.7	1	-1	-0.6	-0.4
24	0.7	-0.3	-1	1	-1	0
25	-0.6	-0.25	1	-1	0	-0.75
26	0	0	0	-1	0	0
27	0	0	0	-1	0	0
28	0	0	0	-1	0	0

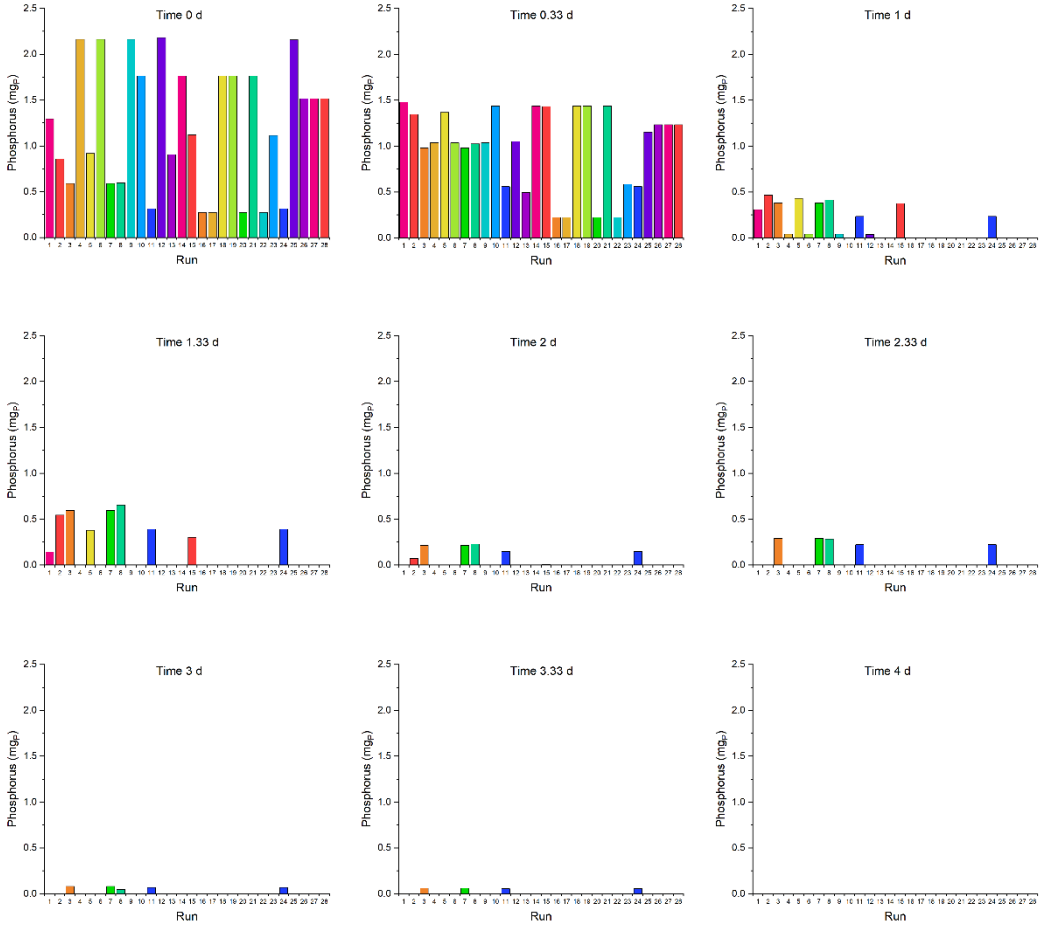

Figure 3A.1. Discrete amount of phosphorus added for each experiment at each time instant

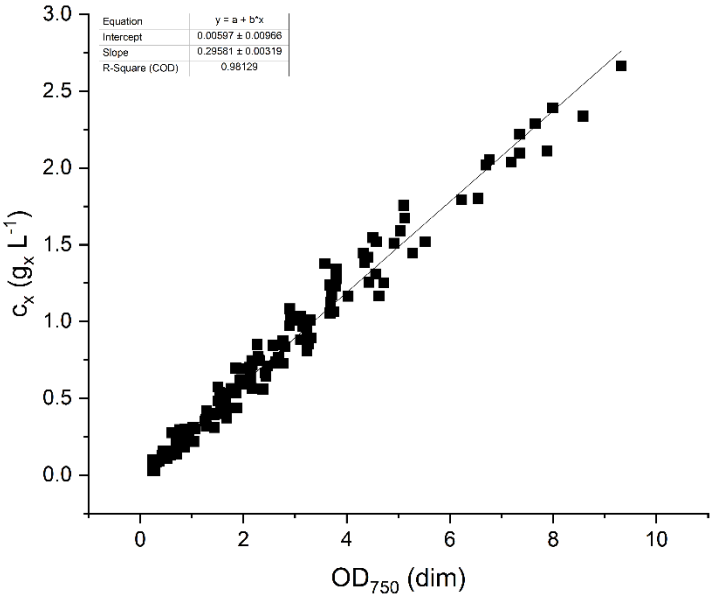

Figure 3A.2. Linear correlation between OD_{750} and biomass concentration (c_x, $g_x\ L^{-1}$)

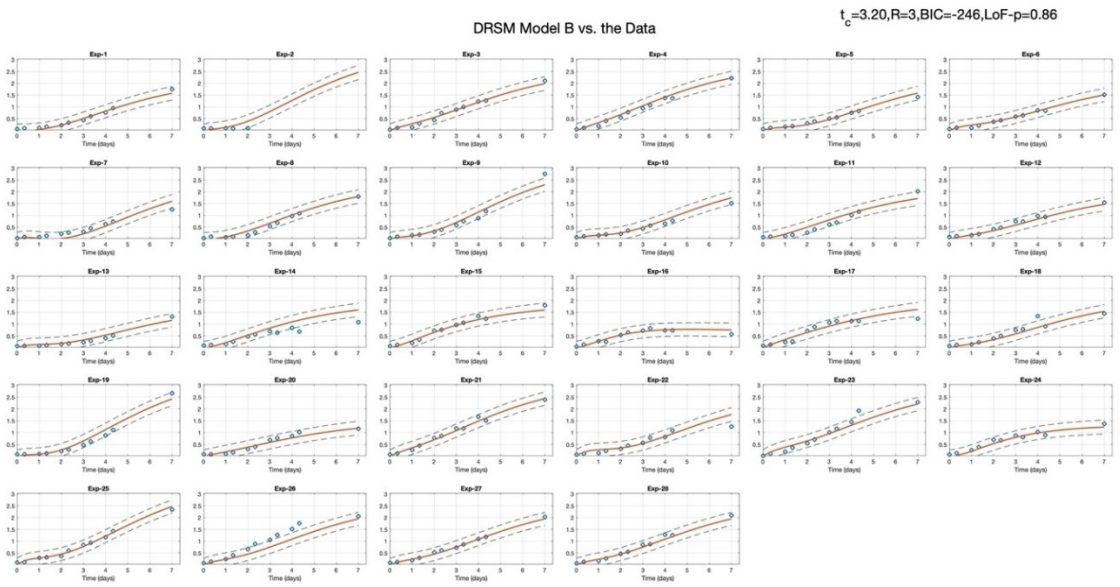

Figure 3A.3. Nominal predictions and corresponding prediction intervals of Model B against the experimental data in 28 experiments

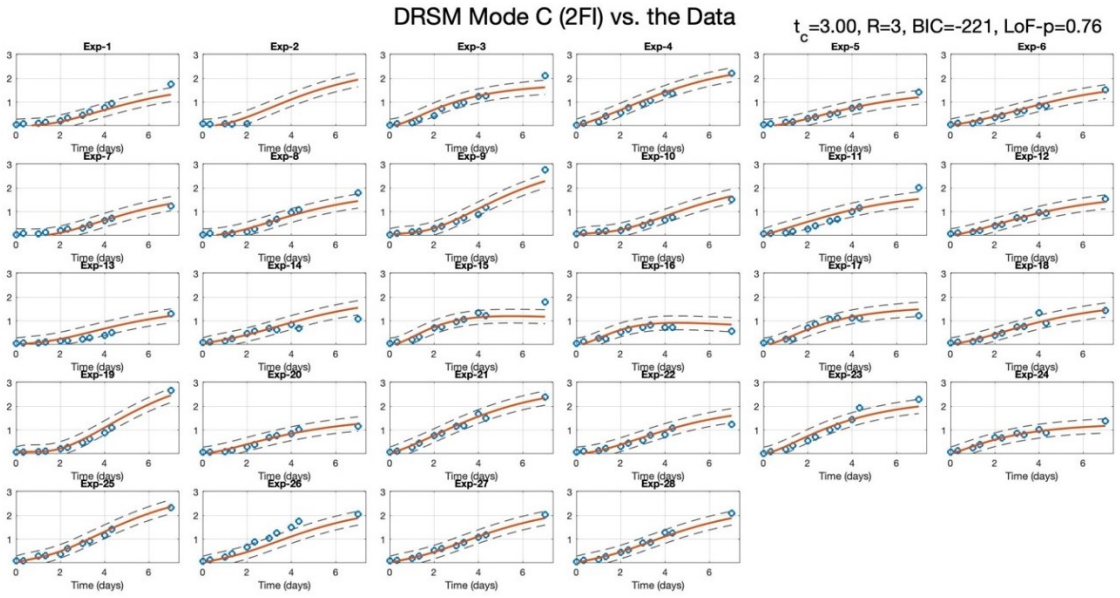

Figure 3A.4. Nominal predictions and corresponding prediction intervals of Model C, the 2FI model, against the experimental data in 28 experiments

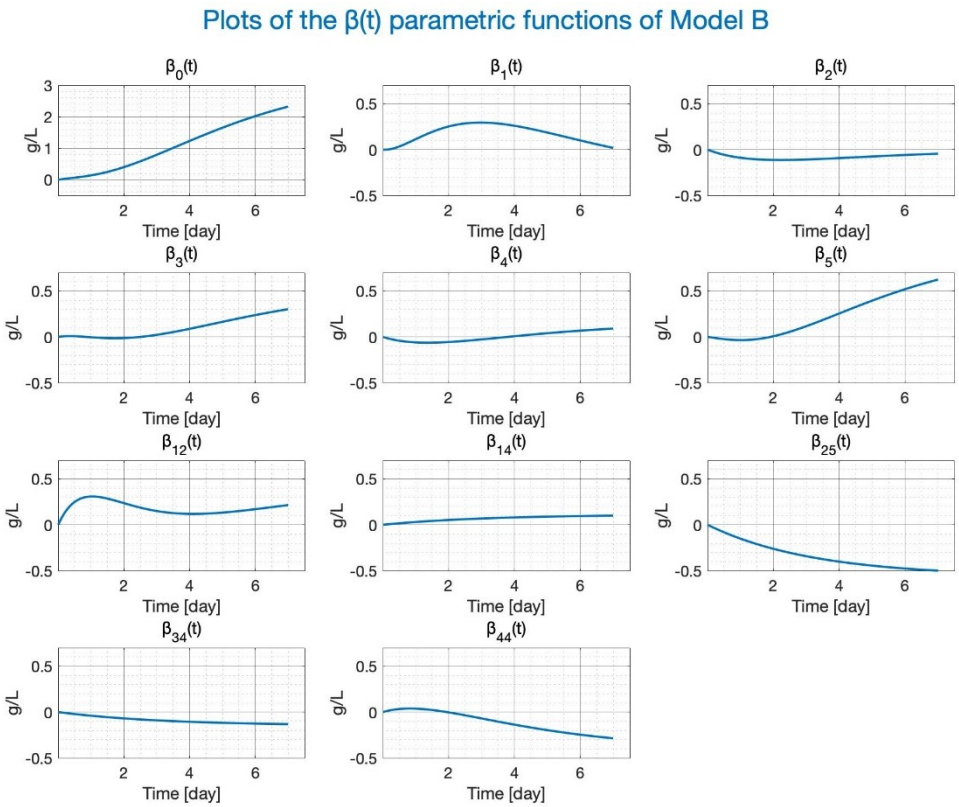

Figure 3A.5. Plots of the β(t) parametric functions of Model B

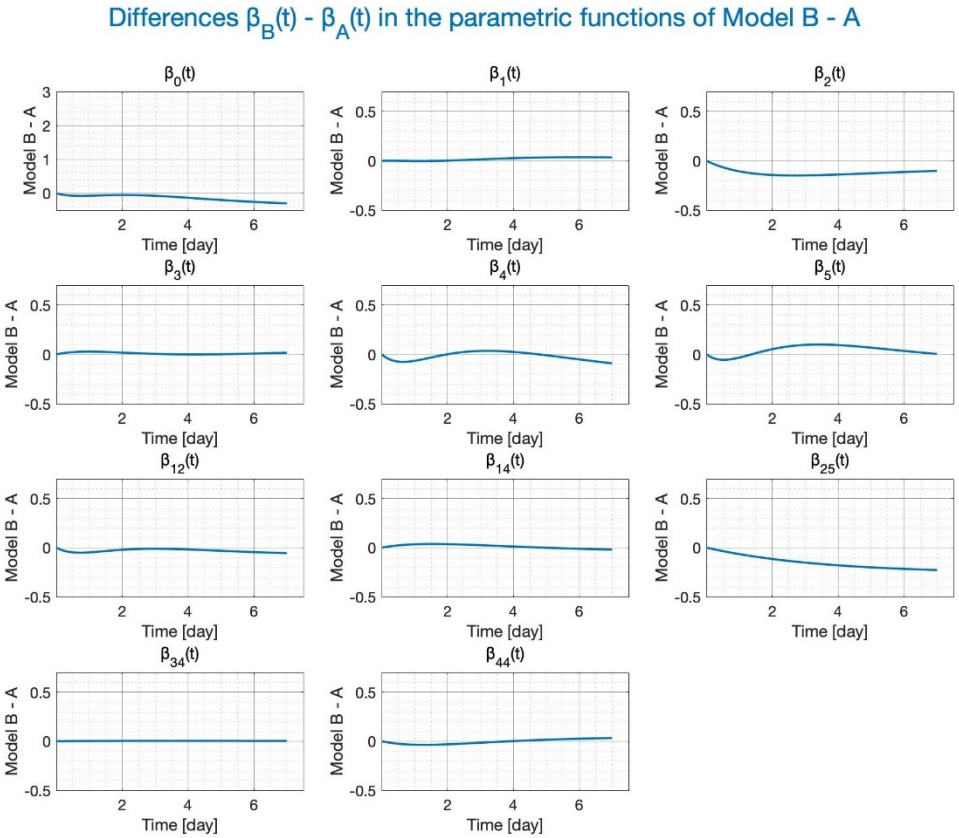

Figure 3A.6. Plots of β_B(t)- β_A(t) the difference between the parametric functions of Model B and A (Note that the y scale is the same as in Figure 3A.5 for easy comparison)

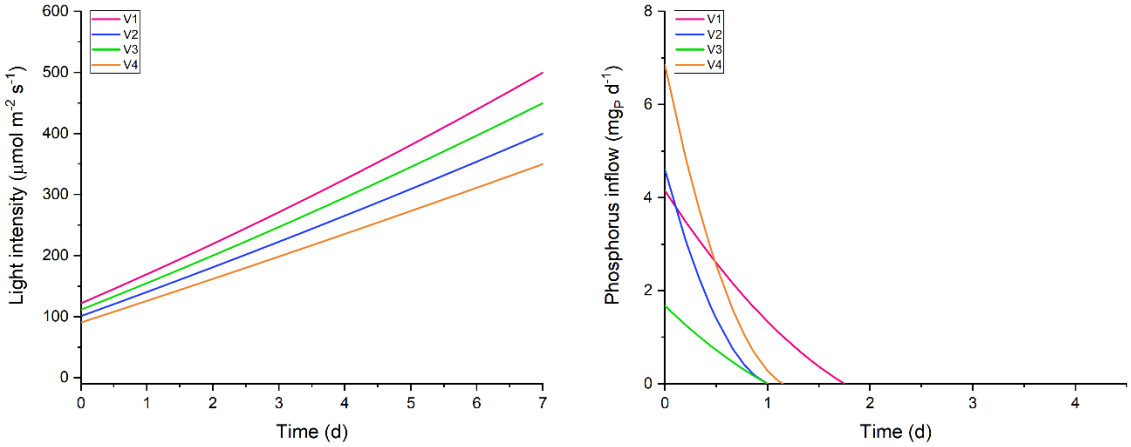

Figure 3A.7. Incident light intensity and inlet phosphorus profiles for each of the cross validation experiments

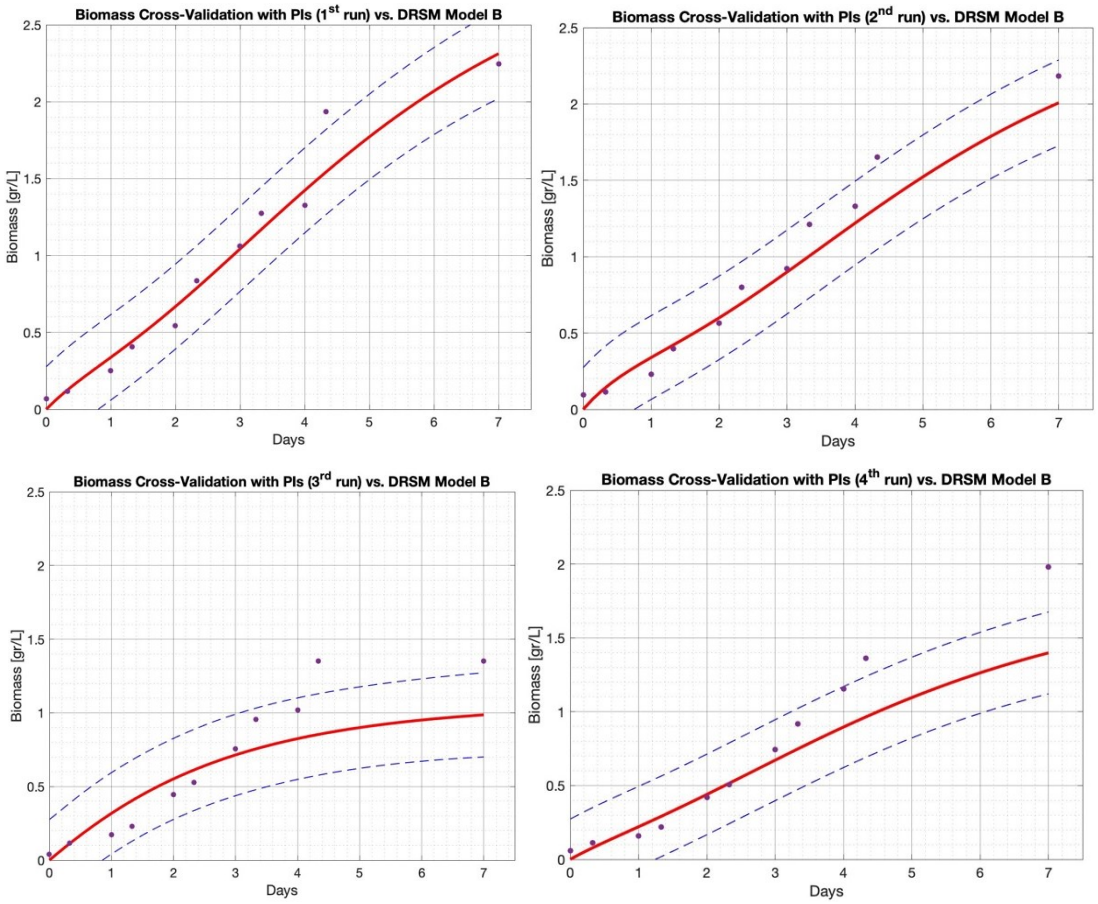

Figure 3A.8. Comparison of the experimental data against Model B and its *prediction* intervals for the four cross-validation runs

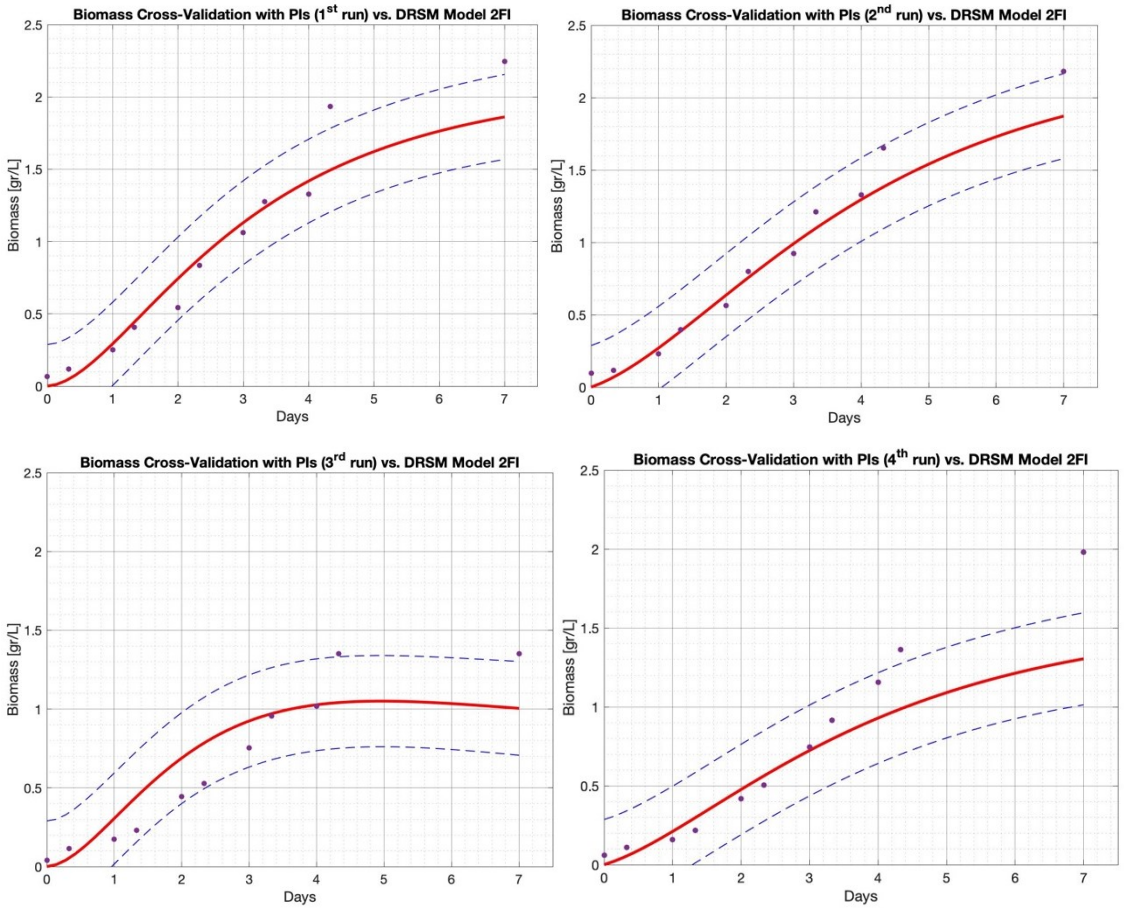

Figure 3A.9. Comparison of the experimental data against Model C (2FI) and its *prediction* intervals for the four cross-validation runs

Chapter 4

Stabilizing autotrophic cyanophycin production in continuous photobioreactors

Cyanophycin, an intracellular reserve molecule synthetized by cyanobacteria, is considered as a potential biobased raw material for the industrial sector. It is usually produced through the cultivation of photosynthetic microorganisms in batch systems, which are affected by the high variability of cyanophycin accumulation due to varying growth phases, which lower the overall productivity. In this Chapter, *Synechocystis* sp. PCC 6803 was cultivated in a continuous photobioreactor to increase cyanophycin productivity and to assess the feasibility of large-scale application. A stable production of the compound was obtained at steady-state. The effect of residence time and inlet phosphorus concentration on the biomass and cyanophycin productivity was evaluated, to identify the optimal conditions for its accumulation. A maximum value of cyanophycin productivity of about 30 mg_{CGP} L^{-1} d^{-1} was obtained, doubling the one achieved in the batch system. A quantitative correlation between the phosphorus quota and the cyanophycin produced was eventually proposed, highlighting a threshold of 4 mg of phosphorus per g of biomass for cyanophycin accumulation.

Part of this Chapter was published as a scientific paper in *Algal Research* (Trentin, G., Lucato, V., Sforza, E., Bertucco, A., 2021, https://doi.org/10.1016/j.algal.2021.102518)

4.1 Introduction

Population growth and new living standards are posing new challenges to be faced towards a sustainable bio-based industry development, including the one related to plastic production. Indeed, bio-based processes exploiting microorganisms, such as microalgae and cyanobacteria are one of the possibilities to avoid ethical conflicts and dodge a disadvantageous development on the resource market. Photosynthetic microorganisms might be the ideal biorefinery feedstock as a sustainable factory, thanks to their attractive features: they have the ability of growing autotrophically, using sunlight energy, and they are able to exploit CO_2 as carbon source, thus minimizing greenhouse gas emissions. Moreover, they require non-potable water and minimal nutrients supply, which can be also derived from wastewater [1,2]. Furthermore, photosynthetic microorganisms provide many commercially relevant compounds that are often related to reserve molecules accumulation, and they can find many interesting applications in several commercial fields [3–9].

Recently, cyanophycin aroused a lot of interest as a potential raw material for the industrial sector. It is a reserve molecule present as insoluble inclusions (optically opaque granules) in the cytoplasm, commonly also referred to as the Cyanophycin Granule Polypeptide (CGP) [10,11]. Known also as multi-arginyl-L-polyaspartate, CGP serves as an intracellular energy reservoir within cyanobacteria under nutrient limitations, hence a storage compound for carbon, nitrogen and energy [12]. It is synthetized by several species of cyanobacteria, but it has also been found in a few heterotrophic bacteria [13]. As recently reviewed by Du et al. [14], cyanophycin accumulation has been found to occur in several cyanobacterial strains, such as *Scytonema* genus, *Nostoc ellipsosporum* NE1, *Synechococcus* sp. MA19, *Synechococcus* sp. G2.1, *Anabaena* sp. PCC7120, *Anabaena variabilis* ATCC29413, *Thermosynechococcus elongatus* BP-1, *Agmenellum quadruplicatum* and *Toxyfilum mysidocida*. Hai et al. [15] cultivated *Synechococcus* sp. MA19 in a 80-L closed photobioreactor in batch mode, with an incident light intensity of 300 μmol photons m^{-2} s^{-1}, and at a temperature of 50°C, obtaining an accumulation of CGP up to 3.5% of the cell dry matter. *Aphanocapsa* 3608, instead, grown at 35°C and 10800 lx accumulates up to 16% of CGP in late limited stationary phase [11]. However, the effect of the main operative variables affecting the accumulation of cyanophycin are still largely unknown [16].

Cyanophycin molecules consist of a polyaspartic backbone and arginine residues linked to the β-carboxylic group of each aspartic acid via isopeptide bonds [12]. The molecular mass

of the polymer ranges from 25 to 100 kDa [17]. In water, it is soluble under acidic (pH<2) or alkaline (pH>9) conditions, and insoluble at physiological pH [10,11].

Cyanophycin has recently attracted the attention of the scientific community as a biodegradable replacement for petrochemical-based industrial products. It can be hydrolysed to its constituent amino acids, arginine and aspartic acid, to a derivative with reduced arginine content or even to polyaspartic acid (PAA) [14]. PAA is a biodegradable polymer where the abundance of negatively charged carboxyl groups makes it a promising substitute for non-biodegradable polyacrylates [18]. It can also be used as an anti-precipitant, a detergent and an industrial additive [14,16,19,20], as well as a precursor to produce nitrogen-containing chemicals [18]. For example, acrylonitrile, which has a market volume of 6 million tonnes per year and price of € 1000 per tonne, can be derived from aspartic acid. Likewise, urea, a fertilizer, and 1,4-butanediamine, a building block for nylon-4,6, could be produced from arginine, the other aminoacidic constituent of CGP [20]. Cyanophycin is, thus, a valuable source of dipeptides and amino acids for food, feed, and pharmaceutical industries, with a competitive predicted market price for CGP-dipeptides [18].

To increase its productivity, various microbial strains, such as *Escherichia coli*, *Pseudomonas putida*, *Ralstonia eutropha*, *Rhizopus oryzae* and *Saccharomyces cerevisiae* have been exploited for cyanophycin production through heterologous expression of diverse cyanobacterial cyanophycin synthetases (CphAs). However, these species need organic carbon as raw material, differently from photoautotrophic microorganisms, which then emerge as a green alternative to heterotrophic bacteria [21]. The main drawback of cyanophycin accumulation in autotrophic organisms is the high variability of the related synthesis and accumulation processes, as its intracellular content depends on the growth phase and on environmental conditions: it is low during the exponential phase, while it increases when cells get into the stationary phase, reaching 18% (w/w) of the cell dry mass [22]. It has been demonstrated that a higher production of cyanophycin can be reached under conditions of imbalanced growth, where nutrient starvation occurs, together with adverse light intensity and low temperature [17,23], that however strongly impact the biomass productivity. Phosphate starvation has been identified as the most efficient method to boost cyanophycin accumulation, even though the biological mechanisms involved have not been clarified yet [24]. Indeed, as a result of phosphate starvation, Trautmann et al. [25] obtained 0.18 g of cyanophycin per g of biomass in *Synechocystis* PCC 6803 in batch system. The production was also increased with overproducing mutant species (BW86) up

to 0.40 g per g of biomass [24], highlighting the high potential of the species as a cell factory.

On the other hand, even though some attempts of high density cultivation of cyanobacteria for enhancing cyanophycin production have been already carried out [26], the actual capability of growing cyanobacteria for cyanophycin production in large scale reactors has not been fully understood and little is known in the literature in view of an industrial and extensive application. Moreover, it is still not clear if the transient production of this compound can be stabilized for prolonged industrial campaigns.

This Chapter aims at giving a contribution to the lack of literature addressing the issue of cyanophycin production in continuous cultivation systems. Indeed, the main advantage of cultivating microorganisms in a continuous system is linked to the possibility of stabilizing conditions inside the reactor over time, both in terms of quantity and quality of the biomass produced, thus allowing to obtain higher and stable productivity, required for large-scale operation [27,28]. Accordingly, the effects of operating variables, such as phosphorous concentration and residence time, on cyanophycin accumulation and its stability were assessed, to find the best compromise between the growth of biomass and the production of cyanophycin and considering that this compound is accumulated under unbalanced conditions, which affects biomass productivity.

4.2 Materials and methods

4.2.1 Experimental Strain and Culture Medium

The cyanobacterial strain *Synechocystis* sp. PCC 6803 (Pasteur Culture collection of Cyanobacteria, France) was used in this study. It was maintained and propagated in sterilized BG11 medium [29], modified by substituting HEPES with 1.5 g L^{-1} of sodium hydrogen carbonate, to maintain the pH within the optimal interval of 7.5-8. pH was monitored daily using a Hanna portable pH-meter (code HI9124), in 250 mL Erlenmeyer flasks placed in an orbital shaker.

4.2.2 Experimental setup

Experiments were carried out in batch and continuous cultivation systems, in a thermostated incubator (Frigomeccanica Andreaus, Padova) at a constant temperature of 30 °C.

For batch experiments, Quickfit® Drechsel Bottles with a volume of 250 mL and a diameter of 5 cm were used. A CO_2-air (5% v/v) mixture was bubbled continuously at the bottom of the bottle, with a total gas flow rate of 1 L h^{-1}. Additionally, a magnetic stirrer was used to prevent any deposition of biomass, thus ensuring a good mixing within the reactor. Reactors were illuminated by a continuous light of 150 μmol photons m^{-2} s^{-1}, provided by a white LED lamp. Photon flux density (PFD) was measured using a photoradiometer (HD 2101.1 from Delta OHM), which quantifies the photosynthetically active radiation (PAR). Cyanobacteria culture used as inoculum was cultivated at the same temperature and light intensity of batch experiments. Initial concentration of potassium hydrogen phosphate in the cultivation medium was modified to assess the effect on cyanophycin accumulation. In these preliminary batch experiments, performed in at least two/three independent biological replicates, two concentrations of the substrate (c_P^0) were used: 4.67±0.17 mg_P L^{-1} (as a control, corresponding to the concentration of the standard BG11) and 1.48±0.04 mg_P L^{-1} (condition of P limitation).

Continuous experiments were carried out in vertical flat-panel polycarbonate photobioreactors having a working volume of 150 mL (V_{PBR}), an irradiated surface equal to 0.005 m^2 and a thickness of 0.03 m. A stirring magnet, placed at the bottom of the reactor, and the bubbling of 1 L h^{-1} CO_2-enriched air (5% v/v) ensured a good mixing and non-limiting CO_2 supply. Light was provided by a white LED lamp with the incident light intensity equal to 250 μmol photons m^{-2} s^{-1}. The incident light intensity and temperature are given in a way that they are not limiting for the growth of this cyanobacterial species. The fresh medium was continuously fed at a constant flowrate (Q) by a peristaltic pump (Watson-Marlow 120U/DM3), whereas the working volume (V_{PBR}) was controlled by an overflow tube properly placed, from which the exhaust biomass was constantly withdrawn (Figure 4.1). Therefore, the residence time τ (d) was inversely proportional to the flow rate (Q) provided by the pump, according to:

$$\tau = \frac{1}{D} = \frac{V_{PBR}}{Q} \tag{4.1}$$

Since the dilution rate D is equal to the specific growth rate μ (d^{-1}), by changing the residence time, a different growth rate can be imposed on the culture. The reactor was firstly operated in batch to increase the biomass concentration for about 4 days, the pump was then activated to continuously supply the fresh medium. After a transitory period of about 3 times the value of the residence time, steady state was achieved with constant biomass

concentration. Steady state was kept for at least a period equal to three times the residence time, and biomass samples were taken daily for analysis. In continuous systems, if the experimental conditions are changed, a new variable transient period is observed, after which a new steady state is reached.

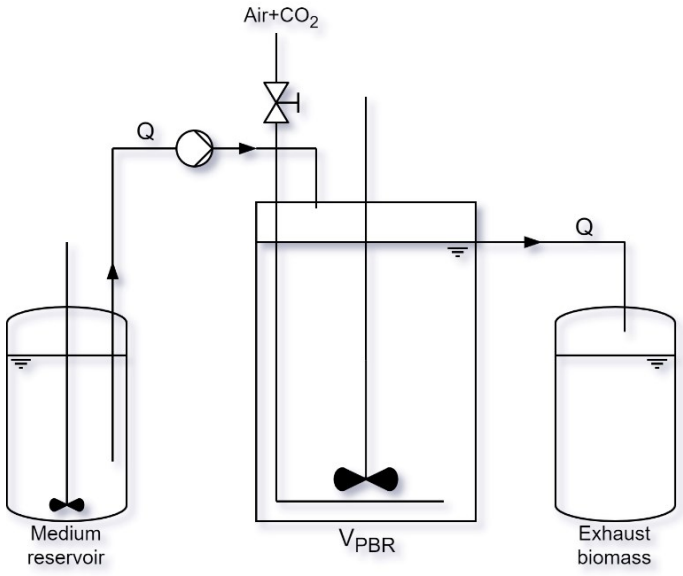

Figure 4.1. Experimental set-up of the continuous experiments

The biomass volumetric productivity P_x (g_x L^{-1} d^{-1}) was calculated as

$$P_x = \frac{c_x}{\tau} \tag{4.2}$$

where c_x is the biomass concentration measured at steady state. Accordingly, cyanophycin productivity P_{CGP} (mg_{CGP} L^{-1} d^{-1}) was calculated as

$$P_{CGP} = P_x \cdot q_{CGP} \tag{4.3}$$

where q_{CGP} is the cyanophycin quota (g_{CGP} g_x^{-1}) measured at steady state.

The residence time (τ) and the inlet concentration of phosphorus (c_P^{inlet}) in the cultivation medium were changed to assess their effect on cyanophycin accumulation and productivity. Specifically, c_P^{inlet} were chosen based on the standard BG11 P concentration that is equal to about 5 mg_P L^{-1} (P1): the concentration was doubled (P2), as a negative control, and reduced to a half (P1/2) and one quarter (P1/4) to induce cyanophycin accumulation. A first set of experiments was carried out at a residence time of 2.28 d, selected considering a possible reduction of the maximum growth rate due to the P limitation. Residence time was then changed to assess its influence on biomass and cyanophycin productivity. Phosphorus

limitation was ascertained by measuring the P concentration in the reactor inlet stream. The experimental conditions are summarized in Table 4.1.

Table 4.1. Summary of operating conditions of continuous experiments

	c_P^{inlet} ($mg_P\ L^{-1}$)	τ (d)
P2	9.88	2.28
P1	5.46±0.29	0.91
		2.28
		3.56
		8.51
P1/2	2.70±0.29	0.91
		1.54
		2.28
		3.56
		11.5
P1/4	1.37±0.16	1.54
		2.28
		3.56
		11.5

4.2.3 Growth analysis

The biomass concentration was monitored daily by spectrophotometric analysis at 750 nm with a UV-Visible double beam spectrophotometer (UV1900, by Shimadzu, Japan). To measure dry cell weight concentration (c_x), a known volume of culture sample was filtered thorough 0.22 μm previously dried nitrocellulose filters, which then were dried for 2 h at 105°C in a laboratory oven. Axenic condition of the reactor was checked periodically, by plating the samples in LB Petri dishes.

4.2.4 Nutrient analysis

Nutrients concentration was measured in the fresh inlet cultivation medium and in the outlet stream after biomass removal by filtration, to assess the nutrient consumption. Detection of orthophosphates was carried out following the method described by Innamorati et al. in Nova Thalassia vol. 11 [30], whereas nitrates are quantified with the diagnostic kit Hyrocheck Spectratest (Code 6223). Biomass composition at steady state was characterized in terms of phosphorus, nitrogen, carbohydrates and pigment internal quotas on centrifuged

samples, to remove the supernatant cultivation medium, at 9960 rcf for 10 min. Phosphorus and nitrogen content in the biomass were determined thanks to an alkaline persulfate digestion [31], followed by the quantification of released orthophosphates and nitrates. Carbohydrate content was determined by the Anthrone method [32]. Pigment extraction by N,N-dimethylformamide (DMF) was carried out: after the supernatant was removed, 1 mL of solvent was added. Samples were then stored in a freezer for at least 48 h to ensure complete pigment extraction. After further centrifugation, the absorption spectrum of the extract was measured, using DMF as reference. The final concentration of total chlorophyll and carotenoids was determined according to Bryant (1994) [33].

4.2.5 Cyanophycin extraction and quantification

Extraction and quantification of cyanophycin was developed based on the Elbahloul et al. [34] and Trautmann et al. [25] protocols. The extraction was carried out with a known volume of culture, which was centrifuged to remove the supernatant. Subsequently, the pellet was resuspended in acetone at room temperature to increase the permeability of the membrane. Following a second centrifugation step, the pellet was washed twice with Tris-HCl 50 mM to remove soluble proteins. At the end of the second wash, the pellet was resuspended in HCl 1M to solubilize the compound of interest. CGP was precipitated by adding 500 µL of Tris-HCl 100 mM. The opalescent-looking cyanophycin granules thus became visible. Finally, before proceeding with the quantification of the cyanophycin quota (q_{CGP}) based on the Bradford [35] colorimetric assay, a final centrifuge was performed to precipitate any residual cell debris. This extraction protocol ensures that proteins are not extracted, thus avoiding possible interference in the Bradford method.

4.2.6 Statistical analysis

Statistical tests were applied to data acquired at steady state, specifically on biomass concentration and productivity, on cyanophycin quota and productivity and on carbohydrate content. The existence of equal variance among data was verified with Levene's test using a confidence level of 95%. Then, one-way ANOVA analysis was performed to find statistically significant differences among the data. Grouping was done according to Tukey's multiple comparison procedure with a 95% confidence interval. Data that do not share a letter are significantly different.

4.3 Results and discussion

4.3.1 Stabilizing cyanophycin content and productivity in continuous systems

Continuous experiments with *Synechocystis* sp. PCC 6803 were performed to verify that it was possible to produce cyanophycin with this mode of operation, by carefully adjusting the operative conditions. The main advantage of working in a continuous system is linked to the possibility of stabilizing the conditions inside the reactor over time, thus allowing to obtain a specific and constant quality of the biomass [28]. Other advantages such as the reduction of volume requirement, lower labour capital and operational costs, the decrease of the unprofitable periods needed for cleaning and sterilization of batch equipment, make continuous cultivation systems an attractive solution for the large-scale production [36]. In addition, in the case of photosynthetic microorganisms, by adjusting the residence time, it is possible to operate the system near to the optimal cell-to-light density, resulting in a maximum volumetric productivity [37]. Finally, to our knowledge, there are no examples in the literature of cyanophycin production in continuous systems.

Initially, the reactor was run with a residence time of 2.28 d (i.e. a dilution rate of 0.439 d^{-1}), at a constant incident light intensity of 250 μmol photons m^{-2} s^{-1}, close to the saturation point, with decreasing P concentration in the inlet. The results of biomass growth and cyanophycin production are summarized in Table 4A.1 (Appendix) and Figure 4.2.

As the phosphorus inlet concentration decreased, also biomass concentration and productivity were lower. The highest volumetric biomass productivity of 0.439±0.008 g_x L^{-1} d^{-1} was measured under non-limiting P concentration (two times the BG11 standard). This value is greater than the one measured by Touloupakis et al. [38], which however could be due to the lower incident light intensity, which is the main variable affecting biomass production.

Cyanophycin was not accumulated with P inlet concentration higher than 5.46 mg L^{-1}, while an internal quota of such a compound was detected when using lower P concentrations. It should be highlighted that the increase of cyanophycin content fully compensated the decreased biomass productivity, with a maximum in productivity of about 27 mg_{CGP} L^{-1} d^{-1}, a value greater than the one found in literature [25] and measured in our batch experiments, which were carried out to verify the effect of phosphorus limitation on cyanophycin production. It is known that the accumulation of reserve compounds such as

CGP is related to the growth phase, in particularly when stationary phase is eventually reached [17]. The nitrogen quota in the biomass was also measured, but being nitrate provided in excess to accumulate CGP [16], no differences in nitrogen accumulation were observed, with an average content of about 11-12% (data not shown).

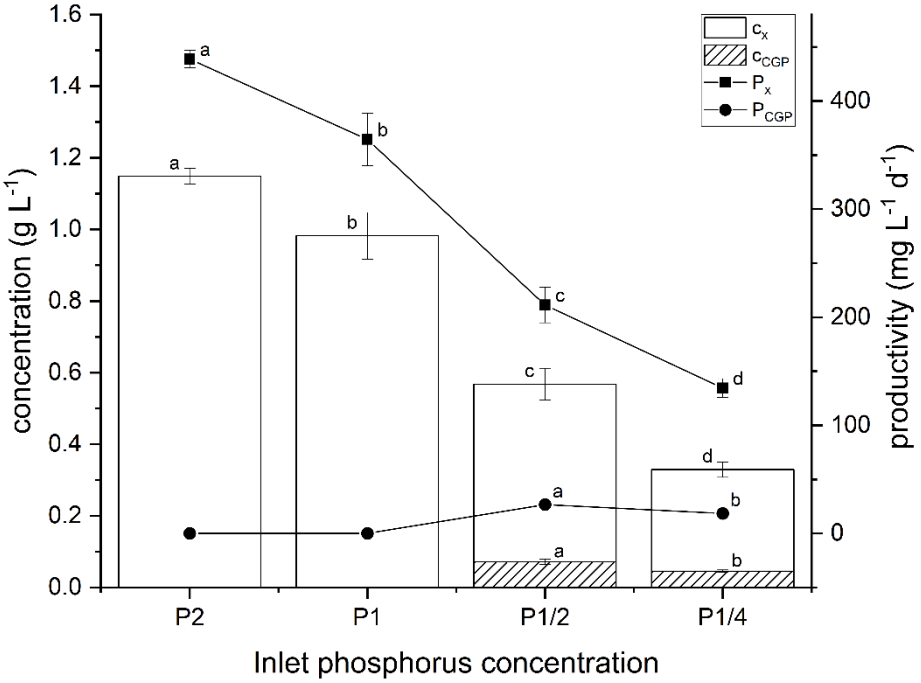

Figure 4.2. Steady state biomass concentration (c_x), cyanophycin concentration (c_{CGP}), biomass productivity (P_x), cyanophycin productivity (P_{CGP}), at a residence time of 2.28 d, with different inlet phosphorus concentrations. Error bars represent the standard deviation of at least 4 samples for each steady state (n≥4). Statistical analysis was conducted separately for each category of data. Data that do not share a letter are significantly different. Lines are just eye guides.

In batch experiments, the initial phosphorus concentrations were selected on the basis of the results obtained by Trautmann et al. [25]. The accumulation of CGP was found negligible with an initial phosphorus concentration around 5 $mg_P\ L^{-1}$ (the concentration of standard growth medium), whereas it became relevant when the substrate concentration was reduced to 1.5 $mg_P\ L^{-1}$. Results are shown in Figure 4.3.

After a comparable initial growth rate for P-limited and control runs, a decrease was observed when P became limiting. The stationary phase was reached on the fourth day (Figure 4.3B) in the case of P limitation, later if the nutrient was provided in excess. At the end of the batch curve, the biomass concentration (c_x) reached 0.76±0.02 and 2.0±0.08 $g\ L^{-1}$, in limited and control conditions, respectively.

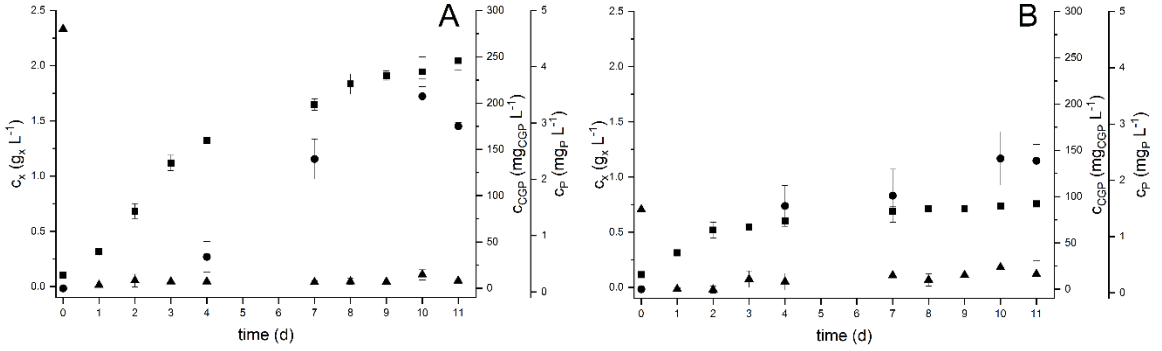

Figure 4.3. Biomass (*squares*), cyanophycin (*circles*) and phosphorus (*triangles*) concentration in batch growth curves of *Synechocystis* sp. PCC 6803 for control (panel A) and P-limited condition (panel B). Error bars represent the standard deviation (n=4, two technical replicates for two biological replicates).

Concentration of CGP (c_{CGP}), initially absent in both conditions tested, gradually increased reaching its maximum value at stationary phase, as the progressive P starvation forced the cell to downregulate the synthesis of nucleic acids and cell division. It should be noted that the CGP content was not stable in the stationary phase of batch experiments, with a significant decrease after the tenth day in the control (Figure 4.3A). Cyanophycin quota (q_{CGP}) measured at stationary phase was equal to 0.18±0.02 and 0.086±0.002 $g_{CGP}\ g_x^{-1}$, respectively, in the limited and control conditions. These values are slightly higher than those measured by Trautmann et al. [25], using the same limiting substrate concentrations in the medium. However, the difference is possibly due to the different temperature and light conditions at which the experiments were performed.

Certainly, the most interesting comparison between batch and continuous system is related to the cyanophycin productivity: Table 4.2 shows production values (P_{CGP}, not including the additional time for reinoculating a batch reactor between two sequential production cycles) much lower than that obtained in continuous. Nevertheless, P_{CGP} was higher in the case of the control than in the P-limited condition, but the higher biomass productivity (P_x) compensated the lower quota, thus resulting in a higher cyanophycin productivity of the control, which however is about half of that obtained in continuous.

Table 4.2. Summary of data obtained from batch experiments with *Synechocystis* sp. PCC 6803 (± SD; n=4, two technical replicates for two biological replicates).

	c_P^0 $mg_P\ L^{-1}$	c_x $g_x\ L^{-1}$	q_{CGP} $g\ g_x^{-1}$	P_x $mg_x\ L^{-1}\ d^{-1}$	P_{CGP} $mg_{CGP}\ L^{-1}\ d^{-1}$
Phosphorus limitation	1.48±0.04	0.76±0.02	0.18±0.02	58.4±0.91	10.7±1.37
Control condition	4.67±0.17	2.0±0.08	0.086±0.002	176.7±9.37	15.1±0.35

The results of batch experiments are possibly related to the dynamics of phosphorus uptake: Figure 4.3 shows that the external concentration of phosphorus rapidly decreased in the first day for both conditions, with a common trend attributable to the luxury uptake phenomenon [39]. Microalgae and cyanobacteria are able to sequester from the environment much more phosphorus than that immediately required for growth. The intracellular phosphorus accumulation is complex [40], but P is generally stored as reserve polymer in the form of polyphosphates [41], which can be used as a phosphorus source when phosphate becomes depleted in the surrounding medium. This explains the results obtained in the batch system, with different dynamics of cyanophycin accumulation, but poses a strong limitation to a quantitative description of the effect of P concentration on CGP synthesis when using a batch system.

Therefore, despite their wide application for microalgal cultivations, batch systems lack in performance, as they offer lower productivity, uncertain reliability and variable product quality [36], owing to the continuous change of external conditions, in particular concerning the availability of light and nutrients. Such behavior is worsened under P limitation, with severe consequences on productivity. It means that batch cultivation is not the preferred choice in view of massive biomass production, while continuous systems generally allow a productivity at least 2-5 times higher [38,42].

More interestingly, the possibility of managing the operative conditions to stabilize in continuous system the production of the compound was demonstrated. A relation between P content and CGP production was already proposed, but a more quantitative approach is needed, to setup the optimum operating conditions that are focused on the productivity of the product, more than on its quota in the biomass.

4.3.2 The combined effect of residence time and phosphorus limitation on cyanophycin production in continuous reactor

Other continuous experiments were carried out to assess the combined effect of phosphorus inlet concentration and residence time on biomass and cyanophycin productivity. For each condition of P inlet, the effect of residence time was investigated, as it was previously found to be responsible for differences in biomass composition. Indeed, since in a continuously stirred biological reactor working at steady state, the average growth rate is equal to the dilution rate, at lower residence times cells undergo faster duplication, accumulating protein [43], while at higher residence time the average growth rate is lower, and cells

accumulate reserve materials, like carbohydrates [28]. Touloupakis et al. [38] also found a relationship between the dilution rate and the biochemical composition of biomass, with the protein content that decreased as the dilution rate increased, the chlorophyll content that was maximum at the lowest dilution rate, while phycocyanin and total carotenoids decreased. Thus, by varying the residence time, it is possible to stimulate a greater accumulation of a specific compound of interest. Based on the observation of preliminary experiments, it should be hypothesized a possible accumulation of cyanophycin when working at higher residence time.

Figure 4.4 reports the biomass productivity obtained at steady state for each value of residence time and different P feeds. It showed a classical trend as a function of residence time [37] with a maximum between 1 and 2 days.

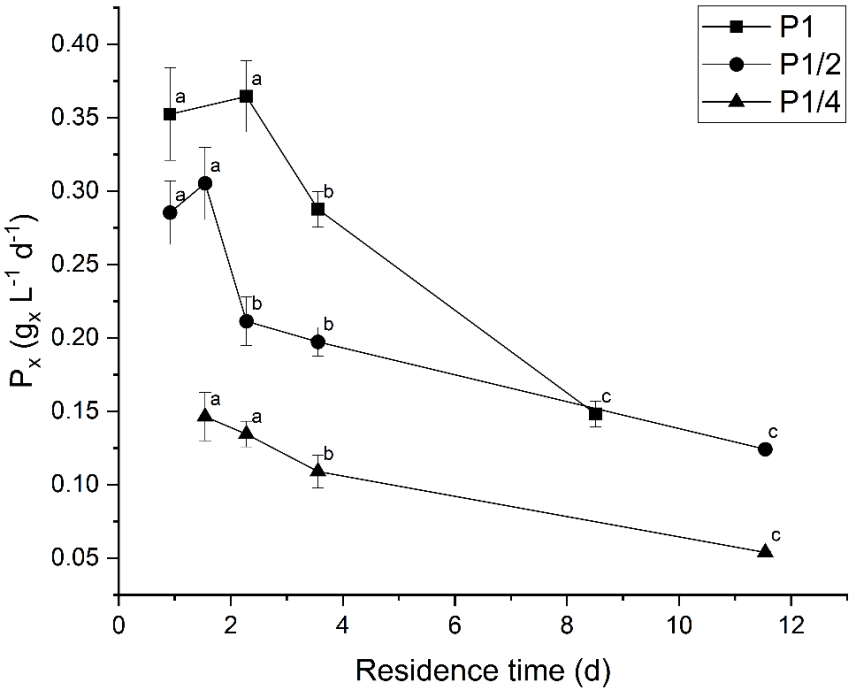

Figure 4.4. Biomass productivity (P_x) as a function of residence time, parametric to the inlet phosphorus concentration. Error bars represent the standard deviation of at least 4 samples for each steady state (n≥4). Statistical analysis was conducted separately for each series obtained under the same phosphorus inlet concentration. Data that do not share a letter are significantly different. Lines are just eye guides.

The higher value obtained is equal to about 0.35 g_X L^{-1} d^{-1}, a value comparable to the one found in literature for the same species [38]. Instead, under limiting P conditions, the biomass production was lower. Indeed, in all experiments, the outlet P concentration measured was always below 1 mg_P L^{-1} (data not shown), demonstrating that the P supplied was almost completely consumed during cultivation. Therefore, a contextual reduction of

the internal phosphorus quota was also measured, with values of about 0.2%, close to the minimum phosphorus quota found in the literature [44]. However, our goal was to find the best compromise between biomass productivity and cyanophycin productivity in this stressful condition: indeed, a completely different trend was observed in the case of cyanophycin accumulation and productivity, as reported in Figure 4.5.

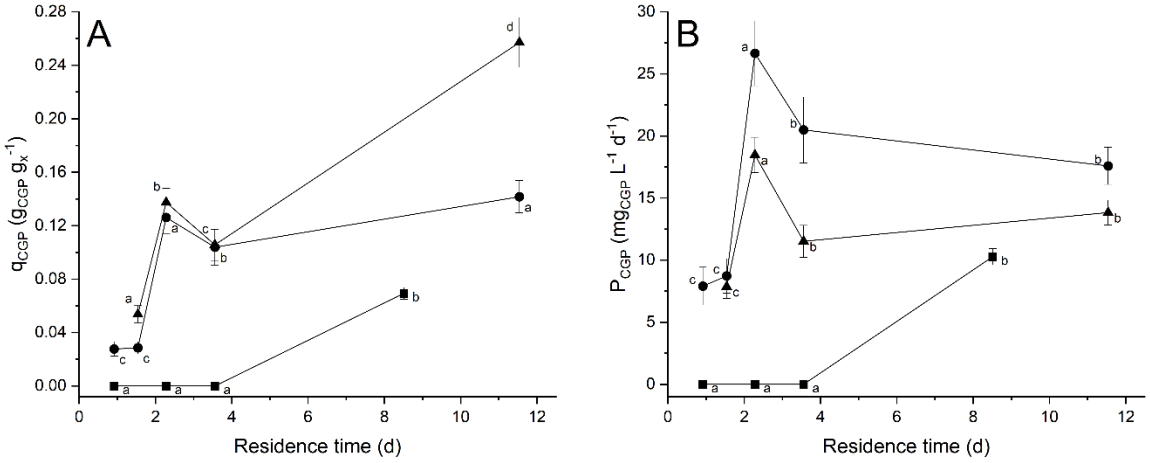

Figure 4.5. Cyanophycin quota (q_{CGP}) in panel A and productivity (P_{CGP}) in panel B as a function of residence time, parametric to the inlet phosphorus concentration (*squares* for P1, *circles* for P1/2 and *triangles* for P1/4). Error bars represent the standard deviation of at least 4 samples for each steady state (n≥4). Statistical analysis was conducted separately for each series obtained under the same phosphorus inlet concentration. Data that do not share a letter are significantly different. Lines are just eye guides.

The CGP productivity showed a maximum whose value depends on the inlet concentration of phosphorus. When working at higher concentration (P1=5.46 mg_P L^{-1}), CGP was accumulated under higher residence times only, as expected, and in agreement with the observation in batch systems. Under lower inlet P concentration, the maximum cyanophycin productivity was observed at a residence time of about 2 days, slightly shifted than the one of biomass productivity. The maximum value reached was almost 30 mg_{CGP} L^{-1} d^{-1}, i.e. the productivity was doubled compared to the one obtained in batch cultivation systems, thus confirming the potential of the continuous cultivation system. A similar value of productivity was obtained by Trautmann et al. [25] cultivating the engineered strain BW86 that overproduces such a compound in a batch system. Considering that the productivity we obtained in the continuous system was double than that achievable in the batch one, it would be interesting to cultivate this genetically modified organism in a continuous system, but unfortunately this strain is not commercially available. Such an idea looks promising in view of a large-scale production of cyanophycin by a photoautotrophic microorganism.

It is interesting to see also the relationship between phosphorus quotas and the corresponding cyanophycin content (Figure 4.6). Besides the residence time, a clear correlation between P and CGP internal quota exists, which can be used to find the proper condition to be set in an operating system. It is shown, particularly, that a threshold of P quota exists, evaluated at about 4 mg of phosphorus per g of biomass, beyond which cyanophycin is not accumulated anymore. When the amount of phosphorus in the biomass is reduced, CGP accumulation is significantly boosted. Specifically, it is noted that a small change in the internal phosphorus quota leads to a rapid increase in the cyanophycin content.

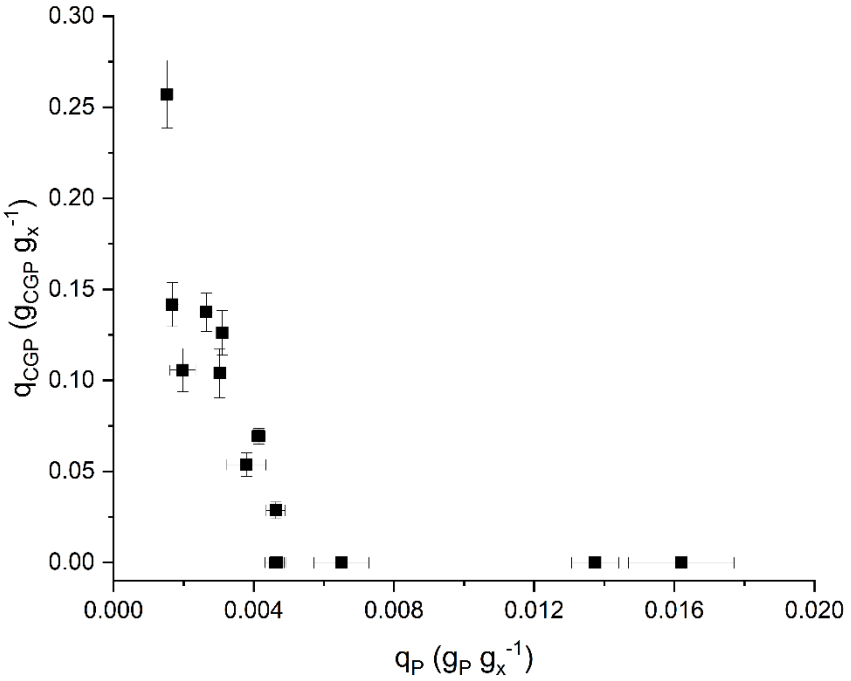

Figure 4.6. Cyanophycin quota (q_{CGP}) as a function of phosphorus quota (q_P) measured at steady state. Error bars represent the standard deviation of at least 4 samples for each steady state (n≥4).

Noticeably, Trautmann et al. [25] found a similar trend in a batch cultivation system, and the same limit value for the phosphorus quota was found. However, differently from that work, our finding is independent of the time of measure, while in the batch system there is a strong time dependence. On the other hand, the occurrence of this correlation between P and CGP quotas also in a continuous system is promising in view of applying a modeling approach to describe cyanophycin production, using a model that relates the microorganism growth to the nutrient internal quota as the Droop model. Indeed, because of the relation existing between the CGP and the P quota, it is possible to connect the cyanophycin production to the internal quota of the nutrient.

Pigment content was also measured in continuous, as an index of the physiological state of the cells. As the residence time increased, a decrease in the chlorophyll content was found. On the other end, carotenoids have a much more linear trend and their partial degradation occurred only at the highest residence time (Figure 4A.1, Appendix). This behavior reflects the increased stress perceived by the cells as the residence time increased in a situation with limiting concentration of phosphorus, probably due to a chlorosis phenomenon. This is an evolutionary mechanism of quiescence that allows the microorganism to survive even prolonged periods of stress [33], but strongly affects the biomass productivity. Its hallmark is the rapid degradation of the light-gathering complexes, resulting in a yellow-green color of the biomass, due to the predominance of yellow coloration of carotenoids [45]. This phenomenon was observed in *Synechocystis* sp. PCC 6803 by Trautmann et al. [25] as well as in *Synechococcus* sp. PCC 7942 [45], in both cases as a response to phosphorus limitation. This phenomenon was also observed during batch experiments (Figure 4A.2, Appendix): the concentration of chlorophyll, which generally decreases along with time in the growth curve, was remarkably lower under P limitation (Figure 4A.2B).

However, despite the lower content of pigments, the stability of the steady state obtained in the continuous cultivation system confirmed that the viability of the culture was not compromised. This also explains the higher productivity achieved in the continuous system.

From a physiological perspective, it is also interesting to observe the effect of P quota on carbohydrate content (Figure 4.7). With an inlet phosphorus concentration of about that of a standard freshwater media (P1), the carbohydrates measured are in line with data found in literature for the same species (about 10% of c_x) [38]. Instead, as the inlet phosphorus concentration decreased, an opposite trend was observed for carbohydrates, reaching a maximum value measured of 39.8±2.08 % with P of 1.37 mg L^{-1} and 11.5 days of residence time, corresponding to the lowest P quota of 0.001. This relation between intracellular phosphorus and carbohydrate content was already pointed out by Markou [46] in the case of *Arthrospira platensis*: under phosphorus limitation, the synthesis of carbohydrates is strongly stimulated, and in this case their content is even quadrupled. This side effect makes the continuous production process of cyanophycin even more interesting from the perspective of exploitation of photosynthetic microorganisms as novel cell factories. Indeed, after the extraction of the molecule of interest (CGP), the carbohydrate-rich exhausted algal biomass could be exploited, for instance, as a raw material for bioethanol production through anaerobic fermentation [47].

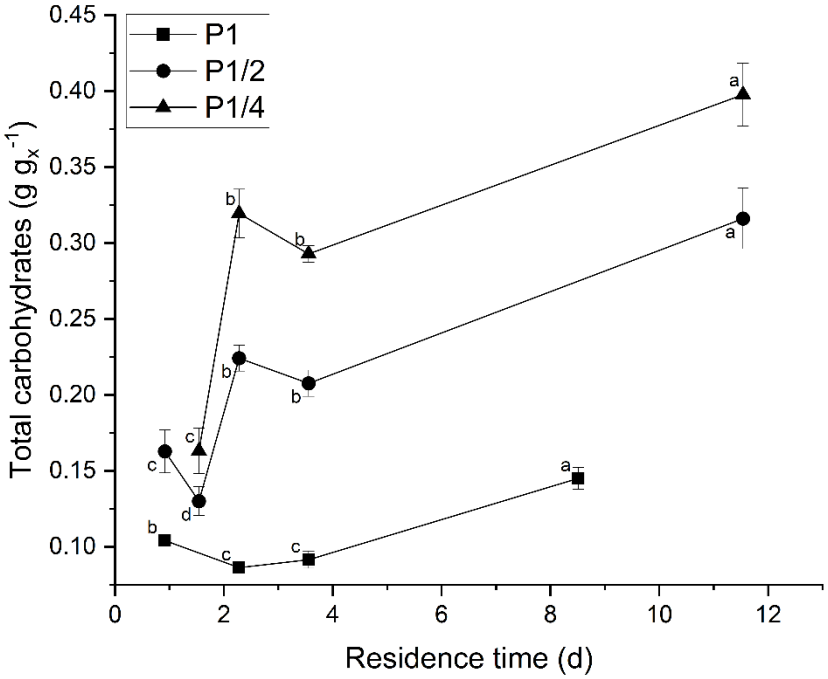

Figure 4.7. Steady state biomass carbohydrates content as a function of residence time, parametric to the inlet phosphorus concentration. Error bars represent the standard deviation of at least 4 samples for each steady state (n≥4). Statistical analysis was conducted separately for each series obtained under the same phosphorus inlet concentration. Data that do not share a letter are significantly different. Lines are just eye guides.

Even though the productivity of cyanophycin achieved in our work is still not compatible with an industrial scale production, the results obtained are significant in view of finding an alternative system of production. Nowadays, indeed, cyanophycin is produced by recombinant heterotrophic microorganisms like *E. coli*, but also *Ralstonia eutropha*, *P. putida* and yeast accumulated cyanophycin in their cells up to 50% of their dry weight [48]. It is necessary to consider that for heterotrophic cultivation, one third of the total cost of the process is attributable to the cost of the substrates needed for microorganisms growth [49]. For this reason, cyanobacteria have emerged as promising candidates to produce chemicals. In the case of cyanophycin, the engineered strain BW86 was capable of accumulating up to 57% (w/w) per cell dry mass [24]. This is the highest cellular cyanophycin content in bacteria ever reported. However, the volumetric productivity is low due to lower cell density in photobioreactors [14]. In this context, the possibility of maximizing and stabilizing the productivity of a properly engineered strain using a continuous cultivation system seems the key to obtain an industrial production of cyanophycin exploiting phototrophic microorganisms.

4.4 Final remarks

Synechocystis sp. PCC 6803 was cultivated in a continuous photobioreactor to optimize the accumulation of cyanophycin. This cultivation system proved effective to achieve higher and stable productivity of cyanophycin. Moreover, it allowed to characterize the effect of the operating variables and the physiological effect of the growth conditions, to find the optimal conditions to increase the productivity of the biopolymer. Namely, 2.7 mg_P L^{-1} of phosphorus in the inlet and a residence time of 2.28 d were identified as the cultivating condition able to guarantee the best compromise between the cyanophycin quota and the biomass productivity, resulting in a production of 30 mg_{CGP} L^{-1} d^{-1} of cyanophycin. The analysis of the composition of the biomass showed that the viability of the microorganism in the continuous cultivation system was not compromised by the limitation conditions imposed. Therefore, the system proved efficient for potential large-scale production of cyanophycin. Finally, regardless of the residence time, the existence of a correlation between the internal quota of phosphorus and the internal content of cyanophycin was highlighted, founding a threshold of 4 mg per g of biomass to trigger the accumulation of cyanophycin.

Nomenclature

Q	Volumetric flowrate ($m^3\ d^{-1}$)
V_{PBR}	Flat-panel photobioreactor volume (mL)
τ	Residence time (d)
μ	Biomass specific growth rate (d^{-1})
D	Dilution rate (d^{-1})
c_x	Biomass concentration ($g_x\ L^{-1}$)
c_{CGP}	Cyanophycin concentration ($mg_{CGP}\ L^{-1}$)
q_{CGP}	Cyanophycin quota ($g_{CGP}\ g_x^{-1}$)
P_x	Biomass productivity ($g_x\ L^{-1}\ d^{-1}$)
P_{CGP}	Cyanophycin productivity ($mg_{CGP}\ L^{-1}\ d^{-1}$)
c_P^{inlet}	Inlet phosphorus concentration ($mg_P\ L^{-1}$)
c_P^0	Initial phosphorus concentration ($mg_P\ L^{-1}$)
q_P	Phosphorus quota ($g_P\ g_x^{-1}$)

Literature cited

[1] D.C. Ducat, J.C. Way, P.A. Silver, Engineering cyanobacteria to generate high-value products, Trends Biotechnol. 29 (2011) 95–103. https://doi.org/10.1016/j.tibtech.2010.12.003.

[2] E. Bugnicourt, P. Cinelli, A. Lazzeri, V. Alvarez, Polyhydroxyalkanoate (PHA): Review of synthesis, characteristics, processing and potential applications in packaging, Express Polym. Lett. 8 (2014) 791–808. https://doi.org/10.3144/expresspolymlett.2014.82.

[3] J. Fiedor, K. Burda, Potential role of carotenoids as antioxidants in human health and disease, Nutrients. 6 (2014) 466–488. https://doi.org/10.3390/nu6020466.

[4] N.-S. Lau, M. Matsui, A.A.-A. Abdullah, Cyanobacteria: Photoautotrophic Microbial Factories for the Sustainable Synthesis of Industrial Products, Biomed Res. Int. 2015 (2015) 1–9. https://doi.org/10.1155/2015/754934.

[5] S. Singh, B.N. Kate, U.C. Banecjee, Bioactive compounds from cyanobacteria and microalgae: An overview, Crit. Rev. Biotechnol. 25 (2005) 73–95. https://doi.org/10.1080/07388550500248498.

[6] B.H.A. Rehm, Bacterial polymers: Biosynthesis, modifications and applications, Nat. Rev. Microbiol. 8 (2010) 578–592. https://doi.org/10.1038/nrmicro2354.

[7] S. Alcantara, S. Sanchez, Influence of carbon and nitrogen sources on Flavobacterium growth and zeaxanthin biosynthesis, J. Ind. Microbiol. Biotechnol. 23 (1999) 697–700. https://doi.org/10.1038/sj.jim.2900688.

[8] K.D. Snell, V. Singh, S.M. Brumbley, Production of novel biopolymers in plants: Recent technological advances and future prospects, Curr. Opin. Biotechnol. 32 (2015) 68–75. https://doi.org/10.1016/j.copbio.2014.11.005.

[9] A.K. Koyande, K.W. Chew, K. Rambabu, Y. Tao, D.T. Chu, P.L. Show, Microalgae: A potential alternative to health supplementation for humans, Food Sci. Hum. Wellness. 8 (2019) 16–24. https://doi.org/10.1016/j.fshw.2019.03.001.

[10] N.J. Lang, R.D. Simon, C.P. Wolk, Correspondence of cyanophycin granules with structured granules in Anabaena cylindrica, Arch. Mikrobiol. 83 (1972) 313–320. https://doi.org/10.1007/BF00425243.

[11] M.M. Allen, P.J. Weathers, Structure and composition of cyanophycin granules in the cyanobacterium Aphanocapsa 6308, J. Bacteriol. 141 (1980) 959–962. https://doi.org/10.1128/jb.141.2.959-962.1980.

[12] R.D. Simon, P. Weathers, Preparation and Derivatization of Cyanophycin Granule Polypeptide The filamentous cyanobacterium Anabaena cylindrica Lemm . was grown as, 420 (1976) 165–176.

[13] J. Aravind, T. Saranya, G. Sudha, P. Kanmani, Integrated Waste Management in India, (2016) 49–58. https://doi.org/10.1007/978-3-319-27228-3.

[14] J. Du, L. Li, S. Zhou, Microbial production of cyanophycin: From enzymes to biopolymers, Biotechnol. Adv. 37 (2019). https://doi.org/10.1016/j.biotechadv.2019.05.006.

[15] T. Hai, F.B. Oppermann-Sanio, A. Steinbüchel, Purification and characterization of cyanophycin and cyanophycin synthetase from the thermophilic Synechococcus sp. MA19, FEMS Microbiol. Lett. 181 (1999) 229–236. https://doi.org/10.1016/S0378-1097(99)00544-3.

[16] B. Watzer, K. Forchhammer, Cyanophycin: A Nitrogen-Rich Reserve Polymer, in: K.F.E.-A. Tiwari (Ed.), IntechOpen, Rijeka, 2018: p. Ch. 5. https://doi.org/10.5772/intechopen.77049.

[17] R.D. Simon, Measurement of the cyanophycin granule polypeptide contained in the blue green alga Anabaena cylindrica, J. Bacteriol. 114 (1973) 1213–1216. https://doi.org/10.1128/jb.114.3.1213-1216.1973.

[18] A. Steinbüchel, A. Sallam, Dipeptides in nutrition and therapy: Cyanophycin-derived dipeptides as natural alternatives and their biotechnological production, Appl. Microbiol. Biotechnol. 87 (2010) 815–828. https://doi.org/10.1007/s00253-010-2641-0.

[19] D. Hasson, H. Shemer, A. Sher, State of the art of friendly "green" scale control inhibitors: A review article, Ind. Eng. Chem. Res. 50 (2011) 7601–7607. https://doi.org/10.1021/ie200370v.

[20] J. Sanders, E. Scott, R. Weusthuis, H. Mooibroek, Bio-refinery as the bio-inspired process to bulk chemicals, Macromol. Biosci. 7 (2007) 105–117. https://doi.org/10.1002/mabi.200600223.

[21] A.M. Ruffing, T. Kallas, Editorial: Cyanobacteria: The Green E. coli, Front. Bioeng. Biotechnol. 4 (2016) 7. https://doi.org/10.3389/fbioe.2016.00007.

[22] F. Shi, Z. Xu, P. Cen, Microbial production of natural poly amino acid, Sci. China, Ser. B Chem. 50 (2007) 291–303. https://doi.org/10.1007/s11426-007-0061-5.

[23] M. Obst, A. Steinbüchel, Microbial degradation of poly (amino acid)s, Biomacromolecules. 5 (2004) 1166–1176. https://doi.org/10.1021/bm049949u.

[24] B. Watzer, A. Engelbrecht, W. Hauf, M. Stahl, I. Maldener, K. Forchhammer, Metabolic pathway engineering using the central signal processor PII, Microb. Cell Fact. 14 (2015). https://doi.org/10.1186/s12934-015-0384-4.

[25] A. Trautmann, B. Watzer, A. Wilde, K. Forchhammer, C. Posten, Effect of phosphate availability on cyanophycin accumulation in Synechocystis sp. PCC 6803 and the production strain BW86, Algal Res. 20 (2016) 189–196. https://doi.org/10.1016/j.algal.2016.10.009.

[26] L. Lippi, L. Bähr, A. Wüstenberg, A. Wilde, R. Steuer, Exploring the potential of high-density cultivation of cyanobacteria for the production of cyanophycin, Algal Res. 31 (2018) 363–366. https://doi.org/10.1016/j.algal.2018.02.028.

[27] A. Bertucco, M. Beraldi, E. Sforza, Continuous microalgal cultivation in a laboratory-scale photobioreactor under seasonal day – night irradiation : experiments and simulation, (2014) 12–18. https://doi.org/10.1007/s00449-014-1125-5.

[28] C.E. de Farias Silva, E. Sforza, A. Bertucco, Stability of carbohydrate production in continuous microalgal cultivation under nitrogen limitation: effect of irradiation regime and intensity on Tetradesmus obliquus, J. Appl. Phycol. 30 (2018) 261–270. https://doi.org/10.1007/s10811-017-1252-x.

[29] R. Rippka, J.J.B.W. Deruelles, J.B. Waterbury, M. A. Herdman, R.Y. Stanier, Generic Assignments, Strain Histories and Properties of Pure Cultures of Cyanobacteria, Microbiology-Sgm. 111 (1979) 1–61. https://doi.org/10.1099/00221287-111-1-1.

[30] M. Innamorati, I. Ferrari, D. Marino, M. Ribera D' Alcala, Metodi nell' ecologia del plancton marino. In Nova Thalassia, Edizioni L, 1990.

[31] J.J. Ameel, R.P. Axler, C.J. Owen, Persulfate digestion for determination of total nitrogen and phosphorus in low-nutrient waters, Am. Environ. Lab. 5 (1993) 1–11.

[32] W.E. Trevelyan, J.S. Harrison, Studies on yeast metabolism. I. Fractionation and microdetermination of cell carbohydrates., Biochem. J. 50 (1952) 298–303. https://doi.org/10.1042/bj0500298.

[33] D. A. Bryant, The Molecular Biology of Cyanobacteria in Advances in Photosynthesis book series (AIPH, volume 1), Springer, Dordrecht, 1994. https://doi.org/10.1007/978-94-011-0227-8.

[34] Y. Elbahloul, M. Krehenbrink, R. Reichelt, A. Steinbüchel, Physiological conditions conducive to high cyanophycin content in biomass of Acinetobacter calcoaceticus

Strain ADP1, Appl. Environ. Microbiol. 71 (2005) 858–866. https://doi.org/10.1128/AEM.71.2.858-866.2005.

[35] M.M. Bradford, A rapid and sensitive method for the quantitation of microgram quantities of protein utilizing the principle of protein-dye binding, Anal. Biochem. 72 (1976) 248–254. https://doi.org/https://doi.org/10.1016/0003-2697(76)90527-3.

[36] B.D. Fernandes, A. Mota, J.A. Teixeira, A.A. Vicente, Continuous cultivation of photosynthetic microorganisms: Approaches, applications and future trends, Biotechnol. Adv. 33 (2015) 1228–1245. https://doi.org/10.1016/j.biotechadv.2015.03.004.

[37] E. Barbera, A. Grandi, L. Borella, A. Bertucco, E. Sforza, Continuous cultivation as a method to assess the maximum specific growth rate of photosynthetic organisms, Front. Bioeng. Biotechnol. 7 (2019) 1–12. https://doi.org/10.3389/fbioe.2019.00274.

[38] E. Touloupakis, B. Cicchi, G. Torzillo, A bioenergetic assessment of photosynthetic growth of Synechocystis sp. PCC 6803 in continuous cultures, Biotechnol. Biofuels. 8 (2015) 1–11. https://doi.org/10.1186/s13068-015-0319-7.

[39] N. Powell, A. Shilton, Y. Chisti, S. Pratt, Towards a luxury uptake process via microalgae - Defining the polyphosphate dynamics, Water Res. 43 (2009) 4207–4213. https://doi.org/10.1016/j.watres.2009.06.011.

[40] Y. Zhou, B.T. Nguyen, C. Zhou, L. Straka, Y.J.S. Lai, S. Xia, B.E. Rittmann, The distribution of phosphorus and its transformations during batch growth of Synechocystis, Water Res. 122 (2017) 355–362. https://doi.org/10.1016/j.watres.2017.06.017.

[41] A. Voronkov, M. Sinetova, Polyphosphate accumulation dynamics in a population of Synechocystis sp. PCC 6803 cells under phosphate overplus, Protoplasma. 256 (2019) 1153–1164. https://doi.org/10.1007/s00709-019-01374-2.

[42] Y.K. Lee, W. Chen, H. Shen, D. Han, Y. Li, H.D.T. Jones, J.A. Timlin, Q. Hu, Basic Culturing and Analytical Measurement Techniques, Handb. Microalgal Cult. Appl. Phycol. Biotechnol. Second Ed. (2013) 37–68. https://doi.org/10.1002/9781118567166.ch3.

[43] L. Borella, E. Sforza, A. Bertucco, How the residence time in continuous photobioreactor affects mass and energy balance of microalgal protein production, New Biotechnol. under Revis. (2020).

[44] L. Straka, B.E. Rittmann, The role of heterotrophic bacteria in assessing phosphorus

stress to Synechocystis sp. PCC6803, J. Appl. Phycol. 29 (2017) 1877–1882. https://doi.org/10.1007/s10811-017-1098-2.

[45] J.L. Collier, A.R. Grossman, Chlorosis induced by nutrient deprivation in Synechococcus sp. strain PCC 7942: Not all bleaching is the same, J. Bacteriol. 174 (1992) 4718–4726. https://doi.org/10.1128/jb.174.14.4718-4726.1992.

[46] G. Markou, Alteration of the biomass composition of Arthrospira (Spirulina) platensis under various amounts of limited phosphorus, Bioresour. Technol. 116 (2012) 533–535. https://doi.org/10.1016/j.biortech.2012.04.022.

[47] C.E. de Farias Silva, A. Bertucco, Bioethanol from microalgae and cyanobacteria: A review and technological outlook, Process Biochem. 51 (2016) 1833–1842. https://doi.org/10.1016/j.procbio.2016.02.016.

[48] E. Aboulmagd, F.B. Oppermann-Sanio, A. Steinbüchel, Purification of Synechocystis sp. Strain PCC6308 Cyanophycin Synthetase and Its Characterization with Respect to Substrate and Primer Specificity, Appl. Environ. Microbiol. 67 (2001) 2176–2182. https://doi.org/10.1128/AEM.67.5.2176-2182.2001.

[49] H. Mooibroek, N. Oosterhuis, M. Giuseppin, M. Toonen, H. Franssen, E. Scott, J. Sanders, A. Steinbüchel, Assessment of technological options and economical feasibility for cyanophycin biopolymer and high-value amino acid production, Appl. Microbiol. Biotechnol. 77 (2007) 257–267. https://doi.org/10.1007/s00253-007-1178-3.

Appendix

Table 4A.1. Summary of data obtained from continuous experiments with *Synechocystis* sp. PCC 6803 at residence time equal to 2.28 d (± SD; n≥4).

Phosphorus inlet concentration	c_x $g_x\ L^{-1}$	P_x $g_x\ L^{-1}\ d^{-1}$	q_{CGP} $g_{CGP}\ g_x^{-1}$	P_{CGP} $g_{CGP}\ L^{-1}\ d^{-1}$
P2	1.15±0.02	0.439±0.008	-	-
P1	0.982±0.07	0.364±0.024	-	-
P1/2	0.568±0.04	0.211±0.017	0.127±0.012	26.7±2.61
P1/4	0.329±0.02	0.134±0.009	0.137±0.011	18.5±1.42

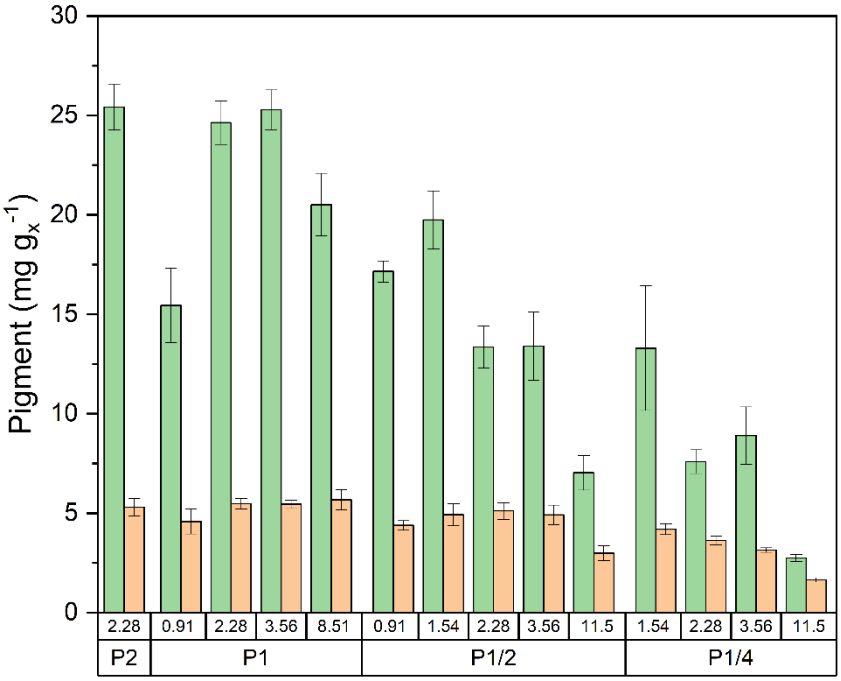

Figure 4A.1. Pigment content in biomass (mg g^{-1}) at different residence time and inlet phosphorus concentration (*green* for chlorophyll; *orange* for carotenoid). Error bars represent the standard deviation of at least 4 samples for each steady state (n≥4).

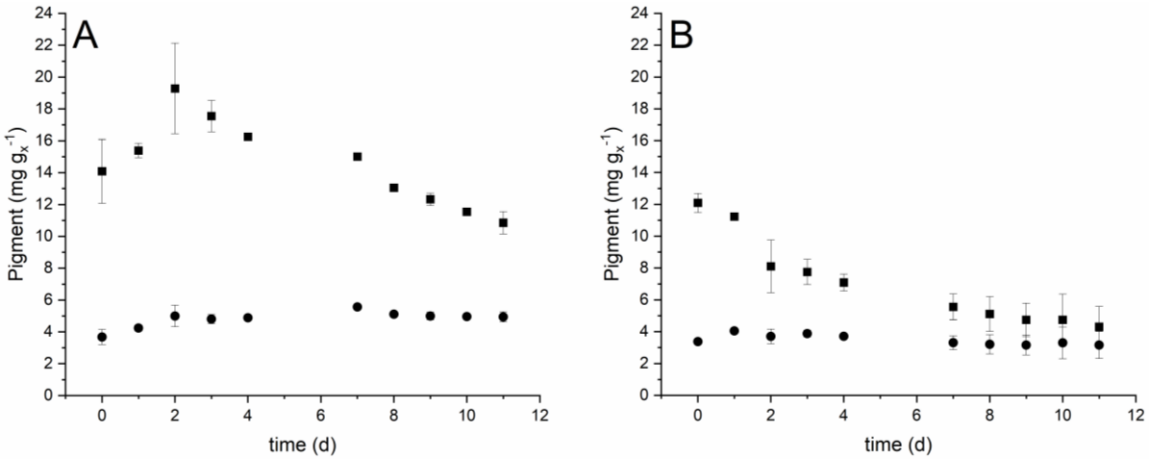

Figure 4A.2. Growth curves of *Synechocystis* sp. PCC 6803 expressed in terms of total chlorophyll (*squares*) and carotenoid (*circles*) in control conditions (panel A) and in phosphorus limited condition (panel B). Error bars represent the standard deviation (n=4, two technical replicates for two biological replicates).

Chapter 5

Fixing N_2 into cyanophycin: continuous cultivation of *Nostoc* sp. PCC 7120

Two diazotrophic cyanobacteria (*Anabaena cylindrica* PCC 7122 and *Nostoc* sp. PCC 7120) were cultivated to produce cyanophycin, a nitrogen reserve compound, under nitrogen fixing conditions. In preliminary continuous experiments, *Nostoc* sp. was shown to be more efficient, accumulating a higher amount of cyanophycin and showing a greater capability to fix atmospheric nitrogen in the biomass (67 mg_N d^{-1} of fixed nitrogen per liter of culture). The operating conditions were then optimized to maximize the cyanophycin productivity: the effect of incident light intensity, residence time and nitrogen availability were investigated. Nitrogen availability and/or pH played a major role with respect to biomass production, whereas phosphorus limitation was the main variable to maximize cyanophycin accumulation. In this way, it was possible to achieve a stable and continuous production of cyanophycin (CGP) under diazotrophic conditions, obtaining a maximum cyanophycin productivity of 15 mg_{CGP} L^{-1} d^{-1}.

Part of this Chapter was published as a scientific paper in *Applied Microbiology and Biotechnology* (Trentin, G., Piazza, F., Carletti, M., Zorin, B., Khozin-Goldberg, I., Bertucco, A., Sforza, E., 2022, https://doi.org/10.1007/s00253-022-12292-4)

5.1 Introduction

Nitrogen is the second most important element for the survival of living organisms: it is a component of amino acids, enzymes, nucleic acids, peptidoglycans and is also required in photosynthetic organisms for the synthesis of chlorophyll [1]. However, gaseous dinitrogen (N_2) is chemically inert and therefore metabolically inaccessible [1], thanks to the high stability of the triple bond between the two nitrogen atoms. Furthermore, to be incorporated into biological macromolecules, it must be reduced to ammonia [2]. For this reason, after sulphuric acid, ammonia is the second largest synthetic inorganic chemical manufactured in the world, and is the basic building block of the world nitrogen industry [3]. It is estimated that the annual production of ammonia is 146 million tons, at an energy cost of 28 GJ per ton, exploiting approximately 1% of the global energy consumed each year [4]. At the industrial level, ammonia is obtained by reacting N_2 with H_2 at high temperatures and pressures according to the Haber-Bosch process, with most plants operated at 200-400 atm and 450-600°C [5].

In recent years, the interest towards bio-sustainable industrial processes able to exploit the great potential of microorganisms for obtaining food, drugs and energy has received increasing interest [6]. Bio-based processes are in fact less energy demanding and more environmentally friendly, as they operate at ambient temperature and pressure. A few species of prokaryotic microorganisms including cyanobacteria, referred to as nitrogen-fixing or diazotrophic ones, are able to enzymatically catalyse the reaction of nitrogen gas fixation to organic molecules at ambient temperature and pressure. Therefore, they do not require the presence of a nitrogen source in the culture medium, but instead use atmospheric nitrogen to support their metabolism [1,7]. These cyanobacteria produce many commercial relevant compounds, such as phycocyanin, zeaxanthin, β-carotene, poly-hydroxy-alkanoates, proteins and PUFAs [8–10], as well as cyanophycin (CGP), a non-ribosomal synthesized polyaminoacid compound, which is interesting as a source of polyaspartic acid (PASP) and arginine, replacing the standard petrochemical-based industrial products [11]. Usually, polyaspartic acid is synthesized by polymerization of aspartic acid or maleic anhydride. In both cases, elevated temperature (greater than 160°C) and by-product removal are required to achieve high molecular weights and reaction yields [12]. On the other hand, amino acids like arginine, instead, are produced through protein hydrolysis, chemical synthesis, and microbiological synthesis. Specifically, most of L-arginine is produced by the direct-fermentation method from natural carbon sources (e.g. sugar, sugar

syrup, glucose from tapioca or corn). Because L-arginine contains 4 atoms of nitrogen, also a source of nitrogen must be supplied, as ammonia or ammonium sulphate [13]. Cyanophycin can be synthetized by both diazotrophic and non-diazotrophic filamentous and unicellular cyanobacteria, and also by some heterotrophic bacteria [14,15]. Cyanophycin acts as a temporary nitrogen reserve compound. In heterocystic diazotrophic cyanobacteria, the accumulation of cyanophycin is correlated to a peak of nitrogenase activity, causing the formation of dense polar nodules in the conjunction between heterocysts and the adjacent vegetative cells. This position facilitates its transportation [16]. Indeed, as early as in 1980, cyanophycin synthetase activity and cyanophycinase activity were measured to be 30- and 70-fold greater in heterocysts than in vegetative cells, thus suggesting that cyanophycin can be rapidly polymerized and depolymerized in such cells. It means that CGP is a dynamic reservoir rather than a passive nitrogen reserve [17]. It has been also shown that iso-aspartyl dipeptidase is preferentially expressed in vegetative cells, to allow the release of the two amino acids arginine and aspartate, once the CGP is converted into dipeptide by cyanophycinase and then transferred into the vegetative cells [14]. The production of cyanophycin in cyanobacteria is limited by their relatively slow growth rate compared to heterotrophic bacteria and by the lower achievable productivities of this biopolymer [11]. Also transgenic plants as *Nicotiana tabacum* and *Solanum tuberosum* were used to produce cyanophycin, even if lower production yields were obtained than with bacterial strains [18]. As regards the production with heterotrophic microorganisms, 970±80 mg L^{-1} and 1.5 g L^{-1} of cyanophycin were produced with *E. coli* BL21 (DE3) and *E. coli* DH1, respectively [15,19]. Although the heterologous CGP production in bacteria is larger than the native one [20], the use of photoautotrophic cyanobacteria for the synthesis of biopolymers allows to develop production processes with a significantly lower impact on the environment [14], as heterotrophic microorganisms require the presence of an organic carbon source [21] and supplementation of reduced nitrogen. In addition, photoautotrophic microorganisms accumulate cyanophycin in its native form (25-100 kDa) [22], while heterologous systems produce smaller size cyanophycin (25-45 kDa), which can contain additional amino acid constituents as lysine [19,23,24]. This suggests that additional factors are involved in the regulation of the polymer length present in native CGP accumulating microorganisms [14,25,26]. The relevant literature about cyanophycin production by diazotrophic cyanobacteria is limited to physiological and molecular studies and cultivation in batch systems [22,27,28]. Due to the transient accumulation during the growth phases of cyanobacteria, batch systems are

not suitable to assess the potential productivity of such a compound: as an example, Simon in 1973 [22] found a maximum CGP quota (7.8% DW) in the stationary phase cells. Then, when this culture was diluted, cyanophycin played its role as a transient N reserve and was completely utilized in beginning of the new growth phase. The same pattern has recently been observed by Canizales et al. [27], who studied the accumulation of cyanophycin using urea and ammonia as nitrogen sources in *Synechocystis* sp. PCC 6803. Other studies carried out in batch systems showed that after the addition to the cultivation medium of a source of nitrogen as ammonia, it was measured a temporary increase in the CGP quota, which however was then rapidly degraded [28,29]. So far, batch cultivation appears to be poorly efficient in boosting the CGP productivity in cyanobacteria.

Recently, Trentin et al. [30] demonstrated that it is possible to obtain a higher and stable production of cyanophycin by continuous cultivation of the unicellular, non-diazotrophic cyanobacterium *Synechocystis* sp. PCC 6803 under balanced phosphorus limitation. Indeed, cyanobacterial growth in phosphate-limited conditions resulted in CGP accumulation [27,31,32]. Stevens et al. [32] observed by electron microscopy that as phosphate depletion proceeded, not only the number of the CGP granules per cells, but also the diameter of each granule, increased. Concerning the possibility of continuously cultivating diazotrophic cyanobacteria, Barbera et al. [33] obtained remarkable productivities with *Anabaena* sp. in a continuous cultivation system, showing that the growth of diazotrophic organisms can be efficient is such operating conditions.

In this work, two diazotrophic cyanobacteria were cultivated in a continuous system under N_2 fixing conditions to possibly assess the possible stable production of cyanophycin. In particular, it was evaluated the effect of operating variables in this continuous system, such as inlet phosphorus concentration, incident light intensity, residence time, and nitrogen availability, on biomass and cyanophycin productivities. The goal is to produce biomass having specific composition and constant quality over time, with high productivities and, at the same time, reducing the costs associated with the process, in view of developing a system compatible with large-scale production.

5.2 Materials and methods

5.2.1 Experimental setup

Anabaena sp. PCC 7122 (*Anabaena cylindrica*) and *Nostoc* sp. PCC 7120 were purchased from UTEX Culture Collection of Algae at The University of Texas at Austin (US). Cyanobacteria were maintained in diazotrophic conditions at a constant temperature of 24±1°C in the BG11 medium [34], modified to remove all nitrogen compounds present: the organic buffer Hepes and Ferric ammonium citrate were substituted with Sodium bicarbonate and Ferric chloride hexahydrate ($FeCl_3 \cdot 6H_2O$), respectively. The final composition of the medium was reported in Table 5A.1 in the Appendix. Before use, the medium was sterilized in autoclave for 20 min at 121°C. Experiments were carried out in a vertical flat-plate polycarbonate photobioreactor with a working volume of 150 mL (V_{PBR}), an irradiated surface of 0.005 m^2 (A_{PBR}) and a thickness of 3 cm. Light (I_0) was provided continuously by a white LED lamp. Photon Flux Density (PFD) was measured using a photoradiometer (HD 2101.1 from Delta OHM), by means of a quantum radiometric probe which quantifies the Photosynthetically Active Radiation (PAR). The mixing was ensured by both a stirring magnet placed at the bottom of the reactor and the bubbling of 1 L h^{-1} of CO_2-air (5% v/v) mixture. The bubbling guaranteed the carbon supply as well the control of the pH within the interval 7.5-8.5, monitored daily using a Hanna portable pH-meter (code HI9124). Moreover, this configuration allows to minimize the cells adhesion to the walls so that the system can be approximated to a Continuous Stirred Tank Reactor (CSTR). In a CSTR, the specific growth rate μ (d^{-1}) is equal to the dilution rate D that is the inverse of the residence time τ (d) (Eq.1). By definition, the residence time is equal to the ratio between the volume of the reactor (V_{PBR}) and the inlet volumetric flowrate (Q).

$$\mu = D = \frac{1}{\tau} = \frac{Q}{V_{PBR}} \tag{5.1}$$

The volume of the reactor (V_{PBR}) was maintained constant thanks to an overflow pipe, which allows the output of the exhausted biomass with the same flowrate (Q) at which the fresh medium is pumped into the reactor, by means of a multichannel peristaltic pump (205S/CA, Watson-Marlow Fluid Technology Group). So, by changing the residence time, i.e. changing the flowrate Q, it is possible to set different growth rates. With this system,

after a transition period of about three times the residence time, steady state was achieved. At this point, nutrient consumption, biomass concentration and composition remained constant until the experimental conditions change, and a new transitory period can be observed. The presence of contaminants in the reactor was checked periodically, by plating the samples in LB Petri dishes, and the culture was discarded in case of contamination. Accordingly, the productivity P_i (g_i L^{-1} d^{-1}) was calculated as the ratio between the concentration of the component *i* measured at steady state (c_i) (e.g., biomass, cyanophycin, nitrogen) and the residence time (τ):

$$P_i = \frac{c_i}{\tau} \tag{5.2}$$

Steady state achievement was monitored daily through optical density measurement at 750 nm, with a UV-visible double beam spectrophotometer (UV1900, by Shimadzu, Japan). When the steady state was reached, it was kept for at least a period equal to three times the residence time, and samples of exhausted culture medium were withdrawn daily from the reactor for quantification and composition analysis. Dry cell weight (c_x) at steady state was measured by vacuum filtration, through 0.45 μm previously dried nitrocellulose filters, which then were dried for 2 h at 105°C in a laboratory oven. Biomass composition at steady state was characterized in terms of phosphorus, nitrogen, pigment, cyanophycin and protein internal quotas. Phosphorus and nitrogen content in the biomass were measured on centrifuged samples to remove the supernatant, at 9960 rcf (relative centrifugal force) for 10 min. The method used is an alkaline persulfate digestion [35], followed by the quantification of released orthophosphates and nitrates. Orthophosphates are quantified following the protocols of Innamorati et al. [36], whereas nitrates are measured with the diagnostic kit Hydrocheck Spectratest (Code 6223). Extraction and quantification of pigments was carried out by N,N-dimethylformamide (DMF). A known volume of the culture was centrifuged at 9960 rcf for 10 min to remove the supernatant. Then, isovolume quantity of solvent was added in the dark, because once taken into solution, pigments are photosensitive. Samples were then stored in freezer for at least 48 h to ensure complete pigment extraction. The absorption spectrum on the extract was measured using DMF as reference solvent, after a further centrifugation step. The final concentration of total chlorophyll and carotenoids was determined according to Bryant [37]. Furthermore, at steady state, the PFD was measured also at the back surfaces of the PBR (*BI*) to calculate photosynthetic efficiency based on the PAR, according to

$$\eta_{PAR} = \frac{c_x \cdot Q \cdot LHV}{PDF_{abs} \cdot E_P \cdot A_{PBR}} \quad (5.3)$$

In Eq. (5.3) c_x is the steady state biomass concentration, Q is flowrate, PFD_{abs} is the difference in the irradiance between the front (I_0) and the back (BI) of the photobioreactor surface, A_{PBR} is the irradiated surface of the reactor, E_P is the average energy of photons (0.223 kJ $mmol^{-1}$), and LHV is the Lower Heating Value of biomass (12.28 kJ g_x^{-1}), calculated with equations reported by Vardon et al. and Sung et al. [38,39].

The effect of the inlet phosphorus concentration on cyanophycin productivity was investigated with both the cyanobacterial species (*Anabaena* cylindrica PCC 7122 and *Nostoc* sp. PCC 7120). The residence time (τ) and the incident light intensity (I_0) were kept constant respectively at 2.3 d and 450 µmol photons m^{-2} s^{-1}, according to previous literature on cyanophycin production in continuous system [30] and on continuous cultivation of diazotrophic cyanobacteria [33]. Inlet phosphorus concentrations were varied from the one commonly present in standard BG11 medium (about 5 mg_P L^{-1}) to about 1 mg_P L^{-1}, modifying the concentration of potassium hydrogen phosphate (K_2HPO_4) in the cultivation medium feed. Phosphorus concentration was ascertained by measuring it in both the reactor inlet and outlet streams, following the procedure proposed by Innamorati et al. [36] after biomass removal by filtration. The operating conditions are summarized in Table 5.1.

Table 5.1. Summary of operating condition in preliminary continuous experiments with *Anabaena cylindrica* PCC 7122 and *Nostoc* sp. PCC 7120

		Inlet phosphorus concentration (c_P^{inlet}) (mg_P L^{-1})	**Residence time (τ) (d)**	**Incident light intensity (I_0) (µmol photons m^{-2} s^{-1})**
Effect of the inlet phosphorus concentration	*Anabaena cylindrica* PCC 7122	5.5±0.5 2.8±0.1 2.0±0.1 1.5±0.1 1.0±0.2	2.3	450
	Nostoc sp. PCC 7120	5.9±0.1 2.2±0.1 2.0±0.2 1.7±0.1 1.2±0.1	2.3	450

A second set of experiments was carried out with *Nostoc* sp. PCC 7120, to further test the effect of incident light intensity, residence time, and nitrogen availability. The effect of the incident light intensity was evaluated using two inlet phosphorus concentrations (2.01±0.17 mg_P L^{-1} and 1.04±0.03 mg_P L^{-1}) at a constant residence time of 2.3 d. When addressing the

effect of the residence time, instead, reactors were illuminated continuously at 450 µmol photons m^{-2} s^{-1} and phosphorus concentration in the inlet stream was set to 1.1±0.03 mg_P L^{-1}. Finally, the effects of nitrogen availability and pH on the reactor productivity were addressed. To change the pH value, the cultivation medium was modified by removing sodium carbonate and reducing sodium bicarbonate concentration to 250 mg L^{-1}. Where specified, the cyanobacteria were grown in the presence of a non-limiting source of nitrogen as $NaNO_3$ (3000 mg L^{-1}). In both cases, the inlet phosphorus concentration, the incident light intensity and the residence time were maintained constant respectively at 1.2±0.03 mg_P L^{-1}, 450 µmol photons m^{-2} s^{-1} and 2.3 d. The operating conditions are summarized in Table 5.2.

Table 5.2. Summary of operating condition in continuous experiments with *Nostoc* sp. PCC 7120

	Inlet phosphorus concentration (c_P^{inlet}) (mg_P L^{-1})	**Residence time (τ) (d)**	**Incident light intensity (I_0) (µmol photons m^{-2} s^{-1})**	**Other modification**
Effect of incident light intensity	2.01±0.17	2.3	200 450 650	-
	1.04±0.03	2.3	200 450 650	-
Effect of residence time	1.1±0.03	1.8 2.3 3 4.7	450	-
Effect of nitrogen availability and pH	1.2±0.03	2.3	450	- low pH low pH+$NaNO_3$

Additional preliminary experiments were carried out with both species in batch systems, in at least two/three independent biological replicates. Quickfit® Drechsel Bottles with a volume of 200 mL and a diameter of 5 cm were used. A mixture of CO_2-air (5% v/v) was bubbled continuously from the bottom of the reactor. Additionally, a good mixing within the reactor was ensured by the presence of a magnetic stirrer. The incident light intensity was provided continuously by a LED lamp at a constant value of 100 µmol photons m^{-2} s^{-1}. Experiments last 10 days and were carried out with two concentration of potassium hydrogen phosphate in the cultivation medium: 7.3±0.1 mg_P L^{-1} and 1.4±0.1 mg_P L^{-1}, to assess the effect of phosphate limitation on CGP accumulation. Quantification of biomass and cyanophycin concentration was done according to the same procedures used in the continuous experiments. By linear regression of experimental points of biomass

concentration measured during the logarithmic phase of growth, it was possible to calculate the cyanobacterial specific growth rate.

5.2.2 Cyanophycin extraction and quantification

Cyanophycin extraction and quantification were done according to the methods proposed by Elbahloul et al. and Trautmann et al. [31,40]. The pellet of known volume of the culture was resuspended in acetone at room temperature to increase the permeability of the membranes. Then, it was washed twice with 50 mM Tris-HCl, to remove soluble proteins. To solubilize cyanophycin, 0.1M HCl was used. The solubilized cyanophycin was then precipitated using 100 mM Tris-HCl. The quantification of this cyanophycin was done according to the Bradford colorimetric assay using CGP standard, isolated from *Nostoc* sp.. This extraction method ensures that the proteins are not extracted, to avoid interference in the Bradford method. The extracted cyanophycin was dried, analysed in terms of amino acid composition and used as the standard for the calibration curve.

5.2.3 Statistical analysis

Statistical tests were applied to data measured at steady state, and were performed separately for each category of data. The existence of equal variance among data was verified with Levene's test using a confidence level of 95%. Statistically significant differences among the data were ascertained through one-way ANOVA analysis. Grouping was done according to Tukey's multiple comparison procedure with a 95% confidence interval. Data that do not share a letter were significantly different.

5.2.4 Calculation of N_2 solubility in the culture

Aspen Plus™ process simulator (V12.1) was used to predict and to carry out sensitivity analysis on nitrogen solubility as a function of operating conditions. A flash unit operated at 24°C and 1 atm was fed with a gaseous stream (75.2% N_2, 20% O_2, 4.8% CO_2, v) and with a liquid stream with the composition of the microalgal cultivation medium. The thermodynamic model was the Elec-NRTL, which can suitably deal with ionic species included in the cultivation medium fed to the process, and with the related chemical equilibria. It was previously validated using literature data of nitrogen solubility in water (data not shown). Table 5.3 reports the equilibrium and dissociation reactions considered

in the simulation. The formation of solid species was neglected, as it would irrelevantly complicate the simulation. The non-condensable components (O_2, CO_2, and N_2) were modelled as Henry components, i.e. their solubility was evaluated according to the Henry's law.

Table 5.3. Equilibrium and dissociation reactions included in the global chemistry

Type	Stoichiometry
Equilibrium	$H_2O + H_2PO_4^- \rightleftharpoons H_3O^+ + HPO_4^{2-}$
	$H_2O + HPO_4^{2-} \rightleftharpoons H_3O^+ + PO_4^{3-}$
	$H_3PO_4 + H_2O \rightleftharpoons H_3O^+ + H_2PO_4^-$
	$H_2O + HCO_3^- \rightleftharpoons CO_3^{2-} + H_3O^+$
	$2H_2O + CO_2 \rightleftharpoons HCO_3^- + H_3O^+$
	$2H_2O \rightleftharpoons OH^- + H_3O^+$
Dissociation	$NaHCO_3 \rightarrow HCO_3^- + Na^+$
	$Na_2CO_3 \rightarrow CO_3^{2-} + 2Na^+$
	$K_2HPO_4 \rightarrow HPO_4^{2-} + 2K^+$

5.3 Results

5.3.1 Preliminary batch experiments

Preliminary batch experiments were carried out to verify the effect of phosphorus limitation on cyanophycin production. Both species were cultivated at two different inlet phosphorus concentration ($c_{P,\ initial}$). Results are reported in Figure 5A.1 of Appendix. A decrease in the growth rate (μ) was observed when cyanobacteria were grown under phosphorus limitation. Specifically, it reduced from 0.38±0.11 d^{-1} and 0.44±0.03 d^{-1} to 0.23±0.02 d^{-1} and 0.33±0.01 d^{-1} for *Anabaena cylindrica* and *Nostoc* sp. PCC 7120, respectively. Indeed, in that case the cells entered the stationary phase already on the seventh day, whereas when P was present in the medium in a higher concentration, cells entered the stationary phase only on the ninth day. Consequently, the final biomass concentration and productivity measured on the tenth day of culture were higher under control conditions, compared to those found under P limitation conditions. The decrease in biomass concentration and productivity occurring in *Nostoc* PCC 7120 under limiting conditions was not as relevant as in the case of *Anabaena cylindrica*: this was probably because the growth of *Nostoc* PCC 7120 was less affected by the P limitation than that of *Anabaena cylindrica*, allowing the cells to

reach a higher concentration. Regarding the cyanophycin accumulation, consistently with the observations made by Simon in 1973 [22] in the first study concerning cyanophycin, the maximum quota of CGP was identified during the stationary phase of growth of the microorganisms, when the nutrients limitation was relevant. Moreover, for both species, the cyanophycin internal quota was greater when they were grown under P limitation condition, as found by Trautmann et al. [31] and Trentin et al. [30] in batch experiments. The maximum cyanophycin productivity was obtained with *Nostoc* sp. PCC 7120, also thanks to the higher biomass productivity obtained with this species. Results are summarized in Table 5.4.

Table 5.4. Summary of data obtained from batch experiments with *Anabaena cylindrica* and *Nostoc* sp. PCC 7120 (± SD; n=4, two technical replicates for two biological replicates)

	UoM	***Anabaena cylindrica***		***Nostoc* sp. PCC 7120**	
$c_{P,\,initial}$	$mg_P\ L^{-1}$	7.26±0.06	1.40±0.01	7.26±0.06	1.41±0.03
μ	d^{-1}	0.38±0.11	0.23±0.02	0.44±0.03	0.33±0.01
$c_{x,\,final}$	$g_x\ L^{-1}$	1.97±0.3	0.82±0.01	1.80±0.30	1.29±0.01
P_x	$mg_x\ L^{-1}\ d^{-1}$	175.5±35.2	62.6±3.9	161±44	116±1
$q_{CGP,\,final}$	%	2.1±0.26	13.5±1.9	4.1±1.68	11.5±0.4
$c_{CGP,\,final}$	$mg_{CGP}\ L^{-1}$	41.9±11.6	110.9±14.0	71.4±17.7	149.2±6.6
P_{CGP}	$mg_{CGP}\ L^{-1}\ d^{-1}$	4.2±1.2	11.1±1.4	7.1±1.8	14.9±0.7

5.3.2 Continuous cultivation of Anabaena cylindrica PCC 7122 and Nostoc sp. PCC 7120 to produce cyanophycin

The effect of different inlet phosphorus concentrations on the growth of two diazotrophic species was addressed, to identify which condition allows to increase cyanophycin productivity. The reactor was run at a residence time of 2.3 d ($D=0.43\ d^{-1}$), at a constant incident light intensity of 450 µmol photons $m^{-2}\ s^{-1}$, with decreasing P concentration in the inlet, as summarized in Table 5.1. The results of biomass and cyanophycin concentrations and productivities are shown in Figure 5.1.

For both of the species, the biomass concentration decreased at a decreasing inlet P concentration (Figure 5.1A and 5.1C), as a result of nutrient limitation. However, as observed for *Synechocystis* sp. PCC 6803 and other species [30–32], when the inlet phosphorus concentration is lower, the cyanophycin quota increases: the inlet concentration of phosphorus fed to the reactor has a trend that is inversely proportional to the cyanophycin quota. It should be mentioned that a commercial standard for cyanophycin quantification is not available yet. For this reason, in this work, a sample of cyanophycin from *Nostoc* sp.

was produced, extracted, dried and used as a reference for the quantification of cyanophycin after the extraction. The absence of a commercial compound and variation of procedures for CGP quantification is an issue when comparing our data with those from the literature, where other aminoacidic compounds are used for calibration, and possibly affected the exact quantification of CGP.

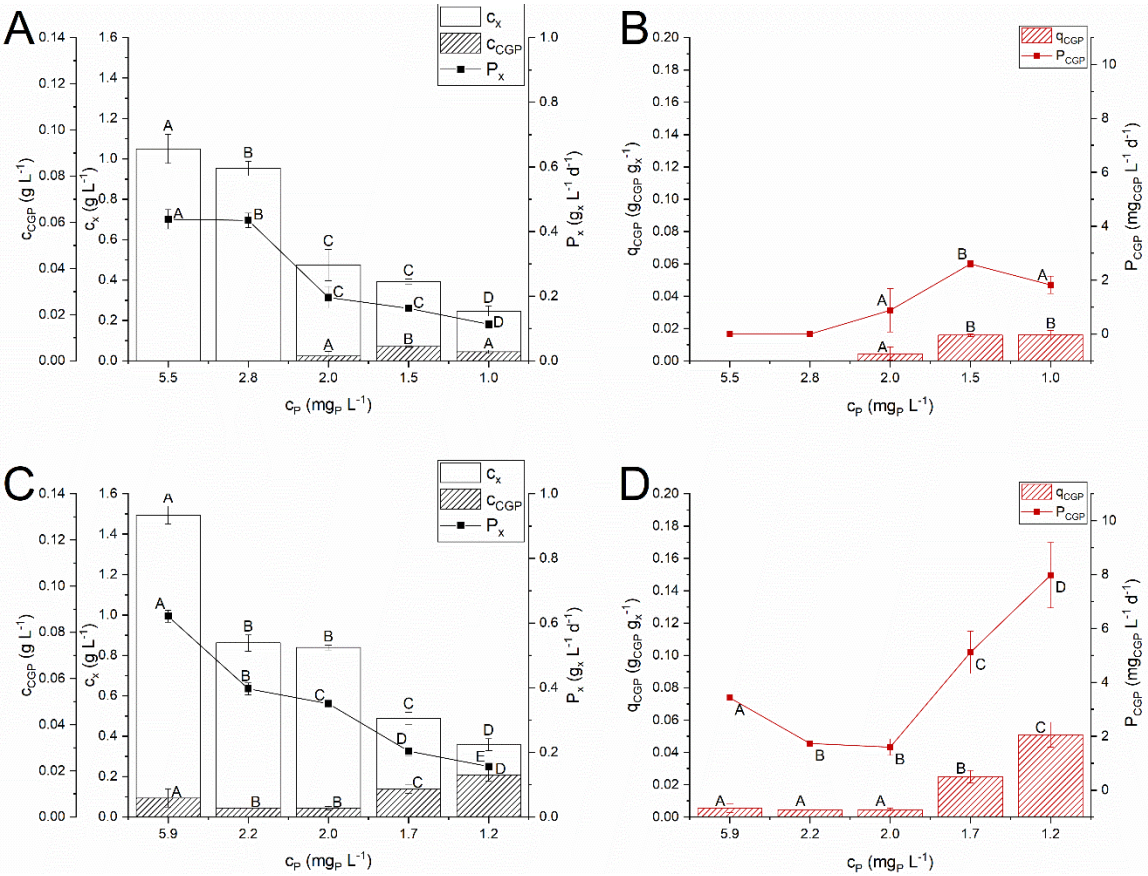

Figure 5.1. Steady state biomass concentration (c_x), cyanophycin concentration (c_{CGP}), biomass productivity (P_x), cyanophycin quota (q_{CGP}) and cyanophycin productivity (P_{CGP}) as function of the inlet phosphorus concentration (c_P) obtained with *Anabaena cylindrica* (panel A and B) and with *Nostoc* sp. PCC 7120 (panel C and D). Error bars represent the standard deviation of at least 4 samples for each steady state (n≥4). Statistical analysis was conducted separately for each category of data. Data that do not share a letter are significantly different. Lines are just eye guides

As for the two species tested, *Nostoc* sp. PCC 7120 appeared the most productive, reaching a higher biomass productivity in all the conditions investigated. This could be due to a greater ability to fix atmospheric nitrogen, allowing a greater biomass productivity even in limiting conditions of phosphorus. Indeed, since nitrogen was not supplied with the culture medium, it is necessary to have a deep insight of nitrogen quota measured in the experiments. Results of nitrogen quota ($Y_{N|X}$) and nitrogen biofixation rate (P_N) are shown in Figure 5.2.

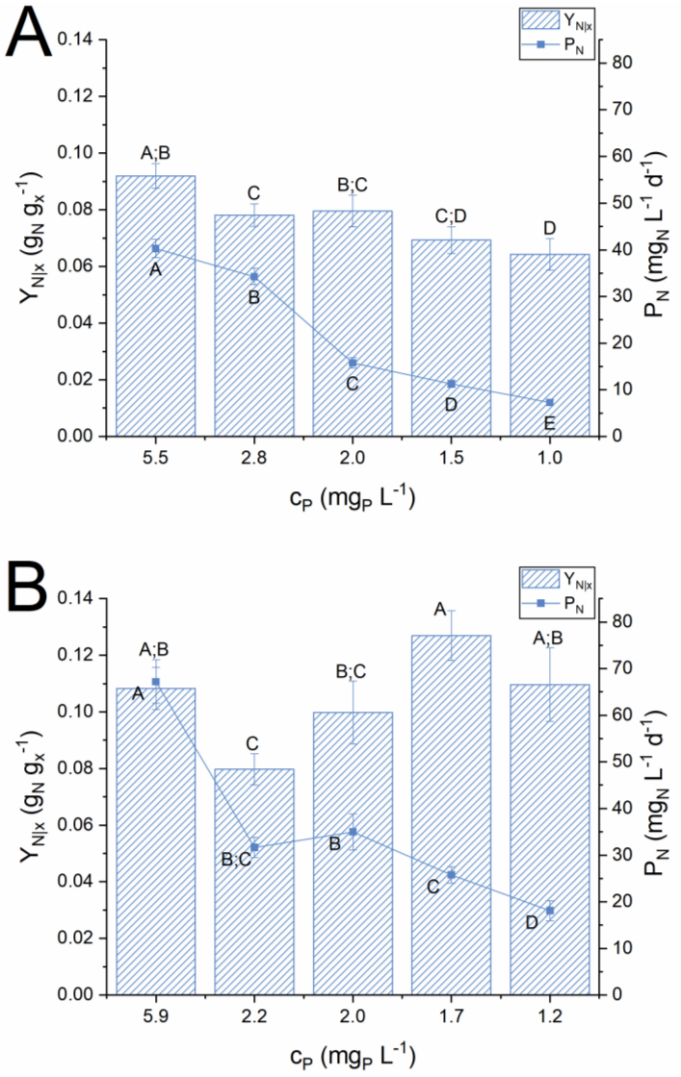

Figure 5.2. Steady-state nitrogen yield ($Y_{N|x}$) and nitrogen fixation rate (P_N) as function of the inlet phosphorus concentration (c_P) obtained with *Anabaena cylindrica* (panel A) and with *Nostoc* sp. PCC 7120 (panel B). Error bars represent the standard deviation of at least 4 samples for each steady state (n≥4). Statistical analysis was conducted separately for each category of data. Data that do not share a letter are significantly different. Lines are just eye guides

For both of the species it is clear that increasing the phosphorus in the inlet medium led to an increase in the nitrogen fixation rate. However, *Nostoc* sp. PCC 7120 achieved a greater quota of nitrogen in the biomass (Figure 5.2B), in all the experimental conditions. Thus, also the nitrogen fixation rate was greater, with a maximum value measured of 67.2±4.7 mg_N L^{-1} d^{-1}, 67% higher than that achieved with *Anabaena cylindrica* in the same experimental conditions. This value was much greater also with respect to the productivity calculated by Do Nascimento et al. [41], that was equal to 20 mg_N L^{-1} d^{-1} under laboratory controlled conditions and 13 mg_N L^{-1} d^{-1} outdoors. Overall, considering these preliminary results, *Nostoc* sp. PCC 7120 showed to be more efficient both in nitrogen fixation, and in biomass and cyanophycin productivity. For this reason, it was selected for the subsequent

studies to find the best operating conditions to maximize the cyanophycin production in a continuous system.

5.3.3 Effect of light intensity and residence time on cyanophycin accumulation at steady state

To find out the best operating conditions to accumulate cyanophycin in continuous cultivation of *Nostoc* sp. PCC 7120, the effects of two variables were studied: the incident light intensity and the residence time. Each one was varied, keeping the other at a constant value, as summarized in Table 5.2. Three incident light intensities were investigated: 200, 450 and 650 µmol photons m^{-2} s^{-1} and two different inlet P concentration were used (2.0±0.2 mg_P L^{-1} and 1.0±0.1 mg_P L^{-1}), as at these concentrations a larger cyanophycin quota was measured in preliminary experiments: the results obtained are reported in Figure 5.3.

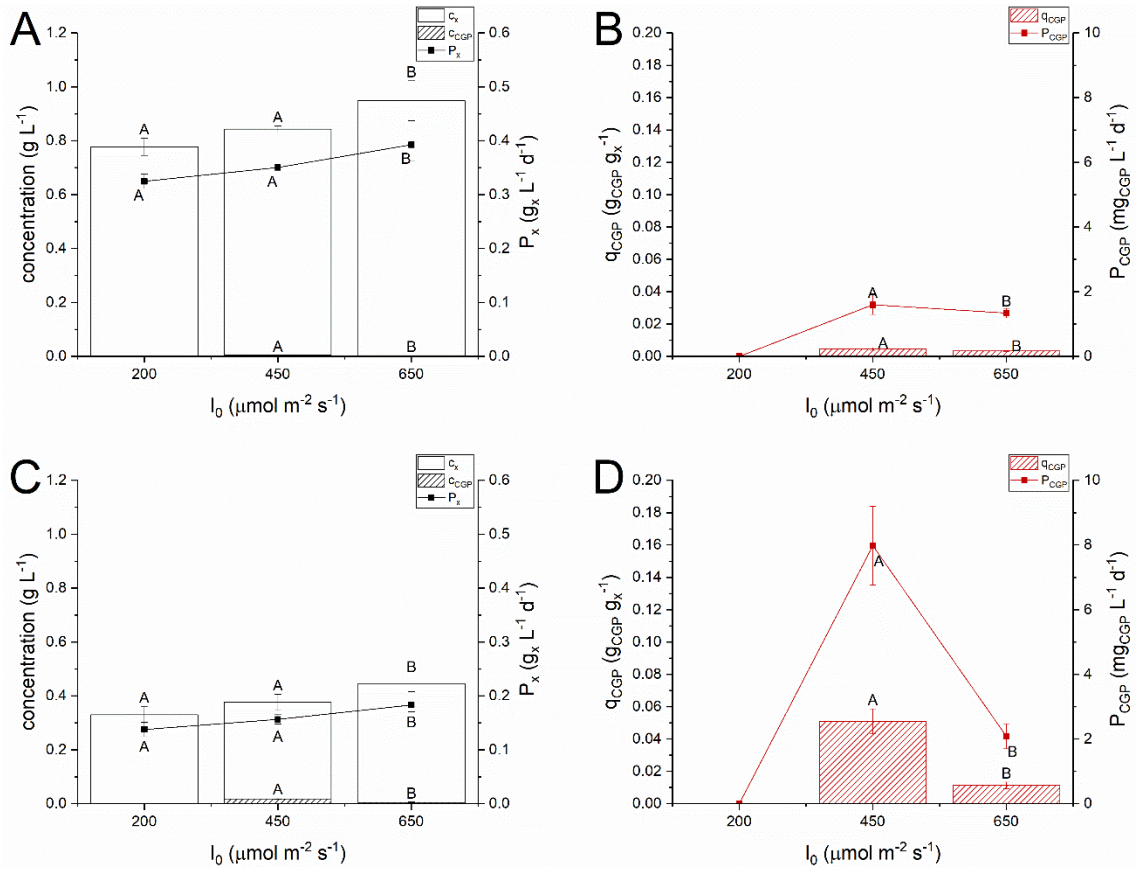

Figure 5.3. Steady state biomass concentration (c_x), cyanophycin concentration (c_{CGP}), biomass productivity (P_x), cyanophycin quota (q_{CGP}) and cyanophycin productivity (P_{CGP}) as function of the incident light intensity (I_0) with inlet P concentration equal to 2.0±0.2 mg_P L^{-1} (panel A and B) and inlet P concentration equal to 1.0±0.1 mg_P L^{-1} (panel C and D). Error bars represent the standard deviation of at least 4 samples for each steady state (n≥4). Statistical analysis was conducted separately for each category of data. Data that do not share a letter are significantly different. Lines are just eye guides

It can be seen that, regardless the inlet phosphorus concentration, the biomass concentration gets higher as the incident light intensity increases, in line with what reported for other microalgal species [42]. However, in this case, the biomass concentration poorly increased under higher light, possibly due to the stronger limitation caused by phosphorus depletion. Indeed, regardless the incident light intensity, also the pigment content was higher when larger amount of phosphorus was provided (2.0±0.2 mg_P L^{-1}). Regarding cyanophycin, no accumulation was observed at 200 μmol photons m^{-2} s^{-1}, similarly to what reported by Kromkamp [43], where *Aphanocapsa* accumulated 1.5% of cyanophycin in the biomass only, a lower value than that measured under high light intensities.

Based on the above results, a light intensity of 450 μmol photons m^{-2} s^{-1} and an inlet concentration of phosphorus equal to 1 mg_P L^{-1} were the conditions used to further study the effect of residence time (τ). Four were the values set (1.8, 2.3, 3.0 and 4.7 d) with results reported in Figure 5A.2 in Appendix. Increasing the residence time, a decrease in the biomass productivity due to self-shading phenomena occurred and at τ=1.8 d the highest biomass productivity was measured. However, the cyanophycin productivity had a maximum at 2.3 d, due to the correspondingly higher CGP accumulation in the biomass.

5.3.4 Nitrogen limitation and pH affect biomass accumulation and cyanophycin production

Further experiments were carried out to ascertain the effects of nitrogen limitation and pH on cyanophycin accumulation. An incident light intensity of 450 μmol photons m^{-2} s^{-1}, a residence time of 2.3 d and an inlet concentration of phosphorus equal to about 1 mg_P L^{-1} were the other operating conditions, as summarized in Table 5.2. First, an experiment in the presence of sodium nitrate (3000 g L^{-1}) (Table 5.2) was performed to assess the effect of nitrogen availability on biomass and cyanophycin productivity. The presence of nitrate ions in the medium allowed a higher biomass concentration at steady state, supporting the hypothesis that atmospheric nitrogen solubility in the medium can be limiting. The larger nitrogen availability in the culture medium caused a 50% increase in photosynthetic yield from 0.89±0.07% to 1.35±0.06%, as also observed by Fernandez Valiente and Leganes in *Nostoc* UAM 205 [44]. Interestingly, the nitrate caused a decrease in the internal quota and productivity of cyanophycin, as cyanophycin seems to play a less important role in non-diazotrophic conditions [45].

The effect of pH was also investigated. To change the pH, the composition of the cultivation medium was modified, removing all the sodium carbonate, and reducing up to 250 mg L^{-1}

the concentration of sodium bicarbonate. Accordingly, the pH was kept at lower values, around 7-7.5, compared to the ones measured in the other experiments (at about pH=8). Thanks to the continuous bubbling of 5% v/v of CO_2, it is reasonable that this variation did not affect the carbon availability. However, the pH change resulted in an increased biomass production, as reported in Figure 5.4. In any case, the cyanophycin internal quota was not affected by the pH-related availability of nitrogen resulting in an overall higher cyanophycin productivity (Figure 5.4B). This resulted in an increased CGP productivity of 34% with respect to the control.

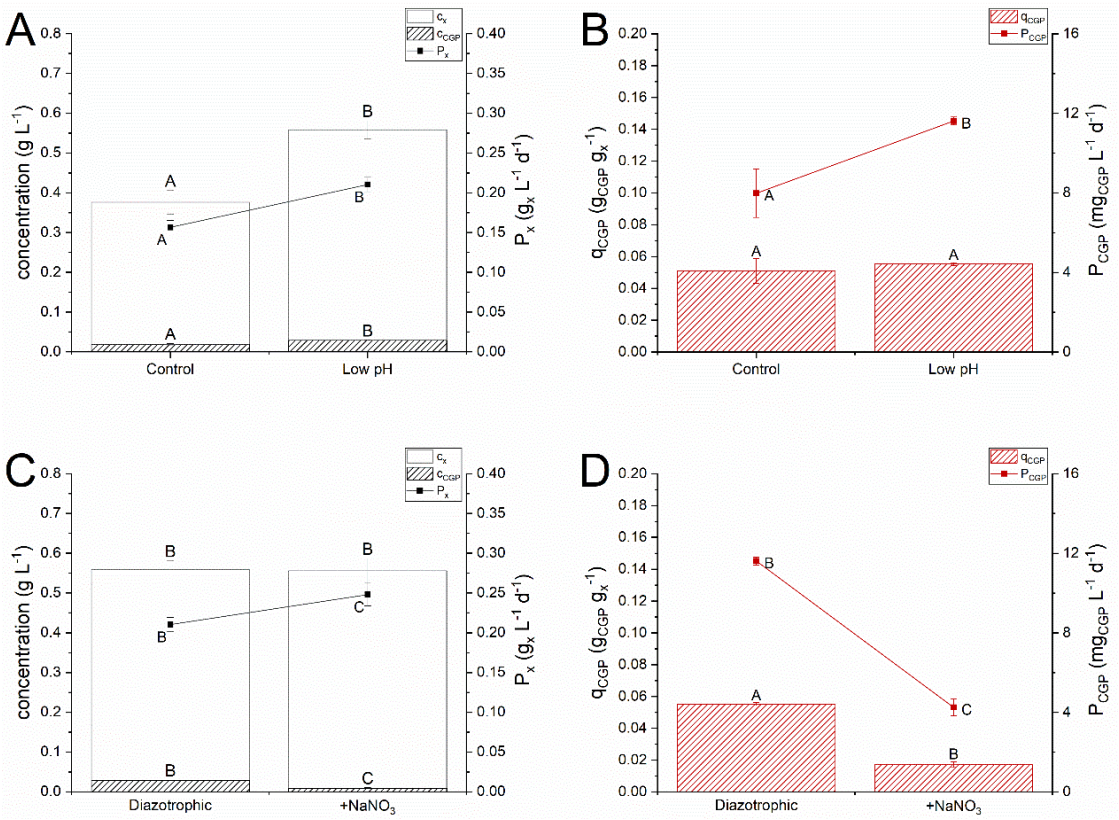

Figure 5.4. Effect of nitrogen availability and pH on *Nostoc* sp. PCC 7120. Steady state biomass concentration (c_x), cyanophycin concentration (c_{CGP}), biomass productivity (P_x) in panel A and C; cyanophycin quota (q_{CGP}) and cyanophycin productivity (P_{CGP}) in panel B and D. Error bars represent the standard deviation of at least 4 samples for each steady state (n≥4). Statistical analysis was conducted separately for each category of data. Data that do not share a letter are significantly different. Lines are just eye guides

5.3.5 Extreme phosphorus limitation to boost cyanophycin accumulation under diazotrophic conditions

After evaluating the effect of light, residence time, phosphorus and nitrogen availability, a clear role of the phosphorus limitation on cyanophycin accumulation was evidenced. In

fact, it was observed that the production of cyanophycin granules was strictly dependent on the concentration of phosphorus present in the culture medium. To better highlight this relation, measurement of cyanophycin quota as a function of the phosphorus quota are reported in the graph of Figure 5.5, to compare the data with the observation made by Trautmann et al. [31] and Trentin et al. [30], both in batch and continuous systems with *Synechocystis* sp.. The two variables were found to be inversely proportional, similarly to the case of *Synechocystis* sp., but with lower average values of internal phosphorus quota (0.0025 g_P g_x^{-1} for *Nostoc* sp. PCC 7120, 0.004 g_P g_x^{-1} for *Synechocystis* sp. PCC 6803). This suggests a possible higher specific P uptake for *Nostoc* sp. PCC 7120, with respect to the other species. For this reason, a test under extreme phosphorus deprivation (0.6 mg_P L^{-1}) was carried out.

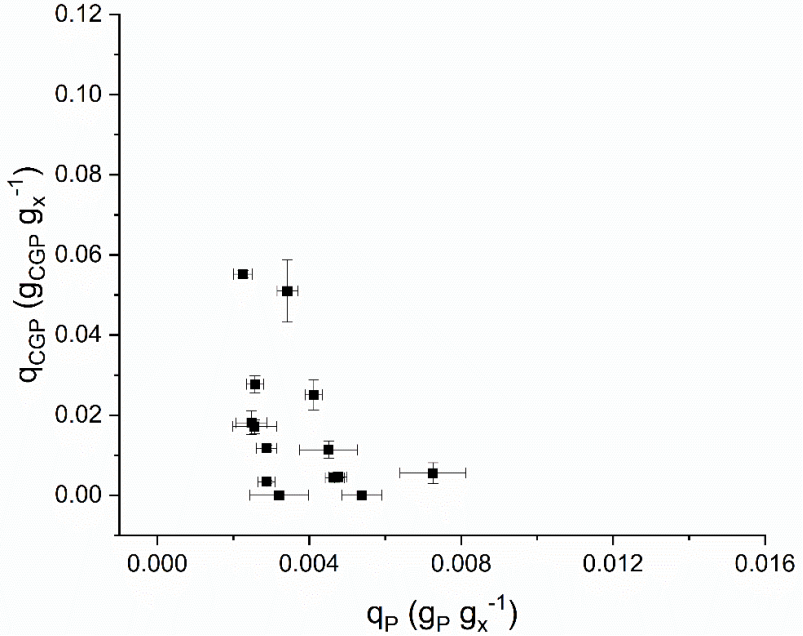

Figure 5.5. Cyanophycin quota (q_{CGP}) as function of phosphorus quota (q_P) in *Nostoc* sp. PCC 7120 cultivated in continuous systems

Results are reported in Figure 5.6, showing that when further decreasing the P quota, it is possible to obtain even higher amount of cyanophycin in the biomass. Indeed, a greater CGP quota was measured in the continuous system when the phosphorus quota q_P was lower than about 0.0025 g_P g_x^{-1}, and precisely equal to 0.0018±0.0001 g_P g_x^{-1}. As expected, decreasing the inlet phosphorus concentration, the biomass concentration decreased and *Nostoc* sp. PCC 7120 was strongly affected by these stressful growth conditions, leading to a more pronounced chlorosis of the biomass. On the contrary, the cyanophycin quota increased, doubling its value when the phosphorus content in the biomass was reduced

down to 0.18±0.01% w. Accordingly, under P limitation also the cyanophycin productivity increased by 27%.

In summary, it was possible to boost the cyanophycin productivity in a continuous system operated at steady state, where the main variables to be managed were phosphorus supply and light intensity.

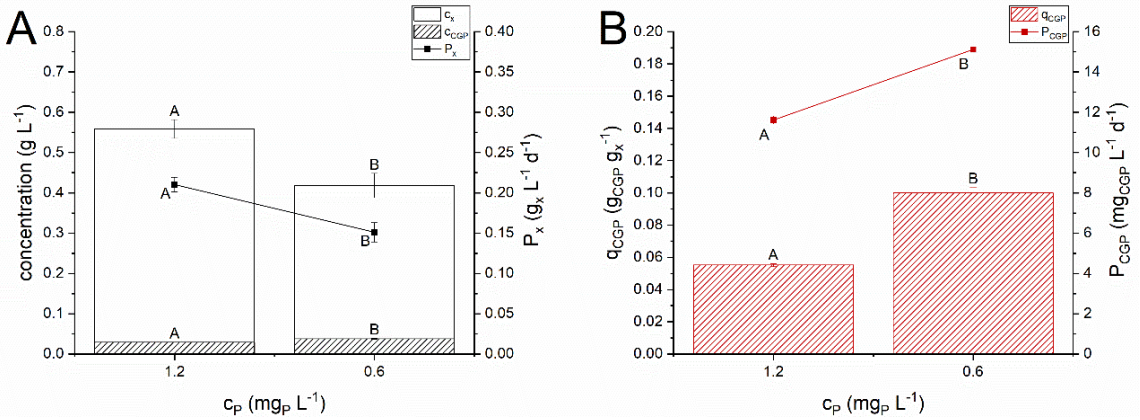

Figure 5.6. Effect of inlet phosphorus concentration on *Nostoc* sp. PCC 7120. Steady state biomass concentration (c_x), cyanophycin concentration (c_{CGP}), biomass productivity (P_x) in panel A; cyanophycin quota (q_{CGP}) and cyanophycin productivity (P_{CGP}) in panel B. Error bars represent the standard deviation of at least 4 samples for each steady state (n≥4). Statistical analysis was conducted separately for each category of data. Data that do not share a letter are significantly different. Lines are just eye guides

3.4 Discussion

The possibility of producing cyanophycin by diazotrophic cyanobacteria in continuous system was assessed by cultivating *Anabaena cylindrica* and *Nostoc* sp. PCC 7120 under progressive phosphorus limitation in the inlet. From the comparison between the two cyanobacteria considered, a species specificity was observed on CGP accumulation: *Anabaena cylindrica* did not produce cyanophycin under non limiting P conditions (5.5-2.8 $mg_P\ L^{-1}$). When the inlet phosphorus concentration was reduced to 2 $mg_P\ L^{-1}$, CGP accumulation occurred (Figure 5.1B). *Nostoc* sp. PCC 7120, instead, was able to produce cyanophycin in all the conditions tested, also in the cases of higher concentration of P fed (5.9-2 $mg_P\ L^{-1}$), even though the internal quota measured was low (Figure 5.1D). Moreover, when the inlet phosphorus concentration was reduced to about 1 $mg_P\ L^{-1}$, *Nostoc* sp. PCC 7120 was more productive reaching a two-fold cyanophycin productivity and accumulating 96% cyanophycin with respect to *Anabaena cylindrica*. Indeed, the contextual decrease in biomass concentration and productivity occurring in *Nostoc* PCC 7120 under limiting conditions was not as relevant as in the case of *Anabaena cylindrica*, thus suggesting a

higher tolerance of *Nostoc* PCC 7120 to P limitation. Accordingly, the maximum cyanophycin productivity was obtained with *Nostoc* sp. PCC 7120, also thanks to the higher biomass productivity and higher internal CGP quota ensured by the species.

Following a decrease in the inlet phosphorus concentration, the cultures changed their colour from a blue-green to a yellow-green: the synthesis of chlorophyll was reduced and the degradation of phycobiliproteins occurred, as observed macroscopically and proved by pigment content (Table 5A.2 in Appendix). As observed by Allen [46] in batch systems, this phenomenon caused the release of high quantities of nitrogen at the intracellular level, that could also explain the greater accumulation of cyanophycin measured under P limitation. Based on data of pigment content, this could also explain what was observed in our work, in a continuous system. All these important changes of the photosynthetic apparatus affected the light capture and, consequently, the photosynthetic yield. This was confirmed by the reduction of the photosynthetic efficiency (η_{PAR}) measured in both species, and reported in Table 5A.3 in Appendix. Indeed, it was previously shown that P limitation causes a decrease in the activity of photosystem II, while there are no important differences with regard to the usual function of photosystem I [47].

Therefore, under phosphorus limitation, the cyanophycin concentration and productivity were improved and *Nostoc* sp. PCC 7120 was more effective than *Anabaena cylindrica*, in terms of both biomass and cyanophycin production. Moreover, *Nostoc* sp. PCC 7120 proved to be quite efficient as a nitrogen fixing organism, resulting in a biofixation rate equal to 67.2 $mg_N\ L^{-1}\ d^{-1}$.

These preliminary results confirmed that in a continuous system the amount of phosphorus fed at the inlet is a fundamental operating variable when studying cyanophycin production, but suggested also that other ones (incident light, residence time, pH and nitrogen availability) can influence its accumulation and productivity in a continuous system. Thus, other experiments were carried out with the more promising of the two species (i.e. *Nostoc* sp. PCC 7120) to obtain a greater productivity of cyanophycin in a continuous system where atmospheric nitrogen is exploited.

The effect of other operating variables on biomass and cyanophycin accumulation was addressed, showing that lights affects the cyanophycin accumulation (Figure 5.3), and specifically no cyanophycin accumulation can be measured at an incident light intensity equal to 200 μmol photons $m^{-2}\ s^{-1}$. Light intensity is one of the major factors in photosynthetic biomass production, however it might impact biomass composition [48], as can be seen in Table 5A.4 in Appendix, reporting the pigment content. Indeed, when

cyanobacteria are exposed to high light intensities, they reduce the chlorophyll content to limit photoinhibition [49]. The level of carotenoids, on the other hand, remained almost constant: these pigments, play an important role in the photoprotection mechanism, so they are not degraded at high light intensities, as also found by Schagerl and Müller in *Anabaena cylindrica* [50]. Limited variation in the cellular nitrogen content was observed under different light intensities (Table 5A.5 of Appendix), suggesting a possible reallocation of intracellular nitrogen to other reserve compounds, like phycobiliproteins. In this regard, recently J. Wang et al. [51] studied the change of phycobiliproteins content under varying light intensity in *Dolichospermum flos-aquae*, a diazotrophic cyanobacterium, observing that pigment concentration is inversely related to light intensity. The photosynthetic efficiency decreased at increasing light intensity due to photosaturation and photoinhibition, which is a common trend for photosynthetic cultures (data not shown). As regards the effect of the residence time, instead, a greater accumulation of cyanophycin was found at 2.3 d.

To address the effect of nitrogen availability, *Nostoc* sp. PCC 7120 was cultivated in the presence of nitrates (Figure 5.4). The accumulation of cyanophycin was higher under diazotrophic conditions, if compared with experiments carried out in the presence of sodium nitrate. Indeed, the addition of combined nitrogen source to the culture medium tends to suppress the formation of heterocysts [52]. As cyanophycin is mainly located at the poles of the heterocysts and in the connections between the heterocysts and the vegetative cells [16], the reduction of its content in non-diazotrophic culture conditions may be due to the decrease in the number of heterocysts, also found by observing the filaments at the optical microscope (data not shown). Furthermore, as pointed out in the literature [53], the expression of the genes encoding cyanophycin synthase and cyanophycinase is greater in the absence of a combined nitrogen source in the medium, both in heterocysts and in vegetative cells.

The role of pH, that may also influence nitrogen availability, was found to majorly affect biomass production, but not cyanophycin accumulation (Figure 5.4). Interestingly, decreasing the pH level, the concentration and productivity of biomass were significantly increased, with comparable results between the nitrate addition and the pH control. A possible explanation could be related to the effect of pH on nitrogen solubility. A sensitivity analysis was carried out using the software AspenPlus™. Results of this simulation are reported in Figure 5A.3 of Appendix.

According to simulations, the N_2 concentration is stable up to a pH equal to 7.75. Then, it rapidly decreases at higher pH values. Specifically, the N_2 concentration is lowered by 8% when increasing pH value from 7 to 8.5. Thus, several factors including the effect of pH itself and the indirect effect on nitrogen solubility should be accounted for in the cultivation of cyanobacteria, where an equilibrium between CO_2, carbonate ions and bicarbonate ions is set.

3.5 Final remarks

In this Chapter, the possibility of cyanophycin production by diazotrophic cyanobacteria was assessed. Two species, *Anabaena cylindrica* PCC 7122 and *Nostoc* sp. PCC 7120 were cultivated in continuous experiments, with different inlet phosphorus concentrations. Under phosphorus limitation, the cyanophycin concentration and productivity were improved and *Nostoc* sp. PCC 7120 was more effective than *Anabaena cylindrica*, in terms of both biomass and cyanophycin production. Moreover, *Nostoc* sp. PCC 7120 proved to be quite efficient as a nitrogen fixing organism, resulting in a biofixation rate equal to 67.2 $mg_N\ L^{-1}\ d^{-1}$. The effect of other operating variables on biomass and cyanophycin accumulation was addressed, showing how light affects the cyanophycin accumulation. A greater accumulation of cyanophycin was found at residence time of 2.3 d. The value of pH, that may also influence nitrogen availability, was found to majorly affect biomass production, but not cyanophycin accumulation. Anyway, the accumulation of cyanophycin was higher under diazotrophic condition, if compared with experiments carried out in the presence of nitrates. Finally, it was confirmed that P limitation is the main variable affecting cyanophycin accumulation, and it was obtained a maximum cyanophycin productivity of 15 $mg_{CGP}\ L^{-1}\ d^{-1}$. Thus, the internal quota of P in the biomass is the trigger for CPG accumulation. However, the relation between internal P concentration and inlet quota is species specific, as highlighted by the comparison with data for other species.

Nomenclature

V_{PBR}	Photobioreactor volume (mL)
A_{PBR}	Photobioreactor surface (m^2)
Q	Volumetric flowrate (mL d^{-1})
τ	Residence time (d)
D	Dilution rate (d^{-1})
μ	Specific growth rate (d^{-1})
P_i	Productivity of species *i* (g_i m^{-3} d^{-1})
c_x	Biomass concentration (mg_x L^{-1})
c_{CGP}	Cyanophycin concentration (mg_{CGP} L^{-1})
q_{CGP}	Cyanophycin quota (mg_{CGP} mg_x^{-1})
q_P	Phosphorus quota (mg_P mg_x^{-1})
I_0	Incident light intensity (µmol photons m^{-2} s^{-1})
BI	Back Irradiance (µmol photons m^{-2} s^{-1})

Acronyms

PUFAs	Polyunsaturated fatty acids
CGP	Cyanophycin Granules Polypeptide
PASP	Polyaspartic acid
DW	Dry weight
PFD	Photon Flux Density
PAR	Photosynthetically Active Radiation
CSTR	Continuous Stirred Tank Reactor
LHV	Lower Heating Value

Literature cited

[1] L.J. Stal, Nitrogen Fixation in Cyanobacteria, ELS. (2015) 1–9. https://doi.org/https://doi.org/10.1002/9780470015902.a0021159.pub2.

[2] I. Berman-Frank, P. Lundgren, P. Falkowski, Nitrogen fixation and photosynthetic oxygen evolution in cyanobacteria, 154 (2003) 157–164. https://doi.org/10.1016/S0923-2508(03)00029-9.

[3] M. Appl, Ammonia, Ullmann's Encycl. Ind. Chem. (2006). https://doi.org/https://doi.org/10.1002/14356007.a02_143.pub2.

[4] J. Nørskov, J. Chen, E. Al., DOE Roundtable Report, 2016.

[5] E. Mariani, L'industria dell'azoto, in: A. Girelli, L. Matteoli, F. Parisi (Eds.), Trattato Di Chim. Ind. e Appl. Vol. 1, Zanichelli, Zanichelli, 1969: pp. 521–590.

[6] N.K. Sharma, A.K. Rai, L.J. Stal, Cyanobacteria : an economic perspective , Wiley Blackwell, Chichester, England, 2014.

[7] N. Rascio, N. La Rocca, Biological Nitrogen Fixation ☆, Elsevier Inc., 2013. https://doi.org/10.1016/B978-0-12-409548-9.00685-0.

[8] W. Levasseur, P. Perré, V. Pozzobon, A review of high value-added molecules production by microalgae in light of the classification, Biotechnol. Adv. 41 (2020) 107545. https://doi.org/10.1016/j.biotechadv.2020.107545.

[9] M.A. Borowitzka, High-value products from microalgae-their development and commercialisation, J. Appl. Phycol. 25 (2013) 743–756. https://doi.org/10.1007/s10811-013-9983-9.

[10] N.-S. Lau, M. Matsui, A.A.-A. Abdullah, Cyanobacteria: Photoautotrophic Microbial Factories for the Sustainable Synthesis of Industrial Products, Biomed Res. Int. 2015 (2015) 1–9. https://doi.org/10.1155/2015/754934.

[11] J. Du, L. Li, S. Zhou, Microbial production of cyanophycin: From enzymes to biopolymers, Biotechnol. Adv. 37 (2019). https://doi.org/10.1016/j.biotechadv.2019.05.006.

[12] H. Adelnia, H.D.N. Tran, P.J. Little, I. Blakey, H.T. Ta, Poly(aspartic acid) in Biomedical Applications: From Polymerization, Modification, Properties, Degradation, and Biocompatibility to Applications, ACS Biomater. Sci. Eng. 7 (2021) 2083–2105. https://doi.org/10.1021/acsbiomaterials.1c00150.

[13] T. Utagawa, Production of Arginine by Fermentation, J. Nutr. 134 (2004) 2854S-2857S. https://doi.org/10.1093/jn/134.10.2854S.

[14] B. Watzer, K. Forchhammer, Cyanophycin: A Nitrogen-Rich Reserve Polymer, in: K.F.E.-A. Tiwari (Ed.), IntechOpen, Rijeka, 2018: p. Ch. 5. https://doi.org/10.5772/intechopen.77049.

[15] N.A. Khlystov, W.Y. Chan, A.M. Kunjapur, W. Shi, K.L.J. Prather, B.D. Olsen, Material properties of the cyanobacterial reserve polymer multi-L-arginyl-poly-L-aspartate (cyanophycin), Polymer (Guildf). 109 (2017) 238–245. https://doi.org/10.1016/j.polymer.2016.11.058.

[16] D.M. Sherman, D. Tucker, L.A. Sherman, Heterocyst development and localization of cyanophycin in N2-fixing cultures of Anabaena sp. PCC 7120 (Cyanobacteria), J. Phycol. 36 (2000) 932–941.

[17] M. Gupta, N.G. Carr, Enzyme Activities Related to Cyanophycin Metabolism in Heterocysts and Vegetative Cells of Anabaena spp, Microbiology. 125 (1981) 17–23. https://doi.org/https://doi.org/10.1099/00221287-125-1-17.

[18] H. Nausch, J. Huckauf, I. Broer, Peculiarities and impacts of expression of bacterial cyanophycin synthetases in plants, Appl. Microbiol. Biotechnol. 100 (2016) 1559–1565. https://doi.org/10.1007/s00253-015-7212-y.

[19] K.M. Frey, F.B. Oppermann-Sanio, H. Schmidt, A. Steinbüchel, Technical-scale production of cyanophycin with recombinant strains of Escherichia coli, Appl. Environ. Microbiol. 68 (2002) 3377–3384. https://doi.org/10.1128/AEM.68.7.3377-3384.2002.

[20] J. Aravind, T. Saranya, G. Sudha, P. Kanmani, Integrated Waste Management in India, (2016) 49–58. https://doi.org/10.1007/978-3-319-27228-3.

[21] A.M. Ruffing, T. Kallas, Editorial: Cyanobacteria: The Green E. coli, Front. Bioeng. Biotechnol. 4 (2016) 7. https://doi.org/10.3389/fbioe.2016.00007.

[22] R.D. Simon, Measurement of the cyanophycin granule polypeptide contained in the blue green alga Anabaena cylindrica, J. Bacteriol. 114 (1973) 1213–1216. https://doi.org/10.1128/jb.114.3.1213-1216.1973.

[23] A. Steinle, F.B. Oppermann-Sanio, R. Reichelt, A. Steinbüchel, Synthesis and accumulation of cyanophycin in transgenic strains of Saccharomyces cerevisiae, Appl. Environ. Microbiol. 74 (2008) 3410–3418. https://doi.org/10.1128/AEM.00366-08.

[24] K. Ziegler, A. Diener, C. Herpin, R. Richter, R. Deutzmann, W. Lockau, Molecular characterization of cyanophycin synthetase, the enzyme catalyzing the biosynthesis of the cyanobacterial reserve material multi-L- arginyl-poly-L-aspartate

(cyanophycin), Eur. J. Biochem. 254 (1998) 154–159. https://doi.org/10.1046/j.1432-1327.1998.2540154.x.

[25] M. Frommeyer, L. Wiefel, A. Steinbüchel, Features of the biotechnologically relevant polyamide family "cyanophycins" and their biosynthesis in prokaryotes and eukaryotes, Crit. Rev. Biotechnol. 36 (2016) 153–164. https://doi.org/10.3109/07388551.2014.946467.

[26] B. Watzer, F. Klemke, K. Forchhammer, The Cyanophycin Granule Peptide from Cyanobacteria, in: D. Jendrossek (Ed.), Bact. Organelles Organelle-like Inclusions, Springer International Publishing, Cham, 2020: pp. 149–175. https://doi.org/10.1007/978-3-030-60173-7_7.

[27] S. Canizales, M. Sliwszcinka, A. Russo, S. Bentvelzen, H. Temmink, A.M. Verschoor, R.H. Wijffels, M. Janssen, Cyanobacterial growth and cyanophycin production with urea and ammonium as nitrogen source, J. Appl. Phycol. 33 (2021) 3565–3577. https://doi.org/10.1007/s10811-021-02575-0.

[28] A.H. Mackerras, N.M. de Chazal, G.D. Smith, Transient accumulations of cyanophycin in Anabaena cylindrica and Synechocystis 6308, Microbiology. 136 (1990) 2057–2065.

[29] A.H. Mackerras, B.N. Youens, R.C. Weir, G.D. Smith, Is cyanophycin involved in the integration of nitrogen and carbon metabolism in the cyanobacteria Anabaena cylindrica and Gleothece grown on light/dark cycles?, Microbiology. 136 (1990) 2049–2056.

[30] G. Trentin, V. Lucato, E. Sforza, A. Bertucco, Stabilizing autotrophic cyanophycin production in continuous photobioreactors, Algal Res. 60 (2021) 102518. https://doi.org/10.1016/j.algal.2021.102518.

[31] A. Trautmann, B. Watzer, A. Wilde, K. Forchhammer, C. Posten, Effect of phosphate availability on cyanophycin accumulation in Synechocystis sp. PCC 6803 and the production strain BW86, Algal Res. 20 (2016) 189–196. https://doi.org/10.1016/j.algal.2016.10.009.

[32] S.E. Stevens, D.A.M. Paone, D.L. Balkwill, Accumulation of Cyanophycin Granules as a Result of Phosphate Limitation in Agmenellum quadruplicatum , Plant Physiol. 67 (1981) 716–719. https://doi.org/10.1104/pp.67.4.716.

[33] E. Barbera, A. Grandi, L. Borella, A. Bertucco, E. Sforza, Continuous cultivation as a method to assess the maximum specific growth rate of photosynthetic organisms, Front. Bioeng. Biotechnol. 7 (2019) 1–12.

https://doi.org/10.3389/fbioe.2019.00274.

[34] R. Rippka, J.J.B.W. Deruelles, J.B. Waterbury, M. A. Herdman, R.Y. Stanier, Generic Assignments, Strain Histories and Properties of Pure Cultures of Cyanobacteria, Microbiology-Sgm. 111 (1979) 1–61. https://doi.org/10.1099/00221287-111-1-1.

[35] J.J. Ameel, R.P. Axler, C.J. Owen, Persulfate digestion for determination of total nitrogen and phosphorus in low-nutrient waters, Am. Environ. Lab. 5 (1993) 1–11.

[36] M. Innamorati, I. Ferrari, D. Marino, M. Ribera D' Alcala, Metodi nell' ecologia del plancton marino. In Nova Thalassia, Edizioni L, 1990.

[37] D. A. Bryant, The Molecular Biology of Cyanobacteria in Advances in Photosynthesis book series (AIPH, volume 1), Springer, Dordrecht, 1994. https://doi.org/10.1007/978-94-011-0227-8.

[38] D.R. Vardon, B.K. Sharma, J. Scott, G. Yu, Z. Wang, L. Schideman, Y. Zhang, T.J. Strathmann, Chemical properties of biocrude oil from the hydrothermal liquefaction of Spirulina algae, swine manure, and digested anaerobic sludge, Bioresour. Technol. 102 (2011) 8295–8303. https://doi.org/10.1016/j.biortech.2011.06.041.

[39] Y.J. Sung, A.K. Patel, B.S. Yu, H. Il Choi, J. Kim, E.S. Jin, S.J. Sim, Sedimentation rate-based screening of oleaginous microalgae for utilization as a direct combustion fuel, Bioresour. Technol. 293 (2019). https://doi.org/10.1016/j.biortech.2019.122045.

[40] Y. Elbahloul, M. Krehenbrink, R. Reichelt, A. Steinbüchel, Physiological conditions conducive to high cyanophycin content in biomass of Acinetobacter calcoaceticus Strain ADP1, Appl. Environ. Microbiol. 71 (2005) 858–866. https://doi.org/10.1128/AEM.71.2.858-866.2005.

[41] M. Do Nascimento, L. Sanchez Rizza, A. Arruebarrena Di Palma, M. de los A. Dublan, G. Salerno, L.M. Rubio, L. Curatti, Cyanobacterial biological nitrogen fixation as a sustainable nitrogen fertilizer for the production of microalgal oil, Algal Res. 12 (2015) 142–148. https://doi.org/10.1016/j.algal.2015.08.017.

[42] E. Sforza, B. Gris, C.E. De Farias Silva, T. Morosinotto, A. Bertucco, Effects of light on cultivation of scenedesmus obliquus in batch and continuous flat plate photobioreactor, Chem. Eng. Trans. 38 (2014) 211–216. https://doi.org/10.3303/CET1438036.

[43] J. Kromkamp, Formation and functional significance of storage products in cyanobacteria, New Zeal. J. Mar. Freshw. Res. 21 (1987) 457–465.

https://doi.org/10.1080/00288330.1987.9516241.

[44] E. Fernandez Valiente, F. Leganes, Regulatory Effect of pH and Incident Irradiance on the Levels of Nitrogenase Activity in the Cyanobacterium Nostoc UAM 205, J. Plant Physiol. 135 (1990) 623–627. https://doi.org/10.1016/S0176-1617(11)80647-4.

[45] H. Li, D.M. Sherman, S. Bao, L.A. Sherman, Pattern of cyanophycin accumulation in nitrogen-fixing and non-nitrogen-fixing cyanobacteria, Arch. Microbiol. 176 (2001) 9–18. https://doi.org/10.1007/s002030100281.

[46] M.M. Allen, Cyanobacterial Cell Inclusions, Annu. Rev. Microbiol. 38 (1984) 1–25. https://doi.org/10.1146/annurev.mi.38.100184.000245.

[47] J.L. Collier, S.K. Herbert, D.C. Fork, A.R. Grossman, Changes in the cyanobacterial photosynthetic apparatus during acclimation to macronutrient deprivation, Photosynth. Res. 42 (1994) 173–183. https://doi.org/10.1007/BF00018260.

[48] I. Krzemińska, B. Pawlik-Skowrońska, M. Trzcińska, J. Tys, Influence of photoperiods on the growth rate and biomass productivity of green microalgae, Bioprocess Biosyst. Eng. 37 (2014) 735–741. https://doi.org/10.1007/s00449-013-1044-x.

[49] E. Sforza, D. Simionato, G.M. Giacometti, A. Bertucco, T. Morosinotto, Adjusted light and dark cycles can optimize photosynthetic efficiency in algae growing in photobioreactors, PLoS One. 7 (2012). https://doi.org/10.1371/journal.pone.0038975.

[50] M. Schagerl, B. Müller, Acclimation of chlorophyll a and carotenoid levels to different irradiances in four freshwater cyanobacteria, J. Plant Physiol. 163 (2006) 709–716. https://doi.org/10.1016/j.jplph.2005.09.015.

[51] J. Wang, N.D. Wagner, J.M. Fulton, J.T. Scott, Diazotrophs modulate phycobiliproteins and nitrogen stoichiometry differently than other cyanobacteria in response to light and nitrogen availability, Limnol. Oceanogr. 66 (2021) 2333–2345. https://doi.org/10.1002/lno.11757.

[52] G.E. Fogg, Growth and Heterocyst Production in Anabaena Cylindrica Lemm.: II. In Relation to Carbon and Nitrogen Metabolism, Ann. Bot. 13 (1949) 241–259. http://www.jstor.org/stable/42907082.

[53] S. Picossi, A. Valladares, E. Flores, A. Herrero, Nitrogen-regulated genes for the metabolism of cyanophycin, a bacterial nitrogen reserve polymer: Expression and mutational analysis of two cyanophycin synthetase and cyanophycinase gene

clusters in the heterocyst-forming cyanobacterium Anabaena sp. PCC 7, J. Biol. Chem. 279 (2004) 11582–11592. https://doi.org/10.1074/jbc.M311518200.

Appendix

Table 5A.1. Composition of the modified BG11 medium

Component	mg L^{-1}
Na_2Mg EDTA	2
$FeCl_3 \cdot 6H_20$	12.43
Citric acid · H_20	12
$CaCl_2 \cdot 2H_20$	72
$MgSO_4 \cdot 7H_20$	150
K_2HPO_4	30.5
H_3BO_3	5.72
$MnCl_2 \cdot 4H_20$	3.62
$ZnSO_4 \cdot 7H_20$	0.44
$CuSO_4 \cdot 5H_20$	0.16
$COCl_2 \cdot 6H_20$	0.1
$Na_2MoO_4 \cdot 2H_20$	0.78
Na_2CO_3	40
$NaHCO_3$	3000

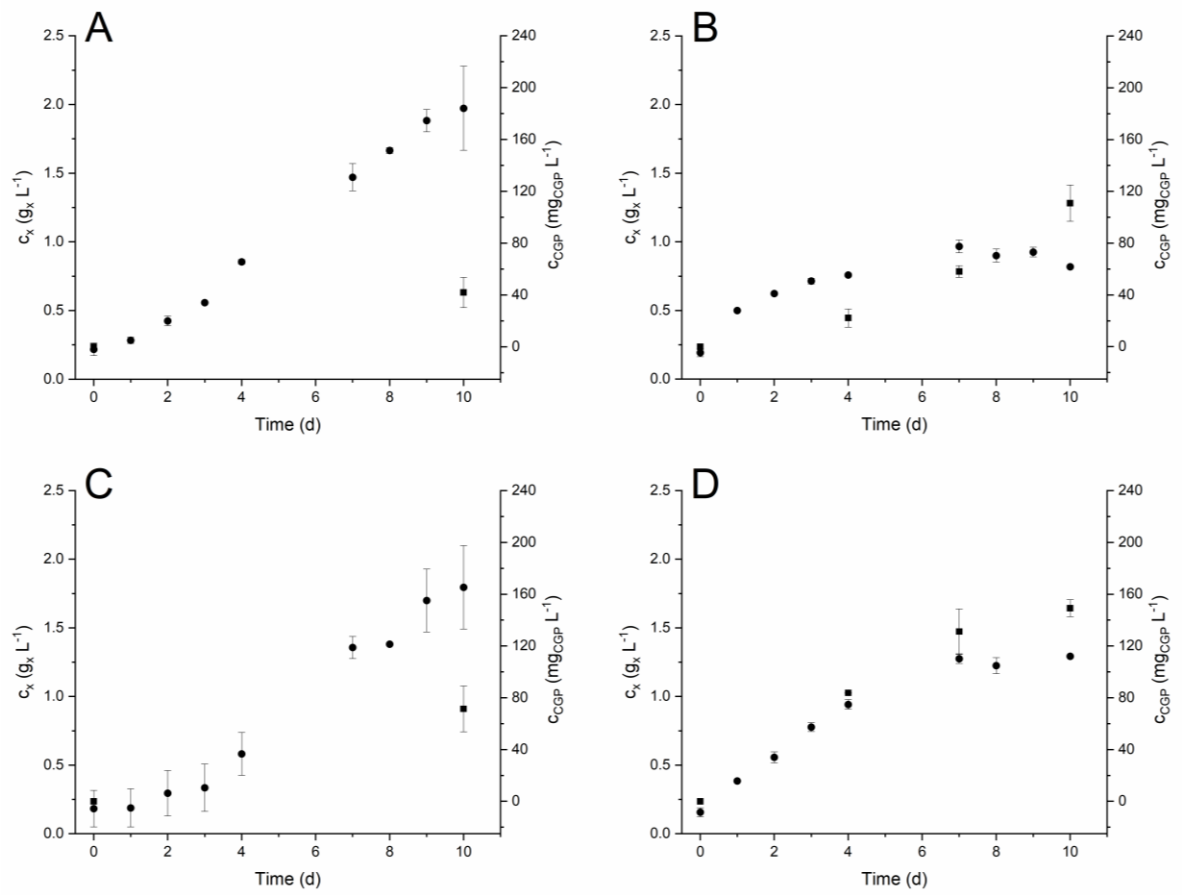

Figure 5A.1. Biomass concentration c_x (g_x L^{-1}) and cyanophycin concentration c_{CGP} (mg_{CGP} L^{-1}) in batch growth curves of *Anabaena cylindrica* and *Nostoc* sp. PCC 7120 respectively for control (panel A and C) and P-limited condition (panel B and D). Error bars represent the standard deviation (n=4, two technical replicates for two biological replicates)

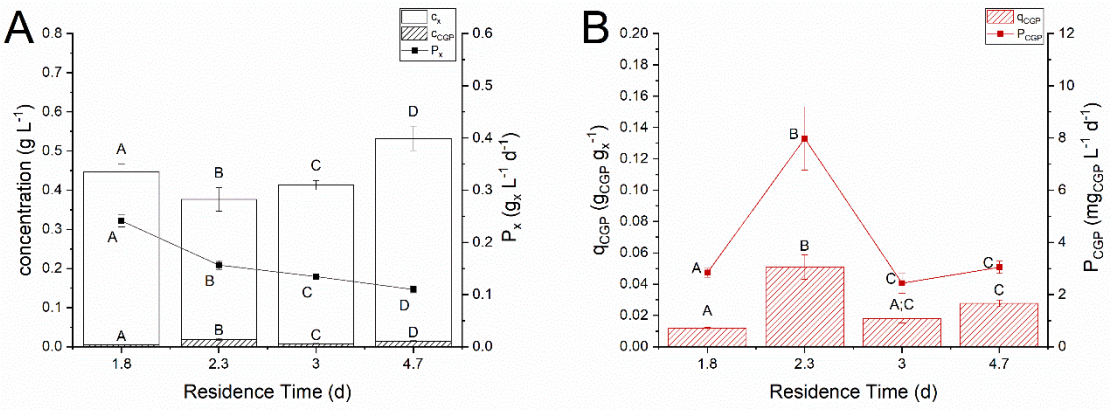

Figure 5A.2. Effect of residence time on *Nostoc* sp. PCC 7120. Steady state biomass concentration (c_x), cyanophycin concentration (c_{CGP}), biomass productivity (P_x) in panel A; cyanophycin quota (q_{CGP}) and cyanophycin productivity (P_{CGP}) in panel B. Error bars represent the standard deviation of at least 4 samples for each steady state (n≥4). Statistical analysis was conducted separately for each category of data. Data that do not share a letter are significantly different. Lines are just eye guides

Table 5A.2. Pigment content in biomass (mg g^{-1}) as function of the inlet phosphorus concentration obtained with *Anabaena cylindrica* PCC 7122 and with *Nostoc* sp. PCC 7120. Errors represent the standard deviation of at least 4 samples for each steady state (n≥4). Data that do not share a letter are significantly different

	Inlet phosphorus concentration (mg_P L^{-1})	**Total chlorophyll (mg g_x^{-1})**	**Carotenoid (mg g_x^{-1})**
Anabaena cylindrica PCC 7122	5.5±0.5	$9.07±0.85^{A}$	$1.53±0.39^{A}$
	2.8±0.1	$6.52±0.62^{B}$	$1.05±0.05^{A;B}$
	2.0±0.1	$2.60±0.27^{C}$	$0.73±0.01^{B}$
	1.5±0.1	$3.04±0.65^{C}$	$1.27±0.43^{A;B}$
	1.0±0.2	$2.85±0.34^{C}$	$0.84±0.16^{B}$
Nostoc sp. PCC 7120	5.9±0.1	$14.83±1.77^{A}$	$2.88±0.24^{A;B}$
	2.2±0.1	$9.31±1.20^{B}$	$2.57±0.32^{A;B}$
	2.0±0.2	$16.80±1.32^{A}$	$4.53±0.57^{C}$
	1.7±0.1	$9.71±1.08^{B}$	$3.35±0.32^{A}$
	1.2±0.1	$6.79±1.20^{B}$	$2.15±0.40^{B}$

Table 5A.3. Effect of inlet phosphorus concentration (c_P^{inlet}) on photosynthetic efficiency η_{PAR}

Anabaena cylindrica PCC 7122		*Nostoc* sp. PCC 7120	
c_P^{inlet} (mg_P L^{-1})	η_{PAR} (%)	c_P^{inlet} (mg_P L^{-1})	η_{PAR} (%)
5.5±0.5	1.89±0.13	5.9±0.1	2.65±0.08
2.8±0.1	1.93±0.07	2.2±0.1	1.77±0.08
2.0±0.1	1.17±0.19	2.0±0.2	1.65±0.02
1.5±0.1	1.04±0.04	1.7±0.1	0.97±0.06
1.0±0.2	0.82±0.08	1.2±0.1	0.89±0.07

Table 5A.4. Pigment content in biomass (mg g^{-1}) as function of the incident light intensity (I_0) with inlet P concentration equal to 2.0±0.2 mg_P L^{-1} and inlet P concentration equal to 1.0±0.1 mg_P L^{-1}. Error represent the standard deviation of at least 4 samples for each steady state (n≥4). Data that do not share a letter are significantly different

	Inlet phosphorus concentration (c_P^{inlet}) (mg_P L^{-1})	Residence time (τ) (d)	Incident light intensity (I_0) (µmol photons m^{-2} s^{-1})	Total chlorophyll (mg g_x^{-1})	Carotenoid (mg g_x^{-1})
Effect of incident light intensity	2.01±0.17	2.3	200	$15.92±2.53^{A}$	$3.20±0.43^{A}$
			450	$16.80±1.32^{A}$	$4.53±0.57^{B}$
			650	$7.44±0.69^{B}$	$2.53±0.22^{A}$
	1.04±0.03	2.3	200	$9.51±0.62^{A;B}$	$2.35±0.23^{A}$
			450	$6.79±1.20^{A}$	$2.15±0.40^{A}$
			650	$11.39±1.48^{B}$	$3.44±0.37^{B}$

Table 5A.5. Effect of incident light intensity on steady state nitrogen yield $Y_{N|x}$ (g_N g_x^{-1}). Statistical analysis was conducted separately for each category of data. Errors represent the standard deviation of at least 4 samples for each steady state (n≥4). Data that do not share a letter are significantly different

	Inlet phosphorus concentration (c_P^{inlet}) (mg_P L^{-1})	Residence time (τ) (d)	Incident light intensity (I_0) (µmol photons m^{-2} s^{-1})	Nitrogen yield ($Y_{N\|x}$) (g_N g_x^{-1})
Effect of incident light intensity	2.01±0.17	2.3	200	$0.101±0.008^{A}$
			450	$0.100±0.011^{A;B}$
			650	$0.082±0.006^{B}$
	1.04±0.03	2.3	200	$0.072±0.012^{A}$
			450	$0.110±0.013^{B}$
			650	$0.107±0.005^{B}$

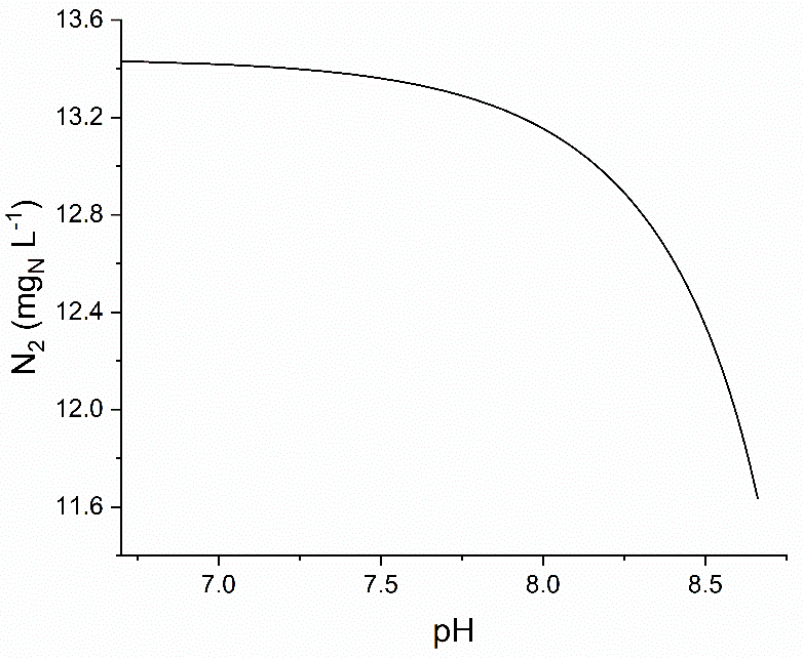

Figure 5A.3. Dissolved nitrogen concentration (N_2) in the culture medium as function of the pH at a constant temperature of 24°C as simulated by AspenPlus™

Chapter 6

Continuous production of cyanophycin by engineered strains of *Nostoc* sp. PCC 7120

Nostoc sp. PCC 7120 was engineered to obtains strains that over accumulate cyanophycin, a high added value nitrogen reserve compound. These strains were cultivated in continuous system under nitrogen fixing condition. It was assessed the effect of the inlet phosphorus concentration, and *Nostoc* 44 resulted the most producing strain, reaching a cyanophycin productivity 3 times higher than *wild type* strain. A quantitative correlation between the phosphorus quota and the cyanophycin quota was proposed, highlighting that these two variables were inversely proportional as resulted for *wild type* strain and also for other cyanobacterial strain.

6.1 Introduction

Thanks to their rapid growth rate, the ability to accumulate high value molecules and the possibility of growing in wastewater, microalgae are being exploited in different areas [1,2]. They produce a wide range of valuable bioproducts, including proteins, polysaccharides, lipids, pigments, vitamins, bioactive compounds, and antioxidants. The microalgal biomass can be used directly as food and nutrient supplements for the food/feed industry, while their processed products are applied in biopharmaceuticals and cosmetics [3,4]. However, the industrial application of microalgae strongly depends on the production yields of the product of interest, obtained by cultivating *wild type* strains. [5]. In this context, genetic engineering of microorganisms can help to overcome the inherent limitation of metabolic capacity for higher accumulation of the desired biomolecules, thus eventually improving the economic feasibility of the production process. On the other hand, although bioengineering of microalgae offers the great potential to improve process economics, the risk assessment, biosafety, and regulatory issues pertaining to the use of genetically engineered microalgae must always be considered. Quite a lot of algal bioengineering research has already been carried out for different purposes. For example, the photosynthetic biomass production in *N. oceanica* was substantially enhanced upon overexpression of RuBisCO activase [6]. The engineering of Calvin cycle through the overexpression of cyanobacterial fructose 1,6-bisphosphate aldolase (FBA) was found to enhance the photosynthetic capacity of *C. vulgaris* [7]. A knock-out mutant of the phospholipase A2 gene (*C. reinhardtii*) had increased the total lipid content up to 64.25% [8]. As regards the high value-added products such as carotenoids with potential application in human health, their productivity has been significantly increased thanks to genetic engineering of microorganisms, as reported by the literature. *Dunaliella salina* produced astaxanthin thanks to the overexpression of *Haematococus pluvialis* gene encoding β-carotene ketolase [9]. The knock-out mutant of zeaxanthin epoxidase in *Chlamydomonas* had significantly increased the zeaxanthin accumulation compared to the *wild type* [10]. The production of sesquiterpenoids and diterpenoids through genetic engineering of *Chlamydomonas* has also been reported [11,12]. The introduction of additional copy of gene encoding gateway enzyme of terpenoid pathway, 1-deoxy-D-xylulose 5-phosphate synthase (dxs), resulted in enhanced accumulation of fucoxanthin in *P. tricornutum* [13].
Whit respect to cyanophycin, a high added value nitrogen reserve compound, its productivity was increased by cultivating engineered microorganisms as *E. coli*, *P. putida*,

Pichia pastoris, *R. eutropha*, *R. oryzae*, *Corynebacterium glutamicum*, and *S. cerevisiae*, through heterologous expression of cphA [14] from *Synechocystis* sp. PCC 6803[15] or *Anabaena* sp. PCC 7120 [16]. The first heterologous production of cyanophycin was obtained with *E. coli* overexpressing the $cphA_{6803}$ gene. Up to 100 mg L^{-1} of insoluble cyanophycin was obtained [17]. The same strain cultured in protamylasse medium, the main waste stream coming from starch extraction from potatoes, allowed to get as much as 28% (w/w) in the cell dry matter [18]. Cyanophycin was also obtained also in transgenic fungi, as *R. orzyae* [19] and in transgenic yeasts, as *S. cerevisiae* and *P. pastoris* [20,21]. Bioreactors of different volumes (30L, 400L and 500L) have been used for large scale production, and 750 g of cyanophycin were obtained with 75% extraction yield [15]. Nevertheless, despite the high yield achieved with engineered heterologous microorganisms, these species need organic carbon as raw material to growth, differently from photoautotrophic microorganisms, which consequently emerge as a greener alternative to heterotrophic bacteria [22]. Indeed, cyanophycin is naturally synthetized by several species of *wild type* cyanobacteria, such as *Anabaena* sp. PCC 7120, *Scytonema* sp., *Anabaena variabilis* ATCC 29413, *Aphanocapsa* 6308, *Synechocystis* sp, PCC 6803, *Agmenellum quadruplicatum*, *Synechococcus* sp. MA19, *Synechococcus* sp. G2.1 and *Nostoc ellipsosporum* [23,24]. To increase the production of cyanophycin in a photoautotrophic way, Watzer developed the mutant *Synechocystis* BW86 [25]. This mutant carries an amino acid substitution (Ile86Asp) in the PII protein, which plays a role in the regulatory cascade of arginine synthesis. It is a protein involved in signal transduction and can interact with different target proteins (enzymes, channels, regulatory proteins), depending on the effector molecule it binds. The bond with different effector molecules (e.g. oxoglutarate, 2-OG, whose concentration depends inversely on the intracellular nitrogen concentration) changes the phosphorylation state of the protein. When dephosphorylated, PII can act with N-acetyl glucosamine kinase (NAGK), an enzyme that catalyses the conversion of N-acetylglutamate (Ac-Glu) to N-acetylglutamate-phosphate (Ac-Glu-P), which represents the limiting step of the cyclic pathway of arginine synthesis. The activity of NAGK is controlled by the formation of the complex with the PII protein: when it is linked to PII it displays a high activity and is less sensitive to the negative feedback effect given by arginine. The PII variant (I86N) of the BW86 strain constitutively binds NAGK, leading to a large production of arginine and thus prompting the formation of cyanophycin from arginine and aspartate [25]. This strain was cultivated under phosphorus limitation, a condition according to the literature able to increase the

cyanophycin concentration [26,27], which reaches values up to 57% of the dry weight, which is the highest cellular content of cyanophycin in a bacterial cell reported so far [25]. In this Chapter, we have addressed the possibility to increase the productivity of cyanophycin by cultivating engineered strains of *Nostoc* sp. PCC 7120 in diazotrophic conditions in continuous systems. This species was already successfully engineered for other purposes, for example to increase the production of hydrogen [28] and that of carotenoids (i.e. echinenone and canthaxanthin) [29]. Despite the potential use of genetically modified microbial factories for the production of high added value compounds, one of the main issues is the drop in productivity due to retro mutation events [30–34]. Additionally, the probability of a loss of the mutation increases when the production of the target compound is a metabolic burden for the cell itself [35,36]. Unfortunately, this aspect is seldom addressed because usually the production is carried out in batch system, or it is not experimented during prolonged cultivation campaign, as in continuous systems [37].
In our study, *Nostoc* sp. PCC 7120 was engineered by a research group at the Ben-Gurion University of the Negev, with whom the Padova group was in a scientific collaboration. The over-accumulating mutants were selected on media containing canavanine, a toxic analogue of arginine. Among the engineered strains, the most promising were selected (*Nostoc* 41, *Nostoc* 44, *Nostoc* 47 and *Nostoc* 53) to be cultivated in a continuous system to assess the effect of the inlet phosphorus concentration on cyanophycin productivity. Cyanobacteria were grown under control (about 6 mg_P L^{-1}) and under P limitation conditions (0.6 mg_P L^{-1}), whereas the other operating variables were set as the optimal conditions found in the experiments carried out with *wild type* strains (§ 5).

6.2 Materials and methods

6.2.1 Experimental Strain and Culture Medium

In order to increase the cyanophycin productivity, *Nostoc* sp. PCC 7120 was engineered to obtain strains that overproduces cyanophycin by a research group at the Ben-Gurion University of the Negev, under the coaching of prof. Inna Khozin-Goldberg. Among the mutants obtained, four strains were selected as the most promising ones (*Nostoc* 41, *Nostoc* 44, *Nostoc* 47 and *Nostoc* 53). Maintenance and propagation of engineered cyanobacteria and *wild type* strain was carried out in modified BG11 medium [38]. All the nitrogen compounds (Hepes, Ferric ammonium citrate) were removed, to maintain the cyanobacteria

in diazotrophic conditions. Before use the medium was sterilized in an autoclave for 20 minutes at 121°C in order to prevent any contaminations. The final composition is reported in Table 6.1.

Table 6.1. Composition of the modified BG11 medium

Component	mg L^{-1}
Na_2Mg EDTA	2
$FeCl_3 \cdot 6H_20$	12.43
Citric acid $\cdot H_20$	12
$CaCl_2 \cdot 2H_20$	72
$MgSO_4 \cdot 7H_20$	150
K_2HPO_4	30.5
H_3BO_3	5.72
$MnCl_2 \cdot 4H_20$	3.62
$ZnSO_4 \cdot 7H_20$	0.44
$CuSO_4 \cdot 5H_20$	0.16
$COCl_2 \cdot 6H_20$	0.1
$Na_2MoO_4 \cdot 2H_20$	0.78
$NaHCO_3$	250

6.2.2 Experimental setup

Two sets of continuous experiments were carried out, to assess the effect of the inlet phosphorus concentration, since in the previous studies carried out with *wild type* strain of *Nostoc* sp. PCC 7120 it resulted the main variable affecting cyanophycin accumulation (§ 5). The inlet phosphorus concentration was set equal to 6.96±0.19 mg_P L^{-1} and then it was reduced down to 0.69±0.20 mg_P L^{-1}, to trigger the cyanophycin accumulation. The inlet phosphorus concentration was varied modifying the concentration of potassium hydrogen phosphate (K_2HPO_4) in the cultivation medium reported in Table 6.1. All mutants were maintained in continuous cultivation without any selective pressure. Experiments were carried out in a polycarbonate flat plate photobioreactor, with an irradiated surface (A_{PBR}) of 0.005 m^2. The working volume (V_{PBR}) equal to 150 mL is kept constant thanks to an overflow tube, which allows the output of the biomass at the same flowrate (Q) at which the medium is pumped into the reactor, by means of a multichannel peristaltic pump (205S/CA, Watson-Marlow Fluid Technology Group). The reactor temperature was maintained constant and equal to 24°C in a thermostated incubator (Frigomeccanica Andreaus, Padova). A constant incident light intensity (I_0) was provided by a white LED lamp at a value of 450 μmol photons m^{-2} s^{-1}. Photon Flux Density (PFD) was measured using a photoradiometer (HD 2101.1 from Delta OHM), by means of a quantum

radiometric probe which quantifies the Photosynthetically Active Radiation (PAR). The cultures in the reactor are mixed by a stirring magnet placed at the bottom and sparged with a CO_2-air mixture (5% v/v). The bubbling guaranteed the carbon supply as well the control of the pH within the range 7.5-8.5, monitored daily using a Hanna portable pH-meter (code HI9124). It was shown that this system can be approximated to a Continuous Stirred Tank Reactor (CSTR). Since the reactor volume (V_{PBR}) is constant, by setting the flowrate (Q) equal to 60.4±1.2 mL d^{-1}, the resulting residence time τ is 2.48 d

$$\tau = \frac{1}{D} = \frac{1}{\mu} = \frac{V_{PBR}}{Q} \tag{6.1}$$

The inverse of the residence time is the dilution rate D, that is the specific growth rate μ, equal to 0.402 d^{-1}. When an experimental condition was set, after a transitory period of about three times the residence time, steady state was achieved. In this state, nutrient consumption, biomass concentration and its composition remained constant until the experimental condition changed. Accordingly, the productivity P_i (g_i L^{-1} d^{-1}) was calculated as the ratio between the concentration of the component i measured at steady state (c_i) (e.g. biomass, cyanophycin, nitrogen) and the residence time (τ):

$$P_i = \frac{c_i}{\tau} \tag{6.2}$$

Steady state achievement was monitored daily through optical density measurement at 750 nm, with a UV-visible double beam spectrophotometer (UV1900, by Shimadzu, Japan). When steady state was reached, it was kept for at least a period equal to three times the residence time, and samples of culture medium were withdrawn daily from the reactor for quantification and composition analysis. Dry cell weight (c_x) at steady state was measured by vacuum filtration, through 0.45 µm previously dried nitrocellulose filters, which were then dried for 2 h at 105°C in a laboratory oven. Biomass composition at steady state was characterized in terms of nitrogen, pigment and cyanophycin content. To measure the nitrogen content ($Y_{N|x}$) an alkaline persulfate digestion was carried out [39], followed by the quantification of released nitrates with the diagnostic kit Hydrocheck Spectratest (Code 6223). Extraction of pigments was obtained by N,N-dimethylformamide (DMF). A known volume of the culture was centrifuged at 9960 rcf for 10 min to remove the supernatant. Then, it was resuspended in an isovolume of DMF. Before quantification, samples were

stored in the dark at -18°C for at least for 24 hours to allow complete pigments extraction. The absorption spectrum of the extract was measured using DMF as reference, after a further centrifugation step. The final concentration of total chlorophyll and carotenoids was determined according to Bryant' procedure [40]. Cyanophycin extraction and quantification was done as reported in §5.2.2. Phosphorus concentration was ascertained by measuring it in both the reactor inlet and outlet streams, with the procedure described by Innamorati et al. [41] after biomass removal by filtration. Finally, axenic condition of the photobioreactor was checked periodically, by plating culture samples in LB Petri dishes.

6.2.3 Statistical analysis

Statistical tests were applied to data acquired at steady state and were conducted separately for each category of data. Levene's test for equal variance ($\alpha = 0.05$) was applied for each group of samples. One-way ANOVA analysis was performed in order to find statistically significant differences among the tested conditions. Grouping was done according to Tukey multiple comparison at 95% confidence interval. Data that do not share a letter were significantly different.

6.3 Results

To assess the effect of the inlet phosphorus concentration on the accumulation of cyanophycin, two sets of experiments were carried out: in control conditions (6.96±0.19 $mg_P\ L^{-1}$) and in P limitation (0.69±0.20 $mg_P\ L^{-1}$). This value for the P concentration was selected based on the results obtained with *wild type* strains (§5). Once the reactors were inoculated, the strains needed about two weeks to adapt to the experimental conditions and reach a steady state. Results of biomass concentrations measured with mutant species are shown in Figure 6.1, along with the data measured in the control, i.e. cultivating the *wild type* strains in the same experimental conditions. As expected, also for engineered strains the biomass concentration decreased as the inlet P concentration decreased. In the control conditions, there was no statistically significative difference between the *wild type* strain and *Nostoc* 44, reaching a biomass concentration equal to about 1.4 $g_x\ L^{-1}$, that corresponds to a biomass productivity equal to 560 $g_x\ m^{-3}\ d^{-1}$. *Nostoc* 41 and *Nostoc* 53, instead, resulted to be less productive strains, reaching the lower biomass concentration and productivity

(about 1 g_x L^{-1} and 400 g_x m^{-3} d^{-1}). When decreasing the inlet P concentration, the biomass concentration decreased. The most producing strain revealed to be *Nostoc* 44, with a biomass concentration equal to 0.56±0.7 g_x L^{-1}, a value significantly greater also with respect to the *wild type* strains. Since the residence time is the same for all the species, also the biomass productivity obtained with *Nostoc* 44 in limiting condition is the greatest one (227±29 g_x m^{-3} d^{-1}).

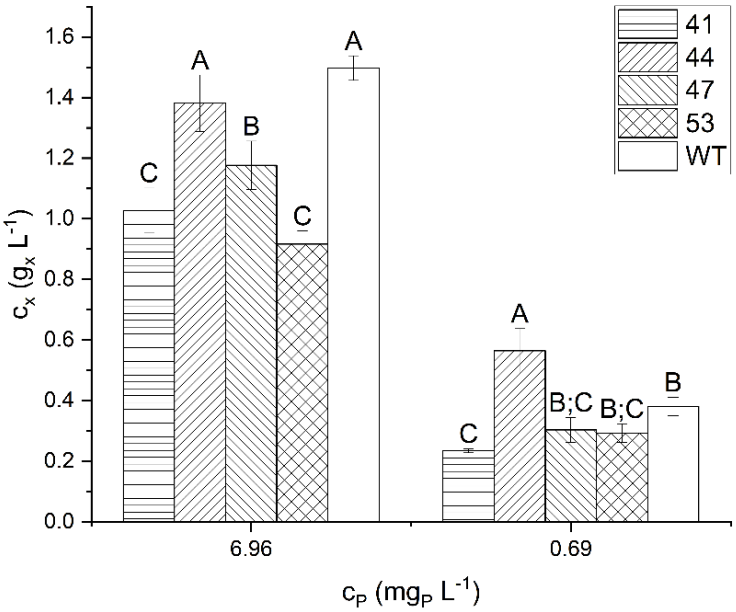

Figure 6.1. Steady state biomass concentration (c_x, g_x L^{-1}) at a residence time of 2.48 d, with different mutant species, as function of the inlet phosphorus concentration (c_P, mg_P L^{-1}). Error bars represent the standard deviation of at least 4 samples for each steady state (n≥4). Statistical analysis was conducted separately for each category of data. Data that do not share a letter are significantly different.

As regards the cyanophycin accumulation, the engineered strains increased their CGP quota when the phosphorus became limiting, as expected. Experimentally measured quotas are reported in Table 6.1. All the strains produced cyanophycin, apart from strain 53, which did not accumulate any of it when cultivated in control conditions. Under P limitation, a great increase of the cyanophycin quota was measured for all the species. Specifically, *Nostoc* 44 increased its cyanophycin quota by 1025%, reaching a value of 0.29 g_{CGP} g_x^{-1}. Other authors reported a cyanophycin accumulation equal to 47.4±2.3% and 57.3±11.1% per cell dry mass, under phosphate and potassium starvation respectively [42]. The optimization led to an accumulation of 40% of cyanophycin per cell dry mass, with a total yield of 340 mg_{CGP} per liter in 9 days [26]. This means that a cyanophycin productivity equal to about 38 mg_{CGP} L^{-1} d^{-1} could be reached. However, these data were obtained in a

batch system with the mutant BW86 of *Synechocystis* sp., a non-diazotrophic cyanobacteria.

Table 6.2. Steady state cyanophycin quota (%) at a residence time of 2.48 d, with different mutant species, as function of the inlet phosphorus concentration (c_P, $mg_P\ L^{-1}$). Error bars represent the standard deviation of at least 4 samples for each steady state (n≥4). Statistical analysis was conducted separately for each category of data. Data that do not share a letter are significantly different.

	c_P^{inlet} ($mg_P\ L^{-1}$) 6.96±0.19	**c_P^{inlet} ($mg_P\ L^{-1}$) 0.69±0.20**
***Nostoc* 41**	0.8±0.3 ^{C}	5.6±1.3 ^{D}
***Nostoc* 44**	2.6±0.4 ^{A}	29.5±1.3 ^{A}
***Nostoc* 47**	1.2±0.2 $^{B;C}$	15.3±1.9 ^{B}
***Nostoc* 53**	-	7.4±1.3 $^{C;D}$
***Nostoc* sp. PCC 7120 (*wild type*)**	1.9±0.7 $^{A;B}$	10.0±0.4 ^{C}

Apart from the cyanophycin quota, it is interesting to consider the cyanophycin productivity. Indeed, as reported in §4.3.2, cyanophycin quota and productivity could have a completely different trend. Results of cyanophycin productivity are shown in Figure 6.2.

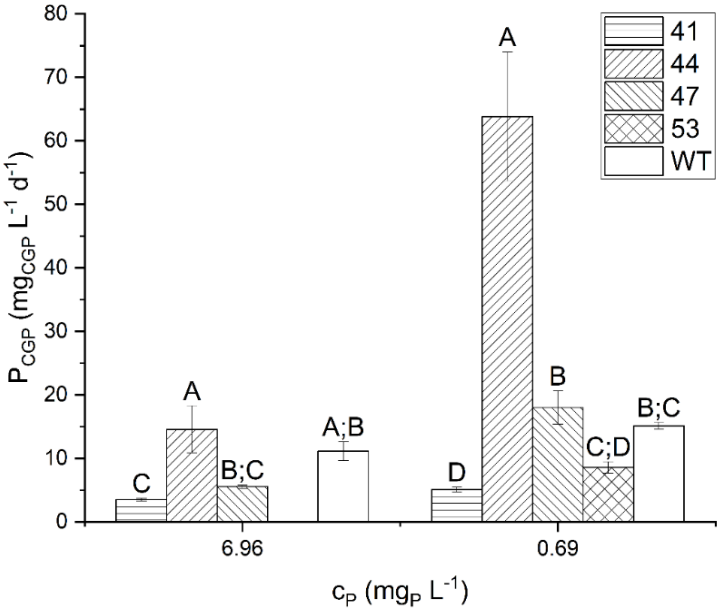

Figure 6.2. Steady state cyanophycin productivity (P_{CGP}, $mg_{CGP}\ L^{-1}\ d^{-1}$) at a residence time of 2.48 d, with different mutant species, as function of the inlet phosphorus concentration (c_P, $mg_P\ L^{-1}$). Error bars represent the standard deviation of at least 4 samples for each steady state (n≥4). Statistical analysis was conducted separately for each category of data. Data that do not share a letter are significantly different.

In this specific case, the cyanophycin obtained with mutant 44 was significantly greater with respect to the other strains. Specifically, a productivity of 63.8±10.2 $g_{CGP}\ m^{-3}\ d^{-1}$ was

reached, that corresponds to an increase of 322% with respect to the maximum productivity measured in the *wild type* (P_{CGP}=15.1±0.5 g_{CGP} m^{-3} d^{-1}). Even if this value is greater by about 65% with respect to the one measured for the non-diazotrophic mutant BW86, the comparison between the two results is not possible. Indeed, the two species were cultivated in two completely different cultivation systems (continuous and batch) and in the case of the batch, the real productivity have to be calculated considering also the additional unproductive time required for operations needed between two sequential production cycles (e.g. cleaning, sterilization), which inevitably reduced their value [43]. Moreover, for a consistent comparison, it must be considered that the two species are completely different in terms of energy, i.e. the light, and nutrients, in particular nitrogen, required for their growth.

The experimental operative conditions were selected based on the results obtained with the *wild type* strains (§5), but these are not necessarily the optimal ones for all the mutants considered in this study. The analysis of nitrogen content of the biomass ($Y_{N|x}$) reported in Figure 6A.1 of Appendix, reveals that there were no significative differences between species both under control and under P limitation conditions, measuring a mean nitrogen content of biomass equal to 8.3±1.3% and 10.0±2.0%, respectively. This suggests that the cultures were at the same time not co-limited by nitrogen. Moreover, the different biomass productivity between strains, resulted in a maximum nitrogen fixation rate equal to 58.9±11.8 mg_N L^{-1} d^{-1}, measured with the *wild type* strain under control conditions. To further qualify the biomass, also its pigments content was measured, reported in Figures 6.3.

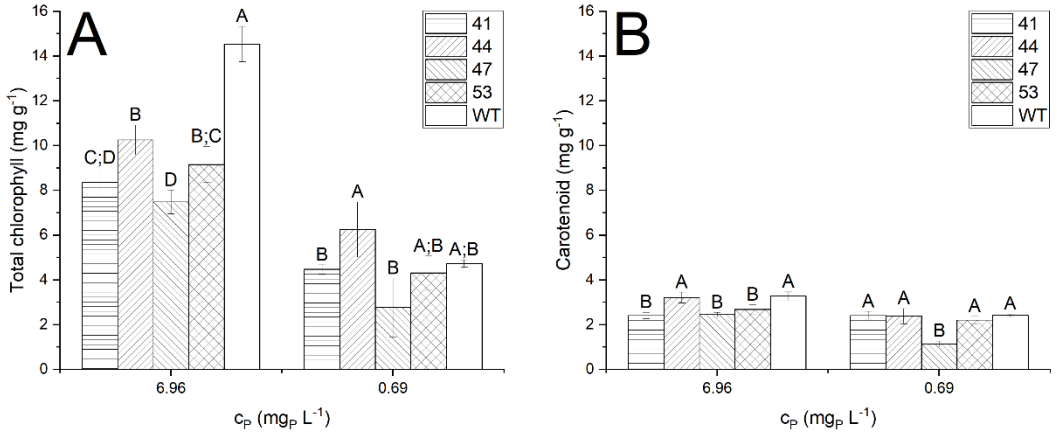

Figure 6.3. Total chlorophyll (panel A) and carotenoid (panel B) content in biomass (mg g^{-1}) at a residence time of 2.48 d, with different mutant species, as function of the inlet phosphorus concentration (c_P, mg_P L^{-1}). Error bars represent the standard deviation of at least 4 samples for each steady state (n≥4). Statistical analysis was conducted separately for each category of data. Data that do not share a letter are significantly different.

It was concluded that for all the species the concentration of chlorophyll decreased as the phosphorus became limiting, instead the concentration of carotenoid remained almost constant and equal to about 2.5 mg g^{-1}. Indeed, visibly, the cultures took a yellowish color, unlike those maintained under control conditions whose color was dark green. This phenomenon was defined as chlorosis [40]. A similar result was obtained by Collier et al. [44], Trautmann et al. [26] and Trentin et al. [27]. It is worth mentioning that the intracellular content of chlorophyll decreased over time during nutrient starvation, because, while its synthesis is stopped, the cells continue to divide [44].

As has emerged from previous works on the production of cyanophycin through the cultivation of photosynthetic microorganisms [26,27,45], there is a strict relationship between the internal quota of phosphorus and the cyanophycin quota. Specifically, they are inversely proportional. So, after measuring the phosphorus concentration in the inlet and outlet streams, the internal quota of phosphorus (q_P, g_P g_x^{-1}) was calculated as the ratio between the amount of the phosphorus internally stored by microorganisms, and the biomass concentration:

$$q_P = \frac{c_P^{inlet} - c_P^{outlet}}{c_x} \tag{6.3}$$

The cyanophycin quota measurements were plotted as function of q_P. Results are shown in Figure 6.4 along with data obtained in §5 with the *wild type* strains (*Nostoc* sp. PCC 7120). Noticeably, data with mutant species are very well in line with those obtained with *wild* type strains, confirming what previously discussed in §5. The productivity of cyanophycin was increased because with *Nostoc* 44, a lower value for the phosphorus internal quota (0.11 ± 0.02 g_P g_x^{-1}) was reached, so the cyanophycin quota was boosted up to about 30%.

Interestingly, Trautman et al. [26] found a similar relationship between cyanophycin and phosphorus quota, with both *wild type* (PCC 6803) and mutant strain (BW86) of *Synechocystis* sp., as reported in Figure 6.5. Also in this case, with the mutant BW86 a lower internal quota of phosphorus was measured, approximately around the same threshold value equal to 0.001 g_P g_x^{-1}. However, the data of Trautmann et al. [26] were obtained in batch system, and so they depends on the time of measure.

In summary, from the preliminary results obtained with the mutants, *Nostoc* 44 resulted as the most promising one, with a cyanophycin productivity equal to 63.8 ± 10.2 g_{CGP} m^{-3} d^{-1}. However, since in this study only two experimental conditions were studied, it is not possible to totally exclude *a priori* the other over-accumulating mutants. More experiments

have to be carried out, aiming to assess the effect of the main operating variables on the cyanobacterial growth. In particular, light availability is a fundamental variable that could promote or limit the cyanobacterial/microalgal growth causing phenomena as photoinhibition, photosaturation, or photolimitation [46,47].

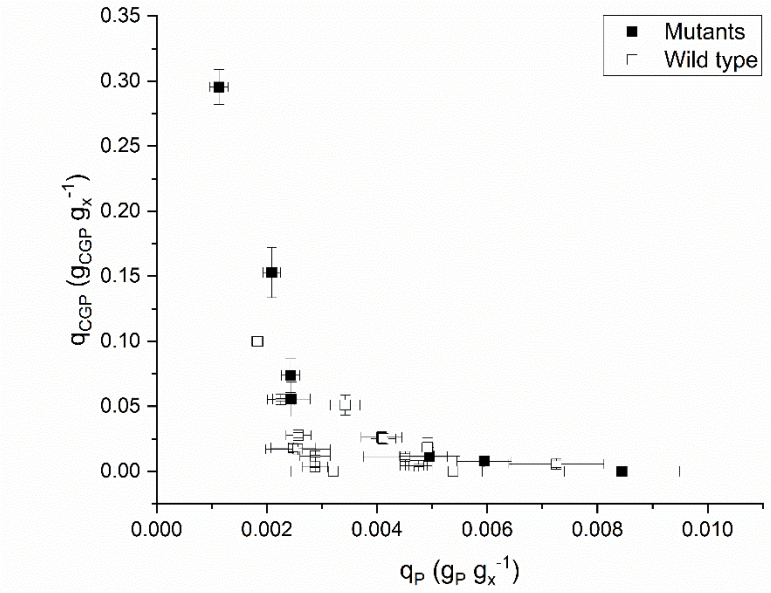

Figure 6.4. Effect of phosphate availability on cyanophycin accumulation in *Nostoc* sp PCC 7120 and in engineered strain of *Nostoc* sp. PCC 7120: cyanophycin quota (q_{CGP}) as a function of phosphorus quota (q_P) measured at steady state. Error bars represent the standard deviation of at least 4 samples for each steady state (n≥4).

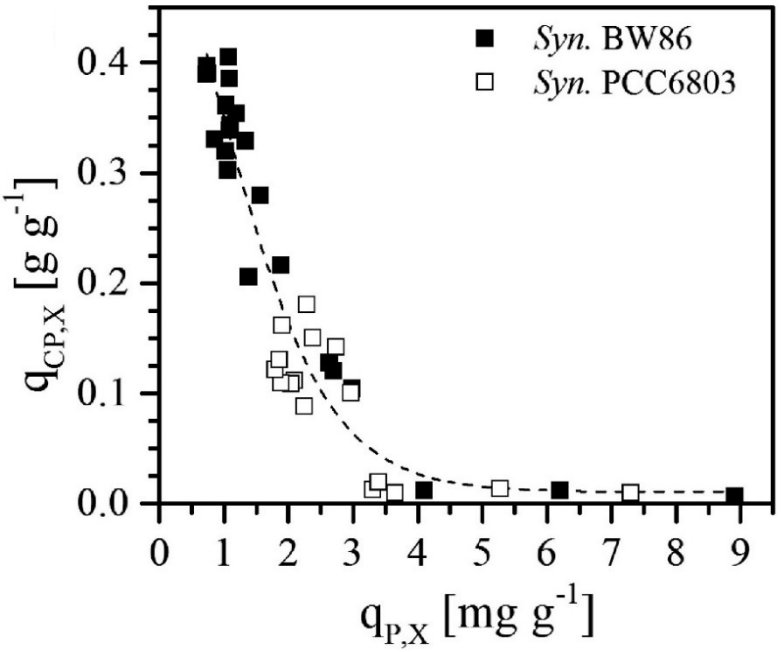

Figure 6.5. Effect of phosphate availability on cyanophycin accumulation in *Synechocystis* sp. 6803 and BW86 cyanophycin quota ($q_{CP,X}$, g_{CGP} g_x^{-1}) in dependence of phosphor quota ($q_{P,X}$, mg_P g_x^{-1}), adapted from [26]

6.4 Final remarks

In this study, engineered strains of *Nostoc* sp. PCC 7120 were cultivated in continuous system to increase the productivity of cyanophycin in diazotrophic conditions under different inlet phosphorus concentrations. *Nostoc* 44 resulted the most promising strains among the ones tested, increasing the cyanophycin productivity by three times. Moreover, the cyanophycin quota expressed as function of the phosphorus internal quota has the same trend with respect to data obtained with *wild type* strain. These two variables are inversely proportional and a decrease in the phosphorus quota triggers the cyanophycin quota. Thus, a promising platform for the biological conversion of atmospheric nitrogen into a valuable nitrogen-rich compound was developed and its high potential was demonstrated. However, more work has to be done in order to find the optimal experimental cultivation condition that ensure a continuous and stable production of cyanophycin.

Nomenclature

Q	Volumetric flowrate ($m^3\ d^{-1}$)
V_{PBR}	Flat-panel photobioreactor volume (mL)
τ	Residence time (d)
μ	Biomass specific growth rate (d^{-1})
D	Dilution rate (d^{-1})
c_x	Biomass concentration ($g_x\ L^{-1}$)
c_{CGP}	Cyanophycin concentration ($mg_{CGP}\ L^{-1}$)
q_{CGP}	Cyanophycin quota ($g_{CGP}\ g_x^{-1}$)
P_x	Biomass productivity ($g_x\ L^{-1}\ d^{-1}$)
P_{CGP}	Cyanophycin productivity ($mg_{CGP}\ L^{-1}\ d^{-1}$)
c_P^{inlet}	Inlet phosphorus concentration ($mg_P\ L^{-1}$)
c_P^{outlet}	Otulet phosphorus concentration ($mg_P\ L^{-1}$)
$Y_{N\|x}$	Nitrogen internal quota ($g_N\ g_x^{-1}$)
q_P	Phosphorus quota ($g_P\ g_x^{-1}$)

Literature cited

[1] Y. Chisti, Biodiesel from microalgae, Biotechnol. Adv. 25 (2007) 294–306. https://doi.org/10.1016/j.biotechadv.2007.02.001.

[2] K.B. Cantrell, T. Ducey, K.S. Ro, P.G. Hunt, Livestock waste-to-bioenergy generation opportunities, Bioresour. Technol. 99 (2008) 7941–7953. https://doi.org/10.1016/j.biortech.2008.02.061.

[3] L. Barsanti, P. Gualtieri, Is exploitation of microalgae economically and energetically sustainable?, Algal Res. 31 (2018) 107–115. https://doi.org/10.1016/j.algal.2018.02.001.

[4] G.L. Bhalamurugan, O. Valerie, L. Mark, Valuable bioproducts obtained from microalgal biomass and their commercial applications: A review, Environ. Eng. Res. 23 (2018) 229–241. https://doi.org/10.4491/eer.2017.220.

[5] S.B. Grama, Z. Liu, J. Li, Emerging Trends in Genetic Engineering of Microalgae for Commercial Applications, Mar. Drugs. 20 (2022) 1–24. https://doi.org/10.3390/md20050285.

[6] L. Wei, Q. Wang, Y. Xin, Y. Lu, J. Xu, Enhancing photosynthetic biomass productivity of industrial oleaginous microalgae by overexpression of RuBisCO activase, Algal Res. 27 (2017) 366–375. https://doi.org/10.1016/j.algal.2017.07.023.

[7] B. Yang, J. Liu, X. Ma, B. Guo, B. Liu, T. Wu, Y. Jiang, F. Chen, Genetic engineering of the Calvin cycle toward enhanced photosynthetic CO2 fixation in microalgae, Biotechnol. Biofuels. 10 (2017) 1–13. https://doi.org/10.1186/s13068-017-0916-8.

[8] Y.S. Shin, J. Jeong, T.H.T. Nguyen, J.Y.H. Kim, E.S. Jin, S.J. Sim, Targeted knockout of phospholipase A2 to increase lipid productivity in Chlamydomonas reinhardtii for biodiesel production, Bioresour. Technol. 271 (2019) 368–374. https://doi.org/10.1016/j.biortech.2018.09.121.

[9] N. Anila, D.P. Simon, A. Chandrashekar, G.A. Ravishankar, R. Sarada, Metabolic engineering of Dunaliella salina for production of ketocarotenoids, Photosynth. Res. 127 (2016) 321–333. https://doi.org/10.1007/s11120-015-0188-8.

[10] K. Baek, J. Yu, J. Jeong, S.J. Sim, S. Bae, E.S. Jin, Photoautotrophic production of macular pigment in a Chlamydomonas reinhardtii strain generated by using DNA-free CRISPR-Cas9 RNP-mediated mutagenesis, Biotechnol. Bioeng. 115 (2018) 719–728. https://doi.org/10.1002/bit.26499.

[11] K.J. Lauersen, T. Baier, J. Wichmann, R. Wördenweber, J.H. Mussgnug, W. Hübner, T. Huser, O. Kruse, Efficient phototrophic production of a high-value sesquiterpenoid from the eukaryotic microalga Chlamydomonas reinhardtii, Metab. Eng. 38 (2016) 331–343. https://doi.org/10.1016/j.ymben.2016.07.013.

[12] J. Wichmann, T. Baier, E. Wentnagel, K.J. Lauersen, O. Kruse, Tailored carbon partitioning for phototrophic production of (E)-α-bisabolene from the green microalga Chlamydomonas reinhardtii, Metab. Eng. 45 (2018) 211–222. https://doi.org/10.1016/j.ymben.2017.12.010.

[13] U. Eilers, A. Bikoulis, J. Breitenbach, C. Büchel, G. Sandmann, Limitations in the biosynthesis of fucoxanthin as targets for genetic engineering in Phaeodactylum tricornutum, J. Appl. Phycol. 28 (2016) 123–129. https://doi.org/10.1007/s10811-015-0583-8.

[14] E. Aboulmagd, I. Voss, F.B. Oppermann-Sanio, A. Steinbüchel, Heterologous Expression of Cyanophycin Synthetase and Cyanophycin Synthesis in the Industrial Relevant Bacteria Corynebacterium glutamicum and Ralstonia eutropha and in Pseudomonas putida, Biomacromolecules. 2 (2001) 1338–1342. https://doi.org/10.1021/bm010075a.

[15] K.M. Frey, F.B. Oppermann-Sanio, H. Schmidt, A. Steinbüchel, Technical-scale production of cyanophycin with recombinant strains of Escherichia coli, Appl. Environ. Microbiol. 68 (2002) 3377–3384. https://doi.org/10.1128/AEM.68.7.3377-3384.2002.

[16] I. Voss, S.C. Diniz, E. Aboulmagd, A. Steinbüchel, Identification of the Anabaena sp. Strain PCC7120 Cyanophycin Synthetase as Suitable Enzyme for Production of Cyanophycin in Gram-Negative Bacteria Like Pseudomonas putida and Ralstonia eutropha, Biomacromolecules. 5 (2004) 1588–1595. https://doi.org/10.1021/bm049861g.

[17] K. Ziegler, A. Diener, C. Herpin, R. Richter, R. Deutzmann, W. Lockau, Molecular characterization of cyanophycin synthetase, the enzyme catalyzing the biosynthesis of the cyanobacterial reserve material multi-L- arginyl-poly-L-aspartate (cyanophycin), Eur. J. Biochem. 254 (1998) 154–159. https://doi.org/10.1046/j.1432-1327.1998.2540154.x.

[18] Y. Elbahloul, M. Krehenbrink, R. Reichelt, A. Steinbüchel, Physiological conditions conducive to high cyanophycin content in biomass of Acinetobacter calcoaceticus Strain ADP1, Appl. Environ. Microbiol. 71 (2005) 858–866.

https://doi.org/10.1128/AEM.71.2.858-866.2005.

[19] B.J. Meussen, R.A. Weusthuis, J.P.M. Sanders, L.H. De Graaff, Production of cyanophycin in Rhizopus oryzae through the expression of a cyanophycin synthetase encoding gene, Appl. Microbiol. Biotechnol. 93 (2012) 1167–1174. https://doi.org/10.1007/s00253-011-3604-9.

[20] A. Steinle, A. Steinbüchel, Establishment of a simple and effective isolation method for cyanophycin from recombinant Saccharomyces cerevisiae, Appl. Microbiol. Biotechnol. 85 (2010) 1393–1399. https://doi.org/10.1007/s00253-009-2213-3.

[21] A. Steinle, S. Witthoff, J.P. Krause, A. Steinbüchel, Establishment of cyanophycin biosynthesis in Pichia pastoris and optimization by use of engineered cyanophycin synthetases, Appl. Environ. Microbiol. 76 (2010) 1062–1070. https://doi.org/10.1128/AEM.01659-09.

[22] A.M. Ruffing, T. Kallas, Editorial: Cyanobacteria: The Green E. coli, Front. Bioeng. Biotechnol. 4 (2016) 7. https://doi.org/10.3389/fbioe.2016.00007.

[23] M. Frommeyer, L. Wiefel, A. Steinbüchel, Features of the biotechnologically relevant polyamide family "cyanophycins" and their biosynthesis in prokaryotes and eukaryotes, Crit. Rev. Biotechnol. 36 (2016) 153–164. https://doi.org/10.3109/07388551.2014.946467.

[24] J. Du, L. Li, S. Zhou, Microbial production of cyanophycin: From enzymes to biopolymers, Biotechnol. Adv. 37 (2019). https://doi.org/10.1016/j.biotechadv.2019.05.006.

[25] B. Watzer, A. Engelbrecht, W. Hauf, M. Stahl, I. Maldener, K. Forchhammer, Metabolic pathway engineering using the central signal processor PII, Microb. Cell Fact. 14 (2015). https://doi.org/10.1186/s12934-015-0384-4.

[26] A. Trautmann, B. Watzer, A. Wilde, K. Forchhammer, C. Posten, Effect of phosphate availability on cyanophycin accumulation in Synechocystis sp. PCC 6803 and the production strain BW86, Algal Res. 20 (2016) 189–196. https://doi.org/10.1016/j.algal.2016.10.009.

[27] G. Trentin, V. Lucato, E. Sforza, A. Bertucco, Stabilizing autotrophic cyanophycin production in continuous photobioreactors, Algal Res. 60 (2021) 102518. https://doi.org/10.1016/j.algal.2021.102518.

[28] M. Nyberg, T. Heidorn, P. Lindblad, Hydrogen production by the engineered cyanobacterial strain Nostoc PCC 7120 δhupW examined in a flat panel photobioreactor system, J. Biotechnol. 215 (2015) 35–43.

https://doi.org/10.1016/j.jbiotec.2015.08.028.

[29] X. Gao, H. Xu, Z. Zhu, Y. She, S. Ye, Improved production of echinenone and canthaxanthin in transgenic Nostoc sp. PCC 7120 overexpressing a heterologous crtO gene from Nostoc flagelliforme, Microbiol. Res. 236 (2020) 126455. https://doi.org/10.1016/j.micres.2020.126455.

[30] K. Takahama, Construction and Analysis of a Recombinant Cyanobacterium Expressing a Chromosomally Inserted Gene for an Ethylene-Forming Enzyme at the psbAI Locus, 95 (2003) 302–305.

[31] J.H. Jacobsen, N. Frigaard, Engineering of photosynthetic mannitol biosynthesis from CO 2 in a cyanobacterium, Metab. Eng. 21 (2014) 60–70. https://doi.org/10.1016/j.ymben.2013.11.004.

[32] K.J. Hellingwerf, F. Branco, Nonhierarchical Flux Regulation Exposes the Fitness Burden Associated with Lactate Production in Synechocystis sp. PCC6803, (2017). https://doi.org/10.1021/acssynbio.6b00235.

[33] P.R. Jones, Genetic instability in cyanobacteria – an elephant in the room ?, 2 (2014) 1–5. https://doi.org/10.3389/fbioe.2014.00012.

[34] A. Hitchcock, C.N. Hunter, D.P. Canniffe, Progress and challenges in engineering cyanobacteria as chassis for light-driven biotechnology, (2020). https://doi.org/10.1111/1751-7915.13526.

[35] P. Rugbjerg, N. Myling-petersen, A. Porse, K. Sarup-lytzen, M.O.A. Sommer, Diverse genetic error modes constrain large-scale bio-based production, Nat. Commun. (n.d.). https://doi.org/10.1038/s41467-018-03232-w.

[36] B.R. Glick, Metabolic load and heterologous gene expression, Biotechnol. Adv. 13 (1995) 247–261. https://doi.org/https://doi.org/10.1016/0734-9750(95)00004-A.

[37] P. Kallio, K. Stensjö, P. Lindblad, Photoautotrophic production of renewable ethylene by engineered cyanobacteria : Steering the cell metabolism towards biotechnological use, (2021) 579–590. https://doi.org/10.1111/ppl.13430.

[38] R. Rippka, J.J.B.W. Deruelles, J.B. Waterbury, M. A. Herdman, R.Y. Stanier, Generic Assignments, Strain Histories and Properties of Pure Cultures of Cyanobacteria, Microbiology-Sgm. 111 (1979) 1–61. https://doi.org/10.1099/00221287-111-1-1.

[39] J.J. Ameel, R.P. Axler, C.J. Owen, Persulfate digestion for determination of total nitrogen and phosphorus in low-nutrient waters, Am. Environ. Lab. 5 (1993) 1–11.

[40] D. A. Bryant, The Molecular Biology of Cyanobacteria in Advances in

Photosynthesis book series (AIPH, volume 1), Springer, Dordrecht, 1994. https://doi.org/10.1007/978-94-011-0227-8.

[41] M. Innamorati, I. Ferrari, D. Marino, M. Ribera D' Alcala, Metodi nell' ecologia del plancton marino. In Nova Thalassia, Edizioni L, 1990.

[42] B. Watzer, K. Forchhammer, Cyanophycin: A Nitrogen-Rich Reserve Polymer, in: K.F.E.-A. Tiwari (Ed.), IntechOpen, Rijeka, 2018: p. Ch. 5. https://doi.org/10.5772/intechopen.77049.

[43] B.D. Fernandes, A. Mota, J.A. Teixeira, A.A. Vicente, Continuous cultivation of photosynthetic microorganisms: Approaches, applications and future trends, Biotechnol. Adv. 33 (2015) 1228–1245. https://doi.org/10.1016/j.biotechadv.2015.03.004.

[44] J.L. Collier, A.R. Grossman, Chlorosis induced by nutrient deprivation in Synechococcus sp. strain PCC 7942: Not all bleaching is the same, J. Bacteriol. 174 (1992) 4718–4726. https://doi.org/10.1128/jb.174.14.4718-4726.1992.

[45] S.E. Stevens, D.A.M. Paone, D.L. Balkwill, Accumulation of Cyanophycin Granules as a Result of Phosphate Limitation in Agmenellum quadruplicatum , Plant Physiol. 67 (1981) 716–719. https://doi.org/10.1104/pp.67.4.716.

[46] E. Sforza, D. Simionato, G.M. Giacometti, A. Bertucco, T. Morosinotto, Adjusted light and dark cycles can optimize photosynthetic efficiency in algae growing in photobioreactors, PLoS One. 7 (2012). https://doi.org/10.1371/journal.pone.0038975.

[47] E.M. Grima, F.G. Acie, Y. Chisti, Photobioreactors : light regime , mass transfer , and scaleup, 70 (1999) 231–247.

Appendix

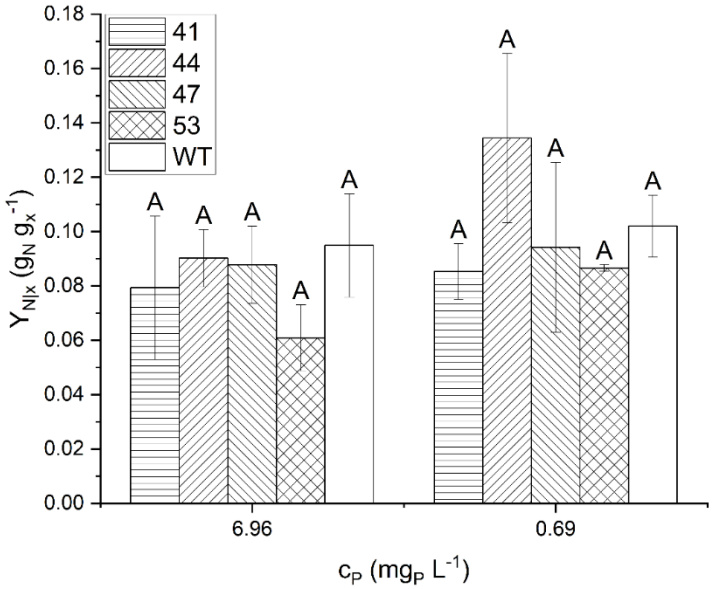

Figure 6A.1. Steady state nitrogen quota ($Y_{N|x}$, g_N g_x^{-1}) at a residence time of 2.48 d, with different mutant species, as function of the inlet phosphorus concentration (c_P, mg_P L^{-1}). Error bars represent the standard deviation of at least 4 samples for each steady state (n≥4). Statistical analysis was conducted separately for each category of data. Data that do not share a letter are significantly different.

Chapter 7

Nutrients uptake in microalgal continuous cultivation system

In this Chapter, data of biomass growth and nutrients uptakes measured in continuous experiments are collected and reorganized to describe the effect of different forms and concentrations of nitrogen and phosphorus as nutrients in microalgal cultivations. Then, a preliminary modified Droop model is implemented using Matlab® with the aim of properly representing the growth of algae in continuous photobioreactors in complex media, where nitrogen was supplied in multiple forms. The model results are compared to data measured in continuous experiments carried out in flat plate photobioreactors, with respect to algal growth rate and the nutrients consumption. A fair approximation of experimental data was achieved for both the microorganisms, although further work has to be done to improve the model and minimize the error between the experimental and the simulated values.

7.1 Introduction

Nowadays, there is a growing interest in the large-scale cultivation and production of microalgae, which have several industrial applications [1]. Microalgae contain carbohydrates, proteins, enzymes, many vitamins, and minerals such as potassium, magnesium and calcium [2]. For this reason, they are largely used in the food industry as additives or nutritional supplements in pasta, snack foods and drinks because they can enhance the nutritional value of food and animal feed [3]. Microalgae can also be incorporated into cosmetics as antioxidants, thickening and water-binding agents in face, skin, and hair care products [2]. Moreover, they can be used as fertilizers or as a tool treatment and biofuel production because of their high oil content and rapid biomass production [4]. Indeed, their biomass is a greener source of energy compared to fossil fuels, and it is preferable to other kinds of feedstock to produce biofuels because it does not require arable land and fresh water [5]. However, even though the biological and technological feasibility of biofuel from microalgae was proved, the process is not considered applicable for the high economic costs associated to cultivation and downstream, that make microalgae not competitive with respect to fossil fuel and other renewable technologies [6]. Another important application of microalgae is the wastewater treatment. Microalgae provide an efficient system for the removal of chemical pollutants, organic contaminants, and heavy metals from wastewater [7]. Domestic, industrial, and animal wastewater are rich in nitrogen and phosphorus that can be assimilated by the microalgae, combining the removal of these pollutants with the production of biomass [8]. In this way, double benefits are obtained: eutrophication problems were avoided and secondly, the biomass is produced without exploiting fertilizers [9]. On the other hand, the utilization of the wastewater limits the potential uses of the biomass, due to regulatory issues [10].

Thus, microalgae can be cultured by different cultivations system and substrates, but they always need light as energy source, and nutrients, among which the major ones are nitrogen and phosphorus [2]. Nitrogen (N) is the second major component of biomass. Its fraction on dry weight basis generally varies between 1% and 14% [11]. Ammonium (NH_4^+), nitrite (NO_2^-) and nitrate (NO_3^-) are some of the inorganic sources of nitrogen assimilated by microalgae [12]. Many cyanobacteria can also fix atmospheric nitrogen (N_2), and some species are able to assimilate organic nitrogen compounds, like urea, proteins, and amino acids, particularly arginine and glutamine [13,14]. Among others, ammonium is the

preferred nitrogen form by microalgae and cyanobacteria because its assimilation and consumption are energetically favourable compared to other inorganic nitrogen forms. However, it has been observed that high concentrations of ammonium are toxic for microalgal growth, mainly by inducing damage to photosystem II. The level of toxicity is species-specific [12]. Moreover, ammonium causes an inhibition of the uptake of other forms of nitrogen [15]. Phosphorus (P) is an important nutrient for microalgae and its biomass content ranges from 0.05% up to 3.3% [11]. In natural environments, phosphorus is often a limiting nutrient for microalgal growth [16]. P is present in various organic and inorganic forms, but algae can only assimilate it as orthophosphates. Anyhow, thanks to intracellular or extracellular enzymes that catalyse the conversion to orthophosphates, microalgae are able to utilize also other phosphorus compounds. The orthophosphate uptake occurs mainly by active transports, while passive diffusion has a minor contribution to the inorganic phosphorus influx [12]. Under certain conditions, microalgae and cyanobacteria can accumulate more phosphorus than necessary in polyphosphate granules. This phenomenon is known as luxury uptake and can be exploited to remove phosphorus from wastewater [17,18].

In this context, mathematical models are useful tools to describe the simultaneous effect of multiple factors affecting microorganisms growth, allowing to predict the final biomass productivity and to optimize the system design in terms of operation and control, and so increasing the process profitability [19]. Therefore, modelling nutrients uptake is seminal not only in the case of wastewater treatment applications, where the goal is to maximize the pollutants uptake, but also in the case of high added-value molecules production under specific nutrient limitation.

Monod model is widely applied to describe the growth kinetics of microorganisms as a function of nutrient concentration [20]. However, the Monod model often fails to fit the experimental data [21]. Indeed, in some conditions, microalgae exhibit a lag between nutrient uptake and growth, suggesting these two processes may be partially decoupled [22]. A model that better explains this phenomenon is the one proposed by Droop [23], which decouples the microorganism growth from the assimilation of the nutrient by introducing a new variable, the cell quota, defined as the weight of internal nutrient per unit of biomass [21]. According to this model, the biomass growth depends on the intracellular nutrient quota, instead of the extracellular available nutrient. The evolution of the nutrient cell quota is determined by two phenomena: the nutrient uptake, which contributes to the accumulation of internal nutrient, and the cellular growth, which consumes the nutrient.

The nutrient uptake depends on external nutrient concentration, but since cells have a limited capacity for nutrient storage, its uptake decreases the closer the internal quota gets to the maximum value [24].

One aspect still to be clarified is the behaviour of microalgae in complex media with multiple nitrogen sources, such as ammonium and nitrate. Ammonium inhibits the uptake of nitrogen compounds, including nitrate, which is abundantly present in wastewaters as a result of nitrification processes [25]. Therefore, in this Chapter, a preliminary modified Droop model is set up to describe the growth of microalgae and cyanobacteria in complex media, where nitrogen is supplied in multiple forms. The model was implemented using Matlab® software and compared to data obtained in continuous experiments carried out in flat plate photobioreactors, with respect to algal growth rate and nutrients consumption, with the aim of representing the growth of algae in continuous photobioreactors at steady state, as a function of incident light intensity, and nitrogen and phosphorus concentrations.

7.2 Materials and methods

7.2.1 Experimental setup

Two photosynthetic microorganisms were used in this study: *Synechocystis* sp. PCC 6803 and *Chlorella protothecoides. Synechocystis* sp. PCC 6803 is a unicellular, non-diazotrophic, coccoid cyanobacterium with a diameter of approximately 2,07 μm [26], which derives from Berkeley strain 6803 isolated from the freshwater Oakland Lake in California. *Chlorella protothecoides* 33.80 is an eukaryotic microalgae with an high specific growth rate, a minimal acclimatization phase (lag) and an early exponential phase [3]. Maintenance and propagation of cultures were performed in freshwater media (BG11) [27] at ambient temperature, under continuous agitation. For batch and continuous experiments, the concentrations of phosphorus and nitrogen were modified to obtain excess and limiting conditions, whereas the concentrations of other nutrients were doubled in order to provide them in excess. Moreover, nitrogen (N) was supplied as ammonium sulphate ($(NH_4)_2SO_4$), sodium nitrate ($NaNO_3$) or as a mixture of both. The media were prepared by mixing the components in demineralized water, and then sterilized in autoclave for 20 minutes at 121°C. Light was provided constantly at 150 μmol photons m^{-2} s^{-1}, unless as specifically stated, by a LED panel, and it was measured using a photoradiometer (HD 2102.1 from Delta Ohm, Italy) which quantifies the photosynthetically active radiation

(PAR). A continuous flow of CO_2 enriched air (5 % v/v) was supplied to the culture, which was also continuously mixed with a magnetic stirrer.

For the batch experiment, Quickfit® Drechsel Bottle with a diameter of 50 mm and a capacity of 250 mL was used. Culture samples were withdrawn at regular intervals of time to verify the growth of the cyanobacteria and nutrient consumption. For continuous experiments, stainless-steel-polycarbonate flat-panel reactor were used, with different reactor depth (z) and volume (V_{PBR}). The medium was continuously supplied to the reactor at a constant flowrate (Q) through a peristaltic pump (Watson -Marlow 120U/DM3). A baffle was placed inside the reactor to prevent short circuiting of nutrients. An overflow tube was located on the opposite side of the medium inlet, to keep the working volume constant. This system can be approximated to a CSTR (Continuous Stirred Tank Reactor). By maintaining constant the flowrate and the working volume, it was possible to operate at steady state with a fixed residence time (ϑ), calculated as:

$$\vartheta = \frac{V_{PBR}}{Q} \tag{7.1}$$

The photobioreactor was monitored by daily sampling. After a transitory time, steady state was achieved, with constant biomass concentration. Steady state was kept for at least a period equal to three times the residence time, and biomass samples were taken daily for analysis.

The cellular growth of photosynthetic microorganism was monitored via assessment of the Optical Density (OD_{750}), and cell dry weight (c_x). The OD_{750} assessment consists in measurements of the sample absorbance at a wavelength of 750 nm, where pigments do not absorb light, allowing a precise measurement of absorbance caused only by diffraction phenomena generated by the suspended cells. For the cell dry weight, a known volume of sample was filtered under vacuum using 0.45 μm nitrocellulose membranes, previously dried for 15 min at 105 ◦C to eliminate moisture. The samples were then placed at 105°C for 2 h and weighed. Nutrients analysis was carried out to measure their concentrations in the biomass and in the exhaust medium. Protocols based on colorimetric tests were used to measure the amount of ammonium, nitrates and orthophosphates. Ammonium concentration was determined using the commercial kit Hydrocheck Spectratest (code 6201), whereas for nitrates it was used the commercial kit Hydrocheck Spectratest (code 6223). Innamorati et al. [28] described the method used for the detection of orthophosphates in Nova Thalassia vol. 11. The nitrogen content in the biomass (q_N) were measured on

centrifuged samples to remove the supernatant, at 9960 rcf (relative centrifugal force) for 10 min. The method used is an alkaline persulfate digestion [29], followed by the quantification of released nitrates. Pigments measurements were done using N,N-dimethylformamide (DMF), a solvent which can solubilise the wall and membrane of cyanobacteria cells and extract the pigments. A known volume of biomass was centrifuged at 9960 rcf for 10 min. The supernatant was discharged, ant the pellet was resuspended in DMF. Before the analysis, the samples were preserved at -18°C at least for 24 hours in the dark because pigments are photosensitive. After centrifugation, the DMF containing the extracted pigments was transferred in a quartz cuvette and analysed with a spectrophotometer. Quantification was done according to Bryant [30].

7.2.2 Statistical analysis

Statistical tests were applied to data acquired at steady state, specifically on biomass concentration and productivity, on cyanophycin quota and productivity and on carbohydrate content. The existence of equal variance among data was verified with Levene's test using a confidence level of 95%. Then, one-way ANOVA analysis was performed to find statistically significant differences among the data. Grouping was done according to Tukey's multiple comparison procedure with a 95% confidence interval. Data that do not share a letter are significantly different.

7.3 Kinetic model

7.3.1 Microalgal growth rate

Biomass growth rate r_x, depends by several factors such as light, the internal nutrient content and the biomass concentration c_x, and is expressed according to:

$$r_x(z) = (\mu_{max} \cdot f(I) \cdot f(q) - k_d) \cdot c_X \tag{7.2}$$

where μ_{max} (d^{-1}) is the maximum specific growth rate, k_d (d^{-1}) is the specific decay rate, and $f(I)$ is the terms accounting for incident light effect on biomass growth.
The term $f(q)$ is described using the Droop model [23]. Compared to the classic Monod model [20], the Droop model does not consider biomass growth to depend on the limiting

nutrient concentration in the reaction environment, but on its internal quota, and is able to better describe the growth of microalgae considering the latency phase due to the nutrient uptake. Hence the function $f(q)$ is expressed as:

$$f(q) = \prod_i \left(1 - \frac{q_i^{min}}{q_i}\right) = \prod_i \left(\frac{R_i}{R_i + q_i^{min}}\right) \tag{7.3}$$

where q_i is the internal cell quota for the limiting nutrient i. As proposed by Barbera et al. [31],the internal quota q_i was equal to the sum of q_i^{min}, which represent the amount of nutrient embedded as structural material within the biomass, and the actual reserve of nutrient i, called R_i.

The effect of light ($f(I)$) on the biomass growth rate is described using the model proposed by Bernard and Rémond [32]:

$$f(I) = \frac{I(z)}{I(z) + K_I \cdot \left(\frac{I(z)}{I_{opt}} - 1\right)^2} \tag{7.4}$$

where $I(z)$ is the light intensity at depth z, K_I (μmol photons m^{-2} s^{-1}) is the half-saturation constant of the light response curve and I_{opt} (μmol photons m^{-2} s^{-1}) is the light intensity at which the growth rate is maximal. Since light does not have a uniform concentration in the reactor and varies along the culture depth, the irradiance at a specific depth z was calculated according to the Lambert-Beer law, considering a rectangular confirmation (i.e. with mono-dimensional light extinction):

$$I(z) = I_0 \cdot \exp\left(-k_a \cdot c_x \cdot z\right) \tag{7.5}$$

where I_0 (μmol photons m^{-2} s^{-1}) is the incident light intensity, k_a (m^2 g^{-1}) is the biomass absorption coefficient, c_x (g_x m^{-3}) is the biomass concentration in the reactor and z (m) is the axial coordinate of the culture depth.

Accordingly, integrating the growth rate of microalgae ($r_x(z)$) along the culture depth (W), it is possible to calculate the average biomass growth rate (r_x^{avg}):

$$r_x^{avg} = \frac{1}{W} \int_0^W r_x(z)\ dz = \frac{1}{W} \int_0^W \left(\mu_{max} \cdot \frac{I(z)}{I(z) + K_I \cdot \left(\frac{I(z)}{I_{opt}} - 1\right)^2} \cdot \prod_i \left(\frac{R_i}{R_i + q_i^{min}}\right) - k_d \right) \cdot C_X\ dz \tag{7.6}$$

7.3.2 Nutrient uptake and storage

Nutrient uptake depends on the external nutrient concentration (c_i) and on its internal quota (q_i). Since the ability of microalgae to accumulate nutrients is limited, the uptake rate decreases as the internal quota of nutrient approaches its maximum value q_i^{max} [24].

$$r_i = \frac{di}{dt} = -\mu_i \cdot c_i = -\rho_i \cdot \frac{c_i}{c_i + K_i} \cdot \left(1 - \frac{q_i}{q_i^{max}}\right) \cdot c_x \tag{7.7}$$

where ρ_i is the maximum uptake rate of nutrient i ($g_i\ g_x^{-1}\ d^{-1}$) and K_i is the nutrient half-saturation constant ($g_i\ m^{-3}$).

The internal reserve, R_i, represents the nutrients storage that occurs in the biomass. At the same time, this is maintained by nutrient uptake, but also dissipated by the cell multiplication [23]. Hence, the variation of the nitrogen internal quota was calculated according to:

$$r_{R,i} = \rho_i \cdot \frac{c_i}{c_i + K_i} \cdot \left(1 - \frac{q_i}{q_i^{max}}\right) - q_i \cdot \frac{1}{W} \int_0^W \left(\mu_{max} \cdot \frac{I(z)}{I(z) + K_I \cdot \left(\frac{I(z)}{I_{opt}} - 1\right)^2} \cdot \prod_i \left(\frac{R_i}{R_i + q_i^{min}}\right) - k_d \right) \cdot dz \tag{7.8}$$

7.3.3 Mass balances in a continuous photobioreactor

A continuous photobioreactor can be approximated to a Continuous Stirred Tank Reactor (CSTR), thus the mass balances for the biomass and nutrients are:

$$c_x^{in} - c_x^{out} + \frac{1}{W} \int_0^W \left(\mu_{max} \cdot \frac{I(z)}{I(z) + K_I \cdot \left(\frac{I(z)}{I_{opt}} - 1\right)^2} \cdot \prod_i \left(\frac{R_i}{R_i + q_i^{min}}\right) - k_d \right) \cdot c_x^{out}\ dz \cdot \vartheta = 0 \tag{7.9}$$

$$c_i^{in} - c_i^{out} - \rho_i \cdot \frac{c_i^{out}}{c_i^{out} + K_i} \cdot \left(1 - \frac{q_i}{q_i^{max}}\right) \cdot c_x^{out} \cdot \vartheta = 0 \tag{7.10}$$

where ϑ (d) is the residence time. As for the internal reserve within the cells, instead, there is no accumulation at steady state, thus the mass balances is:

$$\rho_i \cdot \frac{c_i^{out}}{c_i^{out} + K_i} \cdot \left(1 - \frac{q_i}{q_i^{max}}\right) - q_i \cdot \frac{1}{W} \int_0^W \left(\mu_{max} \cdot \frac{I(z)}{I(z) + K_I \cdot \left(\frac{I(z)}{I_{opt}} - 1\right)^2} \cdot \prod_i \left(\frac{R_i}{R_i + q_i^{min}}\right) - k_d \right) \cdot dz = 0 \tag{7.11}$$

7.3.4 Dixon model

To consider the simultaneous presence of ammonium and nitrate in the cultivation media, the Droop model was modified according to the Dixon's model [33]. This model takes into account the combined effect of two different substrates (A and B), so defining the specific growth rate as

$$\mu_A = \frac{\mu_{max} \cdot c_A}{K_A + c_A + \left(\frac{K_A}{K_B}\right) c_B} \tag{7.12}$$

where μ_{max} is the maximum specific growth rate, c_A and c_B are the substrates concentration, K_A and K_B are the half saturation constants. Considering the Dixon's formulation, the ammonium and nitrate uptake rates can be written as:

$$r_{NO3} = -\rho_{NO3} \cdot \frac{c_{NO3}}{c_{NO3} + K_{NO3} + \alpha\, c_{NH4}} \cdot \left(1 - \frac{q_N}{q_N^{max}}\right) \cdot c_x \tag{7.13}$$

$$r_{NH4} = -\rho_{NH4} \cdot \frac{c_{NH4}}{c_{NH4} + K_{NH4} + \beta\, c_{NO3}} \cdot \left(1 - \frac{q_N}{q_N^{max}}\right) \cdot c_x \tag{7.14}$$

where ρ_{NH4} and ρ_{NO3} are respectively the ammonium and the nitrate maximum uptake rates ($g_N\ g_x^{-1}\ d^{-1}$), c_{NO3} and c_{NH4} are the nitrate and ammonium concentrations ($g_N\ m^{-3}$), α and β are the dimensionless parameter taking into the account the effect of ammonium on nitrate and of nitrate on ammonium, respectively.

7.3.5 Solimeno model

As an alternative to the Dixon model, to consider the simultaneous presence of ammonium and nitrate in the cultivation media, the Droop model has been modified according to a simplified Solimeno model [34], which account for nitrate and ammonium:

$$r_{NO3} = -\rho_{NO3} \cdot \frac{c_{NO3}}{c_{NO3} + K_{N,alg}} \cdot \frac{K_{N,alg}}{K_{N,alg} + c_{NH4}} \cdot \left(1 - \frac{q_N}{q_N^{max}}\right) \cdot c_x \tag{7.15}$$

$$r_{NH4} = -\rho_{NH4} \cdot \frac{c_{NH4}}{c_{NH4} + K_{N,alg}} \cdot \left(1 - \frac{q_N}{q_N^{max}}\right) \cdot c_x \tag{7.16}$$

where $K_{N,alg}$ is the saturation constant of c_x on nitrogen species, and is equal to 0.1 $g_N\ m^{-3}$ [35].

7.3.6 Kinetic parameters

The kinetic parameters used in this study were summarized in the Table 7.1 for *Synechocystis* sp. PCC 6803 and in Table 7.2 for *Chlorella protothecoides*. The experimental values of outlet nitrogen concentration (c_N^{out}), biomass concentration (c_x) and internal nitrogen quota (q_N) were utilised to derive the parameters α and β of the Dixon model (Eq. 7.13 and 7.14), reported in Table 7.1 and 7.2.

Table 7.1. Summary of kinetic parameters for *Synechocystis* sp. PCC 6803

Parameter	UoM	Value	Reference
μ_{max}	d^{-1}	3.3	Calculated from [36–38]
k_d	d^{-1}	0.2	[31]
k_a	$m^2\ g_x^{-1}$	0.1866	[39]
I_{opt}	µmol photons $m^{-2}\ s^{-1}$	350	Calculated from [40]
K_I	µmol photons $m^{-2}\ s^{-1}$	100	Calculated from [40]
ρ_{NO3}	$mg_N\ mg_x^{-1}\ d^{-1}$	1.86	*This work*
ρ_{NH4}	$mg_N\ mg_x^{-1}\ d^{-1}$	0.8	*This work*
K_{NO3}	$mg_N\ L^{-1}$	26.1	*This work*
K_{NH4}	$mg_N\ L^{-1}$	27.78	*This work*
q_N^{max}	$g_N\ g_x^{-1}$	0.18	*This work*
q_N^{min}	$g_N\ g_x^{-1}$	0.014	*This work*
α	dim	20	*This work*
β	dim	0.001	*This work*
$K_{N,alg}$	$g_N\ m^{-3}$	0.1	[35]

Table 7.2. Summary of kinetic parameters for *Chlorella protothecoides*

Parameter	UoM	Value	Reference
μ_{max}	d^{-1}	4.5	[41]
k_d	d^{-1}	0.2	[31]
k_a	$m^2\ g_x^{-1}$	0.09	[42]
I_{opt}	µmol photons $m^{-2}\ s^{-1}$	413	[42]
K_I	µmol photons $m^{-2}\ s^{-1}$	73.4	[42]
ρ_{NO3}	$mg_N\ mg_x^{-1}\ d^{-1}$	0.60	[43]
ρ_{NH4}	$mg_N\ mg_x^{-1}\ d^{-1}$	0.62	[43]
K_{NO3}	$mg_N\ L^{-1}$	14.58	[43]
K_{NH4}	$mg_N\ L^{-1}$	14.23	[43]
q_N^{max}	$g_N\ g_x^{-1}$	0.20	[31]
q_N^{min}	$g_N\ g_x^{-1}$	0.045	[31]
ρ_P	$mg_P\ mg_x^{-1}\ d^{-1}$	0.036	*This work*
K_P	$mg_P\ L^{-1}$	1.85	*This work*
q_P^{max}	$g_P\ mg_x^{-1}$	0.10	[31]
q_P^{min}	$g_P\ mg_x^{-1}$	0.0006	[31]
α	dim	0.056	*This work*
β	dim	17.7	*This work*
$K_{N,alg}$	$g_N\ m^{-3}$	0.1	[35]

7.4 Results and discussion

7.4.1 Experiments with Synechocystis sp. PCC 6803

To assess the effect of varying the nitrogen source and the inlet nitrogen concentration, different experiments were carried out by changing the residence time, the nitrogen source, the inlet nitrogen concentration, and the reactor depth, which affects the average light inside the culture. Data obtained from batch and continuous experiments previously carried out in our laboratory were used to estimate the kinetic nitrogen parameters of the Droop model, solving the mass balances for the biomass, the internal quota, and the nutrient concentration (§7.3). A summary of the estimated value of parameters is reported in Table 7.3.

Table 7.3. Summary of kinetic parameters

Parameter	UoM	Value
q_N^{min}	$mg_N\ mg_x^{-1}$	0.014
q_N^{max}	$mg_N\ mg_x^{-1}$	0.18
ρ_{NO3}	$mg_N\ mg_x^{-1}\ d^{-1}$	1.86
ρ_{NH4}	$mg_N\ mg_x^{-1}\ d^{-1}$	0.8
K_{NO3}	$mg_N\ L^{-1}$	26.1
K_{NH4}	$mg_N\ L^{-1}$	27.78

The reliability of kinetic parameters was verified by carrying out experiments at different operating conditions, and in particular using nitrate or ammonium as nitrogen source. Figure 7.1 reports the results of biomass concentration and nitrogen quota of continuous experiments carried out with nitrate as only nitrogen source, at two different residence time and using reactor with different depth (Table 7.4).

As the inlet nitrogen concentration decreases, there is a significant decrease in biomass, as well as a reduction in the internal nitrogen quota that is significantly different only for the experiment with an inlet nitrogen concentration equal to 23.3 $mg_N\ L^{-1}$. In this case the experiment proved to be carried out under nitrogen limiting condition. Indeed, almost no nitrates are measured in the exhaust medium (Table 7.4).

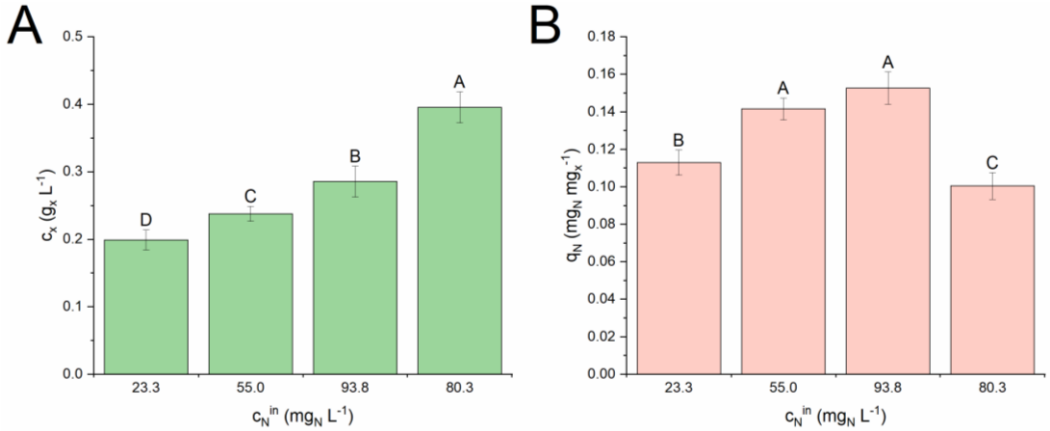

Figure 7.1. Biomass concentration (c_x, panel A) and internal nitrogen quota (q_N, panel B) in continuous experiments with nitrate as nitrogen source. Statistical analysis was conducted separately for each category of data. Data that do not share a letter are significantly different.

Table 7.4. Results obtained in continuous experiments at steady state with nitrate as nitrogen source (± SD; n≥4). Statistical analysis was conducted separately for each category of data. Data that do not share a letter are significantly different.

τ (d)	z (cm)	c_N^{in} (mg_N L^{-1})	c_N^{out} (mg_N L^{-1})	c_x (g_x L^{-1})	q_N (%)
0.8	3	23.3±1.2	$0.9±0.8^{D}$	$0.199±0.015^{D}$	$11.3±0.7^{B}$
0.8	3	55.0±1.0	$19.6±1.5^{C}$	$0.238±0.011^{C}$	$14.1±0.6^{A}$
0.8	3	80.3±1.5	$42.6±2.2^{B}$	$0.396±0.023^{A}$	$10.0±0.7^{C}$
1.1	3.5	93.8±0.9	$51.9±2.4^{A}$	$0.285±0.023^{B}$	$15.3±0.9^{A}$

The internal nitrogen quota (q_N) varies from 11% to 15%. These results are consistent with previous results obtained in our laboratory with the eukaryotic microalga *Chlorella vulgaris* (about 12%) [44] and with values generally reported in literature (between 1% and 14%) [11,12].

For each continuous experiment, the values of outlet nitrogen concentration (c_N^{out}), biomass concentration (c_x) and internal nitrogen quota (q_N) have been simulated using the Droop model. The simulations were performed considering the same experimental conditions under which the experiments were carried out.

A comparison with the simulated values is reported in Figure 7.2. The main differences are observed for the internal nitrogen quota, in particular when the nutrient is limiting (c_N^{in}=23 mg_N L^{-1}), which it is slightly underestimated. Outlet nitrogen concentrations are overestimated, especially when the residence time is higher and equal to 1.1 d and the reactor depth is slightly higher (3.5 cm). Biomass concentration, on the other hand, is evaluated quite accurately, with a minor overestimation at the lower nitrogen concentrations.

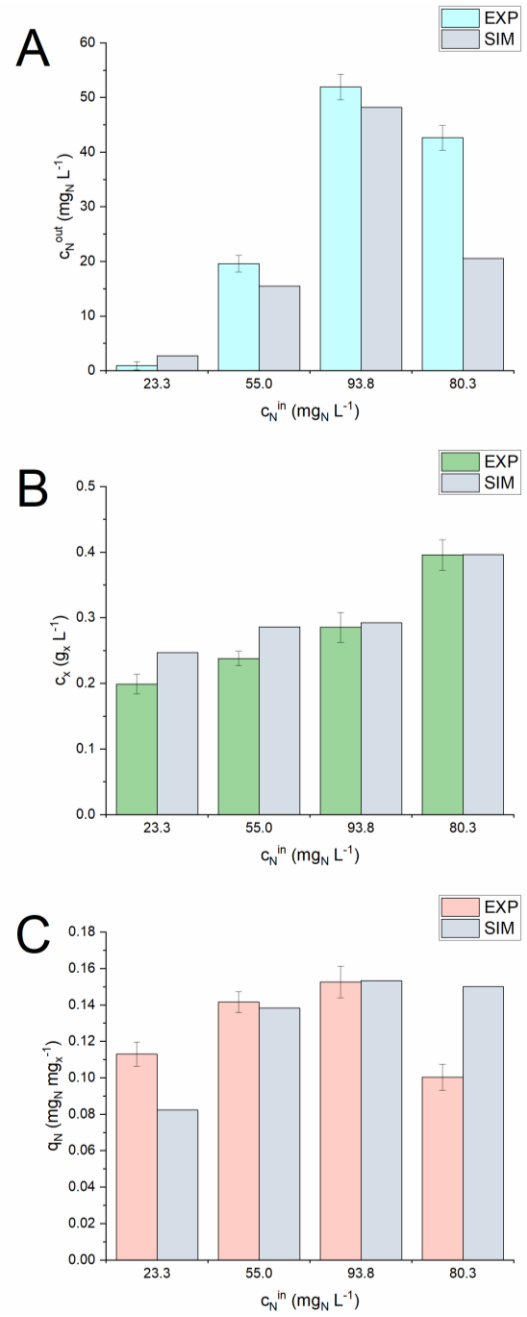

Figure 7.2. Comparison between the experimental and the calculated values for the outlet nitrogen concentration (c_N^{out}), biomass concentration (c_x) and internal quota (q_N) for continuous experiments with nitrate as nitrogen source

Other experiments were carried out using ammonium as only nitrogen source, as a preference for ammonium is observed for *Synechocystis* sp. [45]. This evidence was experimentally confirmed by performing batch experiments, in presence of same quantities of both nitrate and ammonium. In the first 30 hours after the inoculum, only the ammonia was consumed (data not shown). Results obtained from experimental measurements and simulations are reported in Figure 7.3, whereas the operating conditions were summarized in Table 7A.1 of Appendix.

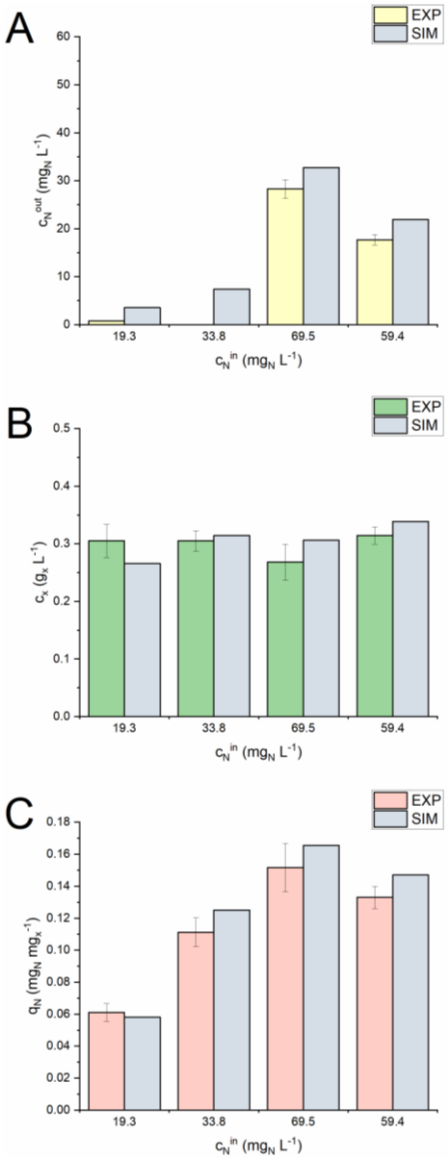

Figure 7.3. Comparison between the experimental and the calculated values for the outlet nitrogen concentration (c_N^{out}), biomass concentration (c_x) and internal quota (q_N) for continuous experiments with ammonium as nitrogen source

The content of pigments in the biomass gives an indication of the health status of microalga, as they reflect the effects of the growth conditions and of stress perceived by cells. When ammonium was limiting (c_N^{in}=19.3 mg_N L^{-1}), the pigment production, usually equal to about 15 mg g_x^{-1} for chlorophyll and 3.5 mg g_x^{-1} for carotenoid, was reduced down to 8.40±0.55 mg g_x^{-1} and 2.85±0.38 mg g_x^{-1}. In fact, a typical response to nitrogen limitation is the discoloration of cells with a decrease in chlorophyll content. This phenomenon was found also for the microalga *Chlorella fusca*, which exhibits a 50% reduction of the total chlorophyll content when cultivated in batch system, after 3 days of nitrogen starvation, whereas in *C. reinhardtii* nitrogen limitation can cause a 78% reduction in chlorophyll. This phenomenon is probably due to the lack of nitrogen atoms needed to form the pigment

itself [46]. As regards the simulated values, the biomass concentrations were quite accurately predicted, and only when nitrogen was limiting, the biomass was slightly underestimated. The nitrogen outlet concentrations, instead, were generally overestimated by about 5 mg_N L^{-1} compared to the experimental measurements. Conversely, internal nitrogen quota (q_N) for ammonium experiments were more accurately predicted.

Furthermore, it is interesting to see the difference due to the use of a different nitrogen source, comparing the results obtained in experiments carried out at the same operating conditions, with about the same inlet nitrogen concentration (c_N^{in}=57.2±3.1 mg_N L^{-1}), but provided alternatively by nitrate or ammonium. As can be seen from Figure 7.4, the internal nitrogen quota is not significantly different, but a different concentration of biomass was obtained, which is significantly higher when ammonium is used as nitrogen source. By the way, the nitrogen source by which the microalgae achieve maximum productivity is species-specific. For example, for the microalgae *Scenedesmus bijugatus* and *Dunaliella salina* the highest productivity is achieved by providing nitrate as a nitrogen source, whereas *Chlorella* sp. preferred the ammonium [47,48]. Otherwise, previous continuous experiments carried out in our laboratory on the microalga *Chlorella protothecoides* show an equal internal nitrogen quota and biomass concentration with ammonium and nitrate [43].

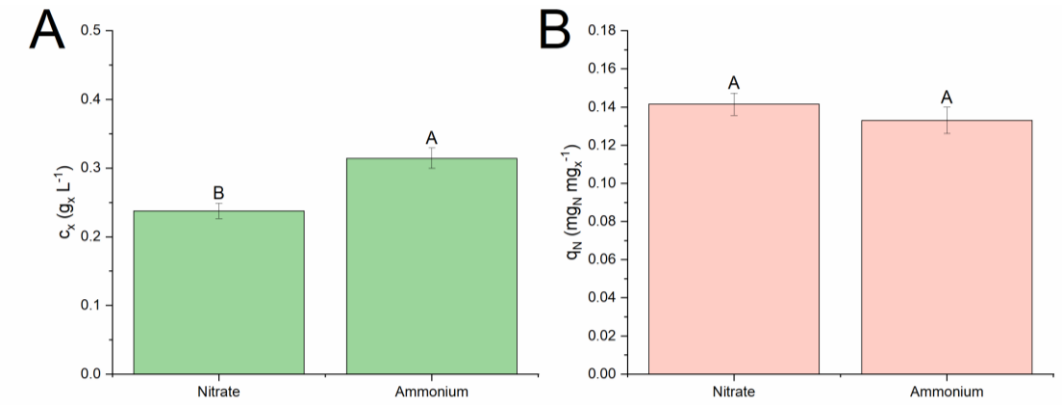

Figure 7.4. Biomass concentration (c_x, panel A) and internal nitrogen quota (q_N, panel B) in continuous experiments with nitrate or ammonium as nitrogen source. Statistical analysis was conducted separately for each category of data. Data that do not share a letter are significantly different.

However, microalgae are often cultivated in batch or continuous system in complex media, i.e. with multiple nitrogen sources, as ammonium and nitrate. Previous studies on the eukaryotic microalga *C. protothecoides* have revealed also a different assimilation of ammonium and nitrate in batch and continuous systems. In fact, while in batch in the presence of both nitrogen forms, ammonium is the only assimilated species, in continuous

systems there is a simultaneous consumption of both species [43]. On the other hand, nutrient consumption in a batch system could be influenced by many variables, such as the initial biomass concentration, the adaptation of the preinoculum, and possibly by the incident light intensity, which is variable due to the effect of self-shading. Thus, a series of continuous experiments with a mixture of ammonium and nitrate were carried out, varying the total inlet nitrogen concentration, the ratio between the two forms and the residence time. Experimental results are reported in Table 7.5.

Table 7.5. Results obtained in continuous experiments with both nitrate and ammonium as nitrogen source (± SD; n≥4). Statistical analysis was conducted separately for each category of data. Data that do not share a letter are significantly different.

Exp. n°	τ (d)	c_{NO3}^{in} ($mg_N\ L^{-1}$)	c_{NH4}^{in} ($mg_N\ L^{-1}$)	c_{NO3}^{out} ($mg_N\ L^{-1}$)	c_{NH4}^{out} ($mg_N\ L^{-1}$)	c_x ($g_x\ L^{-1}$)	q_N (%)
1	1.1	50.3±2.1	15.5±0.3	24.6±1.9	-	$0.407±0.02^{B}$	$11.4±0.7^{A;B}$
2	1.1	37.7±0.1	22.0±1.6	24.4±1.3	0.3±0.01	$0.351±0.03^{B;C}$	$10.6±0.4^{B}$
3	1.1	38.0±0.1	52.2±3.5	31.6±0.7	3.9±1.1	$0.568±0.03^{A}$	$12.2±0.5^{A}$
4	0.9	35.8±1.8	59.2±1.9	32.3±0.9	19.7±3.7	$0.328±0.04^{C}$	$11.1±0.5^{B}$

The measurements of inlet and outlet concentrations of ammonium and nitrate showed that in continuous photobioreactors when ammonium is limiting for biomass growth (Exp. n° 1 and 2), also nitrate is consumed. On the other hand, when ammonium is not a limiting nutrient, the microalgae mainly consume ammonium, and only a minimal nitrate uptake is observed (Figure 7.5).

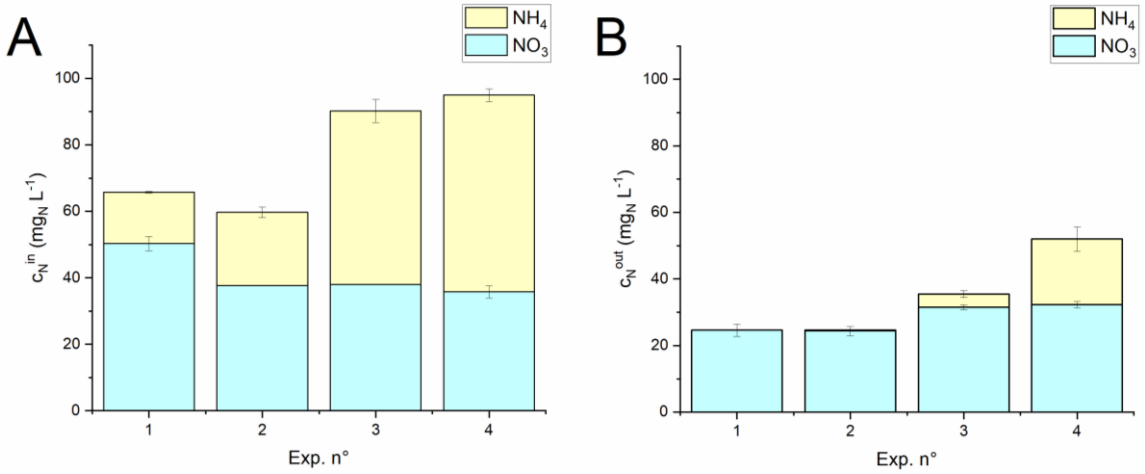

Figure 7.5. Inlet (c_N^{in}, panel A) and outlet (c_N^{out}, panel B) nitrogen concentration in continuous experiments with a mixture of ammonium (*yellow*) and nitrate (*blue*)

The different regulations of nitrogen assimilation in *Synechocystis* sp. PCC 6803 with respect to *Chlorella protothecoides* are clear, comparing the experimental results obtained in the same experimental conditions (i.e. same inlet nitrate and ammonium concentration equal to about 30 mg_N L^{-1} each ones). *Synechocystis* sp. PCC 6803 consumes all the ammonium and part of the nitrate, as ammonium is limiting to its growth (Exp. n°2, Figure 7.5), whereas *C. protothecoides* shows a consumption of both nitrogen sources, although it prefers mainly ammonium [43].

The trend of biomass concentration instead is reported in Figure 7.6. The biomass concentration depends on both the total inlet nitrogen concentration and the residence time. Specifically, increasing the total nitrogen inlet concentration at the same residence time the biomass concentration increase (Exp. n° 1-3). Instead, in the case of about equal inlet amount of ammonia e nitrate, at shorter residence time, the biomass concentration measured is lower (Exp n° 3 and 4). A decrease in biomass concentration with a decrease in residence time is in accordance with the observations of Cho et al. [49] for *Chlorella vulgaris* in continuous cultivation (Figure 7.6).

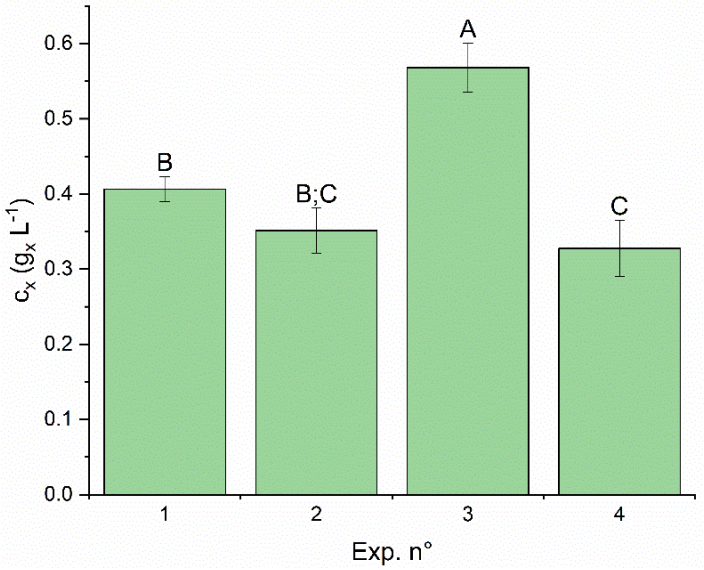

Figure 7.6. Biomass concentration in continuous experiments with a mixture of ammonium and nitrate

To properly simulate these experimental conditions, the Droop model has been modified to account for both the inlet nitrogen sources, as described in §7.3. It was modified according to both the Dixon model (§7.3.4) and the Solimeno model (§7.3.5). Results obtained from experimental measurements and simulations are reported in Figure 7.7.

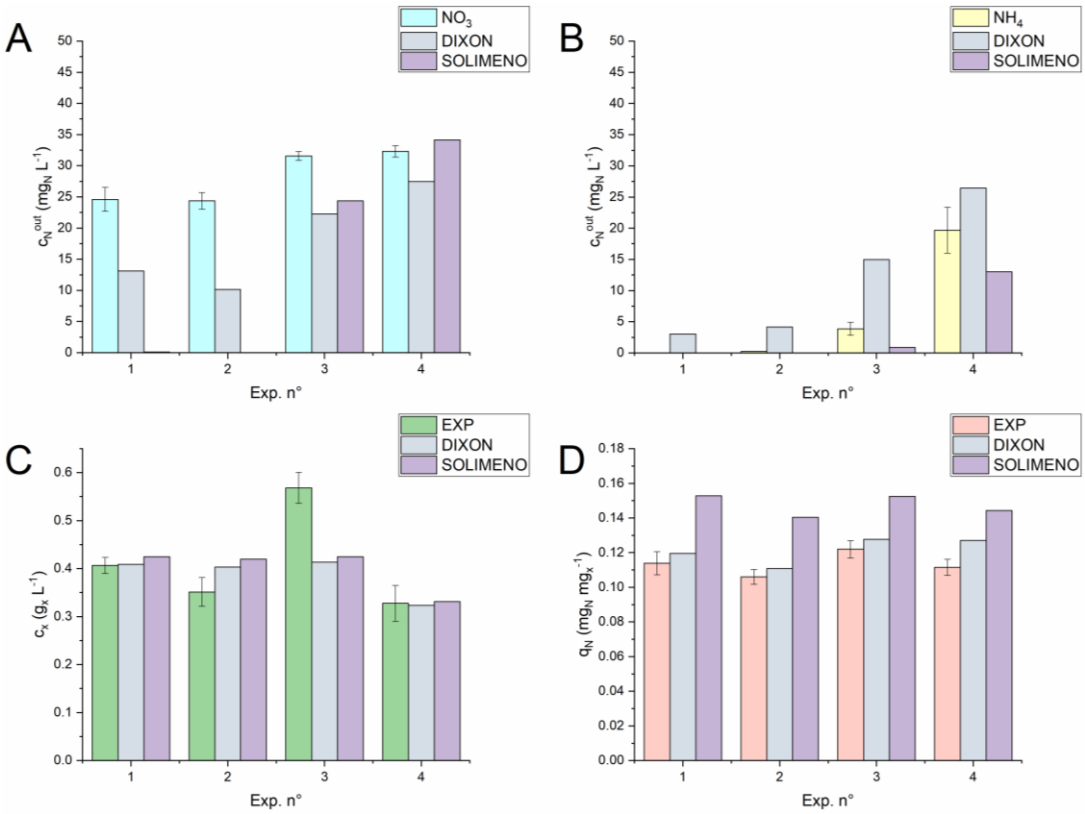

Figure 7.7. Comparison between the experimental and the simulated values for the outlet nitrogen concentration (c_N^{out}), biomass concentration (c_x) and internal quota (q_N) for continuous experiments in complex media

With respect to the nutrient consumptions, the outlet concentration of nitrate is underestimated with both model (Figure 7.7A), whereas the outlet concentration of ammonium, the favourite nutrient of *Synechocystis* sp., is generally overestimated by the Dixon model and underestimated by the Solimeno model (Figure 7.7B). Despite these differences in the nitrogen consumption, the biomass concentration is predicted quite satisfactorily by both models (Figure 7.7C). The nitrogen quota instead, is predicted quite well by the Dixon model, and it is always overestimated by the Solimeno model, probably due to the higher consumption of ammonium that it estimated. Thus, both models proved capable of describing the preference of ammonium over nitrate as a source of nitrogen, even if more work has to be done in order to find the proper value of kinetic parameters to obtain a model that better describe the consumption of both nutrients.

7.4.2 Experiments with Chlorella protothecoides

Other experiments were carried out and simulated with the microalgal species *Chlorella protothecoides*. This species was selected as it was previously used in our research group,

and many of its kinetic parameter were already retrieved and verified in previous work [31,42,43,50]. Here, the aim was to verify both Dixon and Solimeno models on a complex media, axenic o sterile, accounting also for the presence of phosphorus, a macronutrients essential for the algae growth [12], which is frequently a limiting nutrient, especially in natural environment [16]. Preliminarily, some experiments at different concentration of phosphorus were carried out.

Even if the nutrient uptake in batch and continuous system could be different, some batch experiments were carried out at different inlet phosphorus concentration, and were used to evaluate the phosphorus kinetic parameters, ρ_P and K_P, which were then compared to the ones found in literature and verified in continuous experiments. Figure 7.8 shows the biomass growth curve obtained at different inlet phosphorus concentration for *Chlorella protothecoides*. As expected, increasing the inlet phosphorus concentration, a longer exponential phase is observed. Conversely, when the nutrient was limiting, the death phase started earlier.

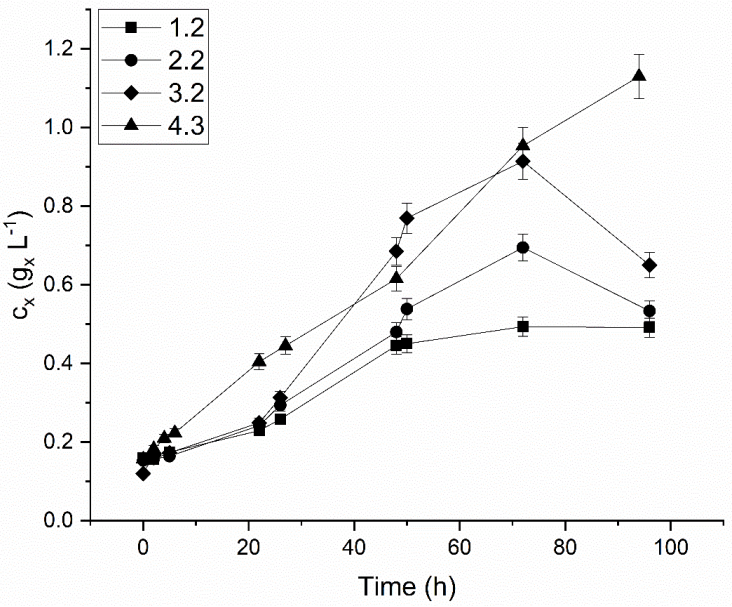

Figure 7.8. Biomass concentration in batch growth curves of *Chlorella protothecoides* carried out at different initial phosphorus concentration (1.2 mg_P L^{-1}, 2.2 mg_P L^{-1}, 3.2 mg_P L^{-1}, 4.3 mg_P L^{-1})

The phosphorus concentration was measured at regular intervals of time during the batch growth curves. As shown in the Figure 7.8, in all the experiments, the initial phosphorous content sharply decreases in the first hours, when greatest amount of nutrient is consumed. After 20 hours, phosphorous concentration starts to decrease slowly until all the nutrient amount present in the cultivation medium is depleted. This trend was already observed in

many microorganisms, both prokaryotes and eucaryotes [17]. It suggests that, like other organisms, *C. protothecoides* is able to perform the luxury uptake and so to take up more phosphorous than the one it need for growth and to use it when external nutrient concentration become limiting. As the nutrients uptake occurs mainly in the first hours, the slopes of the linear interpolation of phosphorus concentration in this period of time represent the experimentally measured nutrient uptake rates (r_P), and were used to find the value of the kinetic parameters ρ_P and K_P (Table 7.6).

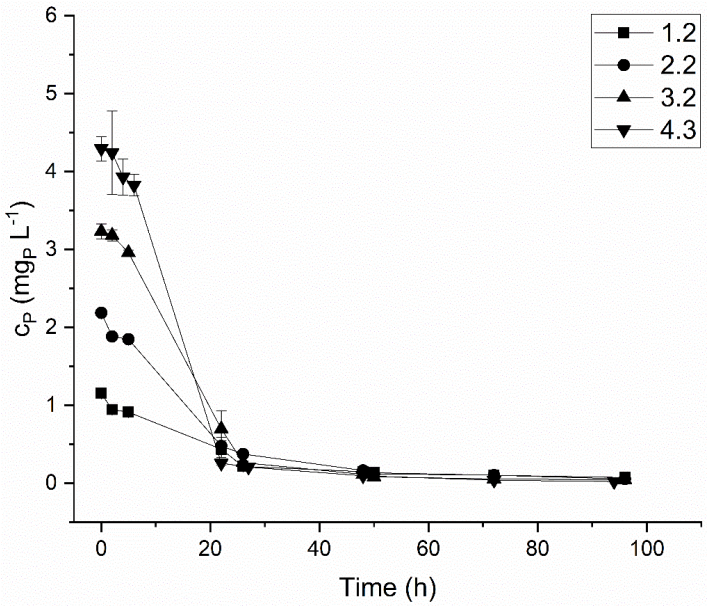

Figure 7.9. Phosphorus concentration in batch growth curves of Chlorella protothecoides.

Table 7.6. Phosphorus uptake rate (r_P) and normalized uptake rate of phosphorus (r_P/c_x) experimentally measured

c_P^0 (mg_P L^{-1})	$-r_P$ (mg_P L^{-1} h^{-1})	$-r_P/c_x$ (g_P g_x^{-1} h^{-1})
1.2±0.1	0.0455	0.00029
2.2±0.01	0.0632	0.00041
3.2±0.1	0.0560	0.00047
4.3±0.2	0.0863	0.00056

Experimental data were fitted by minimizing errors between the experimental and the calculated value of the phosphorous uptake rate normalized on the biomass concentration (r_P/c_x), by means of Eq. (7.7). The fitting procedure is done in iterative way, until a final value of the two parameters (ρ_P and K_P) was obtained. Figure 7.10 shows the comparison between the experimental and the calculated values of the phosphorus uptake rate normalized on biomass concentration.

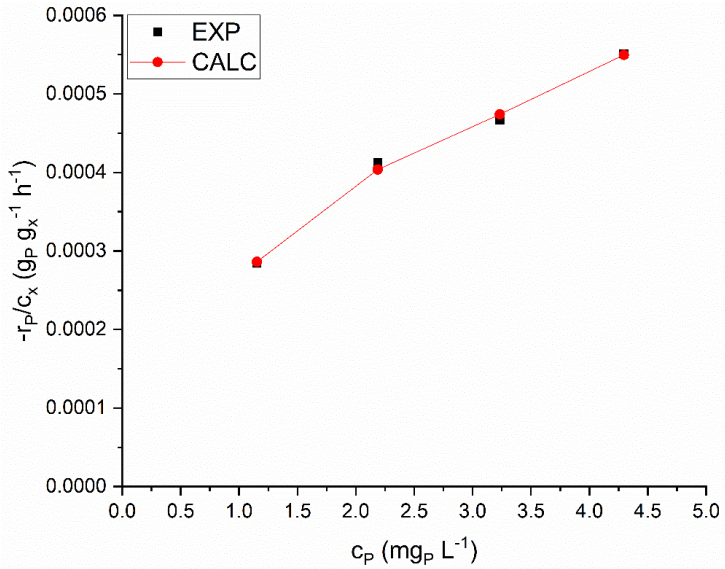

Figure 7.10. Comparison between experimental (*black*)and calculated (*red*) values of the phosphorous uptake rate normalized on the biomass concentration ($-r_P/c_x$).

The kinetic parameter obtained are equal to 0.0036 g_P g_x d^{-1} and 1.85 mg_P L^{-1} for the maximum uptake rate of phosphorus and the phosphorus half saturation constant, respectively. The value of K_P is similar to the one already reported by Sforza et al. [50] (1.8 mg_P L^{-1}) and Barbera et al. [31] (1.86 mg_P L^{-1}). Instead, the value of ρ_P is slightly greater than the one reported by Carpine et al. for *Synechocystis* sp. [51], but is in agreement with the one found by Barbera et al. [31]. Anyway, the kinetic parameters were validated on continuous experiments carried out at different inlet phosphorus concentration. Results of experimental and simulated value of biomass concentration and phosphorus outlet concentration were reported in Figure 7.11. The model is able to represent acceptably the experimental data both when phosphorous is limiting (c_P^{in}=6 mg_P L^{-1}) and when it is provided in excess (c_P^{in}=44 mg_P L^{-1}).

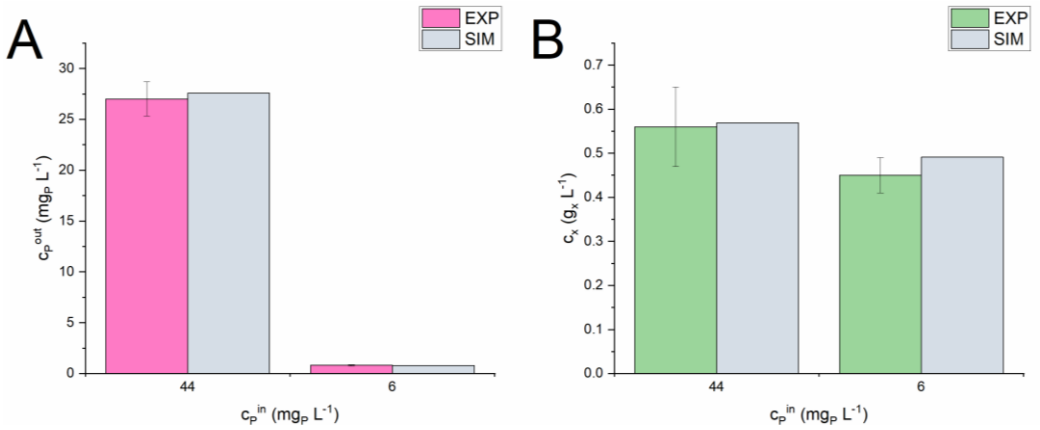

Figure 7.11. Comparison between the experimental and the simulated values for the outlet nitrogen concentration (c_P^{out}), biomass concentration (c_x) for continuous experiments

Therefore, a complete model which account for nitrogen, provided by nitrate and/or ammonium, and phosphorus was set up, using alternatively the Dixon and the Solimeno model. Its reliability was verified comparing experimental and simulated values obtained in axenic culture and using wastewater as cultivation medium. Wastewater, indeed, is a very complex media, in which different nutrients are present, and they can influence each other. Experimental conditions are reported in Table 7.7.

Table 7.7. Experimental condition of validation experiments

	Exp. n°	τ (d)	z (m)	I_0 (μmol photons m^{-2} s^{-1})	c_{NO3}^{in} (mg_N L^{-1})	c_{NH4}^{in} (mg_N L^{-1})	c_P^{in} (mg_P L^{-1})
axenic	6	0.8	6.5	150	30.5	34.4	62.0
wastewater	7	1.3	2.5	100	7.5	44.5	8.0
wastewater	8	2.0	2.5	100	7.5	63.0	8.4
wastewater	9	1.3	2.5	100	11.5	59.9	9.5
wastewater	10	1.0	2.5	100	7.5	63.8	9.4

Both models are able to predict accurately the phosphorus quota, as shown in Figure 7A.1 of the Appendix. As regards the biomass concentration, instead, results of experimental and simulated values were reported in Figure 7.12.

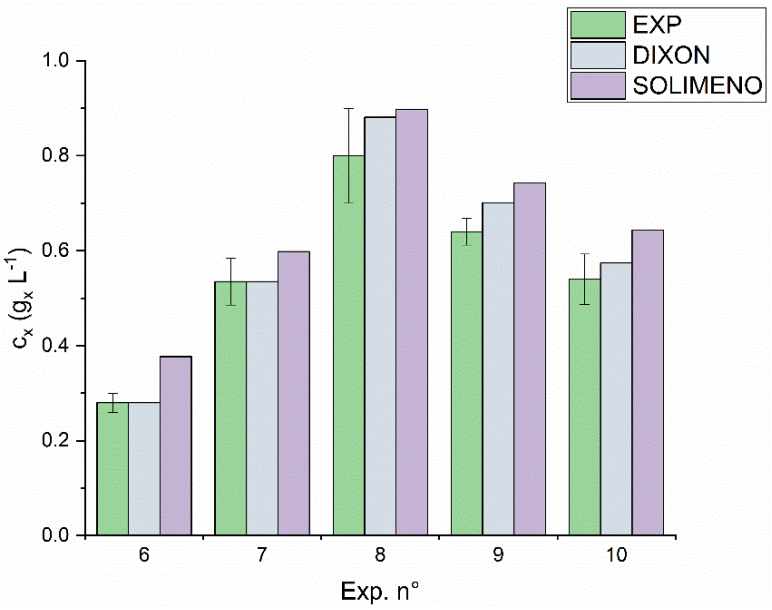

Figure 7.12. Comparison between the experimental and the simulated values for the biomass concentration (c_x) for continuous experiments of *Chlorella protothecoides* in complex media

Biomass concentration is generally evaluated acceptably, although the Solimeno model tends to overestimate its value by about 0.1 g_x L^{-1}. An explanation can be found by looking

at the experimental and simulated value of the ammonium outlet concentration, reported in Figure 7.13.

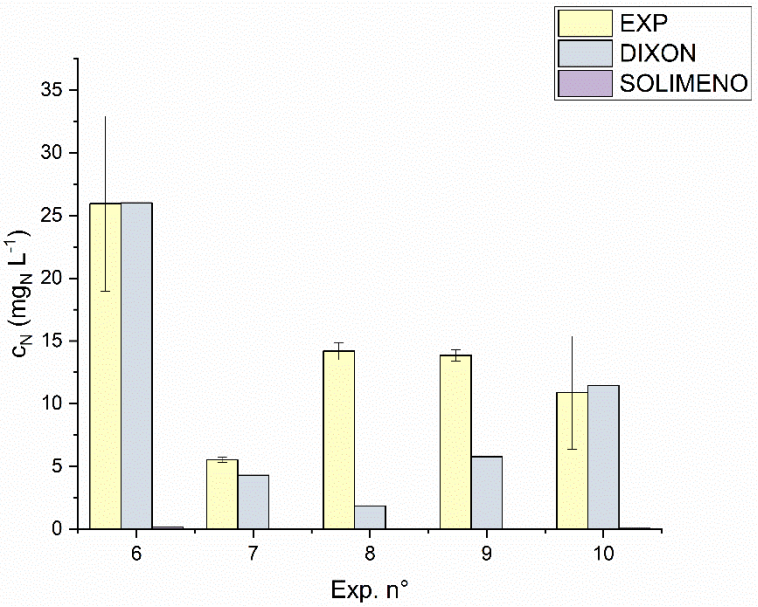

Figure 7.13. Comparison between the experimental and the calculated values for the outlet ammonium concentration (c_N^{out}) for continuous experiments of *Chlorella protothecoides* in complex media

In the case of the Solimeno model, indeed, the ammonia was always totally consumed by the algal growth, justifying the greater biomass concentration simulated at the steady state. Similarly, also the Dixon model generally underestimates the outlet ammonium concentration, suggesting that a greater ammonium uptake is estimated with respect to the real one. This is probably due to the other processes in which ammonium is involved. Indeed, ammonium (NH_4^+) is present in solution in equilibrium with ammonia (NH_3), and the concentrations of the two forms depend manly on the pH. Moreover, part of the ammonia is transferred to the atmosphere, reducing the availability of the nutrient for the microalgal growth [52]. Thus, in order to improve the simulation performance, both models should be integrated considering also the other compounds involved in ammonium processes (NH_3, H^+). However, this will inevitably lead to a more complicated model with 8 variables, in which other kinetic parameters have to be estimated and validated.

7.5 Final remarks

To describe the growth of photosynthetic microorganisms in complex media, where nitrogen was supplied in multiple forms, several experimental measurements were

collected from continuous experiments. Then, a preliminary mathematical model was developed implementing a modified Droop approach, that decouples the microorganism growth from the nutrient assimilation. To consider the simultaneous presence of ammonium and nitrate in the cultivation media, the Droop model was modified according to the Dixon or alternatively to the Solimeno model. These models were implemented using Matlab® software and compared to results measured in continuous experiments carried out in flat plate photobioreactors with a cyanobacterial species (*Synechocystis* sp. PCC 6803) and a microalgal species (*Chlorella protothecoides*), for different operating variables, specifically different values of residence time, reactor thickness and nutrients concentrations, both for axenic cultures and for microalgal cultivation in wastewater. A fair approximation of experimental biomass concentration and internal nutrient quota was achieved for both the microorganisms, although some variables cannot be reproduced accurately, specifically the outlet concentration of both nitrogen sources (ammonium and nitrate). Although applied to specific species, the preliminary model set up is of general validity, and can be further improved and implemented to simulate and optimize the operating conditions of a microalgal cultivation, once all the species-specific kinetic parameters are known.

Nomenclature

μ_{max}	Maximum specific growth rate (d^{-1})
k_d	Specific decay rate (d^{-1})
c_X	Biomass concentration ($g_x\ m^{-3}$)
q_i	Internal cell quota ($g_i\ g_x^{-1}$)
q_i^{min}	Minimum internal cell quota of nutrient i ($g_i\ g_x^{-1}$)
q_i^{max}	Maximum internal cell quota of nutrient i ($g_i\ g_x^{-1}$)
R_i	Actual reserve of nutrient i ($g_i\ g_x^{-1}$)
I_0	Incident light intensity (µmol photons $m^{-2}\ s^{-1}$)
K_I	Half-saturation constant of the incident light intensity (µmol photons $m^{-2}\ s^{-1}$)
I_{opt}	Optimal irradiance (µmol $m^{-2}\ s^{-1}$)
K_a	Biomass light absorption coefficient ($m^2\ g^{-1}$)
z	Axial coordinate of the photobioreactor depth (m)
W	Photobioreactor depth (m)
c_i	Concentration of nutrient i ($g_i\ m^{-3}$)
ρ_i	Maximum uptake rate of nutrient i ($g_i\ g_x^{-1}\ d^{-1}$)
K_i	Nutrient i half-saturation constant ($g_i\ m^{-3}$)
ϑ	Residence time (d)
c_x^{in}	Inlet biomass concentration ($g_x\ m^{-3}$)
c_x^{out}	Outlet biomass concentration ($g_x\ m^{-3}$)
c_i^{in}	Inlet concentration of nutrient i ($g_i\ m^{-3}$)
c_i^{out}	Outlet concentration of nutrient i ($g_i\ m^{-3}$)
α	Dixon parameter (dim)
β	Dixon parameter (dim)
$K_{N,alg}$	Saturation constant of c_x on nitrogen species ($g_N\ m^{-3}$)
V_{PBR}	Photobioreactor volume (m^3)
Q	Volumetric flowrate ($m^3\ d^{-1}$)

Acronyms

CSTR	Continuous Stirred Tank Reactor
OD_{750}	Optical Density

rcf	relative centrifugal force
DMF	N,N-dimethylformamide
ANOVA	ANalysis Of Variance
SD	Standard Deviation

Literature cited

[1] E.C. Odjadjare, T. Mutanda, A.O. Olaniran, E.C. Odjadjare, T. Mutanda, A.O. Olaniran, Critical Reviews in Biotechnology Potential biotechnological application of microalgae : a critical review, 8551 (2015). https://doi.org/10.3109/07388551.2015.1108956.

[2] M.I. Khan, J.H. Shin, J.D. Kim, The promising future of microalgae: Current status, challenges, and optimization of a sustainable and renewable industry for biofuels, feed, and other products, Microb. Cell Fact. 17 (2018) 1–21. https://doi.org/10.1186/s12934-018-0879-x.

[3] M.P. Caporgno, A. Mathys, Trends in Microalgae Incorporation Into Innovative Food Products With Potential Health Benefits, 5 (2018) 1–10. https://doi.org/10.3389/fnut.2018.00058.

[4] F. Camacho, A. Macedo, Potential Industrial Applications and Commercialization of Microalgae in the Functional Food and Feed Industries : A Short Review, (2019).

[5] L. Brennan, P. Owende, Biofuels from microalgae — A review of technologies for production , processing , and extractions of biofuels and co-products, 14 (2010) 557–577. https://doi.org/10.1016/j.rser.2009.10.009.

[6] M. Musa, G.A. Ayoko, A. Ward, C. Rösch, R.J. Brown, T.J. Rainey, Factors Affecting Microalgae Production for Biofuels and the Potentials of Chemometric Methods in Assessing and Optimizing Productivity, Cells. 8 (2019). https://doi.org/10.3390/cells8080851.

[7] R. Muñoz, B. Guieysse, Algal–bacterial processes for the treatment of hazardous contaminants: A review, Water Res. 40 (2006) 2799–2815. https://doi.org/https://doi.org/10.1016/j.watres.2006.06.011.

[8] H. Chen, Q. Wang, Microalgae-based nitrogen bioremediation, Algal Res. 46 (2020) 101775. https://doi.org/10.1016/j.algal.2019.101775.

[9] F.G.A. Fernández, J. María, F. Sevilla, E.M. Grima, Chapter 21 - Costs analysis of microalgae production, Second Edi, Elsevier B.V., 2019. https://doi.org/10.1016/B978-0-444-64192-2.00021-4.

[10] L. Barsanti, P. Gualtieri, Is exploitation of microalgae economically and energetically sustainable?, Algal Res. 31 (2018) 107–115. https://doi.org/10.1016/j.algal.2018.02.001.

[11] J.U. Grobbelaar, Algal Nutrition – Mineral Nutrition, in: Handb. Microalgal Cult.,

2003: pp. 95–115. https://doi.org/https://doi.org/10.1002/9780470995280.ch6.

[12] G. Markou, D. Vandamme, K. Muylaert, Microalgal and cyanobacterial cultivation: The supply of nutrients, Water Res. 65 (2014) 186–202. https://doi.org/10.1016/j.watres.2014.07.025.

[13] E. Flores, A. Herrero, Nitrogen assimilation and nitrogen control in cyanobacteria., Biochem. Soc. Trans. 33 (2005) 164–167. https://doi.org/10.1042/BST0330164.

[14] O. Perez-garcia, F.M.E. Escalante, E. Luz, Y. Bashan, Heterotrophic cultures of microalgae : Metabolism and potential products, Water Res. 45 (2010) 11–36. https://doi.org/10.1016/j.watres.2010.08.037.

[15] E. Sanz-luque, A. Chamizo-ampudia, A. Llamas, A. Galvan, E. Fernandez, Understanding nitrate assimilation and its regulation in microalgae Overview of Nitrate Assimilation, 6 (2015). https://doi.org/10.3389/fpls.2015.00899.

[16] R.L. Oliver, G.G. Ganf, Freshwater Blooms, in: B.A. Whitton, M. Potts (Eds.), Ecol. Cyanobacteria Their Divers. Time Sp., Springer Netherlands, Dordrecht, 2002: pp. 149–194. https://doi.org/10.1007/0-306-46855-7_6.

[17] N. Powell, A. Shilton, Y. Chisti, S. Pratt, Towards a luxury uptake process via microalgae - Defining the polyphosphate dynamics, Water Res. 43 (2009) 4207–4213. https://doi.org/10.1016/j.watres.2009.06.011.

[18] J. Li, M. Dittrich, Dynamic polyphosphate metabolism in cyanobacteria responding to phosphorus availability, Environ. Microbiol. 21 (2019) 572–583. https://doi.org/https://doi.org/10.1111/1462-2920.14488.

[19] A. Solimeno, J. García, Science of the Total Environment Microalgae-bacteria models evolution : From microalgae steady-state to integrated microalgae-bacteria wastewater treatment models – A comparative review, Sci. Total Environ. 607–608 (2017) 1136–1150. https://doi.org/10.1016/j.scitotenv.2017.07.114.

[20] J. Monod, The growth of bacterial cultures, Annu. Rev. Microbiol. 3 (1949) 371–394. https://doi.org/10.1146/annurev.mi.03.100149.002103.

[21] V. Lemesle, L. Mailleret, A mechanistic investigation of the algae growth “Droop” model., Acta Biotheor. 56 (2008) 87–102. https://doi.org/10.1007/s10441-008-9031-3.

[22] O. Bernard, B.D. Shoener, S.M. Schramm, B. Fabrice, S. Snowling, J. Steyer, C. Martínez, B.G. Pl, J.S. Guest, W. Dorottya, B. Valverde-p, Microalgae and cyanobacteria modeling in water resource recovery facilities : A critical review, 2 (2019). https://doi.org/10.1016/j.wroa.2018.100024.

[23] M.R. Droop, 25 Years of Algal Growth Kinetics A Personal View, XXVI (1983) 99–112.

[24] J.T. Lehman, D.B. Botkin, G.E. Likens, The assumptions and rationales of a computer model of phytoplankton population dynamics1, Limnol. Oceanogr. 20 (1975) 343–364. https://doi.org/https://doi.org/10.4319/lo.1975.20.3.0343.

[25] A.E. Walsby, Cyanobacterial heterocysts: terminal pores proposed as sites of gas exchange, Trends Microbiol. 15 (2007) 340–349. https://doi.org/10.1016/j.tim.2007.06.007.

[26] T. Zavřel, P. Očenášová, J. Červený, Phenotypic characterization of Synechocystis sp. PCC 6803 substrains reveals differences in sensitivity to abiotic stress, PLoS One. 12 (2017) e0189130. https://doi.org/10.1371/journal.pone.0189130.

[27] R. Rippka, J.J.B.W. Deruelles, J.B. Waterbury, M. A. Herdman, R.Y. Stanier, Generic Assignments, Strain Histories and Properties of Pure Cultures of Cyanobacteria, Microbiology-Sgm. 111 (1979) 1–61. https://doi.org/10.1099/00221287-111-1-1.

[28] M. Innamorati, I. Ferrari, D. Marino, M. Ribera D' Alcala, Metodi nell' ecologia del plancton marino. In Nova Thalassia, Edizioni L, 1990.

[29] J.J. Ameel, R.P. Axler, C.J. Owen, Persulfate digestion for determination of total nitrogen and phosphorus in low-nutrient waters, Am. Environ. Lab. 5 (1993) 1–11.

[30] D. A. Bryant, The Molecular Biology of Cyanobacteria in Advances in Photosynthesis book series (AIPH, volume 1), Springer, Dordrecht, 1994. https://doi.org/10.1007/978-94-011-0227-8.

[31] E. Barbera, M. Turetta, E. Sforza, The effect of the internal nutrient quota accumulation on algal-based wastewater treatment : Decoupling HRT and SRT to improve the process, J. Water Process Eng. 49 (2022) 103112. https://doi.org/10.1016/j.jwpe.2022.103112.

[32] O. Bernard, B. Rémond, Validation of a simple model accounting for light and temperature effect on microalgal growth, Bioresour. Technol. 123 (2012) 520–527. https://doi.org/10.1016/j.biortech.2012.07.022.

[33] S.K. Padhi, S. Gokhale, Journal of Environmental Chemical Engineering Biological oxidation of gaseous VOCs – rotating biological contactor a promising and eco-friendly technique, Biochem. Pharmacol. 2 (2014) 2085–2102. https://doi.org/10.1016/j.jece.2014.09.005.

[34] A. Solimeno, L. Parker, T. Lundquist, J. García, Integral microalgae-bacteria model

(BIO _ ALGAE): Application to wastewater high rate algal ponds, Sci. Total Environ. 601–602 (2017) 646–657. https://doi.org/10.1016/j.scitotenv.2017.05.215.

[35] P. Reichert, D. Borchardt, M. Henze, W. Rauch, P. Shanahan, L. Somlyódy, P. Vanrolleghem, River Water Quality Model no. 1 (RWQM1): II. Biochemical process equations , Water Sci. Technol. 43 (2001) 11–30. https://doi.org/10.2166/wst.2001.0241.

[36] S. Pcc, H. Kim, S. Park, B.E. Rittmann, Multi-component kinetics for the growth of the cyanobacterium, 20 (2015) 347–355.

[37] P. Van Alphen, H.A. Najafabadi, F. Branco, K.J. Hellingwerf, Increasing the Photoautotrophic Growth Rate of Synechocystis sp . PCC 6803 by Identifying the Limitations of Its Cultivation, (n.d.). https://doi.org/10.1002/biot.201700764.

[38] T. Zavřel, M.A. Sinetova, D. Búzová, P. Literáková, J. Červený, Characterization of a model cyanobacterium Synechocystis sp. PCC 6803 autotrophic growth in a flat-panel photobioreactor, Eng. Life Sci. 15 (2015) 122–132. https://doi.org/https://doi.org/10.1002/elsc.201300165.

[39] M. Turetta, E. Barbera, G. Trentin, A. Bertucco, E. Sforza, Modeling the production of cyanophycin in Synechocystis sp. PCC 6803 cultivated in chemostat reactors, Bioresour. Technol. Reports. 19 (2022) 101132. https://doi.org/10.1016/j.biteb.2022.101132.

[40] A. Cordara, A. Re, C. Pagliano, P. Van, R. Pirone, G. Saracco, F. Branco, Analysis of the light intensity dependence of the growth of Synechocystis and of the light distribution in a photobioreactor energized by 635 nm light, 6803 (2018) 1–28. https://doi.org/10.7717/peerj.5256.

[41] D.S. Wágner, B. Valverde-Pérez, M. Sæbø, M. Bregua de la Sotilla, J. Van Wagenen, B.F. Smets, B.G. Plósz, Towards a consensus-based biokinetic model for green microalgae - The ASM-A., Water Res. 103 (2016) 485–499. https://doi.org/10.1016/j.watres.2016.07.026.

[42] E. Barbera, E. Sforza, A. Grandi, A. Bertucco, Uncoupling solid and hydraulic retention time in photobioreactors for microalgae mass production : A model-based analysis, Chem. Eng. Sci. 218 (2020) 115578. https://doi.org/10.1016/j.ces.2020.115578.

[43] M. Pastore, E. Barbera, A. Panichi, E. Sforza, Application of photorespirometry to unravel algal kinetic parameters of nitrogen consumption in complex media, Algal Res. 47 (2020) 101837. https://doi.org/10.1016/j.algal.2020.101837.

[44] C.E. de Farias Silva, E. Sforza, Carbohydrate productivity in continuous reactor under nitrogen limitation: Effect of light and residence time on nutrient uptake in Chlorella vulgaris, Process Biochem. 51 (2016) 2112–2118. https://doi.org/https://doi.org/10.1016/j.procbio.2016.09.015.

[45] M. Kobayashi, N. Takatani, M. Tanigawa, T. Omata, Posttranslational regulation of nitrate assimilation in the cyanobacterium Synechocystis sp. strain PCC 6803., J. Bacteriol. 187 (2005) 498–506. https://doi.org/10.1128/JB.187.2.498-506.2005.

[46] V. da Silva Ferreira, C. Sant'Anna, Impact of culture conditions on the chlorophyll content of microalgae for biotechnological applications, World J. Microbiol. Biotechnol. 33 (2016) 20. https://doi.org/10.1007/s11274-016-2181-6.

[47] W. Kim, J.M. Park, G.H. Gim, S.-H. Jeong, C.M. Kang, D.-J. Kim, S.W. Kim, Optimization of culture conditions and comparison of biomass productivity of three green algae, Bioprocess Biosyst. Eng. 35 (2012) 19–27. https://doi.org/10.1007/s00449-011-0612-1.

[48] M. Arumugam, A. Agarwal, M.C. Arya, Z. Ahmed, Influence of nitrogen sources on biomass productivity of microalgae Scenedesmus bijugatus, Bioresour. Technol. 131 (2013) 246–249. https://doi.org/https://doi.org/10.1016/j.biortech.2012.12.159.

[49] D.-H. Cho, R. Ramanan, J. Heo, D.-S. Shin, H.-M. Oh, H.-S. Kim, Influence of limiting factors on biomass and lipid productivities of axenic Chlorella vulgaris in photobioreactor under chemostat cultivation, Bioresour. Technol. 211 (2016) 367–373. https://doi.org/https://doi.org/10.1016/j.biortech.2016.03.109.

[50] E. Sforza, M. Pastore, E. Barbera, A. Bertucco, Respirometry as a tool to quantify kinetic parameters of microalgal mixotrophic growth, 2019. https://doi.org/10.1007/s00449-019-02087-9.

[51] R. Carpine, F. Raganati, G. Olivieri, K.J. Hellingwerf, A. Pollio, P. Salatino, A. Marzocchella, Poly- β -hydroxybutyrate (PHB) production by Synechocystis PCC6803 from CO 2 : Model development, Algal Res. 29 (2018) 49–60. https://doi.org/10.1016/j.algal.2017.11.011.

[52] F. Fernandes, A. Silkina, J.I. Gayo-Peláez, R.V. Kapoore, D. de la Broise, C.A. Llewellyn, Microalgae Cultivation on Nutrient Rich Digestate: The Importance of Strain and Digestate Tailoring under PH Control, Appl. Sci. 12 (2022). https://doi.org/10.3390/app12115429.

Appendix

Table 7A.1. Experimental condition of experiments with *Synechocystis* sp. PCC 6803 using ammonium as only nitrogen source

τ (d)	z (m)	I_0 (µmol photons m^{-2} s^{-1})	c_{NH4}^{in} (mg_N L^{-1})
0.95	3.5	150	19.3±0.5
0.95	3.5	150	33.8±1.2
0.85	3.5	150	69.5±0.5
0.85	3	150	59.4±0.7

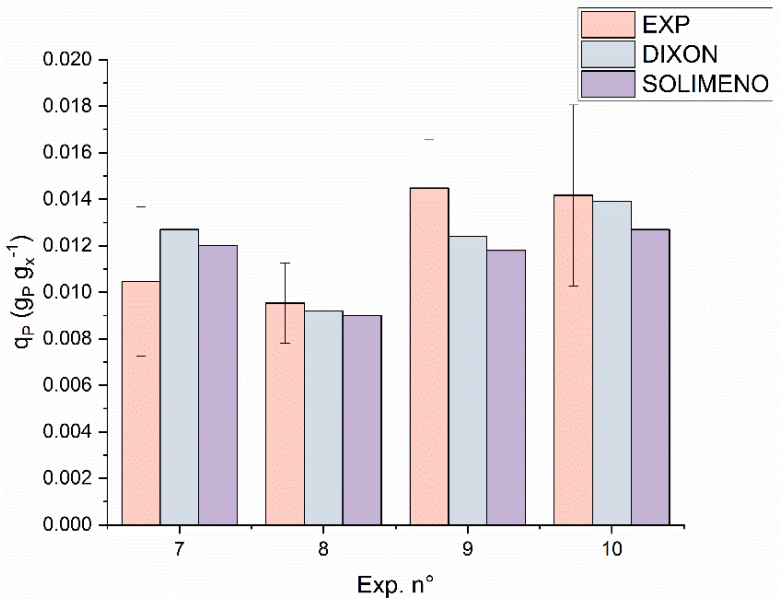

Figure 7A.1. Comparison between the experimental and the simulated values for internal phosphorus quota (q_P) for continuous experiments of *Chlorella protothecoides* in complex media

7A.1 Matlab® code for Synechocystis sp. PCC 6803: Droop model modified with Dixon model

```
clc
clear all
close all
mumax=3.3;
kd=0.2;
Ki=100;
Iopt=350;
ka=0.1866;
KNO3=26.1;
KNH4=27.78;
rhoNO3=1.86;
rhoNH4=0.8;
q_minN=0.014;
q_maxN=0.18;
alpha=20;
beta=0.001;
theta=0.85;
I0=150;
L=3;
z=0:0.05:L;
CqIN=[0 60 0 0 ];
C0=[CqIN(1) CqIN(2) 200 0.01];
```

```
[t,Cq]=ode23(@BM,[0
50],C0,[],I0,mumax,ka,KNO3,KNH4,z,Ki,Iopt,kd,L,theta,CqIN,q_minN,rhoNO3,rhoNH4,q_maxN,alph
a,beta);
function [balances]
=BM(t,Cq,I0,mumax,ka,KNO3,KNH4,z,Ki,Iopt,kd,L,theta,CqIN,q_minN,rhoNO3,rhoNH4,q_maxN,alpha
,beta);
Iz = I0*exp(-ka*Cq(3)*z/100);
rx_z = Cq(3)*mumax*(Cq(4)/(Cq(4)+q_minN))*(Iz./(Iz+Ki.*(Iz./Iopt-1).^2))-kd*Cq(3); %
rx_av = trapz(z,rx_z)/L;
BMx = CqIN(3)-Cq(3)+ rx_av*theta;
uNO3=rhoNO3*(Cq(1)/(KNO3+Cq(1)+alpha*Cq(2)))*(1-((Cq(4)+q_minN)/q_maxN));
rNO3=-uNO3*Cq(3) ;
BMNO3=CqIN(1)-Cq(1)+rNO3*theta;
uNH4=rhoNH4*(Cq(2)/(KNH4+Cq(2)+beta*Cq(1)))*(1-((Cq(4)+q_minN)/q_maxN));
rNH4=-uNH4*Cq(3) ;
BMNH4=CqIN(2)-Cq(2)+rNH4*theta;
uq=mumax*(Cq(4)/(Cq(4)+q_minN))*(Iz./(Iz+Ki.*(Iz./Iopt-1).^2))-kd;
uq_av=trapz(z,uq)/L;
BMqN=(uNO3+uNH4)- uq_av*(Cq(4)+q_minN);
balances=[BMNO3;BMNH4;BMx;BMqN];
end
```

7A.2 Matlab® code for Synechocystis sp. PCC 6803: Droop model modified with Solimeno model

```
clc
clear all
close all
mumax=3.3;
kd=0.2;
Ki=100;
Iopt=350;
ka=0.1866;
KNalg=0.1;
rhoNO3=1.86;
rhoNH4=0.8;
q_minN=0.014;
q_maxN=0.18;
q_maxP=0.10;
I0=150;
L=3.5;
z=0:0.05:L;
CqIN=[80 0 0 0 ];
C0=[CqIN(1) CqIN(2) 200 0.01];
theta=1.1;
[t,Cq]=ode23(@BM,[0
50],C0,[],I0,mumax,ka,KNalg,z,Ki,Iopt,kd,L,theta,CqIN,q_minN,rhoNO3,rhoNH4,q_maxN);
function [balances]
=BM(t,Cq,I0,mumax,ka,KNalg,z,Ki,Iopt,kd,L,theta,CqIN,q_minN,rhoNO3,rhoNH4,q_maxN);
Iz = I0*exp(-ka*Cq(3)*z/100);
rx_z = Cq(3)*mumax*(Cq(4)/(Cq(4)+q_minN))*(Iz./(Iz+Ki.*(Iz./Iopt-1).^2))-kd*Cq(3);
rx_av = trapz(z,rx_z)/L;
BMx = CqIN(3)-Cq(3)+ rx_av*theta;
uNO3=rhoNO3*(Cq(1)/(KNalg+Cq(1)))*(KNalg/(KNalg+Cq(2)))*(1-((Cq(4)+q_minN)/q_maxN));
rNO3=-uNO3*Cq(3) ;
BMNO3=CqIN(1)-Cq(1)+rNO3*theta;
uNH4=rhoNH4*(Cq(2)/(KNalg+Cq(2)))*(1-((Cq(4)+q_minN)/q_maxN));
rNH4=-uNH4*Cq(3) ;
BMNH4=CqIN(2)-Cq(2)+rNH4*theta;
uq=mumax*(Cq(4)/(Cq(4)+q_minN))*(Iz./(Iz+Ki.*(Iz./Iopt-1).^2))-kd;
uq_av=trapz(z,uq)/L;
BMqN=(uNO3+uNH4)- uq_av*(Cq(4)+q_minN);
balances=[BMNO3;BMNH4;BMx;BMqN];
end
```

7A.3 Matlab® code for Chlorella protothecoides: Droop model modified with Dixon model

```
clc
clear all
close all
mumax=4.5;
```

```
kd=0.2;
Ki=73.4;
Iopt=413;
ka=0.09;
KNO3=14.58;
KNH4=14.23;
KP=1.86;
rhoNO3=0.60;
rhoNH4=0.62;
rhoP=0.036;
q_minN=0.045;
q_minP=0.0006;
q_maxN=0.20;
q_maxP=0.10;
alpha=0.056;
beta=17.7;
phiT=1;
I0=150;
L=6.5;
z=0:0.05:L;
CqIN=[250 0 44 0 0 0];
C0=[CqIN(1) CqIN(2) CqIN(3) 200 0.01 0.0001];
theta=1.4;
[t,Cq]=ode23(@BM,[0
50],C0,[],I0,mumax,ka,KNO3,KNH4,KP,z,Ki,Iopt,kd,L,theta,CqIN,phiT,q_minN,q_minP,rhoNO3,rho
NH4,rhoP,q_maxN,q_maxP,alpha,beta);
function [balances]
=BM(t,Cq,I0,mumax,ka,KNO3,KNH4,KP,z,Ki,Iopt,kd,L,theta,CqIN,phiT,q_minN,q_minP,rhoNH4,rhoN
O3,rhoP,q_maxN,q_maxP,alpha,beta);
Iz = I0*exp(-ka*Cq(4)*z/100);
rx_z =
Cq(4)*mumax*phiT*(Cq(5)/(Cq(5)+q_minN))*(Cq(6)/(Cq(6)+q_minP))*(Iz./(Iz+Ki.*(Iz./Iopt-
1).^2))-kd*Cq(4);
rx_av = trapz(z,rx_z)/L;
BMx = CqIN(4)-Cq(4)+ rx_av*theta;
uNO3=rhoNO3*(Cq(1)/(KNO3+Cq(1)+alpha*Cq(2)))*(1-((Cq(5)+q_minN)/q_maxN));
rNO3=-uNO3*Cq(4) ;
BMNO3=CqIN(1)-Cq(1)+rNO3*theta;
uNH4=rhoNH4*(Cq(2)/(KNH4+Cq(2)+beta*Cq(1)))*(1-((Cq(5)+q_minN)/q_maxN));
rNH4=-uNH4*Cq(4) ;
BMNH4=CqIN(2)-Cq(2)+rNH4*theta;
uP=rhoP*(Cq(3)/(KP+Cq(3)))*(1-((Cq(6)+q_minP)/q_maxP));
rP=-uP*Cq(4);
BMP=CqIN(3)-Cq(3)+rP*theta;
uq=mumax*phiT*(Cq(5)/(Cq(5)+q_minN))*(Cq(6)/(Cq(6)+q_minP))*(Iz./(Iz+Ki.*(Iz./Iopt-
1).^2))-kd;
uq_av=trapz(z,uq)/L;
BMqN=(uNO3+uNH4)- uq_av*(Cq(5)+q_minN);
BMqP=uP - uq_av*(Cq(6)+ q_minP);
balances=[BMNO3;BMNH4;BMP;BMx;BMqN;BMqP];
end
```

7A.4 Matlab® code for Chlorella protothecoides: Droop model modified with Solimeno model

```
clc
clear all
close all
mumax=3.3;
kd=0.2;
Ki=100;
Iopt=350;
ka=0.1866;
KNalg=0.1;
rhoNO3=1.86;
rhoNH4=0.8;
q_minN=0.014;
q_maxN=0.18;
q_maxP=0.10;
I0=150;
L=3.5;
z=0:0.05:L;
CqIN=[80 0 0 0 ];
C0=[CqIN(1) CqIN(2) 200 0.01];
```

```
theta=1.1;
[t,Cq]=ode23(@BM,[0
50],C0,[],I0,mumax,ka,KNalg,z,Ki,Iopt,kd,L,theta,CqIN,q_minN,rhoNO3,rhoNH4,q_maxN);
function [balances]
=BM(t,Cq,I0,mumax,ka,KNalg,z,Ki,Iopt,kd,L,theta,CqIN,q_minN,rhoNO3,rhoNH4,q_maxN);
Iz = I0*exp(-ka*Cq(3)*z/100);
rx_z = Cq(3)*mumax*(Cq(4)/(Cq(4)+q_minN))*(Iz./(Iz+Ki.*(Iz./Iopt-1).^2))-kd*Cq(3); %
rx_av = trapz(z,rx_z)/L;
BMx = CqIN(3)-Cq(3)+ rx_av*theta;
uNO3=rhoNO3*(Cq(1)/(KNalg+Cq(1)))*(KNalg/(KNalg+Cq(2)))*(1-((Cq(4)+q_minN)/q_maxN));
rNO3=-uNO3*Cq(3) ;
BMNO3=CqIN(1)-Cq(1)+rNO3*theta;
uNH4=rhoNH4*(Cq(2)/(KNalg+Cq(2)))*(1-((Cq(4)+q_minN)/q_maxN));
rNH4=-uNH4*Cq(3) ;
BMNH4=CqIN(2)-Cq(2)+rNH4*theta;
uq=mumax*(Cq(4)/(Cq(4)+q_minN))*(Iz./(Iz+Ki.*(Iz./Iopt-1).^2))-kd;
uq_av=trapz(z,uq)/L;
BMqN=(uNO3+uNH4)- uq_av*(Cq(4)+q_minN);
balances=[BMNO3;BMNH4;BMx;BMqN];
end
```

Chapter 8

Role of oxygen in tubular photobioreactors: model-based design and operating conditions to minimize productivity losses

Tubular photobioreactors (PBRs) guarantee high microalgal productivities but suffer from oxygen accumulation. It is known that the tube length must be limited to prevent build-up of high oxygen levels, but the combined effect of other variables (light intensity and biomass concentration) was not fully addressed. In this Chapter, a mathematical model is developed to understand the influence of oxygen on biomass productivity in a continuous tubular PBR. Material balances are applied to investigate the behavior of a single tube reactor and of a complete process flowsheet of a commercial plant. Biomass concentration at the inlet resulted the key variable to minimize oxygen inhibition, confirming the solid retention time (SRT) as the main operating variable. However, an optimized length of the tube can minimize the effect of biomass concentration. Finally, it was observed that measuring the O_2 concentration alone is not a reliable index of the overall productivity in a PBR.

Part of this Chapter was published as a scientific paper in *Chemical Engineering and Processing: Process Intensification* (Trentin, G., Barbera, E., Bertucco, A., Sforza, E., 2020, https://doi.org/10.1016/j.cep.2020.108151)

8.1 Introduction

In a world where population is fast growing, future generations will face with severe challenges linked to mass and energy resources availability and compliance with environmental issues. Thus, the key is to develop new biorefining technologies to sustainably transform renewable natural resources into bio-based products, materials and fuels. Photosynthetic microorganisms boost a number of attractive features to this scope [1], and are currently and deeply exploited for food and feed, but also to extract bio-active compounds for nutraceuticals, high-value pharmaceuticals, cosmeceuticals and biomedical applications [2–5]. The commercial exploitation of photosynthetic microorganisms is closely linked to the need of implementing reliable, efficient, and economic industrial processes, able to guarantee high throughput as well as constant product quality. Compared to open systems, closed photobioreactors (PBRs) are certainly more expensive to build but ensure better control of crucial operating variables. They have higher productivity, higher photosynthetic efficiencies, and reduced contamination risks compared to open systems, and allow the production of high value algal products [6–8]. In this context, continuous production plants are the most suitable way to obtain high value biomass production, mainly due to the higher and stable productivity achievable in these systems compared to batch ones [9,10]. Several types of closed PBRs are available, such as tubular, column and flat plate ones.

Tubular PBRs are most suitable configurations for outdoor mass cultivation thanks to their higher surface-to-volume ratio. Tubes can be arranged in different patterns and orientations in order to maximize the photosynthetic efficiency, and the culture is circulated by pumps or by airlift systems [11]. However, a number of issues have to be considered when using tubular PBRs for biomass cultivation [12]. For instance, temperature variations, photolimitation, O_2 accumulation and CO_2 depletion are important phenomena that have to be taken into account when designing this type of reactors. In particular, the accumulation of dissolved oxygen represents one of the major obstacles to algae growth in closed tubular photobioreactors. It is known that a high dissolved oxygen concentration inhibits microalgal growth, and that the extent of this inhibition is species specific [13–19]. Oxygen inhibitory concentration values can easily occur in a tube without gas exchange [13]. In fact, long tubular PBRs suffer of mass transfer issues, and considerable spatial gradients of O_2 and CO_2 concentrations along the axis may occur [11,20]. To prevent build-up of high oxygen levels, several authors stated that the tube length must be limited [20–24]. Torzillo

and Chini Zittelli [20] and Vonshak [24] have calculated the maximum admissible tube length for a given culture velocity, which allows to maintain the level of oxygen below the inhibition threshold for the culture, thanks to the relation proposed by Pirt et al. [22], where the oxygen production is directly proportional to the biomass growth. Acién Fernández et al. [23] proposed another relation to calculate the maximum length of the tubes. According to the authors, this length is limited by a combination of the acceptable upper limit of dissolved oxygen concentration (i.e. the one that does not inhibit photosynthesis), the liquid velocity through the tube, and the rate of photosynthesis. In both of these models, however, the oxygen concentration is related only to biomass productivity. Generally, most of the papers assessing the effect of high oxygen level on biomass productivity partially neglect the combined effect of other variables, such as light intensity and biomass concentration. In a recently published paper, Sforza et al. [25] proposed a new mathematical model able to describe oxygen effect on growth, including the effect of sub-saturating oxygen concentration on basal respiration, the effect of oxygen to carbon ratio, and the effect of inhibition at supersaturated oxygen concentration. Thus, for tubular photobioreactors, a mutual influence exists among oxygen concentration and the other variables, i.e. light intensity, reactor geometry, and biomass concentration, which should be properly accounted for. With a comprehensive model for oxygen, the design and operation of a tubular photobioreactor may ensure maximum biomass productivity. Specifically, the choice of the diameter and the length of the tubes is not only related to the surface-to-volume ratio, to land requirement and to power consumption, but also to light uptake by the culture and to the temperature profile. In the same way, these factors affect, but also are affected, by the biomass and oxygen concentrations inside the tubes and are strongly interrelated one with each other.

From a process perspective, in a previous work by Barbera et al. [26], it has been demonstrated that models are a powerful tool to optimize the performances of photobioreactors. By simulating microalgal growth including both photolimitation and photoinhibition in a continuous stirred-tank photobioreactor (CSTR), it was shown that the hydraulic retention time (HRT) does not affect the biomass productivity, while the key variable is the solid retention time (SRT). Accordingly, it was suggested that a continuous system working with SRT lower than HRT allows keeping the biomass concentration at the optimum value, which depends on the light attenuation profile, and that the biomass productivity can be maximized together with a strong reduction in water and nutrient consumptions.

On the other hand, to properly account for the effect of oxygen on biomass production, in tubular PBRs, the kinetics must be also described as a function of dissolved oxygen and carbon dioxide concentrations as well. In this Chapter, the mathematical model proposed by Sforza et al. [25] is applied to understand the influence of oxygen concentration on the biomass productivity in a tubular PBR operated in continuous mode for the cultivation of *C. protothecoides*, by implementing the oxygen kinetics model according to Barbera et al. [26]. The mathematical model developed is used to investigate first the behaviour of a single tube reactor, and then to analyse a complete process flowsheet including all the main units involved in a commercial production plant. Sensitivity analyses are carried out to investigate the effect of the main process variables, such as tube length, incident light intensity, and SRT, with the aim of identifying the optimal configuration and the operating conditions that allow to minimize the loss of productivity due to oxygen inhibition.

8.2 Materials and methods

8.2.1 Mass balances and kinetic model

The model of a tubular PBR is the one of a Plug Flow Reactor (PFR):

$$\frac{dc_i}{dz} = \frac{Y_{i/x} \cdot R_x}{u} \tag{8.1}$$

where z is the axial coordinate, c_i is the concentration of the species i, u is the convective velocity inside the reactor (m s^{-1}) and $Y_{i/x}$ are the mass yields of the species i, with respect to the biomass x (g_i g_x^{-1}). These are calculated based on the autotrophic stoichiometric equation of photosynthesis proposed by Sforza et al. [27]. In Eq. (8.1), R_x is the net biomass growth rate (g_X m^{-3} d^{-1}) and is expressed as a function of light intensity, temperature, oxygen and carbon dioxide concentrations, while other nutrients, such as N and P, are assumed to be provided in excess. According to these assumptions we have:

$$R_x = \mu_{max} \cdot \phi(T) \cdot \frac{I_{avg}}{I_{avg} + K_I \cdot \left(\frac{I_{avg}}{I_{opt}} - 1\right)^2} \frac{c_{CO2}}{c_{CO2} + K_C\left(1 + \frac{c_{O2}}{K_{ph}}\right)} \cdot c_x - k_{resp} \cdot \frac{c_{O2}}{K_{O2} + c_{O2}} \cdot c_x - k_{inh} \cdot e^{n \cdot c_{O2}} \cdot c_x \tag{8.2}$$

where μ_{max} is the maximum specific growth rate of the microorganism (d^{-1}), c_x, c_{CO2} and c_{O2} are respectively the biomass, carbon dioxide and oxygen concentrations (g m^{-3}); k_{resp} is the maximum oxygen respiration rate (d^{-1}), K_{O2} is the oxygen half-saturation constant for respiration (g m^{-3}), K_C is the half-saturation constant for CO_2 (g m^{-3}), K_{ph} is the photorespiration constant (g m^{-3}), k_{inh} is the oxygen inhibition rate (d^{-1}) and n is the oxygen inhibition exponent (m^3 g^{-1}) as proposed by Sforza et al. [25]. K_I and I_{opt} are respectively

the light half-saturation constant and the irradiance at which the growth rate is maximum (μmol m^{-2} s^{-1}) according to the model proposed by Bernard and Rémond [28]. To consider the light extinction profile along the reactor depth in a cylindrical system illuminated by unidirectional parallel flux, the light function is expressed in terms of average light intensity (I_{avg}), as proposed by Molina-Grima et al. [29]:

$$I_{avg} = \frac{2 \cdot I_0}{r \cdot K_a \cdot c_x \cdot \pi} \cdot \left(1 - \int_0^{\pi/2} cos(\varphi) \cdot e^{[-2 \cdot r \cdot K_a \cdot c_x \cdot cos(\varphi)]} \, d\varphi\right) \tag{8.3}$$

where I_0 is the incident light intensity (μmol m^{-2} s^{-1}), K_a is the biomass light absorption coefficient (m^2 g^{-1}) and r is the radius of the pipe (m). The effect of temperature is described by the term $\phi(T)$, according to the model proposed by Bernard and Rémond [28], based on the Cardinal Temperature Model with Inflexion previously presented by Rosso et al. [30]:

$$\phi(T) = \frac{(T - T_{max}) \cdot (T - T_{min})^2}{(T_{opt} - T_{min}) \cdot [(T_{opt} - T_{min}) \cdot (T - T_{opt}) - (T_{opt} - T_{max}) \cdot (T_{opt} + T_{min} - 2T)]} \tag{8.4}$$

In Eq. (8.4) T_{max} and T_{min} (°C) represents the temperatures above and below which the growth rate is approximated zero respectively and T_{opt} (°C) is the temperature at which it has a maximum.

Therefore, knowing the inlet concentration of the species i (c_i^E), it is possible to integrate and solve Eq. (8.1) to find the outlet concentrations (c_i^U) as well as the profile of concentrations and of the reaction rate along the axial coordinate z. Mass balances were solved using MATLAB® software.

The microalgal species of reference for this study is *Chlorella protothecoides*, a widely studied organism, and its kinetic parameters were experimentally determined via respirometric assays in our laboratory, as described by Barbera et al. [26], Sforza et al. [31]and Sforza et al. [25]. In particular, the values of k_{resp} and k_{inh} used in this work, were calculated starting from those identified by Sforza et al. [25], where they were expressed in terms of oxygen. For this reason, the parameters were recalculated based on the mass oxygen-biomass yield ($Y_{O2/x}$). All the values of the parameters used in the simulations are summarized in Table 8.1. A constant operating temperature was assumed equal to 24°C, and the reactor is made of tubes with a constant diameter (d) of 0.1 m. The velocity inside the tubes is kept equal to 0.26 m s^{-1}, in agreement with the values suggested by Uggetti et al. [32] in similar systems. We notice that, while our study is based on a specific species, if the kinetic parameters and the geometric characteristics of the reactor are known or can be measured, it is easily extendable to other microalgal production plants.

Table 8.1. Value of the parameters used in the simulation

Parameters	M.U.	Value	Reference
μ_{max}	d^{-1}	1.9	[31]
K_I	μmol m^{-2} s^{-1}	73.4	[26]
I_{opt}	μmol m^{-2} s^{-1}	413	[26]
K_a	m^2 g^{-1}	0.09	[26]
T_{max}	°C	39.07	[26]
T_{min}	°C	10.21	[26]
T_{opt}	°C	30.24	[26]
K_C	g m^{-3}	0.005	[25]
K_{O2}	g m^{-3}	0.2	[25]
K_{ph}	g m^{-3}	0.16	[25]
k_{resp}	d^{-1}	0.29	[25]
k_{inh}	d^{-1}	0.0024	[25]
n	m^3 g	0.2232	[25]
$Y_{x/x}$	dim	1	Calculated from [27]
$Y_{O2/x}$	g_{O2} g_x^{-1}	1.7033	Calculated from [27]
$Y_{CO2/x}$	g_{CO2} g_x^{-1}	-2	Calculated from [27]

8.2.2 Process Flow Diagram for the cultivation of C. protothecoides in tubular photobioreactors

The process flowsheet proposed for a commercial microalgae production plant is reported in Figure 8.1.

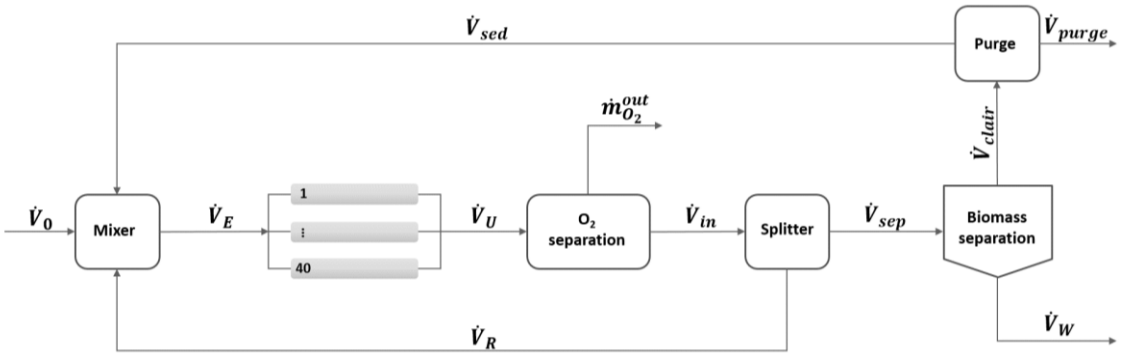

Figure 8.1. Process Flow Diagram for the cultivation of *C. protothecoides* in tubular photobioreactors

The reactor considered is made of 40 parallel tubes, 250 m long, with an internal diameter of 0.1 m, leading to a total irradiated surface equal to 1000 m^2. The tubes length was determined according to the results reported in the following section 8.3.1. In the base case, the incident light intensity (I_0) was taken equal to 1000 μmol m^{-2} s^{-1}. The total volumetric flowrate processed in the reactor ($\dot{V}_E$=$\dot{V}_U$=$\dot{V}$) is equal to 7180.8 m^3 d^{-1}, which is split evenly in the 40 tubes, to maintain a velocity inside them equal to 0.26 m s^{-1}. The biomass leaving the photobioreactor enters a degassing section, with the aim to remove all the produced

oxygen, in such a way to have an oxygen concentration equal to the saturation one in all the units downstream. Then, the biomass is split into two streams. The first one ($\dot{V}_R$) is recycled back to guarantee a constant biomass concentration in the inlet stream to the tubular reactors ($\dot{V}_E$). The other one ($\dot{V}_{sep}$) enters a biomass separation section, where water and nutrients are removed, and the biomass is concentrated. As found by Fasaei et al. [33], an efficient separation system is supposed to be used, able to obtain a highly concentrated stream ($\dot{V}_W$), with a biomass concentration equal to 300 kg m^{-3}. Water and nutrients ($\dot{V}_{clair}$), instead, are recycled back to the reactor, after purging a fraction of the stream. It is assumed that no biomass is lost in this effluent, i.e. an ideal solid separation efficiency of 100% is considered. The purge unit is needed as, while it is desirable to recycle water and nutrients as much as possible to reduce costs, it is also essential to avoid the accumulation of possible metabolites or other compounds that, in the long term, can inhibit the biomass growth. Hence, while this stream ($\dot{V}_{purge}$) is purged, the rest is recirculated back to the top of the plant ($\dot{V}_{sed}$). Here, a make-up stream ($\dot{V}_0$) is needed to restore nutrients, so that their concentration at the reactor inlet is constant. It is assumed that the oxygen concentration (c_{O2}^E) is the one at the saturation value, while the carbon dioxide concentration (c_{CO2}^E) corresponds to nearly equilibrium conditions when bubbling the suspension with pure CO_2. All the values of the variables used in the simulation are summarized in Table 8.2.

Table 8.2. Value of the variables of the production process of *C. protothecoides*

Variables	Symbol	M.U.	Value
Tube length	z	m	250
Number of tubes	-	dim	40
Tubes diameter	d	m	0.1
Total volume of reactor	V_R	m^3	78.54
Irradiated surface of the reactor	S_t	m^2	1000
Velocity inside tubes	u	m s^{-1}	0.26
Total volumetric flow rate	$\dot{V} = \dot{V}_E = \dot{V}_U$	m^3 d^{-1}	7180.8
Incident light intensity	I_0	µmol m^{-2} s^{-1}	1000
Biomass concentration at the reactor inlet	c_x^E	g m^{-3}	500
Oxygen concentration at the reactor inlet	c_{O2}^E	g m^{-3}	8.4
Carbon dioxide concentration at the reactor inlet	c_{CO2}^E	g m^{-3}	1400
Solid separation efficiency	-	%	100
Purge fraction	-	dim	0.03

Mass balances in the reactor section are the ones of Eq. (8.1), while in all the other units of the plant the general mass conservation balance is applied, considering that there is neither accumulation nor production. Mass balances are solved for all the species considered in

this work (biomass, CO_2 and O_2). Because part of the biomass is recirculated back to the plant, it is possible to decouple the retention time of solids (SRT) from the hydraulic retention time (HRT), as recently proposed by Barbera et al. [26]. Accordingly, we have:

$$HRT = \frac{V_R}{\dot{V}_0} \tag{8.5}$$

$$SRT = \frac{V_R \cdot \frac{1}{z}\int_0^z c_x(z)dz}{\dot{m}_x^W} \tag{8.6}$$

In Eq. (8.5) the HRT is defined as the ratio between the volume of the reactor (V_R) and the inlet volumetric flow rate ($\dot{V}_0$), instead the SRT is defined as the ratio between the total amount of biomass retained in the reactor and the biomass flowrate produced and extracted from the plant ($\dot{m}_x^W$).

8.3 Results and discussion

8.3.1 Results of oxygen inhibition in the photobioreactor

First, the effect of the tube length and of the value of inlet biomass concentration is considered, solving the mass balances of Eq. (8.1), to obtain the profiles inside a single tube. To evaluate the performances of the reactor it is interesting to calculate the ratio between the reaction rate along the axial coordinate *z*, *R(z)*, and the reaction rate at the inlet of the reactor, R_0. In fact, at the inlet, the reaction rate is maximum (the limiting variable is light intensity only), because the oxygen concentration is at saturation value, so that no inhibiting effect due to oxygen accumulation occur. Figure 8.2 shows the profiles of the ratio R/R_0. In particular, the results for two values of inlet biomass concentration are shown, respectively 500 g m^{-3} (Figure 8.2A) and 1000 g m^{-3} (Figure 8.2B) and, for each one, the profiles are plotted at three incident light intensities, 1000, 400 and 150 μmol m^{-2} s^{-1}.

As expected, reasonably, in all the cases the reaction rate decreases along the reactor. As the biomass concentration is not sufficiently changing to produce a self-shading effect along *z*, the reduction of the growth rate is due to the increased oxygen concentration (Figure 8A.1 of Appendix) resulting in a remarkable inhibition of growth. In Figure 8.3 an example of the different contributions to reaction rate is shown, demonstrating that the total reaction rate reflects the trend of the inhibition rate. In fact, the photosynthetic and the respiration contribution to the reaction rate are almost constant along the reactor: according to Eq. (8.2), both the light and the photorespiration factors of the photosynthetic term do not vary significantly due to an almost constant biomass concentration and the large excess

of CO_2 in the medium. Regarding the respiration rate, the value of the half-saturation constant for oxygen limitation (0.2 g m^{-3}, Table 8.2) is such that, at oxygen levels higher than the air saturation, this term is always almost equal to 1. On the other hand, the inhibition term increases along the reactor, until the total reaction rate results equal to zero. In that case the negative contributions of the respiration rate and of the inhibition rate equal the positive term of the reaction rate in Eq. (8.2), meaning that no net biomass production occurs inside the reactor.

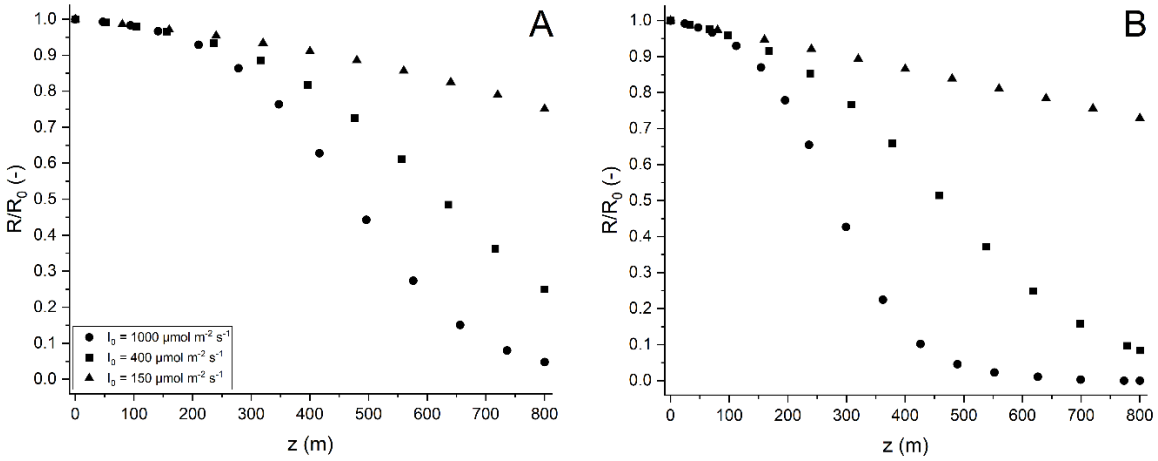

Figure 8.2. Reaction rate normalized on that one at the inlet of the reactor (R/R_0), calculated at different tubes length (z), with an inlet biomass concentration equal to 500 g m^{-3} (panel A) and 1000 g m^{-3} (panel B), parametric at different incident light intensity (I_0) (*circles* for 1000 µmol m^{-2} s^{-1}, *squares* for 400 µmol m^{-2} s^{-1} and *triangles* for 150 µmol m^{-2} s^{-1})

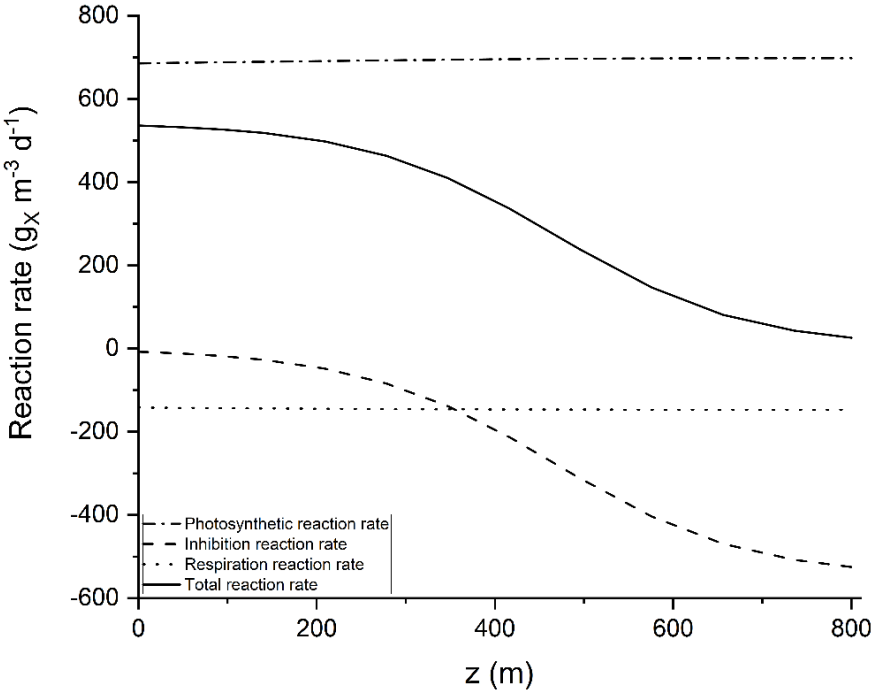

Figure 8.3. Reaction rate with different contributions separately showed: photosynthesis, basal respiration and inhibition due to oxygen, as specified in Eq. 8.2

Previously, Camacho Rubio et al. [15] observed that a great portion of the tubes length was unproductive due to oxygen inhibition. Indeed, it was noted that an inhibition due to oxygen toxicity can occur after only one minute in a tube without gas exchange [13]. The accumulation of oxygen is a relevant problem for closed reactors, especially in case of small diameter tubular PBRs. At maximal rates of photosynthesis, a tubular reactor of 1 cm of diameter may accumulate 8-10 mg_{O2} L^{-1} min^{-1}, that would result in oxygen concentration reaching 100 mg L^{-1} [8]. In the case of *Arthrospira* cultures, Torzillo and Chini Zittelli [20] found that oxygen concentration can rise at a rate of 2-3 mg_{O2} L^{-1} min^{-1}, resulting in oxygen build-up inside tubes up to 70-80 mg L^{-1}.

Moreover, the authors found that the correlated reduction in productivity is greater if a suboptimal temperature is used. It is also interesting that, as reported in Figure 8.2, a different slope is predicted depending on the intensity of incident light and on the concentration of biomass entering the reactor. When this gets higher, the reaction rate drops much more rapidly along the tube, and reaches zero at a length of 800 m. It is noteworthy that the biomass concentration at the entrance of the reactor is a crucial variable. For example, at 250 m length, with a concentration of 500 g m^{-3} the reaction rate is always higher than 80% with respect to the initial one, while in the case of a biomass concentration of 1000 g m^{-3} inside the tubes, the reaction rate drops to almost 60%. Obviously, it is possible to represent the effect of different light intensities for each concentration of biomass inside the reactor, thus creating surfaces that describe the trend of the ratio R/R_0 with respect to light intensity, at different lengths of the photobioreactor (Figure 8A.2 of Appendix).

The biomass productivity is strictly dependent on the average irradiance in the reactor. Indeed, scattering and absorption phenomena due to the algal particles affect light penetration. It means that an optimum cells concentration value should be maintained to achieve higher photosynthetic rate [12]. So, it would be desirable for a correct design and operation of a plant, to develop a unique criterion that allows to identify the right concentration of biomass to be kept at the PBR inlet, depending on the incident light intensity and on the length of the tubes. To this scope, it is proposed to use the reduction in the reaction rate inside the tube. For example, accepting a maximum reduction of the reaction rate equal to 87%, a surface like the one shown in Figure 8.4 can be obtained. This surface identifies the length of the tube to be used, according to different light intensities and different inlet biomass concentrations to ensure such a performance. In this case, an almost planar surface is observed, with the length of tube ranging between 300 m and 200

m. A longer length is needed in case of lower light intensity, because in that case the culture may experience photolimitation.

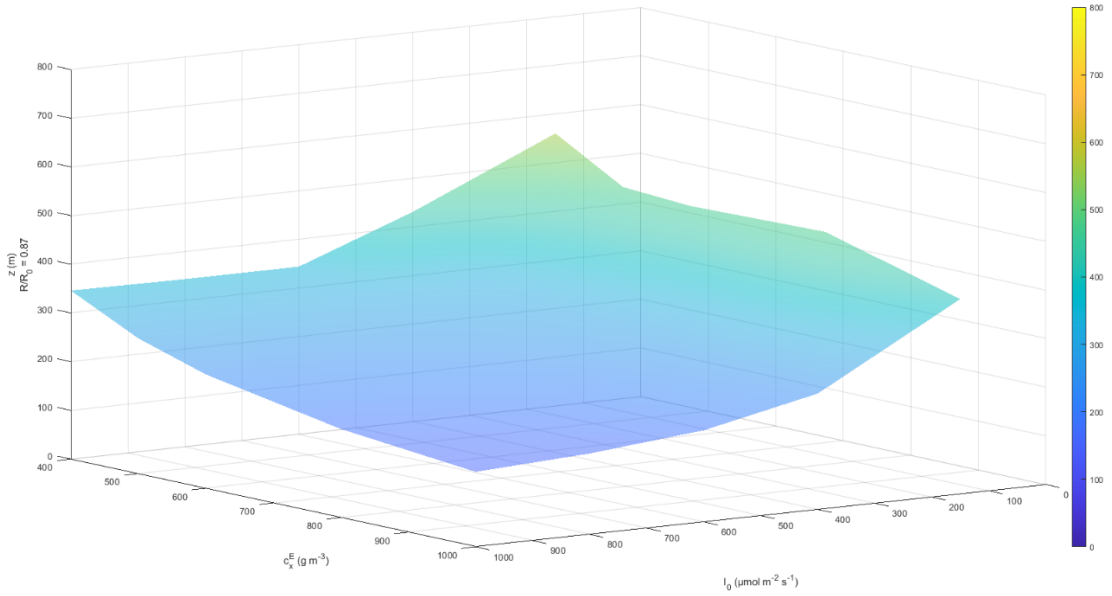

Figure 8.4. Length of the tubes (m) at which the ratio between the reaction rate and the inlet reaction rate (R/R_0) is equal to about 87% as function of the inlet biomass concentration (c_x^E) and of incident light intensity (I_0)

In the case of an already existing photobioreactor, our analysis can be used to determine the optimal microalgal concentration that must be kept at the reactor inlet. In that way, in fact, it is possible to maximize the biomass productivity. Figure 8.5 shows how biomass productivity changes as a function of biomass concentration at the reactor inlet, for two PBR lengths, namely 800 m (Figure 8.5A) and 250 m (Figure 8.5B).

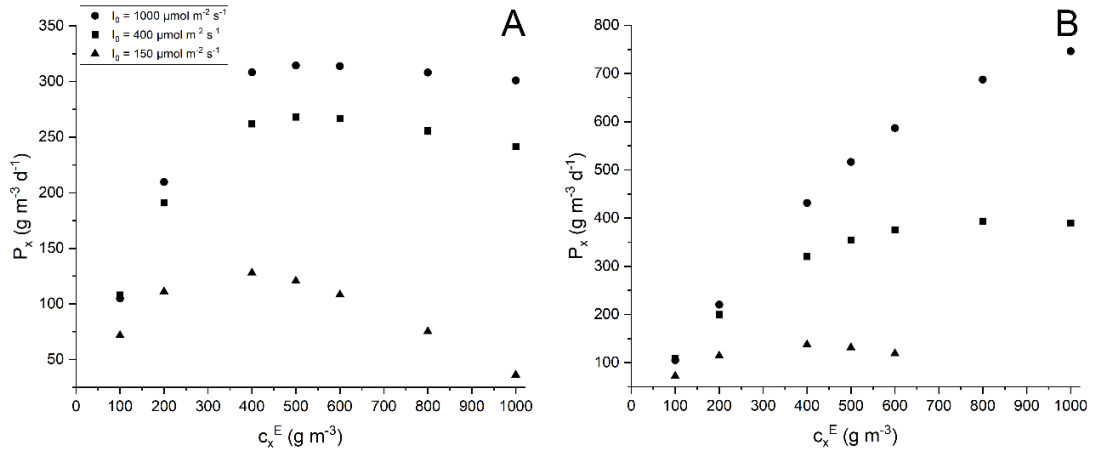

Figure 8.5. Biomass productivity (P_x) as function of different inlet biomass concentration (c_x^E), with length of the tubular rector equal to 800 m (panel A) and 250 m (panel B), parametric at different incident light intensity (I_0) (*circles* for 1000 μmol m^{-2} s^{-1}, *squares* for 400 μmol m^{-2} s^{-1} and *triangles* for 150 μmol m^{-2} s^{-1})

In both cases the effect of three different incident light intensities is considered. It is concluded that with a shorter tube, the productivity is considerably greater, almost double compared to that achieved with the longer one. The concentration of biomass entering the reactor has different effects, depending on the length of tubes. If it is not an optimal one (Figure 8.5A), the productivity reaches a maximum value which will not increase even if the inlet biomass concentration is raised. In the other case, instead, the productivity considerably increases with the inlet biomass concentration (Figure 8.5B).
However, at lower light intensity, increasing the value of the biomass over 400 g m^{-3}, leads to a reduction of the volumetric productivity. In fact, if light intensity is not high, it is better to maintain a lower concentration of biomass in the reactor, in order to have a better light profile along the tube diameter, thus avoiding problems of photolimitation. It is widely known that photolimitation problem occurs very frequently in outdoor cultivations, and especially in tubes with relatively large diameters [11]. Along the section of the pipe, indeed, the culture can be divided into layers, with the external ones highly illuminated, and the inner ones where the cells are in the dark. Moreover, to obtain a high surface-to-volume ratio, bioreactors made with small diameter tubes are preferred. Often they range from 30 to 100 mm [34], but other authors suggested to use a greater depth of reactor [14,32]. Therefore, photoinhibition and photolimitation are not only connected to biomass concentrations, but also to the reactor diameter [12,35]. Certainly, a sufficiently high flow rate ensuring a turbulent flow allows to have a good mixing inside the tubes. However, excessive turbulence can damage cells, and this poses a limit on the convective velocity. Damages associated with turbulence occur when the size of the eddies approaches that of the algal cells. Accepting a safe limit on eddy length of 50 μm, the maximum culture velocity, if a water-like behaviour is considered, cannot exceed 1.0 m s^{-1} [23]. Usually velocities ranging from 0.2 m·s^{-1} to 0.5 m s^{-1} are adopted for biomass cultivation [13], also considering the limited mechanical resistance imposed by the piping construction materials [23].

8.3.2 Role of oxygen in the entire process

In this section, the overall production process described in Section 8.2.2 is analysed. Initially, mass balances are solved for a base case, then the effect of the tubes length and of the inlet biomass concentration on the biomass areal productivity are assessed. The values of the variables used for the base case are the ones described in the Table 8.2. The calculated

mass flow rates for all the species in each stream are reported in Table 8A.1 of the Appendix. The biomass areal productivity obtained is equal to 40.57 g m^{-2} s^{-1}. The calculated HRT is of 31 days, while the SRT is lower, equal to 0.97 day. Barbera et al. [26] have already proved that SRT is the main variable to be used to maximize productivity. On the other hand, the SRT, as can be seen from Eq. (8.6), is directly proportional to the average concentration inside the reactor, i.e. to the inlet biomass concentration. In fact, the microalgal growth occurring in the single tube pass is very small (the residence time per single pass is approximately 16 min). In Figure 8.6, SRT is represented as a function of the inlet biomass concentration (c_x^E), parametric at different incident light intensity (I_0).

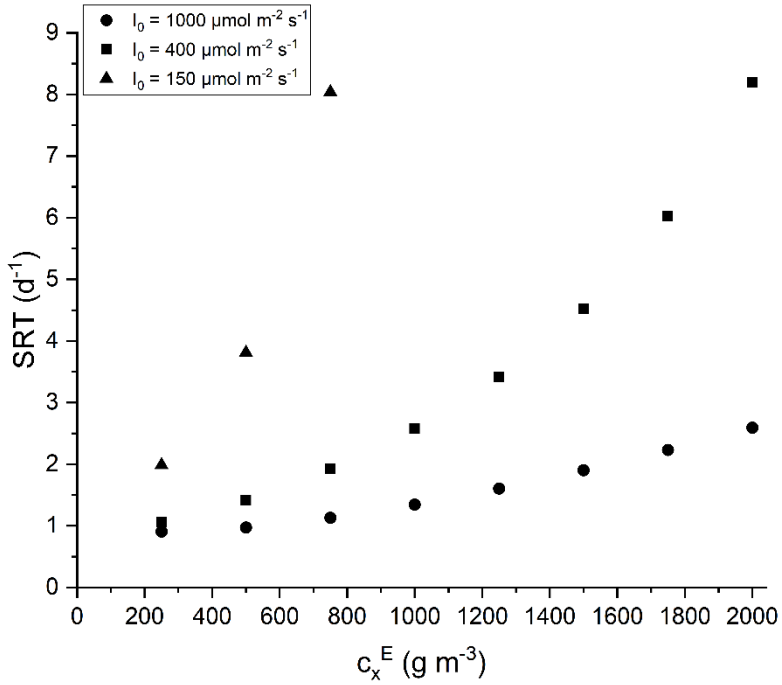

Figure 8.6. Solid Retention Time (*SRT*) as function of the inlet biomass concentration (c_x^E), parametric at different incident light intensity (I_0)

It can be seen how it increases exponentially with the inlet biomass concentration. Therefore, the higher the concentration of biomass used at the PBR inlet, the greater the retention time of the solids. Moreover, as light decreases, less biomass is produced in the reactor. To maintain the concentration entering the reaction section at a stable value (c_x^E), only the biomass that is produced has to be removed ($\dot{m}_x^W$). For this reason, the SRT increases much more rapidly with lower light intensities with respect to a reactor irradiated with higher light intensity. Thus, it is confirmed that the fundamental operating variable is the biomass concentration at the reactor inlet. Controlling its value, it is possible to maintain the SRT around its optimum value, so maximizing the productivity, and reducing also the

consumption of nutrients and water. Sensitivity analyses were performed to understand the influence of the PBR length, by testing in each condition different inlet biomass concentrations, when the *C. prothotecoides* productivity can be maximized. As shown in Figure 8.7, by using tubes of 250 m and increasing the value of inlet biomass concentration, biomass productivity also increases. In addition, the productivity values obtained are significantly higher than when opting for a design with longer tubes. In fact, by increasing the biomass concentration at the entrance of a photobioreactor longer than 250 m, productivity remains unchanged or decreases. An optimal concentration can therefore be identified, which allows to maximize the biomass productivity.

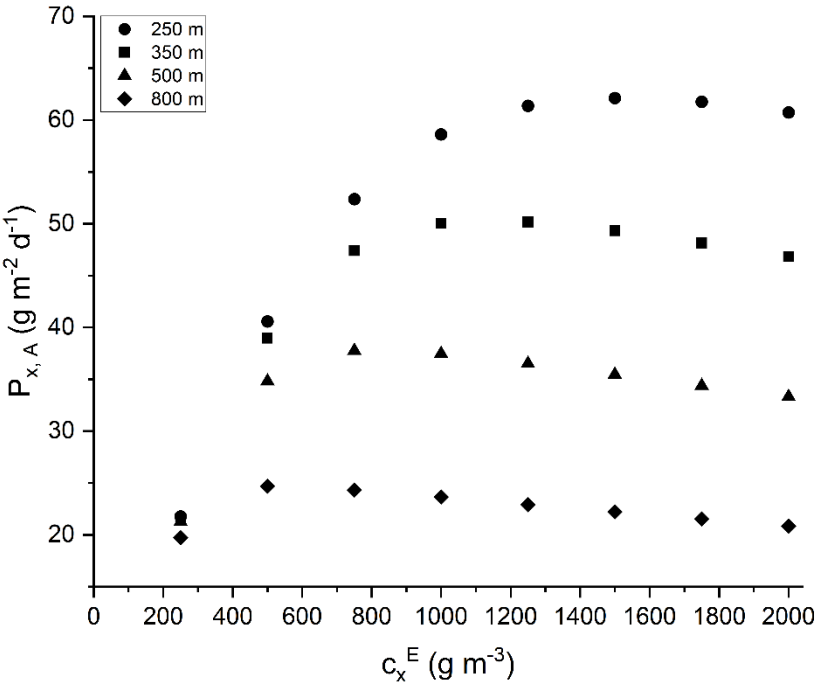

Figure 8.7. Biomass areal productivity ($P_{x,A}$) as function of the inlet biomass concentration (c_x^E), parametric at different length of the tubes

The same analysis was carried out for tube lengths shorter than 250 m (Figure 8A.3): the simulations show that for tube lengths down to 100 m, the productivity keeps increasing, while at even lower lengths, the value becomes steady. However, the lower the tube length, and the higher is the recycle ratio to be applied in order to keep the same value of SRT (e.g., for L = 50 m, R = 13000-30000), which is not realistic in practice. Also, from a technological point of view, using short tubes increases the complexity of the plant (pumps, fittings, connections and so on), which is not feasible at large scale.

Finally, it is useful to see how the concentration of oxygen at the reactor outlet varies at different tube lengths and inlet biomass concentration. As can be seen from Figure 8.8, by

using longer tubes a greater amount of oxygen is produced. It is also possible to identify a c_x^E at which the concentration of oxygen leaving the PBR is maximum. Beyond that value, the oxygen concentration decreases, because in this case the productivity of the system is also decreasing. If the tubes are of an optimal length, increasing the concentration of biomass at the inlet also increases the production of oxygen. This trend reflects the biomass productivity profile reported in Figure 8.7.

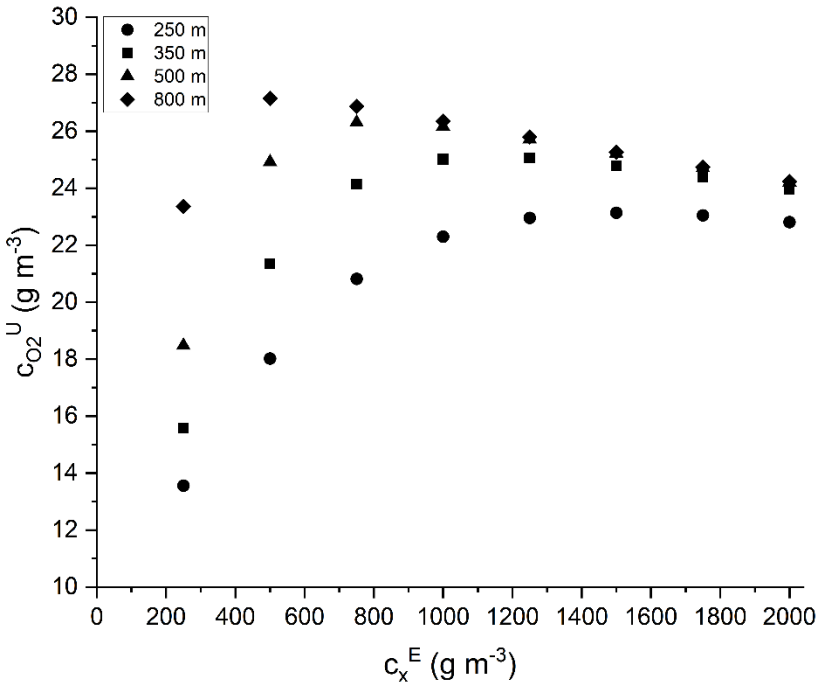

Figure 8.8. Outlet oxygen concentration (c_{O2}^U) as function of the inlet biomass concentration (c_x^E), parametric at different length of the tubes

The results reported in Figure 8.8 allow also to draw some considerations about the current methods to assess the possible occurrence of oxygen inhibition in real plants, which are based on the measurement of its concentration at the tube outlet. It is concluded that the mere measurement of the oxygen concentration in the PBRs is not significant to evaluate the performances of the biomass production process. For sure, a high concentration of oxygen inhibits the microalgal growth, but to properly account for this phenomenon it is necessary to use a kinetic model that describes it in its complexity: as shown in Figure 8.8, the final concentration of oxygen cannot be generically used as a reliable index, because it is a complex result of different kinetic contributions of production and consumption, related to biomass concentration, light intensity and the other variables. For this reason, in this Chapter a comprehensive model that includes photorespiration, basal respiration and inhibition was used. In that way, the length of the tubes and the biomass concentration are

optimized, not simply considering an inhibition threshold, but taking instead into account the close relation existing between the operating variables (biomass inlet level, oxygen concentration and light effect). According to our model, in the case of the design of a new process, the optimal configuration can be identified, while for an existing process, the best operating conditions that let to minimize the loss of productivity, can be detected. In any case the knowledge of the growth kinetic parameters is essential.

8.4 Final remarks

In this Chapter, a systematic analysis of microalgal production in tubular photobioreactors was carried out, based on a simple but comprehensive kinetic model accounting for oxygen inhibition. Simulations were carried out for both a single tubular PBR and for a process with biomass recycle. Through this analysis, it was possible to investigate the effect of main operating variables, such as light intensity and biomass concentration within the reactor. Specifically, the biomass concentration at the tube inlet was found to be the key variable to control oxygen accumulation and consequent growth inhibition. From the overall growth rate profile along the pipe length, it was possible to define a general criterion to determine the optimal tube length that minimizes the effect of the other operating variables (biomass and oxygen concentration) on oxygen inhibition. The analysis also revealed that monitoring the oxygen concentration at the reactor outlet is not sufficient to understand the productivity behaviour. Although here applied to a specific case, the present analysis is of general validity, and can be a useful tool to optimize the operating conditions of an existing plant, or alternatively to find the optimal design of a new one.

Nomenclature

c_i	Concentration of the species *i* (g m^{-3})
c_i^E	Inlet concentration of species *i* (g m^{-3})
c_i^U	Outlet concentration of species *i* (g m^{-3})
u	Convective velocity (m s^{-1})
$Y_{i/x}$	Mass yields of the species *i* (g_i g_x^{-1})
z	Axial coordinate (m)
R_x	Net biomass growth rate (g_x m^{-3} d^{-1})
μ_{max}	Maximum specific growth rate of the microorganism (d^{-1})
k_{resp}	Maximum oxygen respiration rate (d^{-1})
K_{O2}	Oxygen half-saturation constant for respiration (g m^{-3})
K_C	Half-saturation constant for CO_2 (g m^{-3})
K_{ph}	Photorespiration constant (g m^{-3})
k_{inh}	Oxygen inhibition rate (d^{-1})
n	Oxygen inhibition exponent (m^3 g^{-1})
I_0	Incident light intensity (µmol m^{-2} s^{-1})
K_I	Light half-saturation constant (µmol m^{-2} s^{-1})
I_{opt}	Optimal irradiance (µmol m^{-2} s^{-1})
K_a	Biomass light absorption coefficient (m^2 g^{-1})
r	Radius (m)
T	Temperature (°C)
T_{max}	Maximum temperature (°C)
T_{min}	Minimum temperature (°C)
T_{opt}	Optimal temperature (°C)
d	Tubes diameter (m)
V_R	Total volume of the reactor (m^3)
S_t	Irradiated surface of the reactor (m^2)
$\dot{V}_0$	Volumetric flowrate of the make-up stream (m^3 d^{-1})
$\dot{V}_E$	Inlet volumetric flowrate (m^3 d^{-1})
$\dot{V}_U$	Outlet volumetric flowrate (m^3 d^{-1})
$\dot{V}_{in}$	Inlet volumetric flowrate of the splitter unit (m^3 d^{-1})
$\dot{V}_R$	Volumetric flowrate of the biomass recycle stream (m^3 d^{-1})
$\dot{V}_{sep}$	Inlet volumetric flowrate of the biomass separation section (m^3 d^{-1})

$\dot{V}_W$	Outlet volumetric flowrate of the biomass separation section (m^3 d^{-1})
$\dot{V}_{clair}$	Inlet volumetric flowrate of the purge unit (m^3 d^{-1})
$\dot{V}_{purge}$	Outlet volumetric flowrate of the purge unit (m^3 d^{-1})
$\dot{V}_{sed}$	Volumetric flowrate of the biomass recycle stream from purge unit (m^3 d^{-1})
$\dot{m}_x^W$	Biomass flowrate extracted from the plant (g_x d^{-1})
HRT	Hydraulic Retention Time (d)
SRT	Solid Retention Time (d)
P_x	Biomass volumetric productivity (g_x m^{-3} d^{-1})
$P_{x,A}$	Biomass areal productivity (g_x m^{-2} d^{-1})

Literature cited

[1] D.C. Ducat, J.C. Way, P.A. Silver, Engineering cyanobacteria to generate high-value products, Trends Biotechnol. 29 (2011) 95–103. https://doi.org/10.1016/j.tibtech.2010.12.003.

[2] N.-S. Lau, M. Matsui, A.A.-A. Abdullah, Cyanobacteria: Photoautotrophic Microbial Factories for the Sustainable Synthesis of Industrial Products, Biomed Res. Int. 2015 (2015) 1–9. https://doi.org/10.1155/2015/754934.

[3] S. Singh, B.N. Kate, U.C. Banecjee, Bioactive compounds from cyanobacteria and microalgae: An overview, Crit. Rev. Biotechnol. 25 (2005) 73–95. https://doi.org/10.1080/07388550500248498.

[4] M. Bilal, T. Rasheed, I. Ahmed, H.M.N. Iqbal, High-value compounds from microalgae with industrial exploitability - A review, Front. Biosci. - Sch. 9 (2017) 319–342. https://doi.org/10.2741/s490.

[5] A.K. Koyande, K.W. Chew, K. Rambabu, Y. Tao, D.T. Chu, P.L. Show, Microalgae: A potential alternative to health supplementation for humans, Food Sci. Hum. Wellness. 8 (2019) 16–24. https://doi.org/10.1016/j.fshw.2019.03.001.

[6] B. Drosg, I. Fritz, F. Gattermayr, L. Silvestrini, Photo-autotrophic production of poly(hydroxyalkanoates) in cyanobacteria, Chem. Biochem. Eng. Q. 29 (2015) 145–156. https://doi.org/10.15255/CABEQ.2014.2254.

[7] H. Takenaka, Y. Yamaguchi, Chapter 18 Commercial-scale culturing of cyanobacteria : an industrial, (2014) 293–301.

[8] J.C. Weissman, R.P. Goebel, J.R. Benemann, Photobioreactor Design : Mixing , Carbon Utilization , and Oxygen Accumulation, 31 (1988) 336–344.

[9] A. Bertucco, M. Beraldi, E. Sforza, Continuous microalgal cultivation in a laboratory-scale photobioreactor under seasonal day – night irradiation : experiments and simulation, (2014) 12–18. https://doi.org/10.1007/s00449-014-1125-5.

[10] C.E. de Farias Silva, E. Sforza, A. Bertucco, Stability of carbohydrate production in continuous microalgal cultivation under nitrogen limitation: effect of irradiation regime and intensity on Tetradesmus obliquus, J. Appl. Phycol. 30 (2018) 261–270. https://doi.org/10.1007/s10811-017-1252-x.

[11] Q. Huang, F. Jiang, L. Wang, C. Yang, Design of Photobioreactors for Mass Cultivation of Photosynthetic Organisms, Engineering. 3 (2017) 318–329.

https://doi.org/10.1016/J.ENG.2017.03.020.

[12] K.K. Vasumathi, M. Premalatha, P. Subramanian, Parameters influencing the design of photobioreactor for the growth of microalgae, Renew. Sustain. Energy Rev. 16 (2012) 5443–5450. https://doi.org/10.1016/j.rser.2012.06.013.

[13] C. Posten, Design principles of photo-bioreactors for cultivation of microalgae, Eng. Life Sci. 9 (2009) 165–177. https://doi.org/10.1002/elsc.200900003.

[14] G. Torzillo, B. Pushparaj, F. Bocci, W. Balloni, R. Materassi, G. Florenzano, Production of Spirulina biomass in closed photobioreactors, 1986. https://doi.org/10.1016/0144-4565(86)90021-1.

[15] F. Camacho Rubio, F.G. Acién Fernández, J.A. Sánchez Pérez, F. García Camacho, E. Molina Grima, Prediction of dissolved oxygen and carbon dioxide concentration profiles in tubular photobioreactors for microalgal culture, Biotechnol. Bioeng. 62 (1999) 71–86. https://doi.org/10.1002/(SICI)1097-0290(19990105)62:1<71::AID-BIT9>3.0.CO;2-T.

[16] S. Raso, B. van Genugten, M. Vermuë, R.H. Wijffels, Effect of oxygen concentration on the growth of Nannochloropsis sp. at low light intensity, J. Appl. Phycol. 24 (2012) 863–871. https://doi.org/10.1007/s10811-011-9706-z.

[17] A. Vonshak, G. Torzillo, P. Accolla, L. Tomaselli, Light and oxygen stress in Spirulina platensis (cyanobacteria) grown outdoors in tubular reactors, Physiol. Plant. 97 (1996) 175–179. https://doi.org/10.1111/j.1399-3054.1996.tb00494.x.

[18] A. Kazbar, G. Cogne, B. Urbain, H. Marec, B. Le-Gouic, J. Tallec, H. Takache, A. Ismail, J. Pruvost, Effect of dissolved oxygen concentration on microalgal culture in photobioreactors, Algal Res. 39 (2019) 101432. https://doi.org/10.1016/j.algal.2019.101432.

[19] C. Sousa, A. Compadre, M.H. Vermuë, R.H. Wijffels, Effect of oxygen at low and high light intensities on the growth of Neochloris oleoabundans, Algal Res. 2 (2013) 122–126. https://doi.org/10.1016/j.algal.2013.01.007.

[20] G. Torzillo, G. Chini Zittelli, Tubular Photobioreactors, in: 2015: pp. 187–212. https://doi.org/10.1007/978-3-319-20200-6_5.

[21] M. Janssen, J. Tramper, L.R. Mur, R.H. Wijffels, Enclosed outdoor photobioreactors: Light regime, photosynthetic efficiency, scale-up, and future prospects, Biotechnol. Bioeng. 81 (2003) 193–210. https://doi.org/10.1002/bit.10468.

[22] S.J. Pirt, Y.K. Lee, M.R. Walach, M. Watts Pirt, H.H.M. Balyuzi, M.J. Bazin,

Tubular Bioreactor for Photosynthetic Production of Biomass From Carbon Dioxide: Design and Performance., J. Chem. Technol. Biotechnol. Biotechnol. 33 B (1983) 35–58. https://doi.org/10.1002/jctb.280330105.

[23] F.G. Acién Fernández, J.M. Fernández Sevilla, J.A. Sánchez Pérez, E. Molina Grima, Y. Chisti, Airlift-driven external-loop tubular photobioreactors for outdoor production of microalgae: Assessment of design and performance, Chem. Eng. Sci. 56 (2001) 2721–2732. https://doi.org/10.1016/S0009-2509(00)00521-2.

[24] A. Vonshak, Spirulina Platensis Arthrospira : Physiology, Cell-Biology And Biotechnology., (1997). http://public.ebookcentral.proquest.com/choice/publicfullrecord.aspx?p=169889.

[25] E. Sforza, M. Pastore, S.M. Franke, E. Barbera, Modeling the oxygen inhibition in microalgae: an experimental approach based on photorespirometry, Accept. New Biotechnol. (n.d.).

[26] E. Barbera, E. Sforza, A. Grandi, A. Bertucco, Uncoupling solid and hydraulic retention time in photobioreactors for microalgae mass production : A model-based analysis, Chem. Eng. Sci. 218 (2020) 115578. https://doi.org/10.1016/j.ces.2020.115578.

[27] E. Sforza, M. Pastore, A. Spagni, A. Bertucco, Microalgae-bacteria gas exchange in wastewater: how mixotrophy may reduce the oxygen supply for bacteria, Environ. Sci. Pollut. Res. 25 (2018) 28004–28014. https://doi.org/10.1007/s11356-018-2834-0.

[28] O. Bernard, B. Rémond, Validation of a simple model accounting for light and temperature effect on microalgal growth, Bioresour. Technol. 123 (2012) 520–527. https://doi.org/10.1016/j.biortech.2012.07.022.

[29] E.M. Grima, F.G. Camacho, J.A.S. Pérez, F.G.A. Fernéndez, J.M.F. Sevilla, Evaluation of photosynthetic efficiency in microalgal cultures using averaged irradiance, Enzyme Microb. Technol. 21 (1997) 375–381. https://doi.org/10.1016/S0141-0229(97)00012-4.

[30] L. Rosso, J. Lobry, J.-P. Flandrois, An Unexpected Correlation between Cardinal Temperatures of Microbial Growth Highlighted by a New Model, J. Theor. Biol. 162 (1993) 447–463. https://doi.org/10.1006/jtbi.1993.1099.

[31] E. Sforza, M. Pastore, E. Barbera, A. Bertucco, Respirometry as a tool to quantify kinetic parameters of microalgal mixotrophic growth, 2019. https://doi.org/10.1007/s00449-019-02087-9.

[32] E. Uggetti, J. García, J.A. Álvarez, M.J. García-Galán, Start-up of a microalgae-based treatment system within the biorefinery concept: From wastewater to bioproducts, Water Sci. Technol. 78 (2018) 114–124. https://doi.org/10.2166/wst.2018.195.

[33] F. Fasaei, J.H. Bitter, P.M. Slegers, A.J.B. van Boxtel, Techno-economic evaluation of microalgae harvesting and dewatering systems, Algal Res. 31 (2018) 347–362. https://doi.org/10.1016/j.algal.2017.11.038.

[34] J.H. De Vree, R. Bosma, M. Janssen, M.J. Barbosa, R.H. Wijffels, Biotechnology for Biofuels Comparison of four outdoor pilot - scale photobioreactors, Biotechnol. Biofuels. (2015) 1–12. https://doi.org/10.1186/s13068-015-0400-2.

[35] E. Molina, J. Ferna, F.G. Acie, Y. Chisti, Tubular photobioreactor design for algal cultures, 92 (2001) 113–131.

Appendix

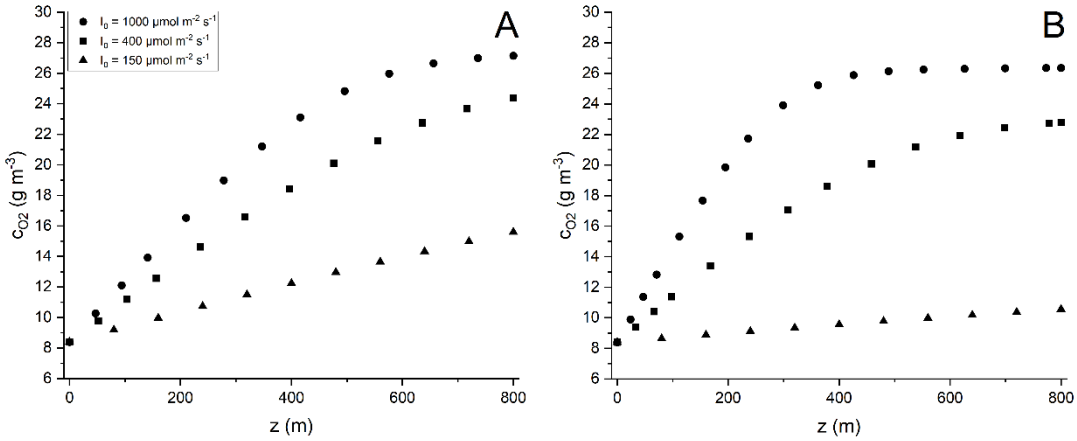

Figure 8A.1. Outlet oxygen concentration (c_{O2}) calculated at different tubes length (z), with an inlet biomass concentration equal to 500 g m^{-3} (panel A) and 1000 g m^{-3} (panel B), parametric at different incident light intensity (I_0) (*circles* for 1000 µmol m^{-2} s^{-1}, *squares* for 400 µmol m^{-2} s^{-1} and *triangles* for 150 µmol m^{-2} s^{-1})

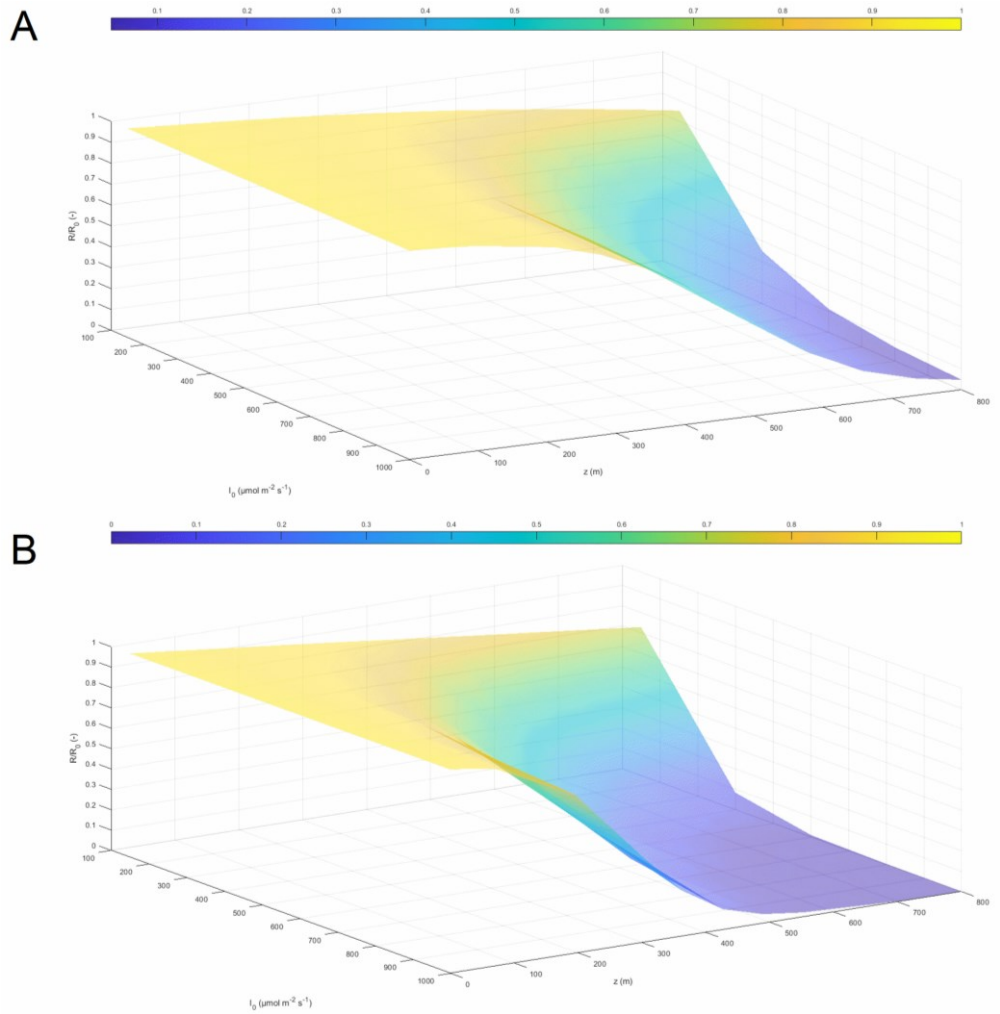

Figure 8A.2. Reaction rate normalized on that one at the inlet of the reactor (R/R_0) at different length of the tubes (z) and at different incident light intensity (I_0), with an inlet biomass concentration equal to 500 g m^{-3} (panel A) and 1000 g m^{-3} (panel B)

Table 8A.1. Mass flow rate of the base case referred to the Process Flow Diagram of Figure 8.1

Stream	Variable	g d^{-1}
Make up stream ($\dot{V}_0$)	$\dot{m}_{O2}{}^{0}$	21,3
	$\dot{m}_{CO2}{}^{0}$	84667,7
Reactor inlet ($\dot{V}_E$)	$\dot{m}_x{}^{E}$	3,59E+06
	$\dot{m}_{O2}{}^{E}$	6,03E+04
	$\dot{m}_{CO2}{}^{E}$	1,01E+07
Reactor outlet ($\dot{V}_U$)	$\dot{m}_x{}^{U}$	3,63E+06
	$\dot{m}_{O2}{}^{U}$	1,29E+05
	$\dot{m}_{CO2}{}^{U}$	9,97E+06
O_2 separation unit outlet	$\dot{m}_{O2}{}^{out}$	69079,1
Splitter inlet ($\dot{V}_{in}$)	$\dot{m}_x{}^{in}$	3,631E+06
	$\dot{m}_{O2}{}^{in}$	60318,6
	$\dot{m}_{CO2}{}^{in}$	9,972E+06
Biomass recycle stream ($\dot{V}_R$)	$\dot{m}_x{}^{R}$	3,59E+06
	$\dot{m}_{O2}{}^{R}$	59644,6
	$\dot{m}_{CO2}{}^{R}$	9,861E+06
Biomass separation section inlet ($\dot{V}_{sep}$)	$\dot{m}_x{}^{sep}$	40571,4
	$\dot{m}_{O2}{}^{sep}$	674,0
	$\dot{m}_{CO2}{}^{sep}$	111424
Biomass separation section outlet ($\dot{V}_W$)	$\dot{m}_x{}^{W}$	40571,4
	$\dot{m}_{O2}{}^{W}$	1,14
	$\dot{m}_{CO2}{}^{W}$	187,8
Purge unit inlet ($\dot{V}_{clair}$)	$\dot{m}_{O2}{}^{clair}$	672,8
	$\dot{m}_{CO2}{}^{clair}$	111236,2
Purge unit outlet ($\dot{V}_{purge}$)	$\dot{m}_{O2}{}^{purge}$	20,2
	$\dot{m}_{CO2}{}^{purge}$	3337,1
Recycle stream from purge unit ($\dot{V}_{sed}$)	$\dot{m}_{O2}{}^{sed}$	652,7
	$\dot{m}_{CO2}{}^{sed}$	107899,1

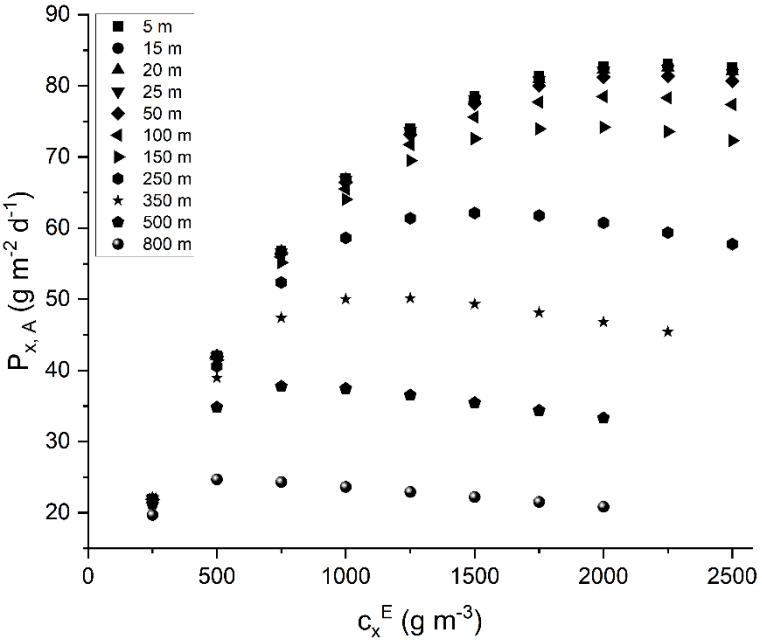

Figure 8A.3. Biomass areal productivity ($P_{x,A}$) as function of the inlet biomass concentration ($c_x{}^{E}$), parametric at different length of the tubes, down to 5 m

Chapter 9

Techno-economic analysis

Even thought, microalgae have been object of increasing interest due to the attractive potential as an innovative sector within the bioeconomy, the development of microalgal culture technologies at a commercial scale is limited by the production costs, which define their potential market sector. Due to the different scales, technologies and assumptions it is necessary to proceed with a case-by-case study. In the case of a new product as cyanophycin, the production process has to be specified first. Based on results obtained by laboratory experiments, capital and operating costs can be evaluated for each section of the envisaged production plant, in order to evaluate a preliminary production cost. Capital and operation costs are affected by several variables, which can limit the industrial applicability of the biomass production. Specifically, in the case of artificially illuminated photobioreactor, the cost is mainly and greatly influenced by the incident light intensity. Therefore, cyanophycin production by photosynthetic microorganism will be attractive only if photosynthetic efficiency will be significantly improved at larger scale.

9.1 Introduction

Currently, photosynthetic microorganisms are being studied in view of applications related to human consumption, including food, nutraceuticals, cosmetic and pharmaceuticals, but also for a wide range application in other markets, such as the production of bulk chemicals or commodities to aquafeed, biofertilizers, CO_2 capture, wastewater treatment and biofuels [1–4]. Therefore, microalgae are proposed to be used as whole biomass, as well as for the extraction of high value compounds. Noticeably, the market size and characteristic between the different application sectors are completely different. In the case of biofuels production, the market size reaches approximatively 1e+6 ton y^{-1}, but to be competitive, the price should remain below 1 € kg^{-1} [5]. A completely different scenario occurs in the case of microalgal cultivation for markets related to human applications. The market size is four orders of magnitude smaller (1e+2 ton y^{-1}), but the market price could rise up to 1000 € kg^{-1} [5]. At present, the highest selling prices in the market are those of isoprenoids as antioxidants (900.000 € ton^{-1}), followed by polysaccharides as immune-stimulant (200.000 € ton^{-1}), polyunsaturated fatty acids (PUFAs) and oxylipins as micronutrients and anti-inflammatory compounds (30.000 to 75.000 € ton^{-1}) [6]. However, compared to biofuels, this is indeed a very restrictive market, which has to follow many regulatory and safety requirements, such as the GRAS (Generally Regarded As Safe) designation, regarding the use of a compound for animal and human consumption [5,6]. Between these two extremes, there is the market with minimum safety requirement which includes biofertilizers, biostimulants, biopesticides and bioplastics [5].

In the other hand, the microalgal production is still a small-scale industrial activity, with a global production that is estimated to be equal to 25,000 ton, more than half of which is produced in China [7]. Indeed, one of the main issues is related to the ability to produce large amount of biomass required by products with high production volume and low market value, as the biofuels. So, the current technology and the gaps in scientific knowledge of large-scale cultivation limits the current microalgal production to high-value products. Nevertheless, the total market was estimated equal to 50 M€ in 2021, and this is set to grow to 70 M€ by 2025 [8].

The operating conditions such as the pH, the nutrient availability, temperature and the incident light intensity have a significant influence on the growth of the photosynthetic microorganisms and, depending on the target product, can be suitably modulated to maximize its productivity [9]. Accordingly, microalgae are cultivated in different systems,

open and closed photobioreactor, affecting the global economics of the process. Open ponds require lower investment costs and easier maintenance with respect to closed photobioreactors, which, on the other hand, guarantee higher productivity, higher photosynthetic efficiencies and reduced contamination risks [10]. The photosynthetic efficiency is the key factor to define the unit selling price, considering that the theoretical maximum value for microalgae is estimated to be 13%, and that less than 10% of the theoretical value is achieved using conventional microalgal culture conditions [11]. Last but not least, biomass biorefining costs accounted for 50-60% of the total microalgal production costs, due to underdeveloped technologies [12].

For this reason, evaluating a production cost is not straightforward, as can be seen from the variability of the results found in the literature. Schipper et al. [13] calculated a biomass production cost of 2.9 € kg^{-1} in the Arabian Gulf. On the opposite, Oostlander et al. [14] evaluated it about one hundred times larger (290 € kg^{-1} and 329 € kg^{-1} for tubular reactors under artificial light and in a greenhouse). Thus, due to different scales, operating conditions and assumptions, it is always necessary to do a case-by-case study.

In this Chapter, a preliminary techno-economic analysis of a one-hectare plant for the production of cyanophycin was performed. Initially, the issue about the lack of a cyanophycin commercial standard was addressed. Then, a Block Flow Diagram (BFD) for a complete cyanophycin production process was proposed. The process is divided into three parts: the biomass production section, the pre-treatment section and the extraction and separation section. Mass balances were done considering three scenarios, where cyanophycin was produced respectively cultivating *Synechocystis* sp. PCC 6803, *Nostoc* sp. PCC 7120 and *Nostoc* 44, at the best operating condition found in the laboratory experiments. Thus, taking into account capital and operating costs, it was possible to preliminarily estimate the total cyanophycin production cost in the three scenarios considered.

9.2 Issues with cyanophycin quantification

9.2.1 Calibration curves for cyanophycin quantification

Cyanobacterial cyanophycin is a non-protein, non-ribosomally produced amino acid copolymer, composed of equimolar amounts of aspartic acid and arginine which has molecular weight ranging from 25 to 100 kDa [15]. The polydispersity is lower and ranges

between 25 and 30 kDa, if the cyanophycin is produced by recombinant microorganisms or transgenic plant [16,17]. Moreover, the native cyanophycin is exclusively composed of aspartate and arginine, whereas in recombinant strain, also lysine has been found [16–18], which influences its solubility [19]. In literature many protocols are proposed for its measurement, but they are all based on a two-step procedure, composed of an extraction phase and a quantification phase. The extraction phase is performed exploiting one of its properties. Indeed, cyanophycin is soluble under a specific range of pH (pH<2; pH>9), and insoluble at physiological pH [20,21]. The quantification, instead, is done alternatively by the Sakaguchi reaction [22], a detection method for arginine or with the Bradford reaction, a detection method for the protein [23]. The main issue, however, is the absence of a commercial standard when comparing experimental data with those from the literature. Indeed, it was found that different aminoacidic compounds as L-arginine or Bovine Serum Albumin (BSA) were used for calibration curves [24,25]. Nevertheless, cyanophycin consists of a polyaspartic acid backbone and arginine residues, which are linked to the β-carboxyl group of each aspartic acid by their α-amino groups. So, both L-arginine or BSA have a completely different composition with respect to cyanophycin structure, possibly affecting its exact quantification. As can be seen in Figure 9.1, the calibration curves obtained using different standards are completely different. Three standards were tested: Bovine Serum Albumin (BSA), Lysozyme, an enzyme with lower molecular weight with respect to BSA, and a sample of cyanophycin produced by another research laboratory. The quantification was done according to the Bradford reaction and alternatively by the Bicinchoninic Acid, another assay for the protein quantification [26]. The calibration curves obtained with the three standards for each detection method revealed to be quite different. For example, at an absorbance of 0.4 measured by the Bradford assay (Figure 9.1A, Figure 9.1C, Figure 9.1E), the concentration of the cyanophycin samples is about 200 $\mu g\ mL^{-1}$, whereas the lysozyme and the BSA are equal to about 500 and 400 $\mu g\ mL^{-1}$, respectively. Thus, if a calibration curve made with BSA was used to quantify the cyanophycin concentration, it would result in an overestimation of the concentration, doubling its quantity. Similar consideration can be drawn for the detection by the Bicinchoninic Assay (Figure 9.1B, Figure 9.1D, Figure 9.1F). Moreover, this method proved unable to detect the cyanophycin, as the absorbance measured at 562 nm at different cyanophycin concentration samples was almost always equal to 0 (Figure 9.1F).

Thus, until a commercial standard will be available, to which everybody can refer experimental data, the best solution appears the production of a cyanophycin internal

standard. Given the specificity of its composition and structure, this seems to be the best solution to avoid overestimation errors. In any case, the comparison with literature remains tricky due to the variability of its composition and polydispersity, depending on the producing microorganism or plant exploited [16,17].

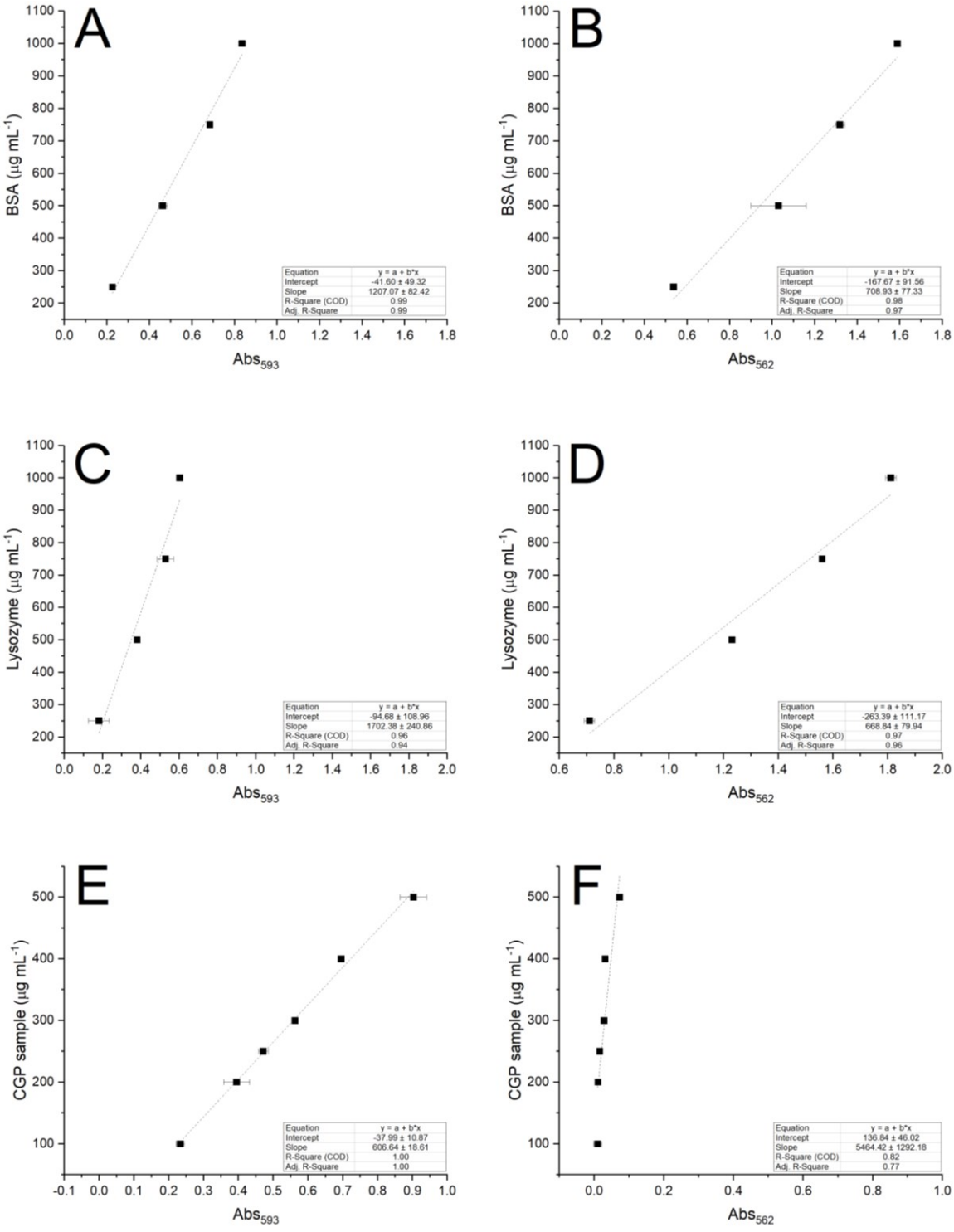

Figure 9.1. Calibration curves obtained with Bovine Serum Albumin (BSA), lysozyme and cyanophycin sample (CGP sample) with Bradford reagent (panels A, C, E) and Bicinchoninic Acid assay (panels B, D, F)

9.2.2 Production and qualification of a cyanophycin internal standard

To overcome the issue about the absence of a commercial standard for cyanophycin quantification, a sample of cyanophycin from *Nostoc* sp. was produced, extracted, dried, and used as a reference for the quantification of cyanophycin after extraction. The amino acid content of the fraction extracted was analysed to verify its composition, according to the following protocol.

Samples of cyanophycin were exactly weighted (5 mg) and dissolved in 10 mL of 6M HCl in sealed tubes, added with a solution of gamma-aminobutyric acid (GABA) used as internal standard (IS), then nitrogen was sparged in the solution to reduce oxygen concentration and the tubes were hermetically closed with Teflon caps. At this point the material was subjected to 10 minutes of sonication and the mixture was heated at 100°C for 48 hours to obtain complete hydrolysis of the cyanophycin. The liquid was then subjected to vacuum evaporation for 2 hours to eliminate the HCl and the volume of the liquid was then dried using gentle flow of nitrogen. Finally, the volume was adjusted to 5mL in a volumetric flask, and the solution was used for the LC-MS/MS analysis, carried out in a Agilent 1260 chromatograph, with autosampler and oven column. As detector a Varian 500MS mass spectrometer (Ion Trap) was used with electrospray (ESI) operating in positive ion mode. For the detection of the target amino acids the following transitions were selected: for Aspartic acid (Asp) m/z 134 and fragment at m/z 74, for Arginine (Arg) m/z 175 and fragment at m/z 70. Calibration curves were obtained preparing different ratio of Asp, Arg and IS and correlating the ratio of amount (amount of analyte/amount of IS) and the ratio of areas (area of analyte/area of IS). Calibration curves were

$$y = 3941\,x + 135 \quad \text{and} \quad y = 5483\,x + 123 \tag{9.1}$$

where y represents the area ratio, and x the amount ratio.

The LC separation was obtained by an Agilent Z-Hilic column (3.0 x 10 mm 2.7 µm), as mobile phases acetonitrile (A), water 0,1% formic acid (B) were used. Flow rate was 0.4 mL min^{-1}. Gradient starts with 2: 98:0 % A:B isocratic for 5 minutes, then 10:90 % A:B at 10 minutes, 40:60% A:B at 20 minutes, then back to initial conditions with five minutes for equilibration. Results are reported in Figure 9A.1 of Appendix. The cyanophycin produced by *Nostoc* sp. is composed by Arginine (Arg) and Aspartic Acid (Asp) only, as expected with the following composition: 36.2% was Arg and 48.5% was Asp, confirming the high quality of the produced and extracted cyanophycin.

9.2.3 Recalculation of the results based on a common calibration curve obtained with the internal standard

Accordingly, to properly compare the experimental data, a new calibration curve was made, using the cyanophycin internal standard. The solutions were prepared by dissolving known concentrations of cyanophycin in HCl 0.1M. Then, the cyanophycin was quantified according to Bradford [23]. Results are reported in Figure 9.2.

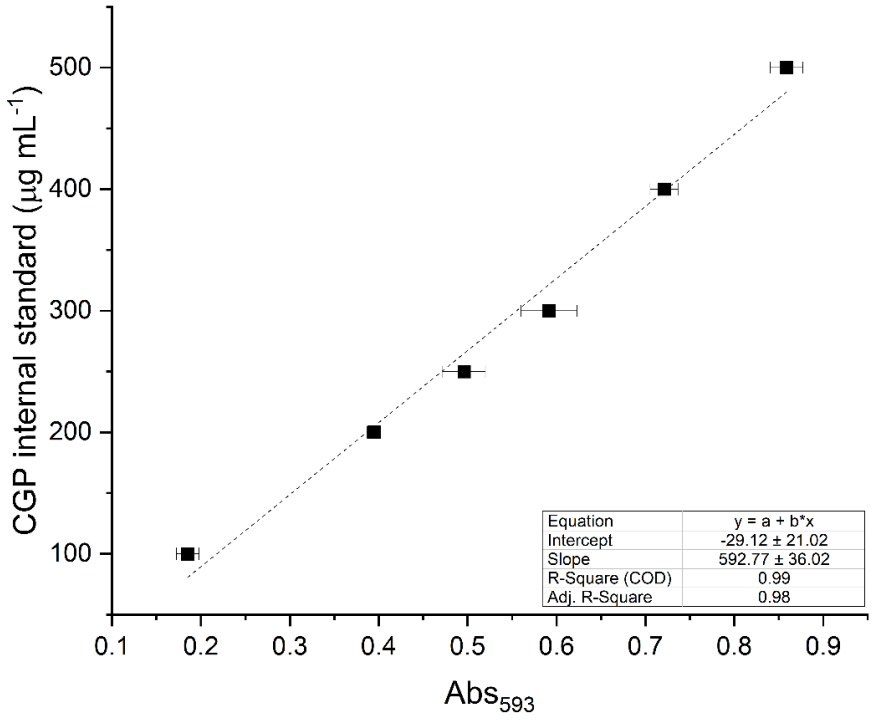

Figure 9.2. Calibration curves obtained with the cyanophycin internal standard (CGP internal standard) obtained with Bradford reagent

The linear relation between the absorbance and cyanophycin concentration (c_{CGP}) is:

$$c_{CGP} = 592.77 Abs_{593} - 29.12 \quad (9.2)$$

where Abs_{593} is the absorbance measured at 593 nm. This linear correlation is almost equal to the one previously obtained with another cyanophycin sample in §9.2.1 (Figure 9.1E). Thus, cyanophycin experimental data obtained in the laboratory experiments with *Synechocystis* sp. PCC 6803 (§4), *Nostoc* sp. PCC 7120 (§5) and *Nostoc* 44 (§6) were recalculated to refer all to the same calibration curve, so that data can be compared with each other and can be properly used in the techno-economic analysis. Results are shown in Table 9.1.

Table 9.1. Cyanophycin production recalculated with the calibration curves obtained with the internal standard, in the best operating conditions obtained with three cyanobacterial species

Variables	UoM	*Synechocystis* sp. PCC 6803	*Nostoc* sp. PCC 7120	*Nostoc* 44
Cyanophycin quota (q_{CGP})	$g_{CGP}\ g_x^{-1}$	0.041±0.003	0.100±0.004	0.295±0.013
Cyanophycin concentration (c_{CGP})	$g_{CGP}\ m^{-3}$	0.023±0.002	0.038±0.001	158.6±25.2
Cyanophycin productivity (P_{CGP})	$g_{CGP}\ m^{-3}\ d^{-1}$	8.65±0.65	15.1±0.54	63.8±10.2

9.3 Methods

9.3.1 Proposal for a cyanophycin production process

In this analysis, a proposal for a cyanophycin production process by cyanobacteria is presented according to Figure 9.3, the process was divided into three sections: a biomass production one, a biomass pre-treatment one and a section for the extraction and separation of the cyanophycin.

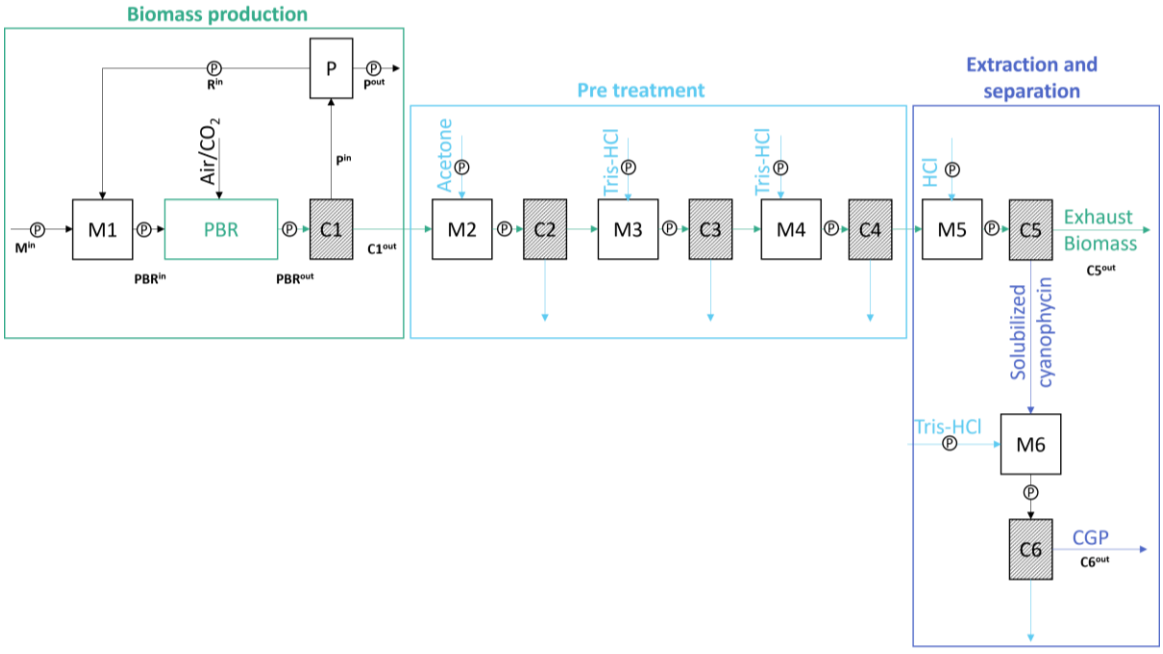

Figure 9.3. Block flow diagram of the cyanophycin production process proposed (M: mixer; PBR: photobioreactor; C: centrifugal separator; P: purge)

For the biomass production section, a one-hectare plant made of flat photobioreactors was considered. Green Wall Panel – II® (GWP-II®) costs were used, gathering data from Tredici et al. [27], since they ensures good productivities compared to other flat panel photobioreactors [28]. The biomass leaving the reactor (PBR^{out}) enters a centrifugal separator (C1), where water and nutrients are removed, and recycled back to the inlet of

the photobioreactor (R^{in}), after purging a fraction of the stream (P^{out}). A makeup stream (M^{in}) is needed to restore nutrients, so that their concentration at the reactor inlet (PBR^{in}) is kept constant. The concentrated biomass ($C1^{out}$), enters a pre-treatment section, where the biomass is washed with different solvents (Acetone and Tris-HCl 50 mM) and then centrifuged. Then, in the extraction section, the cyanophycin is extracted from the exhaust biomass ($C5^{out}$), solubilized thanks to HCl 0.1M, and then precipited with Tris-HCl 100 mM set to pH 12 by NaOH and finally separated ($C6^{out}$). It has been assumed that the pre-treatment and extraction operations are carried out as they were performed in the laboratory experiments, since at present there are no commercial industrial plants for cyanophycin extraction.

9.3.2 Calculation assumptions and methodology

Calculations were done considering three scenarios, where cyanophycin was produced respectively cultivating *Synechocystis* sp. PCC 6803, *Nostoc* sp. PCC 7120 and *Nostoc* 44, at the best operating condition found in the laboratory experiments (§4, §5, §6), and summarized in Table 9.2.

Table 9.2. Results obtained in the best operating conditions by cultivating three cyanobacterial species

Variables	UoM	*Synechocystis* sp. PCC 6803	*Nostoc* sp. PCC 7120	*Nostoc* 44
BI	µmol m^{-2} s^{-1}	9.87	85.3	59.2
η_{PAR}	%	3.19	0.84	1.17
P_x	g_x m^{-3} d^{-1}	211.3±16.5	151.2±12.0	227.1±29
P_{CGP}	g_{CGP} m^{-3} d^{-1}	8.65±0.65	15.1±0.54	63.8±10.2

Thus, the plant was considered as operated continuously during the year and constantly illuminated by artificial light. Specifically, it was assumed that the same areal productivities were obtained because the photobioreactor maintained the same surface-to-volume ratio and the same operating conditions that was found for each species. These are summarized in Table 9.3. The complete cultivation medium used for each species is reported in Table 9A.1 of Appendix. Similarly, it was assumed that the cyanophycin extraction process has the same efficiency as the one experimentally obtained in the laboratory.

Other general assumptions valid in all the scenarios were done to perform the calculation. The biomass leaving the photobioreactor enters a centrifugal separation section for the recovery of 95% of the biomass [29]. Water and nutrients are recycled back to the reactor, but to avoid the accumulation of possible metabolites or other compounds that in the long

term can inhibit the biomass growth, a purge fraction of 0.03 has been fixed. As regards the biomass growth, the photobioreactor was sparged with a mixture of air/CO_2 (95/5 v), with a flow rate of 1 L h^{-1} m^{-2}. Finally, it was assumed that 50% of the biomass was made of carbon. The uptake of the carbon from nutrients was assumed to be split between CO_2 (25%), Na_2CO_3 (12.5%) and $NaHCO_3$ (12.5%). Thus, mass balances were done in all the three scenarios, to calculate the flowrates for each component in each stream, and specifically the ones of the makeup streams, needed to restore the principal macronutrients at the reactor inlet, to match the concentrations values reported in Table 9.3.

Table 9.3. Experimental conditions used in the best operating conditions obtained with three cyanobacterial species

Variable	UoM	*Synechocystis* sp. PCC 6803	*Nostoc* sp. PCC 7120	*Nostoc* 44
V_{PBR}/A_{PBR}	m^{-3} m^{-2}	0.03	0.03	0.03
I_0	µmol m^{-2} s^{-1}	250	450	450
τ	d	2.69	2.52	2.49
c_N^{inlet}	mg_N L^{-1}	494	-	-0
c_P^{inlet}	mg_P L^{-1}	2.72	0.6	0.6
c_{Na2CO3}^{inlet}	mg L^{-1}	1.63	-	-
c_{NaHCO3}^{inlet}	mg L^{-1}	122.1	10.9	11.0

On this basis, it was possible to estimate the CAPital EXpenditure (CAPEX) and the OPerational EXpenditure (OPEX) singularly for each of the three sections of the production plants. As regards the CAPEX, the Fixed Capital Investment (FCI) was calculated as the sum of the Total Direct Capital costs (TDC) and the Total Indirect Capital costs (TIC). TDC costs are in turn the sum of the TDC Inside Battery Limits (ISBL), which accounts for the cost of all the equipment and the instrumentation, and Offsite Battery Limits (OSBL), which accounts for buildings, yard improvements, service facilities, and that are estimated as 30% of ISBL. Depreciation was calculated considering components lifespan, as indicated in Tredici et al. [27]. TIC costs were calculated as the sum of the cost for engineering and supervision (5% ISBL), installation (10% ISBL) and taxes and insurance (1% ISBL), and were distributed over the 25-year lifespan of the plant. CAPEX is equal for all the three scenarios, as the reactor geometry was the same. With respect to the OPEX, they were calculated as the sum of the Total Direct Operating costs (TDO) and the Total Indirect Operating costs (TIO). The first ones accounted for the costs of labour, nutrients, solvents, and electricity, considering current market quota, while TIO costs was calculated as the sum of the cost of overhead (10% TDO), administration (10% TDO) and

maintenance (5% TDC). Specifically, calculations of TDO costs were done retrieving the labour cost from Tredici et al. [27], whereas the costs of nutrients and solvents were obtained from online databases (https://www.chemanalyst.com/Pricing-data; https://tradingeconomics.com/commodity/). In this analysis, the costs related to water were not considered, given that it can come from different sources, e.g. seawater, wastewater. Instead, the energy cost to operate the electric equipment and irradiate the photobioreactor was considered equal to 135 € MWh^{-1}, a value quite conservative for the near future (https://tradingeconomics.com/commodity/).

9.4 CAPital EXpenditure

9.4.1 Mass Balances of 1 ha biomass production plant

In order to perform the economic analysis, the flowrate of all components in each stream must be known. So, the mass balances were done for each species, applying the general mass conservation balance, at steady state. As indicated in Figure 9.4, the cyanophycin extraction section was neglected, because the separation section was supposed to have the same efficiency found in laboratory experiments, resulting in the same cyanophycin productivity reported in Table 9.2. Results for all the three scenarios are shown in Table 9.4.

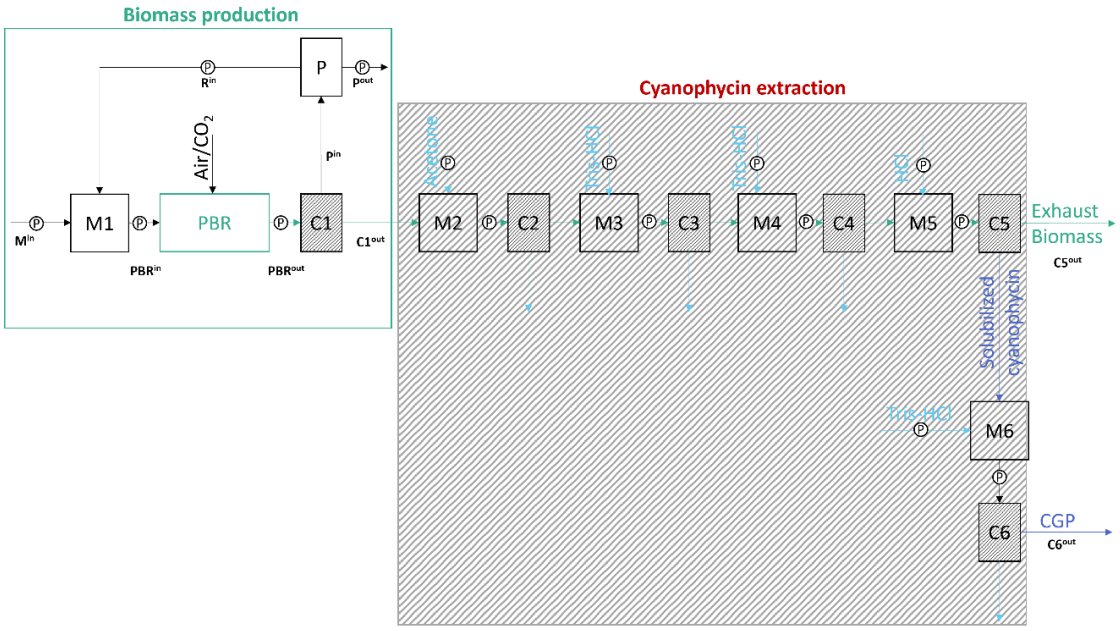

Figure 9.4. Simplified block flow diagram of the cyanophycin production process proposed, with indications of the streams name

Table 9.4. Mass flow rate (ton y^{-1}) referred to the block flow diagram of Figure 9.4

	***Synechocystis* sp. PCC 6803**	***Nostoc* sp. PCC 7120**	***Nostoc* 44**
Photobioreactor inlet (PBR^{in})	ton y^{-1}	ton y^{-1}	ton y^{-1}
$\dot{m}_x$	0	0	0
$\dot{m}_N$	20.1	0	0
$\dot{m}_P$	0.11	0.03	0.03
$\dot{m}_{Na2CO3}$	1.63	0	0
$\dot{m}_{NaHCO3}$	122.1	10.9	11.0
$\dot{m}_{CO2}$	7.84	7.84	7.84
Photobioreactor outlet (PBR^{in})	ton y^{-1}	ton y^{-1}	ton y^{-1}
$\dot{m}_x$	23.14	16.56	24.87
$\dot{m}_N$	17.93	0	0
$\dot{m}_P$	0	0	0
$\dot{m}_{Na2CO3}$	0.18	0	0
$\dot{m}_{NaHCO3}$	114.9	4.65	1.67
Biomass centrifuge outlet ($C1^{out}$)	ton y^{-1}	ton y^{-1}	ton y^{-1}
$\dot{m}_x$	23.14	16.56	24.87
$\dot{m}_N$	17.03	0	0
$\dot{m}_P$	0	0	0
$\dot{m}_{Na2CO3}$	0.17	0	0
$\dot{m}_{NaHCO3}$	109.1	4.42	1.59
Purge outlet (P^{out})	ton y^{-1}	ton y^{-1}	ton y^{-1}
$\dot{m}_N$	0.51	0	0
$\dot{m}_P$	0	0	0
$\dot{m}_{Na2CO3}$	0.01	0	0
$\dot{m}_{NaHCO3}$	3.27	0.13	0.05
Recycle (R^{in})	ton y^{-1}	ton y^{-1}	ton y^{-1}
$\dot{m}_N$	16.52	0	0
$\dot{m}_P$	0	0	0
$\dot{m}_{Na2CO3}$	0.17	0	0
$\dot{m}_{NaHCO3}$	105.9	4.29	1.54
Make up (M^{in})	ton y^{-1}	ton y^{-1}	ton y^{-1}
$\dot{m}_N$	3.61	0.00	0.00
$\dot{m}_P$	0.11	0.03	0.03
$\dot{m}_{Na2CO3}$	1.46	0	0
$\dot{m}_{NaHCO3}$	16.25	6.58	9.46
$\dot{m}_{CO2}$	7.84	7.84	7.84
Biomass centrifuge outlet ($C5^{out}$)	ton y^{-1}	ton y^{-1}	ton y^{-1}
$\dot{m}_x$	22.19	14.90	17.88
Cyanophycin centrifuge outlet ($C6^{out}$)	ton y^{-1}	ton y^{-1}	ton y^{-1}
$\dot{m}_{CGP}$	0.95	1.66	6.99

9.4.2 Capital costs evaluation of the 1 ha biomass production plant

Considering the block flow diagram of Figure 9.3, the CAPEX estimation was done initially in the first section, which relates to the one-hectare plant for the biomass production. Results are reported in Table 9.5. The Fixed Capital Investment (FCI) is equal to 1,964,426

€, and 68% of which are affected by the Total Direct Costs ISBL. Considering the different lifespan of instrumentation, FCI corresponds to a capital cost per annum equal to 107,130 € y^{-1}. As regards the Total Direct Costs ISBL represented in Figure 9.5, they are strongly affected by the cost of the reactor, accounting for 43% of TDC ISBL. Secondly, TDC ISBL cost is affected by electrical equipment, instrumentation and control system (16% of TDC ISBL costs).

Table 9.5. Total Direct Capital costs (TDC) and Total Indirect Capital costs (TIC) of the 1 ha biomass production plant

		Total cost (€)	Lifespan (y)	Capital cost per annum (€ y^{-1})
Reactor		505,320	1-25	35,225
Piping/fittings/valves/tanks		140,945	10-20	9,534
Heat Exchanger		129,792	20	6,490
Pumps		61,512	10	6,151
Blowers		42,400	20	2,120
Centrifugal separator		112,000	25	4,480
Filtration system		30,800	10	3,080
Electrical equipment/instrumentation/control system		272,728	10-25	13,293
Field laboratory		50,000	25	2,000
Total Direct Capital costs (TDC) - ISBL		*1,345,497*	-	*82,373*
Total Direct Capital costs (TDC) - OSBL	*30% ISBL*	*403,649*	*25*	*16,146*
Total Direct Capital costs (TDC)		**1,749,146**	-	**98,519**
Engineering & Supervision	5% ISBL	67,275	25	2,691
Installation	10% ISBL	134,550	25	5,382
Taxes & Insurance	1% ISBL	13,455	25	538
Total Indirect Capital costs (TIC)		**215,280**	**-**	**8,611**

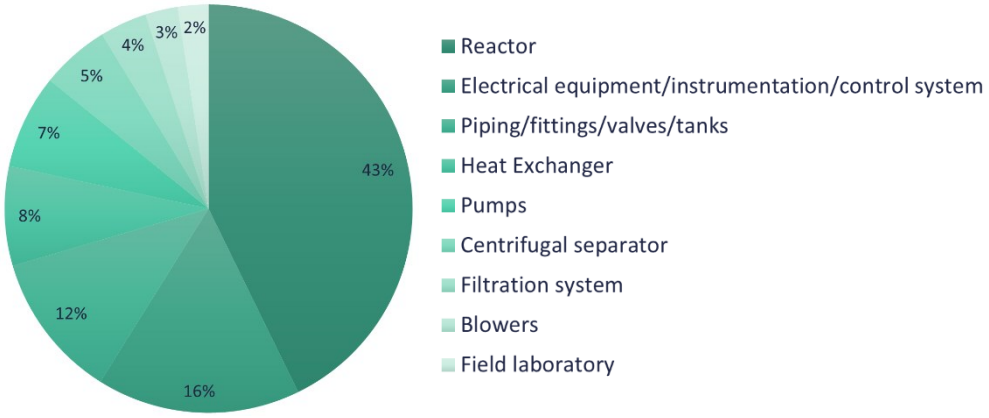

Figure 9.5. Pie chart of Total Direct Capital costs Inside Battery Limits (ISBL) related to the biomass production section

9.4.3 Capital costs evaluation of the cyanophycin extraction section

On the basis of the biomass production section, it was proposed a flowsheet for the pre-treatment of the biomass and the cyanophycin extraction section. The pre-treatment section consists of three mixing tanks, where the biomass is washed with solvents, interspersed with centrifugal separator to remove the spent solvents. Similarly, the extraction section consists of two mixing tanks spaced out by two centrifugal separators. Throughout the sections, the circulation of the biomass was ensured by several pumps. Estimation of the CAPEX was done accordingly to Tredici et al. [27]. Results are summarized in Tables 9.6 and 9.7 for the pre-treatment and the extraction section, respectively. For both sections, the centrifugal separator represents the 72% of the TDC costs (Figure 9A.2 of Appendix).

Table 9.6. Total Direct Capital costs (TDC) and Total Indirect Capital costs (TIC) of the biomass pre treatment section

		Total cost (€)	Lifespan (y)	Capital cost per annum (€ y^{-1})
Piping/fittings/valves/tanks		37,155	20	1,858
Pumps		33,000	10	3,300
Centrifugal separator		336,000	25	13,440
Total Direct Capital costs (TDC) - ISBL		*406,155*	-	*18,598*
Total Direct Capital costs (TDC) - OSBL	*30% ISBL*	*121,847*	*25*	*4,874*
Total Direct Capital costs (TDC)		**528,002**	**-**	**23,472**
Engineering & Supervision	5% ISBL	20,308	25	812
Installation	10% ISBL	40,616	25	1,625
Taxes & Insurance	1% ISBL	4,062	25	162
Total Indirect Capital costs (TIC)		**64,985**	**-**	**2,599**

9.4.4 Fixed Capital Investment of the cyanophycin production plant

Overall, the Fixed Capital Investment for the complete cyanophycin production process is equal to the sum of the FCI calculated for each section, as represented in Table 9.8. The total cost is equal to 2,952,736 €, which corresponds to a total capital cost per annum equal to 150,582 €, considering a 25-year lifespan of the plant. Total Fixed Capital Investment (FCI) is split among the three sections as reported in Figure 9.6, but is strongly affected by the biomass production section, which accounts for 71%.

Table 9.7. Total Direct Capital costs (TDC) and Total Indirect Capital costs (TIC) of the cyanophycin extraction section

		Total cost (€)	Lifespan (y)	Capital cost per annum (€ y^{-1})
Piping/fittings/valves/tanks		24,770	20	1,239
Pumps		22,000	10	2,200
Centrifugal separator		224,000	25	8,960
Total Direct Capital costs (TDC) - ISBL		*270,770*	-	*12,399*
Total Direct Capital costs (TDC) - OSBL	*30% ISBL*	*81,231*	*25*	*3,249*
Total Direct Capital costs (TDC)		**352,001**	**-**	**15,648**
Engineering & Supervision	5% ISBL	13,539	25	542
Installation	10% ISBL	27,077	25	1,083
Taxes & Insurance	1% ISBL	2,708	25	108
Total Indirect Capital costs (TIC)		**43,323**	**-**	**1,733**

Table 9.8. Fixed Capital Investment (FCI) for 1 ha biomass production process, the biomass pretreatment section and the cyanophycin extraction section

	Total cost (€)	Lifespan (y)	Capital cost per annum (€ y^{-1})
1 ha biomass production plant	1,964,426	-	107,130
Pre treatment section	592,986	-	26,071
Extraction section	395,324	-	17,381
Total Fixed Capital Investment (FCI)	**2,952,736**	**-**	**150,582**

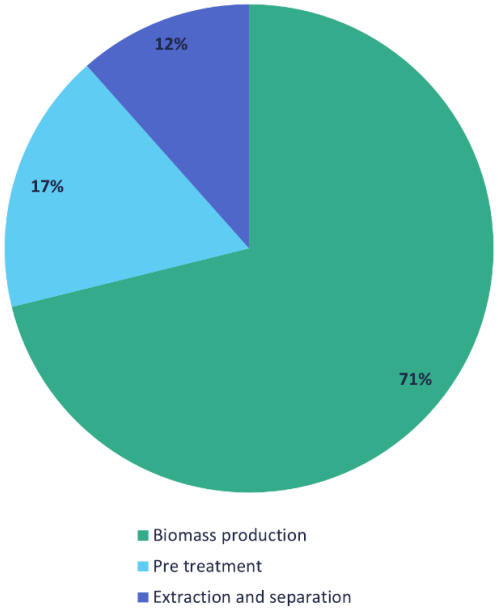

Figure 9.6. Pie chart of total Fixed Capital Investment (FCI)

9.5 OPerational EXpenditure

9.5.1 Operating costs evaluation of the 1 ha biomass production plant

For the three scenarios considered, the OPEX were calculated separately in the biomass production section. Specifically, the main differences between the species regard the intensity of the incident light intensity and the nutrients inlet flowrates. *Synechocystis* sp. PCC 6803 was illuminated at 250 µmol photons m^{-2} s^{-1}, whereas both *Nostoc* species needed 450 µmol photons m^{-2} s^{-1}. As regards the nutrients concentrations, it was calculated the costs of the macronutrients in the makeup stream. With respect to the value reported in Table 9.4, flowrates have been recalculated considering that nitrogen was added as sodium nitrate ($NaNO_3$), whereas phosphorus as disodium hydrogen phosphate (Na_2HPO_4). Results are shown in Table 9.9, along with the current market price for each nutrient.

Table 9.9. Nutrients prices and make up mass flow rates calculated for each cyanobacterial species

Nutrients	Price	*Synechocystis* sp. PCC 6803	*Nostoc* sp. PCC 7120	*Nostoc* 44
	€ ton^{-1}	ton y^{-1}	ton y^{-1}	ton y^{-1}
$NaNO_3$	700	21.89	0.00	0.00
Na_2HPO_4	1,000	0.43	0.10	0.10
Na_2CO_3	372	1.46	0	0
$NaHCO_3$	450	16.25	6.58	9.46
CO_2	390	7.84	7.84	7.84

Table 9.10 reports the values for the TDO and TIO costs. Overall, the OPEX were estimated equal to 1,796,967 € y^{-1}, 2,907,609 € y^{-1} and 2,909,168 € y^{-1} for *Synechocystis* sp. PCC 6803, *Nostoc* sp. PCC 7120 and *Nostoc* 44, respectively. Since the photobioreactor was equal for the three scenarios, the same labour cost was identified, and it was equal to 179,400 € y^{-1}. Nutrients costs was higher for *Synechocystis* sp. PCC 6803 with respect to both *Nostoc* species, and precisely it was about four times higher. In fact, since *Synechocystis* sp. PCC 6803 is not a diazotrophic cyanobacteria, so that nitrogen must be supplied with the cultivation medium. Nevertheless, the major cost among the TDO ones is that of electricity, and precisely of electricity for the illumination of the photobioreactor. Note that reactors were supposed to be constantly illuminated by artificial light. As a result, the TDO costs were affected by electricity for 83% for *Synechocystis* sp. PCC 6803 and for for 91% both *Nostoc* species, respectively.

Table 9.10. Operating cost (OPEX) for 1 ha biomass production process

			***Synechocystis* sp. PCC 6803**	***Nostoc* sp. PCC 7120**	***Nostoc* 44**
Plant supervisor (1)		€ y^{-1}	52,000	52,000	52,000
Biologist (1)		€ y^{-1}	35,000	35,000	35,000
Worker (4)		€ y^{-1}	92,400	92,400	92,400
Total Labour cost		€ y^{-1}	*179,400*	*179,400*	*179,400*
$NaNO_3$		€ y^{-1}	15,320	0	0
NaH_2PO_4		€ y^{-1}	429	101	104
Na_2CO_3		€ y^{-1}	544	0	0
$NaHCO_3$		€ y^{-1}	7,313	2,959	4,255
CO_2		€ y^{-1}	3,058	3,058	3,058
Nutrients		€ y^{-1}	*26,663*	*6,118*	*7,417*
10 kW submersible pump		€ y^{-1}	3,402	3,402	3,402
3.75 kW circulation pump		€ y^{-1}	4,730	4,730	4,730
5.5 kW centrifugal pump		€ y^{-1}	292	292	292
0.75 kW centrifugal pump		€ y^{-1}	61	61	61
7.5 kW centrifugal separator		€ y^{-1}	3,078	3,078	3,078
7.5 kW three-lobe blower		€ y^{-1}	17,386	17,386	17,386
Incident light intensity (I_0)		€ y^{-1}	1,182,600	2,128,680	2,128,680
Electricity costs		€ y^{-1}	1,211,549	2,157,629	2,157,629
Total Direct Operating costs (TDO)		€ y^{-1}	**1,424,591**	**2,350,126**	**2,351,426**
Overhead	10% TDO	€ y^{-1}	142,459	235,013	235,143
Administration	10% TDO	€ y^{-1}	142,459	235,013	235,143
Maintenance	5% TDC	€ y^{-1}	87,457	87,457	87,457
Total Indirect Operating costs (TIO)		€ y^{-1}	**372,376**	**557,483**	**557,742**

9.5.2 Operating costs evaluation of the cyanophycin extraction section

To calculate the operating cost of the biomass pre-treatment section and the cyanophycin extraction section, the flowrates of all solvents were calculated on the basis of the laboratory protocol used for the extraction of cyanophycin (§4). Results of calculation are summarized in Table 9.11, along with solvents prices, as estimated according to current market. The are some differences among the solvents required by the species, mostly due to the different biomass mass flow rate obtained for the species, which required a proportional amount of solvent. With an in-depth study of a large-scale process these differences could probably be minimized.

Table 9.11. Solvents prices and mass flow rates calculated for each cyanobacterial species

Solvents	**Price**	***Synechocystis* sp. PCC 6803**	***Nostoc* sp. PCC 7120**	***Nostoc* 44**
Pre-treatment	€ ton^{-1}	ton y^{-1}	ton y^{-1}	ton y^{-1}
CH_3COCH_3	1,140	609	435	654
Tris HCl 50 mM	5,000	12	4.34	6.52
Extraction	€ ton^{-1}	ton y^{-1}	ton y^{-1}	ton y^{-1}
HCl 0.1 M	140	4.21	3.01	4.52
Tris HCl 0.1 M	5,000	18.22	13.03	19.56
NaOH	715	1.82	1.30	1.96

Thus, it is possible to estimate the OPEX for both sections. Results are reported in Table 9.12 and Table 9.13 for the biomass pre-treatment and the cyanophycin extraction sections, respectively.

Table 9.12. Operating cost (OPEX) for the biomass pretreatment section

			***Synechocystis* sp. PCC 6803**	***Nostoc* sp. PCC 7120**	***Nostoc* 44**
Worker		€ y^{-1}	69,300	69,300	69,300
Total Labour cost		€ y^{-1}	*69,300*	*69,300*	*69,300*
CH_3COCH_3		€ y^{-1}	694,098	496,412	745,098
Tris-HCl 50 mM		€ y^{-1}	60,732	21,717	32,597
Solvent		€ y^{-1}	*754,830*	*518,129*	*777,695*
3.75 kW circulation pump		€ y^{-1}	7,096	7,096	7,096
7.5 kW centrifugal separator		€ y^{-1}	9,234	9,234	9,234
Electricity costs		€ y^{-1}	*16,330*	*16,330*	*16,330*
Total Direct Operating costs (TDO)		€ y^{-1}	**842,204**	**605,504**	**865,069**
Overhead	10% TDO	€ y^{-1}	84,220	60,550	86,507
Administration	10% TDO	€ y^{-1}	84,220	60,550	86,507
Maintenance	5% TDC	€ y^{-1}	26,400	26,400	26,400
Total Indirect Operating costs (TIO)		€ y^{-1}	**194,841**	**147,501**	**199,414**

As regards the cost of labour, to operate the equipment less workers are required with respect to the biomass production section, and their number is equal in the three scenarios. Thus, the OPEX is majorly affected by the solvent cost, which in the pre-treatment section affect the OPEX for a mean value of about 72% for all species. In the cyanophycin extraction section, instead, the solvent cost represents about 45% of OPEX. Electricity costs, which represent the higher operating cost in the biomass production section, here represent less than 6% of the OPEX in all the scenarios.

Details about the contributions to the OPEX for each section are reported in Figure 9A.3 of the Appendix.

Table 9.13. Operating cost (OPEX) for the cyanophycin extraction section

			***Synechocystis* sp. PCC 6803**	***Nostoc* sp. PCC 7120**	***Nostoc* 44**
Worker		€ y^{-1}	46,200	46,200	46,200
Total Labour cost		€ y^{-1}	46,200	46,200	46,200
HCl 0.1 M		€ y^{-1}	590	422	633
Tris-HCl 100 mM		€ y^{-1}	91,097	65,152	97,791
NaOH		€ y^{-1}	1,303	932	1,398
Solvent		€ y^{-1}	92,990	66,506	99,823
3.75 kW circulation pump		€ y^{-1}	4,730	4,730	4,730
7.5 kW centrifugal separator		€ y^{-1}	6,156	6,156	6,156
Electricity costs		€ y^{-1}	10,886	10,886	10,886
Total Direct Operating costs (TDO)		€ y^{-1}	**151,822**	**125,337**	**158,654**
Overhead	10% TDO	€ y^{-1}	15,182	12,534	15,865
Administration	10% TDO	€ y^{-1}	15,182	12,534	15,865
Maintenance	5% TDC	€ y^{-1}	17,600	17,600	17,600
Total Indirect Operating costs (TIO)		€ y^{-1}	**47,964**	**42,667**	**49,331**

9.5.3 Operating cost of the cyanophycin production plant

Overall, the OPEX for the complete cyanophycin production process is equal to the sum of the operating cost calculated for each section (see Table 9.14). The total costs are equal to 3,033,798 € y^{-1}, 3,828,618 € y^{-1}, 4,181,637 € y^{-1}, for *Synechocystis* sp. PCC 6803, *Nostoc* sp. PCC 7120 and *Nostoc* 44, respectively. The OPEX, according to Figure 9.8, are strongly affected by the biomass production section, which accounts for 59%, 76% and 70% of operating costs for the three species, respectively. Indeed, the major cost is due to electricity for the illumination of the photobioreactor, which represent 40%, 56% and 52% of the total OPEX, for *Synechocystis* sp. PCC 6803, *Nostoc* sp. PCC 7120 and *Nostoc* 44, respectively. The lower value obtained for *Synechocystis* sp. PCC 6803 is due to the lower incident light intensity applied in this case. However, such a high impact of incident light intensity could have been foreseen, given that to produce cyanophycin, cyanobacteria were grown under unbalanced conditions, thus reaching very low values of photosynthetic efficiency (about 3% for *Synechocystis* sp. PCC 6803, less than 1.5% for both *Nostoc* species), as shown in Table 9.2.

Table 9.14. Operating costs for 1 ha biomass production process, the biomass pretreatment section and the cyanophycin extraction section

	Capital cost per annum	***Synechocystis* sp. PCC 6803**	***Nostoc* sp. PCC 7120**	***Nostoc* 44**
1 ha biomass production plant	€ y^{-1}	1,796,967	2,907,609	2,909,168
Pre treatment section	€ y^{-1}	1,037,045	753,005	1,064,483
Extraction section	€ y^{-1}	199,786	168,005	207,985
OPEX	€ y^{-1}	**3,033,798**	**3,828,618**	**4,181,637**

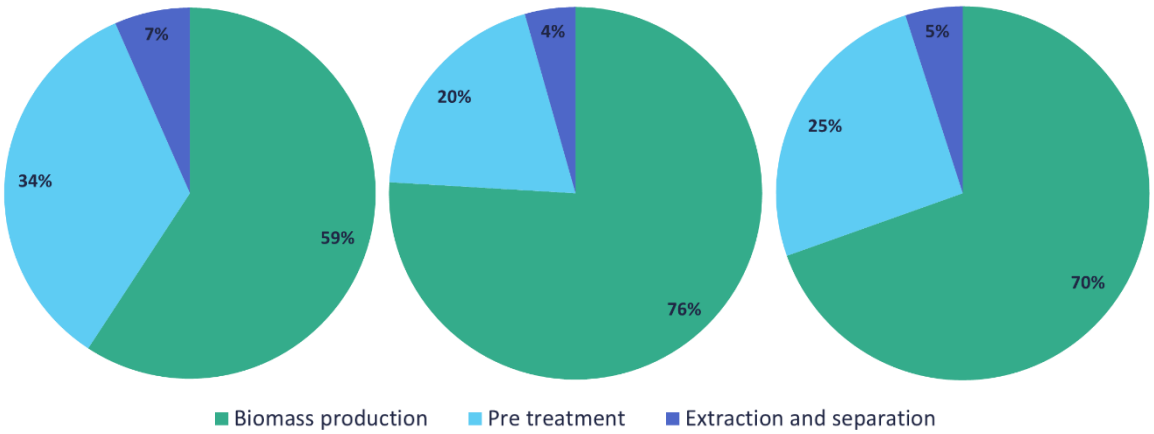

Figure 9.8. Pie charts of total OPEX for *Synechocystis* sp. PCC 6803, *Nostoc* sp. PCC 7120 and *Nostoc* 44

9.6 Production cost

The capital (CAPEX) and the operating (OPEX) cost reported in the previous sections can be used to evaluate the total product cost (TPC) in different scenarios. Initially the biomass price was calculated considering only the one-hectare biomass production process. Results are summarized in Table 9.15.

Table 9.15. Total biomass production cost based of 1 ha biomass production plant

		***Synechocystis* sp. PCC 6803**	***Nostoc* sp. PCC 7120**	***Nostoc* 44**
CAPEX+OPEX	€ y^{-1}	1,904,097	3,014,739	3,016,298
Biomass areal productivity ($P_{x,a}$)	ton_x ha^{-1} y^{-1}	23.14	16.56	24.87
Total Production Cost (TPC)	**€ kg_x^{-1}**	**82.3**	**182.0**	**121.3**

The total production cost per year of *Synechocystis* sp. PCC 6803 is one third smaller with respect to both *Nostoc* species. Thus, the Total Production Cost (TPC) is equal to 82.3 € kg_x^{-1} at a biomass productivity of P_x= 23.14 ton_x ha^{-1} y^{-1}. In the case of *Nostoc* sp. PCC 7120, the TPC rise to 182 € kg_x^{-1}, because the biomass areal productivity is smaller and

equal to 16.56 $ton_x\ ha^{-1}\ y^{-1}$. *Nostoc* 44, instead, has a TPC lower with respect to *Nostoc* sp. PCC 7120 (121.3 € kg_x^{-1}), because even if the cost per annum is almost the same, the biomass productivity is one third higher. These values fall in the range of selling prices typical of medium safety requirements product, as feed additives, livestock feed of for aquaculture [5].

On the other hand, the sum of capital and operating costs of all the three sections of the biomass production plant, gives rise to the Total Production Cost per kg of cyanophycin, as reported in Table 9.16. The values obtained exceed three thousand euros for *Synechocystis* sp. PCC 6803, whereas, for the mutant species *Nostoc* 44, it remains below 700 € kg_{CGP}^{-1}. Obviously, these results are greatly affected by the very low cyanophycin productivities achieved.

However, considering the process flow diagram of Figure 9.3, cyanophycin is not the only product, but once the cyanophycin has been extracted, the exhaust biomass can be available for other use, for example in lower value market. In this way, the Total Production Cost is reduced up to 137.6 € kg_x^{-1} for *Synechocystis* sp. PCC 6803, whereas for both *Nostoc* species the TPC remains higher (240.3 € kg_x^{-1} and 174.2 € kg_x^{-1} for *Nostoc* sp. PCC 7120 and *Nostoc* 44, respectively) due to the higher production cost.

Table 9.16. Total production cost based on total cyanophycin production cost

		***Synechocystis* sp. PCC 6803**	***Nostoc* sp. PCC 7120**	***Nostoc* 44**
CAPEX+OPEX	€ y^{-1}	3,184,380	3,979,200	4,332,219
Cyanophycin areal productivity ($P_{CGP,a}$)	$ton_{CGP}\ ha^{-1}\ y^{-1}$	0.95	1.66	6.99
Total Production Cost (TPC)	**€ kg_{CGP}^{-1}**	**3361.1**	**2402.9**	**619.8**
Biomass areal productivity ($P_{x,a}$)	$ton_x\ ha^{-1}\ y^{-1}$	23.14	16.56	24.87
Total Production Cost (TPC)	**€ kg_x^{-1}**	**137.6**	**240.3**	**174.2**

9.7 Final remarks

In this Chapter, a preliminary economic analysis was performed to evaluate the production cost for cyanophycin, based on a one-hectare biomass production plant, a pre-treatment section and a cyanophycin extraction section. Calculations were done in three scenarios, that correspond to the cyanophycin production as obtained in the best operating condition for the three cyanobacterial species considered.

As regards the biomass production section, it resulted that the reactor accounts for 43% of the Total Direct Costs (TDC). Instead, for both the pre-treatment and the extraction section the centrifugal separator represented the 72% of the TDC. Overall, the Fixed Capital Investment (FCI) for the cyanophycin production plant is equal to 2,952,736 €, with the biomass production section accounting for 71%.

The operating costs in the three scenarios were different because different operating conditions were used for the three cyanobacterial species. Specifically, the nutrients and the electricity duties were different among the species. The labour cost, instead, was the same. As the OPEX were calculated separately for the three sections of the cyanophycin production plant, in the biomass production section about 70% of the OPEX was due to the electricity costs, whereas in the pre-treatment and in the extraction section the highest cost was related to solvents, that represented respectively about 70% and 45% of OPEX.

Eventually, it was possible to evaluate the total product cost that accounts for both capital and operating cost. If we considered only the biomass production section, the total production cost results equal to 82.3 € kg^{-1}, 182.0 € kg^{-1} and 121.3 € kg^{-1} for *Synechocystis* sp. PCC 6803, *Nostoc* sp. PCC 7120 and *Nostoc* 44, respectively. On the other hand, if the cost of all sections of the production plant is accounted for, and assuming as valuable product not only the extracted cyanophycin but also the biomass left after the extraction, the total production cost resulted equal to 137.6 € kg^{-1}, 240.3 € kg^{-1} and 174.2 € kg^{-1} for *Synechocystis* sp. PCC 6803, *Nostoc* sp. PCC 7120 and *Nostoc* 44, respectively. These quite values depend on the fact that to produce cyanophycin, cyanobacteria were grown under unbalanced conditions, thus reaching very low photosynthetic efficiency. For this reason, further experimentation is needed to find the cultivating conditions that can guarantee a high cyanophycin productivity, but at the same time to reduce the operating cost due to electricity, thus increasing the photosynthetic efficiency. These improvements are likely to reduce the total production cost which, at present, are definitely not acceptable.

Nomenclature

q_{CGP}	Cyanophycin quota ($g_{CGP}\ g_x^{-1}$)
c_{CGP}	Cyanophycin concentration ($g_{CGP}\ m^{-3}$)
P_{CGP}	Cyanophycin productivity ($g_{CGP}\ m^{-3}\ d^{-1}$)
BI	Back Irradiance ($\mu mol\ m^{-2}\ s^{-1}$)
η_{PAR}	Photosynthetic efficiency (%)
P_x	Biomass productivity ($g_x\ m^{-3}\ d^{-1}$)
V_{PBR}/A_{PBR}	Ratio between photobioreactor volume and ratio ($m^3\ m^{-2}$)
I_0	Incident light intensity ($\mu mol\ m^{-2}\ s^{-1}$)
τ	Residence time (d)
c_N^{inlet}	Nitrogen inlet concentration ($mg_N\ L^{-1}$)
c_P^{inlet}	Phosphorus inlet concentration ($mg_P\ L^{-1}$)
c_{Na2CO3}^{inlet}	Sodium carbonate inlet concentration ($mg\ L^{-1}$)
c_{NaHCO3}^{inlet}	Sodium bicarbonate inlet concentration ($mg\ L^{-1}$)
$\dot{m}_x$	Biomass mass flow rate ($ton\ y^{-1}$)
$\dot{m}_N$	Nitrogen mass flow rate ($ton\ y^{-1}$)
$\dot{m}_P$	Phosphorus mass flow rate ($ton\ y^{-1}$)
$\dot{m}_{Na2CO3}$	Sodium carbonate mass flow rate ($ton\ y^{-1}$)
$\dot{m}_{NaHCO3}$	Sodium bicarbonate flow rate ($ton\ y^{-1}$)
$\dot{m}_{CO2}$	Carbon dioxide mass flow rate ($ton\ y^{-1}$)
$\dot{m}_{CGP}$	Cyanophycin mass flow rate ($ton\ y^{-1}$)

Acronyms

PUFA	polyunsaturated fatty acids
GRAS	Generally Regarded As Safe
BFD	Block Flow Diagram
BSA	Bovine Serum Albumin
GABA	gamma-aminobutyric acid
CGP	Cyanophycin Granule Polypeptide
IS	Internal Standard
Asp	Aspartic Acid
Arg	Arginine

ESI	electrospray
BCA	Bicinchoninic Acid assay
GWP-II®	Green Wall Panel – II®
CAPEX	CAPital EXpenditure
OPEX	OPerational EXpenditure
FCI	Fixed Capital Investment
TDC	Total Direct Capital costs
TIC	Total Indirect Capital costs
ISBL	Inside Battery Limits
OSBL	Offsite Battery Limits
TDO	Total Direct Operating costs
TIO	Total Indirect Operating costs

Literature cited

[1] M.A. Borowitzka, High-value products from microalgae-their development and commercialisation, J. Appl. Phycol. 25 (2013) 743–756. https://doi.org/10.1007/s10811-013-9983-9.

[2] M. Bilal, T. Rasheed, I. Ahmed, H.M.N. Iqbal, High-value compounds from microalgae with industrial exploitability - A review, Front. Biosci. - Sch. 9 (2017) 319–342. https://doi.org/10.2741/s490.

[3] A.K. Koyande, K.W. Chew, K. Rambabu, Y. Tao, D.T. Chu, P.L. Show, Microalgae: A potential alternative to health supplementation for humans, Food Sci. Hum. Wellness. 8 (2019) 16–24. https://doi.org/10.1016/j.fshw.2019.03.001.

[4] N.-S. Lau, M. Matsui, A.A.-A. Abdullah, Cyanobacteria: Photoautotrophic Microbial Factories for the Sustainable Synthesis of Industrial Products, Biomed Res. Int. 2015 (2015) 1–9. https://doi.org/10.1155/2015/754934.

[5] F.G.A. Fernández, J. María, F. Sevilla, E.M. Grima, Chapter 21 - Costs analysis of microalgae production, Second Edi, Elsevier B.V., 2019. https://doi.org/10.1016/B978-0-444-64192-2.00021-4.

[6] L. Barsanti, P. Gualtieri, Is exploitation of microalgae economically and energetically sustainable?, Algal Res. 31 (2018) 107–115. https://doi.org/10.1016/j.algal.2018.02.001.

[7] B. Vázquez-romero, J. Antonio, H. Pereira, M. Barbosa, J. Ruiz, Science of the Total Environment Techno-economic assessment of microalgae production , harvesting and drying for food , feed , cosmetics , and agriculture, 837 (2022). https://doi.org/10.1016/j.scitotenv.2022.155742.

[8] F.G.A. Fernández, A. Reis, R.H. Wijffels, M. Barbosa, V. Verdelho, B. Llamas, The role of microalgae in the bioeconomy, N. Biotechnol. 61 (2021) 99–107. https://doi.org/https://doi.org/10.1016/j.nbt.2020.11.011.

[9] S. Rezvani, I. Saadaoui, H. Al, N.R. Moheimani, Techno-economic modelling of high-value metabolites and secondary products from microalgae cultivated in closed photobioreactors with supplementary lighting, Algal Res. 65 (2022) 102733. https://doi.org/10.1016/j.algal.2022.102733.

[10] B. Drosg, I. Fritz, F. Gattermayr, L. Silvestrini, Photo-autotrophic production of poly(hydroxyalkanoates) in cyanobacteria, Chem. Biochem. Eng. Q. 29 (2015) 145–156. https://doi.org/10.15255/CABEQ.2014.2254.

[11] L. Ramanna, I. Rawat, F. Bux, Light enhancement strategies improve microalgal biomass productivity, Renew. Sustain. Energy Rev. 80 (2017) 765–773. https://doi.org/10.1016/j.rser.2017.05.202.

[12] M.P. Caporgno, A. Mathys, Trends in Microalgae Incorporation Into Innovative Food Products With Potential Health Benefits, 5 (2018) 1–10. https://doi.org/10.3389/fnut.2018.00058.

[13] K. Schipper, H.M.S.J. Al-jabri, R.H. Wijffels, M.J. Barbosa, Bioresource Technology Techno-economics of algae production in the Arabian Peninsula, Bioresour. Technol. 331 (2021) 125043. https://doi.org/10.1016/j.biortech.2021.125043.

[14] P.C. Oostlander, J. Van Houcke, R.H. Wijffels, M.J. Barbosa, Microalgae production cost in aquaculture hatcheries, Aquaculture. 525 (2020) 735310. https://doi.org/10.1016/j.aquaculture.2020.735310.

[15] M.M. Allen, A.J. Smith, Nitrogen chlorosis in blue-green algae, Arch. Mikrobiol. 69 (1969) 114–120. https://doi.org/10.1007/BF00409755.

[16] K.M. Frey, F.B. Oppermann-Sanio, H. Schmidt, A. Steinbüchel, Technical-scale production of cyanophycin with recombinant strains of Escherichia coli, Appl. Environ. Microbiol. 68 (2002) 3377–3384. https://doi.org/10.1128/AEM.68.7.3377-3384.2002.

[17] A. Steinle, F.B. Oppermann-Sanio, R. Reichelt, A. Steinbüchel, Synthesis and accumulation of cyanophycin in transgenic strains of Saccharomyces cerevisiae, Appl. Environ. Microbiol. 74 (2008) 3410–3418. https://doi.org/10.1128/AEM.00366-08.

[18] K. Ziegler, A. Diener, C. Herpin, R. Richter, R. Deutzmann, W. Lockau, Molecular characterization of cyanophycin synthetase, the enzyme catalyzing the biosynthesis of the cyanobacterial reserve material multi-L- arginyl-poly-L-aspartate (cyanophycin), Eur. J. Biochem. 254 (1998) 154–159. https://doi.org/10.1046/j.1432-1327.1998.2540154.x.

[19] L. Wiefel, A. Steinbüchel, Solubility behavior of cyanophycin depending on lysine content, Appl. Environ. Microbiol. 80 (2014) 1091–1096. https://doi.org/10.1128/AEM.03159-13.

[20] N.J. Lang, R.D. Simon, C.P. Wolk, Correspondence of cyanophycin granules with structured granules in Anabaena cylindrica, Arch. Mikrobiol. 83 (1972) 313–320. https://doi.org/10.1007/BF00425243.

[21] M.M. Allen, P.J. Weathers, Structure and composition of cyanophycin granules in the cyanobacterium Aphanocapsa 6308, J. Bacteriol. 141 (1980) 959–962. https://doi.org/10.1128/jb.141.2.959-962.1980.

[22] L. Messineo, Modification of the Sakaguchi reaction: Spectrophotometric determination of arginine in proteins without previous hydrolysis, Arch. Biochem. Biophys. 117 (1966) 534–540.

[23] M.M. Bradford, A rapid and sensitive method for the quantitation of microgram quantities of protein utilizing the principle of protein-dye binding, Anal. Biochem. 72 (1976) 248–254. https://doi.org/https://doi.org/10.1016/0003-2697(76)90527-3.

[24] H. Li, D.M. Sherman, S. Bao, L.A. Sherman, Pattern of cyanophycin accumulation in nitrogen-fixing and non-nitrogen-fixing cyanobacteria, Arch. Microbiol. 176 (2001) 9–18. https://doi.org/10.1007/s002030100281.

[25] A. Trautmann, B. Watzer, A. Wilde, K. Forchhammer, C. Posten, Effect of phosphate availability on cyanophycin accumulation in Synechocystis sp. PCC 6803 and the production strain BW86, Algal Res. 20 (2016) 189–196. https://doi.org/10.1016/j.algal.2016.10.009.

[26] P.K. Smith, R.I. Krohn, G.T. Hermanson, A.K. Mallia, F.H. Gartner, M.D. Provenzano, E.K. Fujimoto, N.M. Goeke, B.J. Olson, D.C. Klenk, Measurement of protein using bicinchoninic acid, Anal. Biochem. 150 (1985) 76–85. https://doi.org/10.1016/0003-2697(85)90442-7.

[27] M.R. Tredici, L. Rodolfi, N. Biondi, N. Bassi, G. Sampietro, Techno-economic analysis of microalgal biomass production in a 1-ha Green Wall Panel (GWP®) plant, Algal Res. 19 (2016) 253–263. https://doi.org/10.1016/j.algal.2016.09.005.

[28] J. Clippinger, R. Davis, Techno-Economic Analysis for the Production of Algal Biomass via Closed Photobioreactors: Future Cost Potential Evaluated Across a Range of Cultivation System Designs, Natl. Renew. Energy Lab. (2019) 42. https://www.osti.gov/servlets/purl/1566806/.

[29] F. Fasaei, J.H. Bitter, P.M. Slegers, A.J.B. van Boxtel, Techno-economic evaluation of microalgae harvesting and dewatering systems, Algal Res. 31 (2018) 347–362. https://doi.org/10.1016/j.algal.2017.11.038.

Appendix

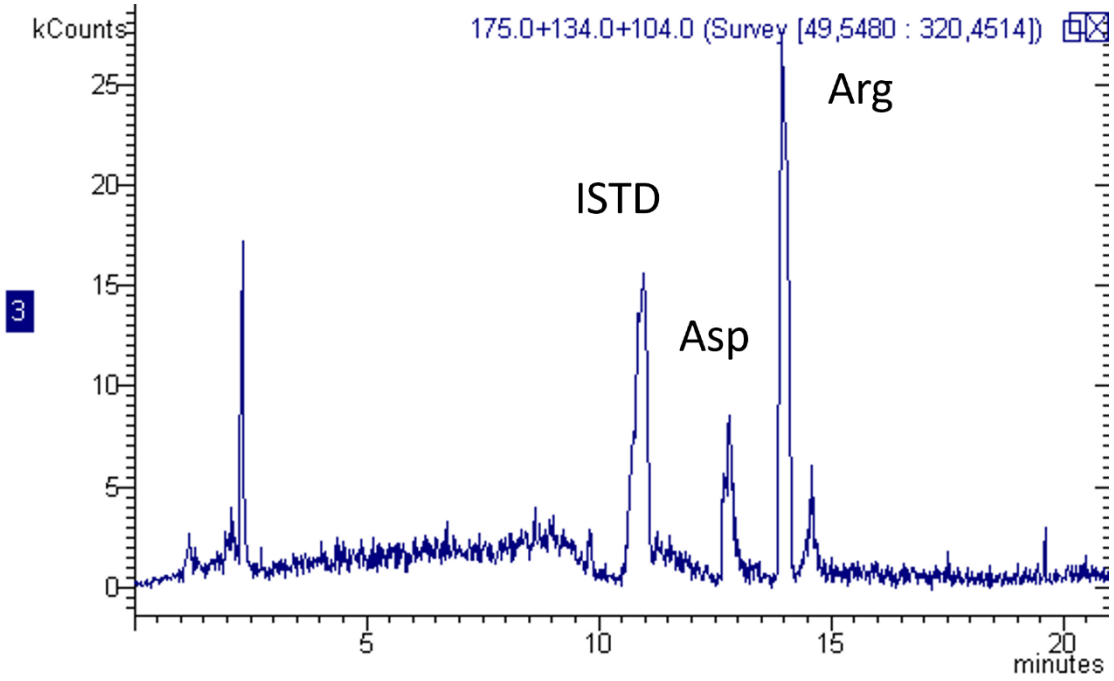

Figure 9A.1. Results of LC-MS/MS analysis of the extracted cyanophycin sample

Table 9A.1. Cultivation medium

Nutrients	***Synechocystis* sp. PCC 6803**	***Nostoc* sp. PCC 7120**	***Nostoc* sp. 44**
	mg L^{-1}	mg L^{-1}	mg L^{-1}
Na_2Mg EDTA	2	2	2
Ferric ammonium citrate	12	-	-
$FeCl_3 \cdot 6H_20$	-	12.43	12.43
Citric acid · H_20	12	12	12
$CaCl_2 \cdot 2H_20$	72	72	72
$MgSO_4 \cdot 7H_20$	150	150	150
K_2HPO_4	15.25	3.05	3.05
H_3BO_3	5.72	5.72	5.72
$MnCl_2 \cdot 4H_20$	3.62	3.62	3.62
$ZnSO_4 \cdot 7H_20$	0.444	0.444	0.444
$CuSO_4 \cdot 5H_20$	0.158	0.158	0.158
$COCl_2 \cdot 6H_20$	0.1	0.1	0.1
$Na_2MoO_4 \cdot 2H_20$	0.782	0.782	0.782
Na_2CO_3	40	-	-
$NaNO_3$	3000	-	-
$NaHCO_3$	3000	250	250

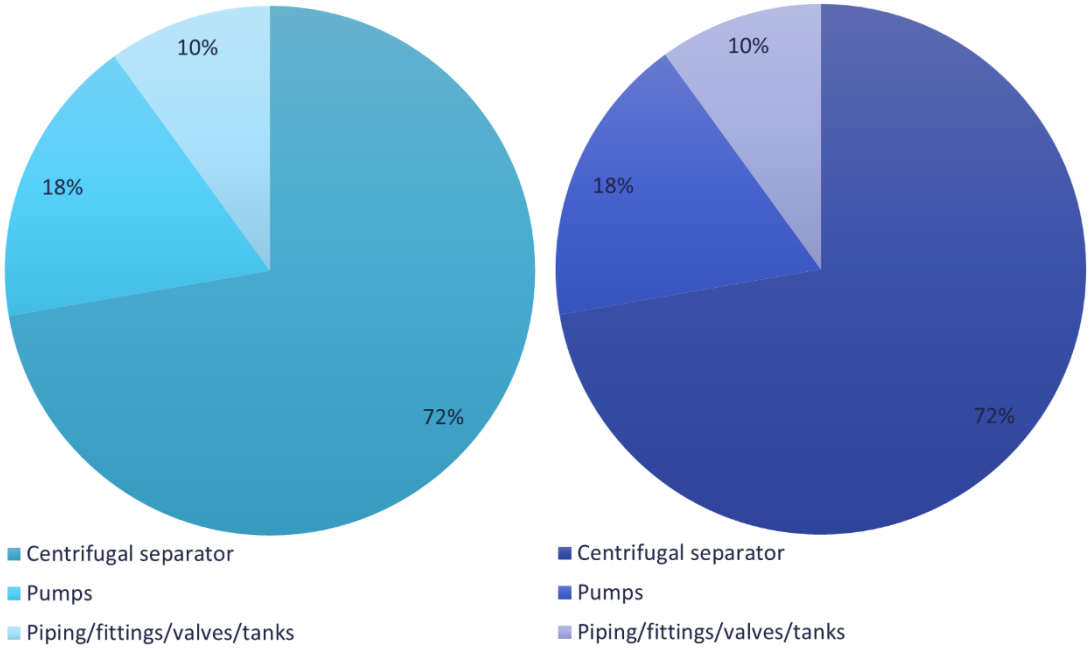

Figure 9A.2. Pie chart of Total Direct Capital cost Inside Battery Limits (ISBL) related to the pretreatment section (*light blue*) and cyanophycin extraction and separation section (*blue*)

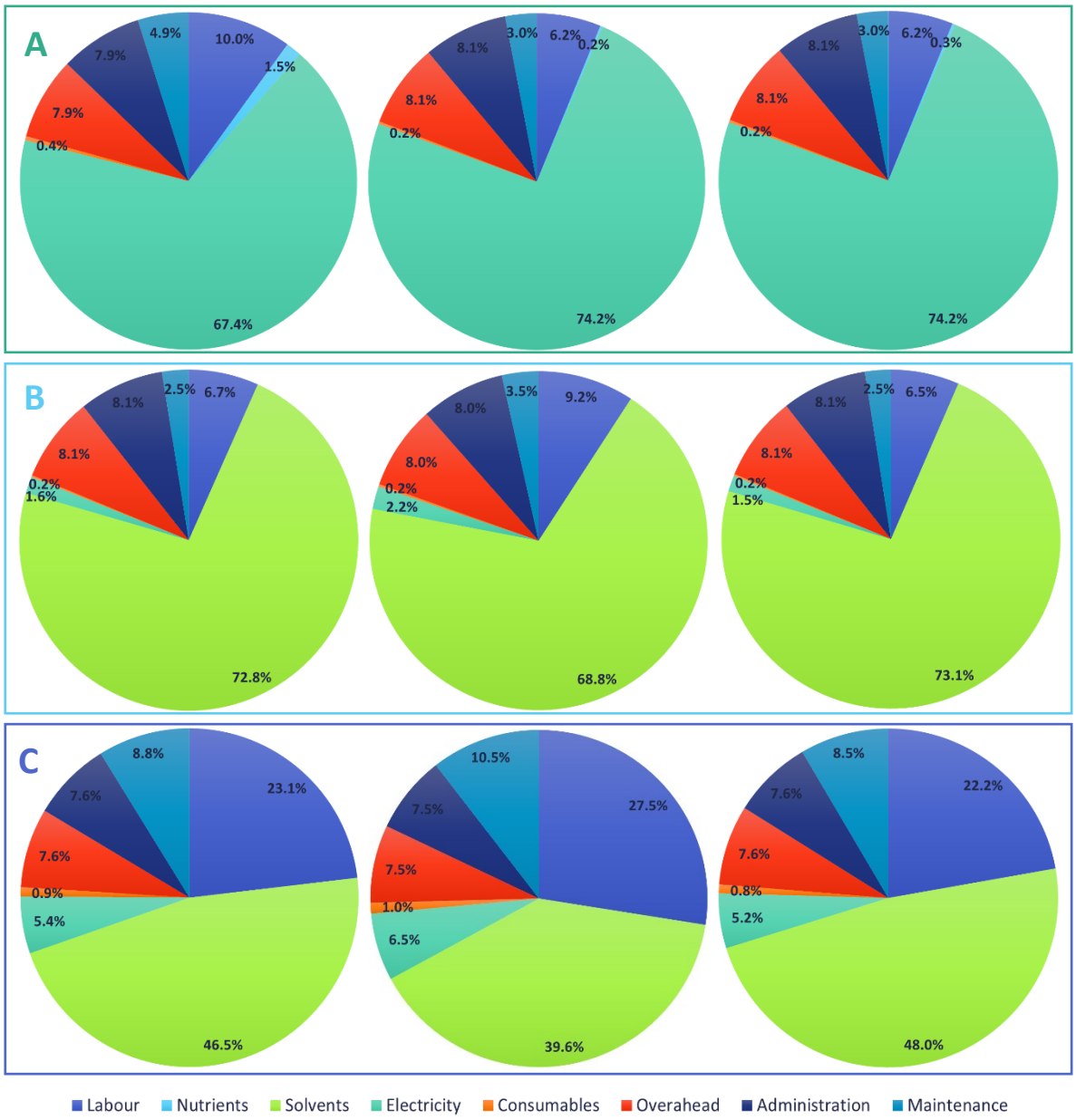

Figure 9A.3. Pie charts of operating costs (OPEX) of 1 ha biomass production plant (panel A), of biomass pre-treatment section (panel B) and of cyanophycin extraction section (panel C). Pie charts of first column is for *Synechocystis* sp. PCC 6803, the second column is for *Nostoc* sp. PCC 7120, and the third column is for *Nostoc* 44

Conclusions

The aim of this PhD research project was to assess the feasibility of using cyanobacteria as factories for the industrial production of cyanophycin as a relevant example of hig value compound. This topic was addressed from different points of view, through both laboratory experiments and mathematical modelling.

The Design of Dynamic Experiments (DoDE) combined with the Response Surface Model (RSM) were applied to model the effect of three operating variables (incident light intensity, temperature, and inlet phosphorus concentration) on cyanophycin production by *Synechocystis* sp. PCC 6803. By applying an evolutionary optimization approach, the best operating conditions ensuring a significant increase in cyanophycin production (about 20%) were identified. The Design of Dynamic Experiments (DoDE) combined with the Dynamic Response Surface Model (DRSM) were instead applied to model the growth of a photosynthetic microorganism, and three models that represent accurately enough data were obtained. Thus, DoDE, RSM and DRSM proved to be powerful tools even when dealing with extremely complex and highly variable bioprocess.

Subsequently, it was demonstrated that a stable production of cyanophycin can be obtained by cultivating different species of cyanobacteria, even under nitrogen fixing conditions. By properly changing the operating variables, it was possible to maximize the cyanophycin productivity. Specifically, cyanophycin was produced by continuously cultivating the unicellular cyanobacteria *Synechocystis* sp. PCC 6803, the diazotrophic filamentous cyanobacteria *Anabaena cylindrica* PCC 7122 and *Nostoc* sp. PCC 7120, and the four different engineered filamentous diazotrophic strains of *Nostoc* sp. PCC 7120. It resulted that there is a clear role of phosphorus on the cyanophycin accumulation, with the cyanophycin quota that was found to be inversely proportional to the phosphorus quota. So, to increase the cyanophycin productivity, it is necessary to reduce the phosphorus quota.

With respect to the mathematical modelling, a preliminary model based on the Droop approach was applied to describe the microalgal growth in a continuous cultivation system for different operating conditions. Encouraging results were obtained to simulate the biomass concentration, nutrients consumption and the internal quota. Another

mathematical model was developed to understand the influence of oxygen on the biomass productivity in a continuous tubular photobioreactor. Although applied to a specific case, this analysis is of general validity, and can be a useful tool to optimize the operating conditions of an existing plant, or alternatively to find the optimal design of a new one.
Finally, a preliminary economic assessment was done according to a proposed flowsheet for a cyanophycin production plant artificially illuminated, and the total product cost was evaluated.

In summary, the results obtained during this PhD project can be considered a good starting point for the study of a photosynthetic cyanophycin production process, for which the literature available is at present quite scarce. However, further work has to be done, in particular for the production of a commercial standard to which compare and refer experimental data. In view of a large-scale process, the protocols for the pre-treatment of biomass and the extraction of cyanophycin must be improved and optimized. Further experimentation is needed to find the cultivating conditions that can guarantee a high cyanophycin productivity, but at the same time reduce the operating cost due to electricity by increasing the photosynthetic efficiency.